DISSERTATION / DOCTORAL THESIS

Titel der Dissertation /Title of the Doctoral Thesis

„Soft Lepton Flavour Violation in a
Two-Higgs-Doublet-Seesaw Model“

verfasst von / submitted by

Elke Aeikens, M.Sc., B.Sc.

angestrebter akademischer Grad / in partial fulfilment of the requirements for the degree of

Doktorin der Naturwissenschaften (Dr. rer. nat)

Wien, 2020 / Vienna 2020

Studienkennzahl lt. Studienblatt / degree programme code as it appears on the student record sheet:	UA 796 605 411
Dissertationsgebiet lt. Studienblatt / field of study as it appears on the student record sheet:	Physik
Betreut von / Supervisor:	ao. Univ.-Prof. Dr. Walter Grimus

Abstract

Extensions of the Standard Model with three right-handed neutrinos in a Seesaw Type I mechanism, and two Higgs doublets offer an interesting framework for investigations. As such models have flavour-changing neutral-scalar interactions (FCNIs), we impose a lepton flavour symmetry, which is only broken *softly* by the non-flavour diagonal mass terms of the right-handed neutrino singlets. Within this model, the seesaw mechanism thus not only explains the smallness of the neutrino masses but is the only source of lepton flavour mixing. The subject of the thesis is a thorough investigation of this model through precision tests that restrict the new model parameters. The latter are the Yukawa couplings, Higgs and neutrino masses, vis. the seesaw scale, and the angles of the flavour-mixing matrices. The applied tests comprise the model contributions to oblique parameters, to the anomalous magnetic moment (AMM) of the electron and muon, and clearly, to lepton flavour-changing processes. With respect to the latter, we investigate in this course the impact of one-loop neutrino mass corrections on lepton flavour-changing processes, which are, interestingly, generally not negligible in our model. We further show that this model can solve the experimental and theoretical discrepancy of the muon AMM and provide a region in the parameter space where all FCNI branching ratios of the type $\ell_1^- \to \ell_2^- \ell_3^+ \ell_3^-$ are close to the experimental bounds and could therefore be detectable in the near future.

Zusammenfassung

Erweiterungen der Standardmodells mit drei rechtshändigen Neutrinos in einem Seesaw Type I Mechanismus und zwei Higgs Doublets bieten ein interessantes Forschungsfeld. Da solche Modelle flavour-verletzende Wechselwirkungen mit neutralen Skalaren (FCNI) haben, führen wir eine Flavour Symmetrie ein, welche nur *soft* gebrochen wird von nicht-falvourdiagonalen Massetermen der rechtshändigen Neutrinosinglets. Innerhalb dieses Models erklärt der Seesawmechnaismus nicht nur, warum Neutrinomassen klein sind, sondern stellt auch die einzige Quelle von Leptonenflavour-Mischung dar. Das Thema dieser Dissertation ist eine sorgfältige Untersuchung dieses Modells durch Präzisionstests, welche die neuen Modellparameter einschränken. Die Modellparameter sind die Yukawakopplungen, die Higgs- und Neutrinomasses, die die Seesawskala festlegen, und die Winkel der flavourmischenden Matrizen. Die angewandten Tests umfassen die Modellbeiträge zu Oblique Parametern, zu den anomalen Magnetischen Momenten (AMM) des Elektrons und Myons, und natürlich zu leptonenflavourverletzenden Prozessen. Im Bezug auf letztere untersuchen wir außerdem den Einfluss von einloop Neutrinomassenkorrekturen auf Leptonflavour-verletzende Prozesse, welche interessanterweise in unserem Modell generell nicht vernachlässigbar sind. Wir zeigen weiterhin, dass dieses Modell eine Region im Parameterraum bereitstellt, in der alle FCNI Verzeigungsverhältnisse des Types $\ell_1^- \to \ell_2^- \ell_3^+ \ell_3^-$ nahe an der experimentellen Grenze sind und deshalb detektierbar in voraussichtlich naher Zukunft.

Acknowledgements

First of all I like to thank my supervisor Prof. Grimus for his advice, the fruitful discussions, and his patience, even after his retirement. Further on, my gratitude goes to my co-supervisor Prof. Neufeld and our collaborator Luis Lavoura. A warm thanks to Prof. André Hoang for your support and your humanity in leading everything along the right tracks, that meant a lot to me.

I like to thank Michel Malinský for his infectious enthusiasm for physics and his time and an open ear for interesting discussions that have enriched my horizon. Furthermore, my thanks go to Alexander Merle, Marco Drewes, and Jessica Turner, as well as Massimiliano Procura, for their support and expertise. I would also like to thank you, Julian Leiber, for your immediate help in times of difficulty. Thanks to Birgit Trappel, Marcus Sperling, Christopher Lepenik, Daniel Lechner, Moritz Preißer, Daniel Samitz, and Max Löschner for the fruitful discussions, the time spent together, and the great atmosphere on the fifth floor, and thanks to Adi, who helped me out with Mathematica in times of need. I give a hug to my friends, Angelika Widl, for your apartment in times of need and your continuous support, together with Carla Schuler and Maarten Fox, you have always been my women I can count on. I send kisses to Bahman Dehnadi, who spent a lot of great time with me, correcting my thesis and introduced me to my passion, the swing dance.

My further thanks go to the great doctoral school DKPI, for many unforgettable events and opportunities that enriched my life inside and outside of physics and especially all DKPI students, namely Ece, Navid, Hanno, Maria (thanks for my first Lipstick), Lukas, Daniel, Erica, Alex, Berni, Tobias, Willi, and all those I forgot to mention, for the jumps into cold waters, the sauna, the jokes, and common destiny with peaks and valleys.

A big thank you to all my awesome friends who always stood by my side, believed in me, supported me with loads of love, and accepted me with and because of all my mistakes. These are Martijn (you are the best!), Fanny, Ivana, Lena, Manu, Christoph, Nati, Chris, Anna, Marco, Megan, Jenny, my roommates, and new family Adrian, Moni, Corina and all my other lovely dancers, and furthermore, Julia, Arjen, Michellö, Frauki, Maggy, Maura, Wout, and all the others I forgot to mention, I love you guys! Viki, thank you for the wonderful time, your help and energy, and the relaxation. I hope we remain friends for a long time.

Finally, thanks to my relatives; God blessed me with the best parents you can imagine, a deep thank you to mum and dad for all your love, your inner faith in me, your constant encouragement and great wisdom of life that kept me going until the end, you have the biggest spot in my heart.

E.H.A. is supported by the FWF Austrian Science Fund under the Doctoral Program W1252-N27 "Particles and Interactions."

Contents

Introduction

The Standard Model (SM) is the most successfully tested theory in particle physics. Any theory that does not contain its fundamental parts has very little chance not to be disproved if it aims to describe nature correctly. So far, the SM describes well all reaction terms for particle interaction within three of the four fundamental forces: electromagnetism, weak force, and strong force. On the other hand, it is also well known that the Standard Model is incomplete, that it does not include the fourth fundamental force, gravity, that it fails to describe dark matter, and the observed neutrino oscillations and masses as well as the matter-antimatter asymmetry of the universe. Furthermore, the SM gives neither explanations for the three fermion generations nor parameter values or mass hierarchies [1, 2]. Therefore, new models beyond the SM, like the one in this thesis, are an attempt to solve at least some of the open questions. They are small steps on the way to the sought-for theory of everything.

The model of this thesis extends the electroweak, flavour, and neutrino sector of the SM. It includes

(A) an extended Higgs sector, consisting of two Higgs-doublets,

(B) an extension in the neutrino sector with three right-handed Majorana neutrino fields ν_R in a high-scale Seesaw Type I mechanism,

(C) flavour diagonal Yukawa coupling matrices in the lepton sector so that the family lepton numbers L_α ($\alpha \in \{e,\ \mu,\ \tau\}$) are conserved in the Yukawa interactions, i.e. the lepton flavour symmetry remains preserved. To allow non-trivial lepton mixing, these lepton numbers and thus this symmetry are only softly broken by the mass terms of ν_R.

This model was proposed by Grimus and Lavoura [3] and has a well-founded motivation. It combines the *advantages* of the simple, economical Seesaw Type I in neutrino physics, which are

- the generation of neutrino masses,
- the explanation of the smallness of the neutrino masses,
- leptogenesis (although not studied here!) as is apparent from [4],

with those of soft lepton flavour violation. This ensures that

- flavour violation, and hence the flavour oscillation, is generated exclusively in the non-diagonal, right-handed Majorana mass term; a mechanism that would not work in the quark sector and could therefore explain the difference between the V_{CKM} and U_{PMNS} matrices.

Finally, there are further advantages of combining of a Type I Seesaw mechanism with right-handed neutrinos and soft lepton flavour violation together with a two-Higgs-doublet model (2HDM), which adds a rich part to the new phenomenology.

The model with its three components (A), (B), and (C) exhibits very specific *properties* [3]:

- Typically, models with several Higgs doublets imply flavour-changing neutral interactions (FCNI) at tree level as they can occur specifically from new non-diagonal Yukawa couplings. But FCNIs are experimentally very restricted. In the model of this thesis, this problem is circumvented by diagonal Yukawa couplings (vis. due to the lepton flavour symmetry); in this way, FCNIs initially occur in one-loop order and are therefore small.

- The absence of tree-level FCNIs means that FCNIs are finite at one-loop level since, without a tree-level term, no counterterms can be written.

- In other models, the Yukawa couplings are often unnaturally small to suppress the FCNIs. This is not the case here since the FCNIs are already small so that Yukawa couplings can be of the same order of magnitude as other Fermion-Yukawa couplings, such as e.g. that of the muon $Y_\mu = m_\mu \sqrt{2}/v \sim 0.001$. We will later work with Yukawa couplings in the range 0.0001 up to 0.7.

- Since the lepton flavour is only broken in the mass terms of ν_R, one could assume that the FCNIs decouple themselves with the scale of the heavy right-handed neutrino masses, the Seesaw scale, i.e. contributions of this model to FCNIs could be suppressed. This proved to be the case for decays with gauge bosons, e.g. radiative decays like $\mu \to e\gamma$ or $Z^0 \to e^-\mu^+$. Surprisingly, however, the Seesaw scale is non-decoupling in the case of flavour-violating decays such as $\mu^- \to e^-e^+e^-$, which is due to contributions that contain scalars, actually charged scalars, and no gauge bosons [3]. This is an intrinsic feature of this model and attractive for further investigations. As we will show, this model even allows that the branching ratios of decays like $\mu^- \to e^-e^+e^-$ are close to the experimental limits.

Note that this model is analysed solely in the lepton-scalar sector, vis. the interaction of the new scalar part with the quark sector is not considered[1] Furthermore, we will only define the scalar masses within the Higgs potential. Adding the quark sector and the Higgs self-interactions would enlarge our parameter space and require the inclusion of further precision testing, which was deemed as being beyond the scope of this thesis.

[1]The connection to the quark sector can be manifold, e.g. due to the nearly diagonal quark-flavour mixing matrix V_{CKM} one could introduce small finely-tuned quark-Higgs coupling matrices or add a third Higgs doublet that only couples to the quarks via Z_2 symmetry.

Since this model seems to offer many advantages but has never been tested phenomenologically for consistency with experimental values and limits, **the task of this thesis is to explicitly investigate the phenomenology of this model** in four experimentally tested areas:

1. The general electroweak precision physics in the form of the oblique parameters S, T, U, V, W, X [5],

2. The astonishingly precisely measured anomalous magnetic moment (AMM) of the electron and the muon. In this context, *it will be also examined whether the model contributions can compensate for the experimental and theoretical discrepancy* $a_\mu^{\text{exp}} - a_\mu^{\text{SM}}$ *of the anomalous magnetic moment of the muon.*

3. On the FCNI of the form $\ell_1^- \to \ell_2^- \ell_3^+ \ell_3^-$, there are strong experimental bounds, which provide a good test for this model and its parameter content. In addition, *we will clarify whether there are parameter spaces that bring these decay rates close to the bounds and thus make it possible to detect them in the near future.*

4. The right-handed neutrino masses and the associated mixing matrix play an important role in the FCNIs as well as in the mass matrix of the light neutrinos. Therefore, the strong experimental constraints of the light neutrino sector indirectly influence the FCNIs. This motivates us to *investigate the effects of the one-loop corrections to the light neutrino mass matrix on the FCNIs* since this has never been done before within the type of our model. Interestingly, we found out that neutrino mass corrections are not negligible but can have a significant impact on the value of the right-handed neutrino mass and mixing matrix and thus on the FCNIs. This is true if the experimental data for light neutrinos are inserted, such as the neutrino mixing matrix, mass-squared differences, and limits of the neutrino mass.

These areas of the Tests 1 to 4 are limited to the new phenomena of interaction between (A), (B), and (C) as many of the other phenomenological features of the 2HDM and the Type I Seesaw model are already being studied separately and are found in the literature. These include vacuum stability, unitary bounds, or on the neutrino side, the bounds of the neutrinoless double beta decay [6, 1, 7, 8, 9].

Since this model will contain a set of new parameters, the main purpose of these tests will be *to analyse whether a specific parameter range can be found that is consistent with all tests.* If this is the case, we can further investigate how large this parameter space is and how the constraints on the individual parameters are correlated. In this way, we can *determine whether the model is feasible, realistic, or even advantageous*. With the resulting parameter range one can make statements about the *verifiability of this model parameters in near future experiments* and thus about the verifiability of this model. As a necessary consequence, we derive the formulas for the tests, some of which may be applicable to other models. In addition, we will be able *to examine the characteristics of the tests carried out in terms of general feasibility and impact.*

Let us make a comment on the structure of this thesis. The theory part, Part I, provides the theoretical basis for each component (A), (B), and (C) of the underlying model and its motivation. In this part, all necessary formulas of this model are presented, and further simplifying assumptions for managing the computations in the subsequent part are made. In the subsequent phenomenological part, Part II, the tests of the Areas 1 to 4 are performed on the model. At the end of Part II, conclusions and results are given together with an outlook briefly outlining further useful tests on this model.

This thesis is based on the paper [10], which is incorporated into the text through literal citations.

Part I.

Theoretical Foundations and the Model

1. Introduction: Ansätze in Model Building

As stated in the introduction, there are good reasons to believe that the SM is incomplete, and new models are needed to explain the missing parts. It is therefore easy to guess that there exist a whole bunch of models in particle physics, all of which try to extend the SM in an advantageous way. So, before we dive into the theoretical introduction of this specific model, let us look at different types of model ansätze and classify our model approach on the model-building methods.

Model building can be realized in two ways, the top-down or the bottom-up approach; this classification has its origin in string theory mentioned by [11]. The top-down approach is based on a theory on a higher scale with a larger gauge group, broken down to the groups of the Standard Model. The **bottom-up approach** that we consider within our model starts from the Standard Model and extends it with new features that take into account the known problems. This can be achieved by proposing new symmetries and/or a new particle content. Models created using a bottom-up approach often combine some of the characteristics of the so-called "Hidden Valley" framework [12], in order to clarify the sense of their previous non-detection. These "Hidden Valley" characteristics are: *heavy* when new particles enter with high mass, *hidden* when symmetries are introduced to suppress tree-level values, and *effectively decoupled* when couplings are suppressed [12]. For a more comprehensive categorization, see [13].

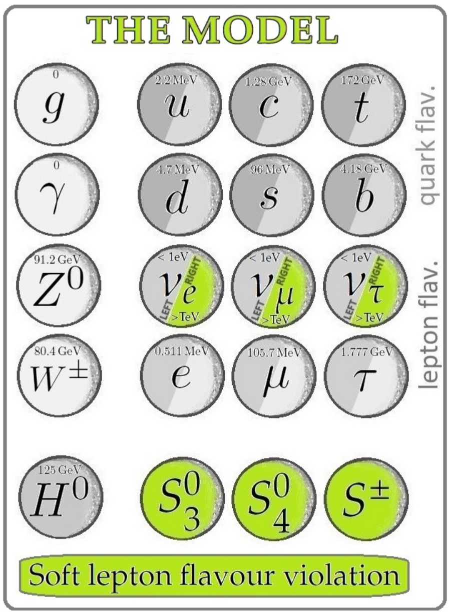

Figure 1.1.: The SM extension of the model of this thesis in green: A new particle content and softly broken lepton-flavour symmetry.

The model to be presented in this thesis has three new features, which are shown in green in Figure 1.1: It contains a new particle content of three *heavy* right-handed Majorana neutrinos and an additional Higgs doublet, the latter being neither very heavy nor decoupled and having a soft, broken lepton flavour symmetry, which is the *hidden* part of this theory and prohibits FCNI at tree level.

In the next three chapters, an introduction to the theory behind each component of this model is given, and the motives and formulas plus assumptions are presented.

2. Neutrino Physics

The recent public perception of the successes in neutrino physics shows that this field has meanwhile developed into an important and renowned area of physics. In 2015, for example, the Nobel Prize was awarded to the neutrino physicists Takaaki Kajita and Arthur B. McDonald for the discovery of neutrino oscillation [14], and in September 2017, it was announced that $\sim 290\,\mathrm{TeV}$ neutrinos were detected in Ice Cube and interpreted as a part of multi-messenger signals from an extragalactic flaring blazar [15].

However, since the beginning of neutrino physics in 1930, when Wolfgang Pauli proposed neutrino particles as a solution to the missing energy in beta decays, it took almost 26 years until the first neutrino discovery in 1956 by C. L. Cowan, F. Reines, F. B. Harrison, H. W. Kruse, and A. D. McGuire [16, 17, 8] with a reactor-neutrino experiment in the USA. Even more time and effort was needed until neutrino physics was established as a separate discipline within physics with a larger community, and the core knowledge from the present day was collected. Two of the important key findings were, first, the neutrino oscillation and thus the indication of the neutrino mass, proposed in a theory by Pontecorvo 1957, which was completed in 1976 by S.M. Bilenky and B. Pontecorvo [17], among others, and experimentally verified in 1987 in the Kamiokande-II experiment. A major breakthrough, however, was the solution to the solar neutrino problem, which was solved in 1986 by the Mikheev–Smirnov–Wolfenstein effect [17].

But why did neutrinos receive such special attention, and why did the progress of neutrino analysis progress so slowly? The reasons for this are that neutrinos have a completely **different character** in certain features than the other SM particles. As we now know, they

1. only interact via the weak force (and gravity),
2. are very light $m_\nu \lesssim 0.1\,\mathrm{eV}$ (CMB data [9]),
3. have flavour states, ν_e, ν_μ, ν_τ, that show a strongly oscillating behaviour, which means that the neutrino mixing matrix U_{PMNS}, which transforms neutrino fields from the flavour to the mass basis, is strongly off-diagonal in contrast to quarks, which have a nearly diagonal mixing matrix V_{CKM}.
4. have so far only been measured with negative helicity and antineutrinos with positive helicity, which corresponds only to left-handed chiral fields.

Points 1 and 2 in particular made it very difficult for the experimentalists to detect neutrinos. The current neutrino detector landscape counts up to almost thirty ongoing experiments and another eight to ten under construction. These include accelerator experiments, experiments to detect terrestrial, solar, atmospheric neutrinos, neutrinos from supernovae and nuclear reactors, and some that attempt to prove the proposed neutrinoless double beta decay [17].

The **current experimental status** of the neutrino parameters shall be presented in the following. In Part II of this thesis, we will use these neutrino precision data as input for our model. Up to now, parameters from the oscillation behaviour (Point 3) have been measured with high precision, such as the neutrino oscillation angles or the mass-squared differences. The best-fit values of the angles are $\sin^2\theta_{12} = 0.304$, determined, among others, from data measured by KamLAND and SuperK in 2016, $\sin^2\theta_{23} = 0.452$ (T2K, MINOS, IceCube, NOvA), and $\sin^2\theta_{13} = 0.0218$ (Double Chooz, Daya Bay, RENO) [18]. Furthermore, the neutrino square mass differences can be extracted from oscillation data, with the best-fit values $\Delta m^2_{12} = 7.50 \times 10^{-5}\,\mathrm{eV}^2$, $\Delta m^2_{13} = 2.457 \times 10^{-3}\,\mathrm{eV}^2$ for the normal mass order being measured by KamLAND and T2K, MINOS, IceCube, NOvA, Daya Bay, and RENO [18], while the first limits for the direct detection of the neutrino mass come from KATRIN with $m_\nu < 1.1\,\mathrm{eV}$ (90% CL) [19]. The best-fit values taken here are the same as those we used in our paper [10]; these deviate slightly from the latest best-fit values in [9], but this deviation is within the range of the uncertainty of the data, so for practical reasons, we have not changed them.

Despite the great achievements in data precision and theory, **neutrino physics still poses great puzzles**,[1] which explains the large number of neutrino experiments that collect data. The puzzles are:

(a) What is the true mass of the lightest neutrino?

(b) Since only mass differences are known: Which mass ordering do neutrinos have, normal or inverted?

(c) Why are neutrinos so light?

We have also mentioned under Points 1 and 4 that neutrinos interact only weakly and are demonstrably only left-handed; this raises the questions:

(d) Do neutrinos have right-handed partners, which are gauge singlets under the SM gauge group?

(e) How are neutrino masses generated, and are they of Dirac or Majorana nature?

(f) Does neutrino oscillation violate the CP by non-zero CP phases in the mixing matrix?

Massive right-handed neutrinos of Majorana nature are fairly good candidates to answer Questions (c) to (f), which is why they are *part of the model* of this thesis. Other

[1] There are also unsolved detected anomalies from early data taken from LSND, MiniBooNE, GALLEX, and SAGE and from several reactor experiences which give an indication of a fourth very light sterile neutrino with masses in the eV range. However, this will not be discussed further here since we are interested in highly massive right-handed neutrinos above the TeV scale.

reasons for including massive right-handed Majorana neutrinos are that it seems only natural to include a right-handed partner for the neutrinos when there exists one for all other SM fermions. Furthermore, right-handed neutrinos of Majorana nature have a defined hypercharge of $Y(\nu_R) = 0$, so that in the theoretical model, a charge quantisation of the SM can be realised, which would not be the case with pure Dirac neutrinos, see e.g. [20, 21]. Within a Seesaw framework, right-handed Majorana neutrinos can additionally explain the smallness of the masses of left-handed neutrinos. Moreover, with a Majorana mass of the right-handed neutrinos of $m_R \gtrsim 10^9$ GeV (Davidson-Ibarra bound) and the CP-breaking Majorana phases, right-handed Majorana neutrinos are good candidates for successful leptogenesis, which explains the matter-antimatter asymmetry in the universe.

In the following, we give an introduction to the theoretical foundations of neutrino physics, provide the necessary formulas used in the second part of this thesis, and try to highlight the advantages of *massive right-handed Majorana neutrinos in a Type I Seesaw framework as we use it in our model*. The first Section 2.1 will deal with the neutrino mass ordering to answer Question (b), followed by an introduction to the Dirac and Majorana masses in Section 2.2 on Question (e). Section 2.3 describes the mass-mixing mechanism for Majorana neutrinos together with the Seesaw mechanism, addressing Questions (c) and (d). Building on this, Section 2.4 briefly summarises the energy scales of our model, while Section 2.5 gives an overview of general extensions of the Standard Model for the generation of neutrino mass with additional scalar multiplets as alternatives to the Seesaw mechanism. To complete the list of Lagrangian terms of neutrino contributions in the SM and beyond, the lepton interactions with the gauge boson are summarized in Section 2.6. Finally, in Section 2.7, assumptions are made about the neutrino sector to simplify the calculations in Part II of the thesis.

2.1. Neutrino Mass Ordering

Although light neutrino masses have never been measured directly before, the detection of neutrino oscillation proves that at least two out of three neutrinos must have mass. Specifically, in neutrino experiments in which oscillating neutrinos, ν, from the atmosphere and the sun were observed, the mass differences from neutrinos, more precisely the mass-squared differences $\Delta m^2_{ij} = |m_i^2 - m_j^2|$ were measured as part of the oscillation probability of the three different-flavoured neutrinos,

$$P_{\alpha\to\beta} = \left|\langle \nu_\beta(t)|\nu_\alpha\rangle\right|^2 = \left|\sum_j U_{\beta j} U^*_{\alpha j} e^{-im_j^2 L/(2E)}\right|^2. \tag{2.1}$$

Here, the neutrinos in flavour basis are marked with Greek indices $\alpha, \beta \in \{e, \mu, \tau\}$, while the Roman indices indicate the mass basis, $i, j \in \{1, 2, 3\}$. Then $U_{\alpha j}$ represents the Pontecorvo–Maki–Nakagawa–Sakata matrix, also often written as U_{PMNS}, which transforms the neutrino states from the flavour to the mass basis, and L is the oscillation distance, E the neutrino energy. The measured numbers with errors for the mass-squared differences, according to [18], are

$$\Delta m^2_{sol} = \Delta m^2_{21} = m_2^2 - m_1^2 = (7.50 \pm 0.19) \times 10^{-5}\,\text{eV}^2, \tag{2.2}$$

$$\Delta m^2_{atm} = \Delta m^2_{31} = |m_3^2 - m_1^2| = \begin{cases} (2.457 \pm 0.047) \times 10^{-3}\,\text{eV}^2 & \textit{(normal mass ord.)}, \quad (2.3) \\ (-2.449 \pm 0.048) \times 10^{-3}\,\text{eV}^2 & \textit{(inverted mass ord.)}. \quad (2.4) \end{cases}$$

With the knowledge of the mass differences, the question remains open as to which of the three neutrinos, ν_1, ν_2, or ν_3, is the lightest and which is the heaviest. There are two discussed mass ordering scenarios: The normal mass ordering, with $m_1 < m_2 < m_3$, and the inverted mass ordering, with $m_3 < m_1 \lesssim m_2$ [17], see also Figure 2.1 for the flavour content. Whether normal or inverted mass ordering is true makes a difference in many types of calculations from neutrino interactions, e.g. the $0\nu\beta\beta$ decay, or lepton flavour-changing cross-sections and already in the extraction of the mass-squared differences from the experimental data, as can be seen from the comparison of Equations (2.3) and (2.4).

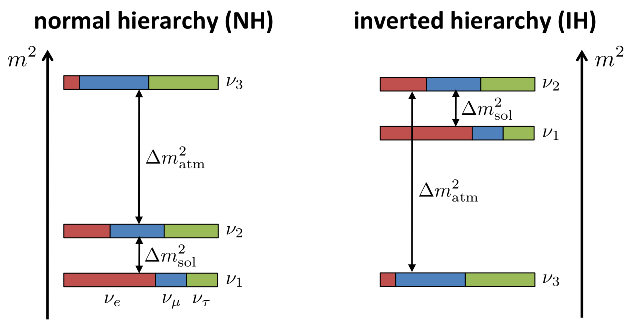

Figure 2.1.: The two possible orderings of neutrino mass eigenstates [22], also often called mass hierarchies.

When considering a hierarchy, e.g. a normal hierarchy, the neutrino masses would be derived from the formulas

$$m_2 = \sqrt{m_1^2 + \Delta m^2_{21}} \quad \text{and} \quad m_3 = \sqrt{m_1^2 + \Delta m^2_{31}}, \tag{2.5}$$

where m_1 remains a free parameter.

2.2. Dirac or Majorana Type

As we saw in the previous chapter, the introduction of neutrino masses is an inevitable extension of the Standard Model simply on account of the detected neutrino oscillations. The concrete implementation of neutrino masses as an extension of the SM, however, always boils down to the question of what type of mass neutrinos have, Dirac or Majorana mass, and whether neutrinos have Dirac or Majorana character. In the following, we first explain Dirac masses, which are the masses that every massive SM fermion has, then we continue with Majorana particles and masses, and finally we clarify the connection with neutrinos.

The general rule for the inclusion of new terms, such as neutrino mass terms, in the SM Lagrange density is that the term must be invariant under Lorentz symmetry. A mass term for a fermion contains fermion fields, ψ, which consist out of two components that transform differently under Lorentz transformation, the left-handed, ψ_L, and right-handed, ψ_R, chiral components,[2] i.e. $\psi = \psi_L + \psi_R$ in Weyl basis, where ψ is a bispinor. The different transforming left- and right-handed components can be projected out of the field using the chirality field operators $\gamma_{R/L} = (1 \pm \gamma_5)/2$, i.e. $\gamma_R\psi = \psi_R$ and $\gamma_L\psi = \psi_L$, with $\gamma_L\gamma_R = 0$. Following up on forming mass terms, a Lorentz-invariant combination of the two chiral fields can be found in a mixture of them, e.g. $\overline{\psi}_L\psi_R$ and thus especially the combination

$$\overline{\psi}\psi = (\overline{\psi}_L + \overline{\psi}_R)(\psi_L + \psi_R) = \overline{\psi}_R\psi_L + \overline{\psi}_L\psi_R \tag{2.6}$$

see Section A.1 for more details on fermion fields. Fermions with a mass term containing this combination

$$\mathcal{L}_{Dirac} = -m_D\overline{\psi}\psi = -m_D(\overline{\psi}_R\psi_L + \overline{\psi}_L\psi_R), \tag{2.7}$$

are called *Dirac fermions* and the mass m_D Dirac mass compared to Majorana fermions with a Majorana mass term. All fermions of the Standard Model are Dirac particles with Dirac masses, with the exception of neutrinos for which the mass terms are not yet defined.

Before we construct Lorentz-invariant Majorana masses, we want to take a brief look at the basic ideas of *Majorana fermions* since Majorana fermions have an additional property. Imagine a fermion like the neutrinos without electromagnetic charge or any other charges from gauged or global $U(1)$ symmetries[3] [23] and consider the antiparticle as the charge conjugation of this fermion, the field of the antifermion would then be described by the charge-conjugated fermion field ψ as

$$\psi^c \equiv C\overline{\psi}^T, \tag{2.8}$$

where C is the charge conjugation operator, see Section A.2.2 for a more detailed definition. Following this thought, if this fermion does have no charges, the antiparticle would not be distinguishable from the particle, and so Ettore Majorana suggested that both could be the same and therefore $\psi = \psi^c$ [24, 25]. Particles with particle fields that obey this condition, the Majorana condition,[4] are called Majorana particles after their discoverer. Now the question arises whether a Lorentz-invariant mass term can be derived for this type of particle. To give an answer, we first need to know under which representation of the Lorentz symmetry a charged-conjugated particle transforms. It can be derived from Equation (2.8) that the left-handed charge-conjugated component

[2] Often the notation of left- and right-handedness is not well-defined in the literature, so that left- and right-handedness is not explicitly assigned to chiral fields but also to helicity states of particles. In order to avoid confusion, helicity states are only set to be positive here (often referred to as right-handed) or negative (often referred to as left-handed).

[3] Actually, neutrinos are charged under the Lepton number symmetry, but let us ignore that for a moment.

[4] It is important to note that the Majorana condition applies only to particle fields in the mass basis.

is of right-handed chirality, as well as the right-handed charge conjugated field is of left-handed chirality,[5] as you can see with Equation (A.9) and $C^{-1}\gamma_5 C = \gamma_5$, it is

$$(\psi_L)^c = (\gamma_L \psi)^c = \gamma_R \psi^c = (\psi^c)_R, . \tag{2.9}$$

Charge conjugation thus changes the chirality of fields and thus also the transformation under Lorentz symmetry. Therefore, Majorana particles can be described by only a single chiral field, e.g. $\psi = \psi_L + (\psi_L)^c$, where $(\psi_L)^c$ transforms under the same Lorentz transformation as ψ_R. Consequently, there exists also a Lorentz-invariant combination for Majorana fermions [23] to form a Majorana mass term; in the following, it is written in left-handed fields

$$\mathcal{L}_{Majorana} = -\frac{1}{2} m_L (\overline{(\psi_L)^c} \psi_L + h.c.) = -\frac{1}{2} m_L \overline{\psi} \psi, \tag{2.10}$$

$$\text{with } \psi(x) = \int \frac{d^3p}{(2\pi)^3} \frac{1}{\sqrt{2E}} \sum_{s=1,2} \left(a_p^s u(s,p) e^{-ipx} + a_p^{s\dagger} u^c(s,p) e^{ixp} \right), \tag{2.11}$$

where m_L is the Majorana mass and $a^\dagger$, a the creation and annihilation operators [17]; for a more detailed description of ψ, see Section A.1.2.

So where is the connection to neutrinos? As already mentioned, Majorana mass terms for general fermions would violate the symmetries of the Standard Model, like the $U(1)_{EM}$, which preserves the electric charge. For this reason, non-electrically charged neutrinos with non-interacting right-handed partners are the only Standard-Model candidates with Majorana potential. In fact, even for neutrinos, Majorana mass terms such as $\overline{(\psi_L)^c}\psi_L$ or $\overline{(\psi_R)^c}\psi_R$ violate one global $U(1)$ symmetry, the Lepton number L, by 2 units, due to the Majorana condition, with $L\left(\overline{(\psi_L)^c}\psi_L\right) = 2$, see Section 4.2, and thus they also break the individual family lepton numbers.

So how can Majorana and Dirac masses be implemented to construct tree-level mass terms for left-handed neutrinos as a minimal extension of the SM?[6] Consider a pure Majorana mass term with only left-handed neutrinos of the simple form in Equation (2.10). Unfortunately, these terms are prohibited at the tree-level because they violate the conservation of weak isospin, I_3, and hypercharge, Y, being the quantum numbers of $SU(2)_L \times U(1)_Y$. As can be seen in Table 2.1, the term $\overline{(\psi_L)^c}\psi_L$ is an isospin triplet with $I_3\left(\overline{(\psi_L)^c}\psi_L\right) = 1$ and hypercharge $Y\left(\overline{(\psi_L)^c}\psi_L\right) = -2$. Therefore, we have to set the Majorana mass of the left-handed neutrinos to zero, $m_L = 0$, at the tree-level.[7] Therefore,

[5] Note that although the neutrino field $(\nu_R)^c$ has left-handed chirality, it is different from the SM ν_L. Since the charge conjugation switches the signs of all charges and also those of the weak charge, $(\nu_R)^c$ remains a weak-isospin singlet, even if it is left-handed like ν_L, whereas ν_L is defined in the SM as part of a weak doublet. In the same way, also the right-handed $(\nu_L)^c$ remains part of a doublet under the weak symmetry, in contrast to ν_R. This shows that the charge conjugation is maximally broken by the chiral-weak symmetry in the charge-current interactions [26], see Section A.2.2 for details.

[6] Further extensions with additional scalar multiplets are presented in Section 2.5.

[7] We will see in Chapter 9 that a Majorana mass for left-handed neutrinos, δM_L, appears in one-loop order.

the remaining options for the tree-level mass generation of left-handed neutrino fields are limited to mass terms with a combination of right-handed neutrinos and must include Dirac masses. However, the implementation of only Dirac masses with right-handed partners has disadvantages. On the one hand, Yukawa couplings have to be fine-tuned to achieve small left-handed neutrino masses with a fixed Higgs vacuum expectation value (VEV), which is considered an unsatisfactory scenario. On the other hand, the Standard Model with only Dirac masses cannot predict charge quantisation. The hypercharge of right-handed neutrinos is, without experimental input, not fixed and therefore each hypercharge receives a shift since the condition from anomalies would not be sufficient to cancel this additional degree of freedom, [20, 21]. This is another reason to prefer right-handed neutrinos of the *Majorana* type with an additional Majorana mass term, which necessarily have a fixed hypercharge at $Y(\nu_R) = 0$.

The only way to distinguish Dirac from Majorana nature in experiments is to measure the mass effects [17]; the most promising experiment for detecting the Majorana nature of neutrinos is the neutrinoless double beta decay ($0\nu\beta\beta$), more about it in the outlook Chapter 12.

2.3. Neutrino Mass, Mixing Matrix, and Seesaw Mechanism

For the mentioned reasons, many neutrino models use the combination of the two mass terms Dirac and Majorana, which implies that the neutrinos are generally of Majorana type. If these models contain right-handed neutrinos, which are very heavy compared to left-handed neutrinos, they are called Type I Seesaw models. Seesaw models are a typical approach to explain the smallness of left-handed neutrinos, as explained in more detail in the last section of this chapter.

As our model contains the Type I Seesaw model, this chapter is intended to give a brief overview of this topic with the necessary formulas. In the first section, we will combine the Majorana and Dirac mass terms of neutrinos into a total mass matrix. In the following section, we will further explain the flavour and mass basis and then transform the total mass matrix from one basis to the other using the neutrino mixing matrix U, which contains the aforementioned flavour mixing matrix U_{PMNS} for the left-handed neutrinos. In the last section, we briefly focus on the three different cases of Majorana and Dirac mass ratios within the total mass matrix, with special emphasis on the case of the Seesaw mechanism.

2.3.1. Total neutrino mass matrix

The total neutrino mass matrix combines the neutrino masses of the two mass-generating Lagrange terms: the Majorana mass terms according to Equation (2.10),

$$\mathcal{L}_M = \frac{1}{2}\nu_R^T C^{-1} M_R^* \nu_R + h.c., \tag{2.12}$$

whereby, for reasons mentioned above, only the right-handed neutrinos, ν_R, with their Majorana mass, M_R, are taken into account; and the Dirac mass terms $\mathcal{L}_D$, according to

Equation (2.7). The Dirac mass terms are generated by the Higgs mechanism like those of all other Standard Model particles. In electroweak symmetry-breaking (EWSB), the Higgs receives a non-zero VEV, $\langle\phi\rangle_0 = \frac{v}{\sqrt{2}}(0,1)^T$ (in unitary gauge), which is inserted into the Lagrangian of the Yukawa interaction, $\mathcal{L}_Y$. Accordingly, the Dirac mass is $M_D = v\,\Delta/\sqrt{2}$, where Δ and Γ are Yukawa coupling matrices. The formulas[8] for the two Lagrangians $\mathcal{L}_Y$ and $\mathcal{L}_D$ are then

$$\mathcal{L}_Y = -\left(\phi^\dagger \bar{\ell}_R\,\Gamma + \tilde{\phi}^\dagger \bar{\nu}_R \Delta\right) D_L + h.c., \tag{2.13}$$

$$\Rightarrow \qquad \mathcal{L}_Y \supset \mathcal{L}_D = -\frac{1}{\sqrt{2}}(\bar{\nu}_L v \Delta\,\nu_R + h.c.) = -\bar{\nu}_L M_D^\dagger \nu_R - \bar{\nu}_R M_D \nu_L, \tag{2.14}$$

with the Higgs doublet ϕ, the left-handed $SU(2)_L$ doublet $D_L = (\nu_L, \ell_L)^T$, and right-handed leptons ℓ_R and $\tilde{\phi} = i\tau_2\phi^*$, with the Pauli matrix $i\tau_2 = \begin{pmatrix} & 1 \\ -1 & \end{pmatrix}$. Finally, the mass terms in Equations (2.12) and (2.14) can be combined to a total mass matrix called M_{D+M}, which has $(n_L + n_R) \times (n_L + n_R) = 6 \times 6$ dimensions, with the three left-handed neutrinos $n_L = 3$ and the number of right-handed neutrinos n_R, which in our model also corresponds to three. M_{D+M} can be written in the form[9]

$$\mathcal{L}_{M+D} = \frac{1}{2}\left(\nu_L^T, (\nu_R)^{c\,T}\right) C^{-1} \underbrace{\begin{pmatrix} 0 & M_D^T \\ M_D & M_R \end{pmatrix}}_{M_{D+M}} \begin{pmatrix} \nu_L \\ (\nu_R)^c \end{pmatrix} + h.c. \tag{2.15}$$

One can see that the mass matrix M_{M+D} is off-diagonal, which indicates that it is not written in the mass basis of the neutrinos, where it would be diagonal, but in the flavour basis as we will see below. So the chiral states mix: Left-handed neutrinos, ν_L, which carry weak-isospin mix with right-handed neutrinos, $(\nu_R)^c$, which are $SU(2)_L$ singlets [17, 25].

2.3.2. Flavour and mass basis of neutrinos

Before we continue with the analysis of the mixing of the neutrinos by diagonalising the entire neutrino mass matrix and thus perform a basis transformation from flavour basis to mass basis, it is crucial to know these two fundamental bases. Let us first consider the flavour basis associated with the flavours of the charged leptons, ℓ, being e, μ and τ, where $\ell = (e, \mu, \tau)^T$. The flavour basis is accordingly defined as the basis where the

---

[8] For simplicity, $\mathcal{L}_Y$ is written here with only one Higgs doublet. In the next chapter, another Higgs doublet will be introduced, but since we will introduce simplifying assumptions later, the formula in Equation (2.14) is still valid for the calculations in the second part of this thesis.

[9] To arrive at the form of Equation (2.15), the following identity is used for the Dirac masses [24]

$$-\bar{\nu}_R M_D \nu_L \overset{(A.9)}{=} (\nu_R)^{cT} C^{-1} M_D\,\nu_L = -\nu_L^T M_D^T \left(C^{-1}\right)^T (\nu_R)^c = \frac{1}{2}(\nu_R)^{c\,T} C^{-1} M_D\,\nu_L - \frac{1}{2}\nu_L^T M_D^T \left(C^{-1}\right)^T (\nu_R)^c\,.$$

masses of the charged leptons, m_e, m_μ, m_τ, are diagonal, $M_\ell = \mathrm{diag}\big(m_e, m_\mu, m_\tau\big)$, and therefore this basis also corresponds to the mass basis of the charged leptons. In the SM, each left-handed charged lepton flavour field, ℓ_L, couples to a left-handed neutrino field by the weak interaction term

$$\mathcal{L}_{cc} = -\frac{g}{\sqrt{2}}\bar{\ell}_L\gamma^\mu\, \nu_L W_\mu^- + h.c. \qquad (\mathit{flavour\ basis}), \tag{2.16}$$

which is also written in the flavour basis, where $W^\pm$ are the W-bosons and g the weak coupling constant. Since this is the basis in which neutrinos are detected via the charged lepton of the same flavour, neutrino fields via ν_e, ν_μ, ν_τ are assigned to the corresponding lepton flavour with $\nu_L = (\nu_e, \nu_\mu, \nu_\tau)_L^T$, and thus these fields are called neutrino flavour fields.

The flavour basis plays therefore a central role in neutrino physics. Neutrino oscillation experiments additionally show that the flavours of the neutrinos can change and therefore the flavour basis must be different from the neutrino mass basis. The transformation for the left-handed neutrino fields from flavour to their mass basis can be defined by the mixing matrix U_ν to $\nu_L = U_\nu \chi_L'$, where χ_L' are the neutrino fields in their mass basis. Furthermore, U_ν, with

$$U_\nu = e^{i\hat{\alpha}}\, U_{\mathrm{PMNS}}\, e^{i\hat{\beta}}, \tag{2.17}$$

is identical to the well-known lepton mixing matrix U_{PMNS} except for a diagonal matrix of unphysical phases $e^{i\hat{\alpha}}$ on the left side and except for the Majorana phase factors of the diagonal matrix $e^{i\hat{\beta}}$ on the right side. In the Standard Model, the latter are obviously zero. Accordingly, $\mathcal{L}_{cc}$ written in the mass basis is

$$\mathcal{L}_{cc} = -\frac{g}{\sqrt{2}}\bar{\ell}_L\gamma^\mu \underbrace{U_\nu}_{\sim U_{PMNS}} \chi_L' W_\mu^- + h.c. \qquad (\mathit{mass\ basis}). \tag{2.18}$$

If we pursue our goal and extend the SM by three right-handed Majorana neutrinos, ν_R, one for each flavour, as done in Equation (2.15), we can see mixing not only between the flavours of the left-handed electron, muon, and tau neutrinos, but also between the left-handed neutrinos, ν_L, and the right-handed neutrinos, $(\nu_R)^c$, because of the non-diagonal matrix elements of M_{D+M}. The extension with three additional right-handed neutrinos clearly requires an extension of the three-component neutrino mass field χ_L' in Equation (2.18) to a neutrino field, χ, with six components. Consequently, the left- and right-handed neutrino flavour fields are transformed into χ via larger 3×6-dimensional matrices U_L and U_R, which contain U_ν,

$$\nu_L = U_L\,\gamma_L\,\chi = U_L\,\chi_L \quad \text{and} \quad \nu_R = U_R\,\gamma_R\,\chi = U_R\,\chi_R, \tag{2.19}$$

$$U_L \simeq (U_\nu, *)\,, \qquad U_R \simeq (*U_\nu, *)\,, \tag{2.20}$$

with $*$ as placeholders (to be derived). Furthermore, ν_L and ν_R, as well as U_L and U_R, can be combined into a vector as already done in Equation (2.15),

$$\nu = \begin{pmatrix} \nu_L \\ (\nu_R)^c \end{pmatrix}, \quad \text{so that} \quad \begin{pmatrix} \nu_L \\ (\nu_R)^c \end{pmatrix} = \begin{pmatrix} U_L \\ U_R^* \end{pmatrix}\chi = U\,\chi, \tag{2.21}$$

where, as mentioned above, the exact definition of the unitary matrix U combining U_L and U_R must be derived by diagonalising M_{D+M}, which is done in the next section using the formula for U given in Equation (2.26).

2.3.3. Neutrino mass and mixing matrix

We are now ready to study the neutrino mixing of the flavour and chiral states, defining the mixing matrix U with U_L and U_R by diagonalizing the mass matrix M_{D+M} in Equation (2.15). For the diagonalization process of matrices, a useful tool is *Schur's theorem (1945)*, also known as *Takagi's factorization* [27], which states:

$$\text{If } M \text{ is a symmetric and complex } n \times n \text{ matrix, } \exists \text{ a unitary } n \times n \text{ matrix } U \text{ such that } U^T M U = \hat{M}, \text{ where } \hat{M} \text{ is diagonal with non-negative elements.} \tag{2.22}$$

In fact, the Majorana mass, M_R, in M_{D+M} is symmetrical due to the Majorana condition, while the Dirac mass, M_D, is generally not restricted [17]. The diagonalization of M_{D+M} into the mass basis can be regarded as a two-step process, in which the unitary diagonalization matrix U is divided into two factors $U = D\,\mathrm{diag}(U_\nu, U_N)$. First, we block-diagonalize M_{D+M} with an ansatz of the arbitrary unitary matrix D and obtain the division between the small-, M_ν, and the large-scale mass matrix, M_N, as shown in [28],

$$D^T M_{D+M} D = \begin{pmatrix} M_\nu & 0 \\ 0 & M_N \end{pmatrix}, \tag{2.23a}$$

$$\text{with} \qquad M_\nu \simeq -M_D^T M_R^{-1} M_D, \qquad M_N \simeq M_R, \tag{2.23b}$$

$$\text{and} \qquad D = \begin{pmatrix} \sqrt{1 - BB^\dagger} & B \\ -B^\dagger & \sqrt{1 - B^\dagger B} \end{pmatrix} \simeq \begin{pmatrix} \mathbb{1} & (M_R^{-1} M_D)^\dagger \\ -M_R^{-1} M_D & \mathbb{1} \end{pmatrix}. \tag{2.23c}$$

The variable B in the diagonalization matrix D in Equation (2.23c) is approximated in lowest order in m_D/m_R, so that the relationship $B^\dagger = M_R^{-1} M_D + \mathcal{O}(\frac{m_D}{m_R})$ applies, where m_D and m_R are the scales[10] of the same-named matrices M_D and M_R, respectively. In the second step, the submatrices M_ν and M_N are diagonalized,

$$U_\nu^T M_\nu U_\nu = \mathrm{diag}(m_1, m_2, m_3) = \hat{m}_\nu, \qquad U_N^T M_N U_N = \mathrm{diag}(m_4, m_5, m_6) = \hat{m}_R, \tag{2.24}$$

where $m_{1,2,3}$ and $m_{4,5,6}$ are the light and heavy mass eigenstates, respectively. All together Equations (2.23) and (2.24) can be written in a combined form, with the definition of the

[10] The exact definition of the scales is presented in Section 2.4.

full mixing matrix U

$$
\begin{aligned}
U^T M_{D+M} U = (U_L^T, U_R^\dagger) \begin{pmatrix} 0 & M_D^T \\ M_D & M_R \end{pmatrix} \begin{pmatrix} U_L \\ U_R^* \end{pmatrix} &= \begin{pmatrix} U_\nu^T & \\ & U_N^T \end{pmatrix} \begin{pmatrix} M_\nu & \\ & M_R \end{pmatrix} \begin{pmatrix} U_\nu & \\ & U_N \end{pmatrix} \\
&= \begin{pmatrix} \mathrm{diag}(m_1, m_2, m_3) & \\ & \mathrm{diag}(m_4, m_5, m_6) \end{pmatrix} = \begin{pmatrix} \hat{m}_\nu & \\ & \hat{m}_R \end{pmatrix} = \hat{m}, \qquad (2.25) \\
\text{with} \quad U = \begin{pmatrix} U_L \\ U_R^* \end{pmatrix} = D \begin{pmatrix} U_\nu & \\ & U_N \end{pmatrix} &\simeq \begin{pmatrix} U_\nu & (M_R^{-1} M_D)^\dagger U_N \\ -M_R^{-1} M_D U_\nu & U_N \end{pmatrix}. \qquad (2.26)
\end{aligned}
$$

The following useful identities result from the unitarity relation for U and Equations (2.25) and (2.26):

$$
\begin{aligned}
& U^\dagger U = U U^\dagger = U_L^\dagger U_L + U_R^T U_R^* = \mathbb{1}_{6\times 6}, && (2.27\text{a}) \\
\Rightarrow \quad & U_L U_L^\dagger = U_R U_R^\dagger = \mathbb{1}_{3\times 3}, \quad U_L U_R^T = 0_{3\times 3}, && (2.27\text{b}) \\
& M_D = U_R \hat{m} U_L^\dagger, \quad M_R = U_R \hat{m} U_R^T, \quad M_L = U_L^* \hat{m} U_L^\dagger = 0_{3\times 3}. && (2.27\text{c})
\end{aligned}
$$

2.3.4. Different mass mixing scenarios and Seesaw mechanism

Characteristic of the diagonalized matrix $\hat{m}$ in Equation (2.25) are the scales of the light and heavy mass eigenstates, which are after (2.23b) and (2.24)

$$
m_{1,2,3} \sim m_\nu \simeq m_D^2 / m_R \quad \text{and} \quad m_{4,5,6} \sim m_R, \qquad (2.28)
$$

where m_ν is the scale of M_ν (the matrix of light-neutrinos after the first diagonalization step in Equation (2.23a)), for the definition of the scales, see also Section 2.4. The scales in Equation (2.28) imply that if the right-handed neutrinos are heavy and m_R is large, the left-handed neutrinos become light and m_ν becomes small, and vice versa. This gave the Seesaw mechanisms their name when one mass scale goes up, in this case m_R, the other goes down, here m_ν, and vice versa.

The *Type I Seesaw mechanism*, from which formulas were derived in the previous section, has a size ratio between the Majorana and Dirac masses within M_{D+M} of $m_D \ll m_R$. Other mixing scenarios are the pseudo-Dirac case, which occurs when the scale of the Dirac mass, m_D, is much larger than that of the Majorana mass, m_R, which means $m_D \gg m_R$. This case is excluded when $m_R > 10^{-9}$ eV and is therefore in fact excluded since otherwise, the conversion of ν_L to ν_R should have been observable in solar neutrinos, which is contrary to the measurements as stated in [7]. In the case of $m_D \sim m_R$, it leads to possible high mixing effects between ν_L and ν_R [7]. In comparison, the Seesaw limit $m_D \ll m_R$ is the most promising, with the advantage that it is solving the hierarchy problem, which will be presented below.

The *hierarchy problem* in neutrino physics describes the fact that, for no known reason, the left-handed neutrino masses m_i with $i \in \{1, 2, 3\}$ have an experimental upper bound[11]

[11] In fact, the most string-bound on the neutrino mass is $m_{1,2,3} < 1.1$ eV and comes from the KATRIN experiment [19]. The upper bound of $\sum_j m_j < 0.17$ eV and therefore $m_i \lesssim 0.1$ eV was achieved using CMB data, which depends on the model and the input data [9].

of $m_\nu \lesssim 0.1\,\text{eV}$ [9], so a much smaller mass scale than of any other Standard Model particle, where latter range from $m_e \simeq 0.51\,\text{MeV}$ to $m_t \simeq 173\,\text{GeV}$ [9], see Figure 2.2. With the seesaw mechanism one tries to explain the small neutrino masses $m_{1,2,3}$ (mass basis) by declaring not the mass but the flavour basis with the Dirac masses in M_D as the natural scale. Since, within a Seesaw mechanism, Dirac masses may very well be in the range of the other Standard Model particles, e.g. $m_D \sim m_\mu$, the muon mass, while $m_{1,2,3} \sim m_D/m_R$ remain small when the mass of the right-handed neutrino is large, as explained at the end of the previous chapter. The typical Seesaw scale represented by the size of the heavy right-handed neutrino mass, m_R, then appears to be only a few orders of magnitude lower than the GUT scale, which is $\lambda_{GUT} \sim 10^{16}\,\text{GeV}$, with

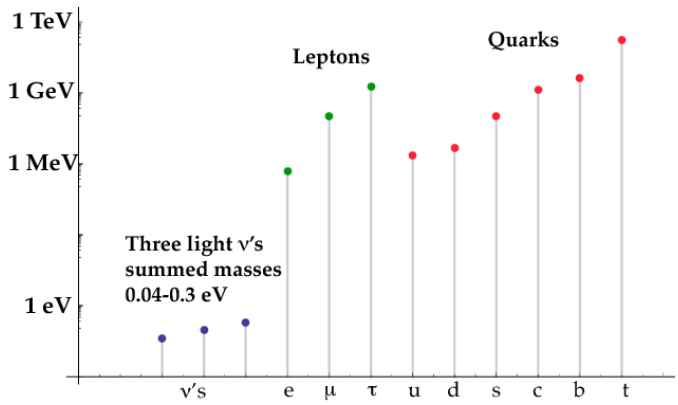

Figure 2.2.: Masses from SM particles [29].

$$m_D \sim 1\,\text{GeV}, \quad m_\nu \lesssim 0.1\,\text{eV}, \quad m_\nu = m_D^2/m_R \;\Rightarrow\; m_R \sim 10^{10}\,\text{GeV}. \tag{2.29}$$

In our model, we will work with the Type I Seesaw mechanism.

2.4. New Scales of Physics

For a better classification of our model and later estimates in the calculations, let us summarise the new energy scales that we have introduced and will introduce into our model:

- The smallest scale is one of the left-handed neutrino masses, which is denoted m_ν and in the order $m_\nu \lesssim 1\,\text{eV}$.
- We call the typical scale of the SM leptons the Dirac scale, m_D, which can be in the order of the electron, m_e, muon, m_μ, or tau mass, m_τ, therefore $m_D \sim 1\,\text{MeV} - 1\,\text{GeV}$. In this model we will work with neutrino Dirac masses in the range $m_D \sim 1\,\text{GeV}$, with correspondingly large Yukawa couplings.
- The Fermi-scale, also called the electroweak scale m_{EW}, is the scale around the SM Higgs VEV ($v \simeq 246\,\text{TeV}$), which is related to the $W^\pm$ and Z boson masses, i.e. $m_{EW} \sim 10\,\text{GeV} - 1\,\text{TeV}$. In the literature, the electroweak scale is also often associated with the scale of the Z or W boson mass, then $m_{EW} \sim m_Z \sim m_W \sim 90\,\text{GeV}$. The scalars of the new Higgs doublet introduced in the next Chapter 3 are all assumed to be of the order m_{EW}.

- The seesaw scale mentioned above is the scale of the right-handed neutrino masses, which are denoted with m_R, *viz.* the scale of the square roots of the eigenvalues of $M_R M_R^*$. m_R is in a high-scale seesaw mechanism[12] like ours typically around $m_R \sim 10^{10}$ GeV and our studies include additionally $m_R \sim 10^{12}$ GeV, which is close to the GUT scale with $\lambda_{GUT} \sim 10^{16}$ GeV.[13]

All in all, the hierarchy of scales is $m_\nu \ll m_D < m_{EW} \ll m_R$. There are a few parameters that are useful to estimate on dimensional grounds. With Equations (2.23b) and (2.26), one has

$$m_i \sim \frac{m_D^2}{m_R} \quad \text{for light neutrinos, } viz. \text{ for } i = 1,2,3, \tag{2.30}$$

$$m_i \sim m_R \quad \text{for heavy neutrinos, } viz. \text{ for } i = 4,5,6, \tag{2.31}$$

$$(U_L)_{\ell i} \sim 1 \text{ and } (U_R)_{\ell i} \sim \frac{m_D}{m_R} \quad \text{for } i = 1,2,3, \tag{2.32}$$

$$(U_R)_{\ell i} \sim 1 \text{ and } (U_L)_{\ell i} \sim \frac{m_D}{m_R} \quad \text{for } i = 4,5,6. \tag{2.33}$$

2.5. Alternatives to the Type I Seesaw Model

In addition to the presented Type I Seesaw model, which represents a minimal extension of the SM, there are other generation mechanisms beyond the SM to create neutrino mass terms. A reasonable starting point for thinking about such SM extensions is to adopt the group theory point of view, to look at the symmetries and their quantum numbers, which belong to the particle fields involved and which must be preserved. Specifically, additional terms in the SM, such as potential mass terms, must preserve the quantum numbers of $U(1)_Y \times SU(2)_L$ and $U(1)_{EM}$. Within a neutrino mass term, the possible

	$D_L = \begin{pmatrix} \nu_L \\ \ell_L^- \end{pmatrix}$	$\phi = \begin{pmatrix} \varphi^+ \\ \varphi^0 \end{pmatrix}$	$\tilde{\phi} = \begin{pmatrix} \varphi^{0*} \\ -\varphi^- \end{pmatrix}$	ℓ_R^-	ν_R
Y	-1	1	-1	-2	0

Table 2.1.: Hypercharge Y and electric charge of several $SU(2)_L$ doublets and singlets.

combinations of particle fields with their corresponding quantum numbers could be,

[12] Note that also other seesaw models with right-handed neutrino masses in the TeV scale where examined, see [30, 31] and references quoted therein.

[13] GUT theories including right-handed neutrinos can have naturally large seesaw scales $m_R \sim 10^{10}$ GeV [30].

see Table 2.1, [32, 33, 34]:

bilinears	relat. I_3-isospin	hypercharge	combinable multiplets with hypercharge			
$\overline{D}_L \otimes \nu_R:$	$\frac{1}{2} \otimes 0 = \frac{1}{2},$	$Y = -1,$	ϕ	doublet,	with $Y = 1,$	(2.34)
$D_L \otimes D_L:$	$\frac{1}{2} \otimes \frac{1}{2} = 0 \oplus 1,$	$Y = -2,$	$\begin{cases} \eta^+ \\ \Delta \end{cases}$	singlet, triplet,	with $Y = 2$ with $Y = 2$,	(2.35)
$\ell_R \otimes \ell_R:$	$0 \otimes 0 = 0,$	$Y = -4,$	k^{++}	singlet,	with $Y = 4,$	(2.36)

which are explained in the following. In the table with the formulas (2.34)-(2.36), every possible combination of leptonic bilinears is shown in the first column and their related I_3 isospin and hypercharge in the second and third columns. These bilinears can couple to the scalar multiplets in the last column that carry the opposite isospin and hypercharge of them. In this way, the allowable Lagrange mass terms for neutrinos can be found, where quantum numbers totalled to zero and are therefore invariant among SM symmetries. The first case (2.34) is the known Yukawa coupling from which the Dirac mass term originates. It is a combination of the SM lepton doublet $D_L = (\nu_\ell, \ell)^T$ with a right-handed singlet ν_R (the right-handed neutrino) together with the Higgs doublet ϕ, in which the Dirac mass M_D is generated at EWSB from the Yukawa couplings together with the vacuum expectation value of the Higgs, as shown earlier in Equation (2.14). The Type I Seesaw, as we have seen in the previous chapters, includes this case together with an ad hoc implementation of a right-handed Majorana neutrino mass M_R, as shown in Figure 2.3, and is therefore the simplest extension of the Standard Model. The second case (2.35) with the scalar triplet Δ is an extension which leads to the Type II Seesaw mechanism, with Δ being a Higgs triplet for the mass vertex as depicted in the diagram in 2.4. Closely connected to the previous case is the Type III Seesaw mechanism, which works with a fermion triplet instead of a scalar triplet and is therefore not part of the table; for more information, see [35]. The other type of neutrino mass terms originate from so-called radiative models, in which neutrino masses are formed from loop corrections of additional particles [36]. These models have the advantage that the neutrino masses are automatically small. To this group belongs the Zee model, which includes the case of (2.35), with a singlet η^+ and additional Higgs doublets, and to this group belongs also the Zee-Babu model, comprising both singlet cases (2.35) with η^+ and (2.36) with k^{++}. At last, the famous Scotogenic model proposed by Ma [37] shall be mentioned, which contains sterile right-handed

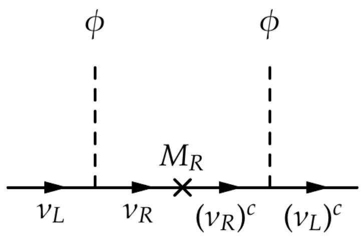

Figure 2.3.: Seesaw type I.

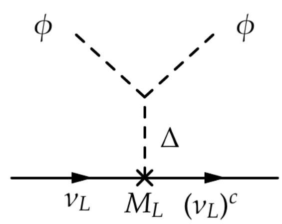

Figure 2.4.: Seesaw type II.

neutrinos, a new Higgs doublet, and a $\mathbb{Z}_2$-symmetry, see [38, 32, 36] for further details[14]. Moreover, a left-handed Majorana mass, M_L, may additionally appear from one-loop contributions to the Type I Seesaw mechanism in the two-Higgs-doublet model of this thesis, as shown in Chapter 9.

Our reasons for working with the Type I Seesaw mechanism are mainly because it can explain the hierarchy problem, it contains favourable right-handed neutrinos as a minimal SM extension, unlike the Type II and Type III Seesaw model or the Zee- and Zee-Babu models, and it is the most simple and economical framework, i.e. its phenomenology is relatively simple as investigated in Part II of this thesis. Note that the concrete implementation of the Type I Seesaw model, which includes right-handed Majorana neutrinos, effectively requires the introduction of three new fields to the Standard Model: A right-chiral neutrino weak-isospin singlet, ν_R, the charge conjugated version $(\nu_R)^c$, which is left-chiral but also an isospin singlet, and the charge-conjugated left-chiral field $(\nu_L)^c$, which is right-chiral but charged under weak-isospin.

2.6. Gauge Boson Interactions with Leptons

In order to have all the neutrino Lagrange terms of our model compiled in this overall Chapter 2, the missing Lagrangians of the interactions between gauge bosons and leptons are to be listed here. From (2.18), we can derive the charged current interaction with the mixing matrix, U_L, and the left-handed neutrino fields, χ_L, in the mass basis,

$$\mathcal{L}_{cc} = \mathcal{L}_W = -\frac{g}{\sqrt{2}}\bar{\ell}_L\gamma^\mu\, U_L\, \chi_L W^-_\mu + h.c. \tag{2.37}$$

The neutral current electroweak interactions with the Z-boson, Z_μ, and photon fields, A_μ, are [6, 3]

$$\begin{aligned}\mathcal{L}_{nc} =& \mathcal{L}_Z + \mathcal{L}_A \\ =& -\frac{g}{4\,c_W} Z_\mu\, \bar{\chi}\gamma_\mu \left(\gamma_L U_L^\dagger U_L - \gamma_R U_L^T U_L^*\right)\chi \qquad \text{(2.38a)} \\ &+ \frac{g}{2\,c_W} Z_\mu\, \bar{\ell}_L\gamma^\mu\ell_L + \left(\frac{g\, s_W^2}{c_W} Z_\mu + eA_\mu\right)\left(\bar{\ell}_L\gamma^\mu\ell_L + \bar{\ell}_R\gamma^\mu\ell_R\right), \qquad \text{(2.38b)}\end{aligned}$$

with the weak angles $s_W = \sin\theta_W$ and $c_W = \cos\theta_W$, where the relation between the coupling constants and the angles is $g\, s_W = g' c_W = e$.

2.7. Simplifying Assumptions

Furthermore, we will need to make simplifying assumptions about the neutrino mixing matrices for left- and right-handed neutrinos, respectively, as well as for light neutrino

[14] Further classification schemes for Majorana masses including two-loop approaches can be found in e.g. [39].

masses, in order to be able to perform the calculations of this model in the second part of this thesis. All assumptions are marked in italics in the following.

Using the standard parametrization for U_{PMNS} *in Ref. [9], we fix the mixing angles to their best-fit values of Ref. [18], viz.* $s_{12}^2 = 0.304$, $s_{23}^2 = 0.452$, *and* $s_{13}^2 = 0.0218$.

U_{PMNS} is part of the mixing matrix for left-handed neutrinos $U_\nu = e^{i\hat{\alpha}} U_{PMNS} e^{i\hat{\beta}}$, see Equation (2.17), together with the Majorana phases $\hat{\alpha}$ and $\hat{\beta}$. These Majorana phases are further rephased and rewritten [17] into the angles ρ and σ and into a more useful convention such as $U_\nu = U_{PMNS} \times \mathrm{diag}(1, e^{i\rho}, e^{i\sigma})$. Overall, the parametrisation of U_ν then reads

$$U_\nu = \begin{pmatrix} c_{12}\, c_{13} & s_{12}\, c_{13} & \epsilon^* \\ -s_{12}\, c_{23} - c_{12}\, s_{23}\, \epsilon & c_{12}\, c_{23} - s_{12}\, s_{23}\, \epsilon & s_{23}\, c_{23} \\ s_{12}\, s_{23} - c_{12}\, c_{23}\, \epsilon & -c_{12}\, s_{23} - s_{12}\, c_{23}\, \epsilon & c_{23}\, c_{13} \end{pmatrix} \begin{pmatrix} 1 & & \\ & e^{i\rho} & \\ & & e^{i\sigma} \end{pmatrix}, \tag{2.39}$$

with $s = \sin\theta$, $c = \cos\theta$, and $\epsilon = \sin\theta_{13} \exp(i\delta_{CP})$, with the angles $\theta_{12}, \theta_{13}, \theta_{23}$, the CP angle δ_{CP}, and the Majorana phases σ, ρ. The notation in Equation (2.39) is equivalent for the matrix U_N of the right-handed neutrinos with the only difference being that each parameter is written with an additional subscript R so that the angles are $\theta_{R12}, \theta_{R13}, \theta_{R23}$, and δ_{CP_R}, and the Majorana phases are σ_R and ρ_R.

We continue to make the simplifying assumption that all the parameters in the model are real, so we put in Equation (2.26) $e^{i\hat{\alpha}} = e^{i\hat{\beta}} = \mathbb{1}$, *and we also assume that* U_{PMNS} *is real. Therefore, the Majorana phases are restricted to* $\hat{\alpha}, \hat{\beta} \in \{0, \pi\}$, *vis.* ρ, $\sigma \in \{0, \pi\}$, *as are the CP-angles within* U_ν *and* U_N *to* $\delta_{CP} \in \{0, \pi\}$. *Finally, for definiteness, we set* $\rho, \sigma = 0$ *and* $\delta_{CP} = \delta_{CP_R}$.

This means that we analyse a parameter space in which leptogenesis is only possible if CP violations is generated from another source, e.g. from the Higgs potential of an extended Higgs sector. In general, however, this model holds the potential for a CP phase $\delta_{CP} \neq \{0, \pi\}$ that makes leptogenesis easy.

Additionally, we have to choose the type of light-neutrino mass spectrum, either normal or inverted – for definiteness, we settle on a normal mass spectrum with the definition of formula (2.5).

Let the lightest neutrino mass m_1, *which is unknown to date, be a free parameter; a reasonable choice for* m_1 *regarding the upper limit on the neutrino mass*[15] *of* $m_1 \lesssim 0.1\, eV$ is e.g.

$$m_1 = \sqrt{\Delta m^2_{atm}} \simeq 0.05\,\mathrm{eV}, \tag{2.40}$$

and with the best-fit values $\Delta m^2_{21} = 7.50 \times 10^{-5}\,\mathrm{eV}^2$ and $\Delta m^2_{31} = 2.457 \times 10^{-3}\,\mathrm{eV}^2$ from Ref. [18], we obtain for the other two light-neutrino masses

$$m_2 \simeq 0.05\,\mathrm{eV} \quad \text{and} \quad m_3 \simeq 0.07\,\mathrm{eV}. \tag{2.41}$$

[15]The upper limit was derived from the CMB bound to the sum of light neutrino masses $\sum_j^{1,2,3} m_j < 0.17\,\mathrm{eV}$ [9], by $m_\nu \simeq \sum_j^{1,2,3} m_j - \sqrt{\Delta m^2_{21}} - \sqrt{\Delta m^2_{31}} \lesssim 0.1\,\mathrm{eV}$.

3. Two-Higgs-Doublet Models

Finding a Higgs-like scalar was a major breakthrough in particle physics in July 2012. It was first detected by the ATLAS [40] and CMS [41] collaborations at the Large Hadron Collider (LHC) at CERN. Since then, with the new update in 2015, the experimental precision at the LHC has risen to a point where the evidence that this scalar is the theoretically predicted Higgs boson is strongly supported. The measured particle is a spin-zero particle with the expected fermion interactions.

Thinking one step ahead, a further extension of the scalar sector to two or more Higgs doublets seems like a plausible option, considering that the SM also includes three non-minimal fermion generations and a non-minimal gauge sector. In principle, it would be possible to include other Higgs multiplets in addition to doublets, but these cases are subject to the strong experimental constraint of the Higgs sector resulting from the global custodial symmetry $SU(2)$. This symmetry connects the two components in a $SU(2)_L$ doublet and is therefore also often referred to as custodial isospin.[1] The effects of custodial symmetry are also reflected in the preservation of the relation between the weak gauge boson masses by the parameter $\rho = m_W/(m_Z \cos\theta_W) = 1$, with the Weinberg angle θ_W (or equivalently, the oblique parameter $T = (\rho - 1)/\alpha = 0$, where α is the fine-structure constant). The parameter ρ exhibits an experimental accuracy below 0.1% [9]. This restricts the enlargement of the Higgs sector to either $SU(2)_L$ singlets, where VEVs do not contribute to gauge boson masses, or doublets exactly resulting in $m_W = m_Z \cos\theta_W$, so that the new singlets or doublets have weak-isospin, I_3, and hypercharge, Y, $I_3 = Y = 0$, or $I_3 = Y = 1/2$, respectively; for more details, see [42, 6]. Thereby Higgs doublets have the added advantage that they can couple with fermions [6].

Nowadays, one can find many models on the market mostly with doublet extensions, especially implementing two and also multi-Higgs doublets, while their reasons for introducing new scalars are manifold. Most of these reasons, apart from the reason of getting a rich phenomenology, can be categorised into three areas, as indicated in [6, 43, 44]:[2]

- First of all, supersymmetry (SUSY) is a well-established motivation, including a second Higgs doublet. Although experimental limits have set hard constraints, SUSY models appeal through their simple elegance, the prediction of the unification of the three forces, the provision of a dark matter candidate, their approaches of supergravity, and other reasons [9]. Two Higgs doublets in SUSY are required

[1]Custodial symmetry is a remnant from an $SU(2) \times SU(2)$ symmetry, see Chapter A.3 for more details.

[2]Additionally, in Ref. [45, 46, 47] the authors used a Higgs doublet extension to explain among others the mass and flavour mixing patterns in the quark and lepton sector.

for the mass-giving process for various chiral multiplets as well as for the cancellation of anomalies [6].

- Second, the inert doublet model predicts an extension with a second Higgs doublet, obeying a $\mathbb{Z}_2$ symmetry that prevents interactions with Standard Model particles. Therefore, this Higgs doublet is a perfect candidate for dark matter [48, 42]. The inert model is further specified in the following text.

- Finally, there are various two-Higgs-doublet model (2HDM) concepts based on CP symmetry. One of them is that multi-Higgs doublets can include an extra source of CP violation, e.g. in their mixing matrix, and thus explain baryogenesis. In principle, the standard model contains CP violation within the CKM matrix, but this amount is too small to explain the matter-antimatter asymmetry that supports this approach.

However, the extension of the SM by two or more Higgs doublets exposes another restriction, which is a major problem stemming from large flavour-changing neutral interactions (FCNIs), such as $\mu \to eee$, $Z \to \mu e$ and the like, which are severely constrained by experiments. FCNIs result from couplings of the new Higgs doublets to fermions, the Yukawa couplings, which are generally not flavour-diagonal and therefore cause FCNIs. As a direct consequence, these models have often suppressed Yukawa couplings, which some of them try to explain via small vacuum expectation values (VEV) from various Higgs doublets. Many other models are equipped with symmetries to bypass tree-level FCNIs. In addressing this problem, Glashow, Weinberg [49], and Paschos found a rule that guarantees the disappearance of tree-level FCNIs when fermions of similar electrical charge receive their mass only from one Higgs doublet and are not connected to further doublets [50]. This led to a categorization of the two-Higgs-doublet models into five types, all of which (except the last one) contain a $\mathbb{Z}_2$ symmetry and couple to the fermions in a different way [50]:

Type I: The inert model, all fermions couple to only one Higgs doublet ϕ_2.

Type II: A model often found in SUSY theories, up-type quarks couple to ϕ_2, while down-type quarks and leptons couple to a separate Higgs doublet ϕ_1.

Type X: In the lepton-specific model, ϕ_2 couples to all quarks, and ϕ_1 to all leptons.

Type Y: The flipped model couples ϕ_2 to up-type quarks and leptons, while down-type quarks couple to ϕ_1.

Type III: Here, every fermion couples to every doublet, and FCNIs appear but are generally assumed to be suppressed.

The model of this thesis contains a 2HDM that is close to Type III, though without defining the relationship to the quark sector.[3] In this 2HDM, tree-level FCNI are prevented

[3] We avoid the quark sector because it would increase our parameter space and require the inclusion of more precision tests that were considered outside the scope of this thesis.

by an additional lepton-flavour symmetry that is softly broken and thus this model does not suffer from small Yukawa couplings. In general, our model has the potential to include CP-violation naturally through the Majorana neutrinos, yet the Higgs potential can provide another source of CP violation to obtain all the necessities for successful leptogenesis (as described in the third bullet point). The primary purpose for an enlargement of the Higgs sector, however, is to achieve interesting, perhaps observable effects such as flavour-change processes and contributions to the magnetic dipole moment of the muon.

In general, two-Higgs-doublet models are limited not only by the custodial symmetry parameter ρ or FCNI but also by the precision measurement of the magnetic dipole moment of the electron and muon and by B-physics, where latter restrict the couplings to the quark sector; and there are further theoretical constraints of the Higgs scalar potential by vacuum stability and unitary constraints [51, 52]. As mentioned earlier in this thesis, the quark sector will not be further specified as it applies to the Higgs potential, with the exception of the definition of the Higgs scalar masses for the same reason given in Footnote 3 on Page 32. Therefore, further investigation of this mode will focus on limit values set by FCNI and magnetic dipole moments of leptons performed in Part II of this thesis.

In this chapter, we provide the motivation and the necessary framework for the implementation of a 2HDM. In the first Section 3.1, we give formulas for the general implementation of multi-Higgs doublets in the Standard Model that focus on describing the Higgs fields and masses. The second Section 3.2 deals with a more concrete realisation of two-Higgs doublets in the Standard Model, defining the scalar fields, masses, and mixing matrices. Furthermore, we will specify the Yukawa interactions with the lepton sector as well as the scalar-gauge interactions. Finally, we will dedicate a section, Section 3.3, to the necessary assumptions made in the Higgs sector to simplify the calculations in Part II of this thesis.

The following text is inspired by [43] and [32] and contains extracts from the paper to this thesis [10].

3.1. Multi-Higgs Doublets in the SM

Let us deduce the 2HDM from the most general approach, namely by including multi Higgs doublets and developing the general formalism, and afterwards restricting it to only two-Higgs doublets.

Higgs fields

A multiple amount, n_H, of Higgs doublets, ϕ_k, can be indicated as

$$\phi_k = \begin{pmatrix} \varphi_k^+ \\ \varphi_k^0 \end{pmatrix} = \begin{pmatrix} \varphi_k^+ \\ \frac{1}{\sqrt{2}}\left(v_k + \rho_k^0 + i\eta_k^0\right) \end{pmatrix} = \begin{pmatrix} \sum\limits_{a=1}^{n_H} \tilde{U}_{ka} S_a^+ \\ \frac{1}{\sqrt{2}}\left(v_k + \sum\limits_{b=1}^{2n_H} V_{kb} S_b^0\right) \end{pmatrix}, \tag{3.1}$$

where the φ_k represent the boson fields in the flavour basis, while $S_a^\pm$ ($a \in \{1 \ldots n_H\}$) and S_b^0 ($b \in \{1 \ldots 2n_H\}$) describe the boson fields in their mass basis. The unitary matrices $\tilde{U}$ and V can be used to rotate separately between the bases for charged and neutral components. Without loss of generality, the Higgs components can be rotated with an $SU(2)_L$ rotation in such a way that for each Higgs doublet, the lower component φ_k^0 inhibits the VEV v_k [43]; furthermore, the VEV v_k can be chosen real and positive with another $U(1)_Y$ rotation, therefore

$$\langle 0|\phi_k|0\rangle = \begin{pmatrix} 0 \\ v_k \end{pmatrix}. \tag{3.2}$$

3.1.1. Higgs potential and scalar masses

Although the derivation of the scalar masses does not play an essential role in the calculation in Part II of this thesis, we will describe it in order to obtain a better understanding of the connection between scalar masses and their rotation matrices in different bases similar to the conditions in the neutrino sector.

The Higgs fields receive masses and their self-interactions through the Higgs potential. The Higgs potential in a general multi-Higgs-doublet model can have the following terms:

$$V_{higgs} = \sum_{ij} \tilde{\mu}_{ij} \phi_i^\dagger \phi_j + \sum_{ijkl} \lambda_{ijkl} \left(\phi_i^\dagger \phi_j\right)\left(\phi_k^\dagger \phi_l\right), \tag{3.3}$$

where $\tilde{\mu}_{ij}^2 = (\mu_{ji}^2)^*$, and $\lambda_{ijkl} = \lambda_{klij} = \lambda_{jilk}^*$. For mentioned reasons, we will only specify the Higgs potential in terms of derivation of the scalar masses. Before electroweak symmetry breaking (EWSB), the scalar mass term in Equation (3.3) is the one proportional to $\tilde{\mu}_{ij}$. After EWSB, in the presence of nonzero VEVs in the Higgs doublets, the contribution to mass terms in Equation (3.3) increase via terms from the quartic scalar coupling proportional to λ_{jilk}. Under this condition, the scalar mass terms turn out to be

$$V_{higgs} \supset V_{mass} = \sum_{ij} \varphi_i^- (M_+^2)_{ij} \varphi_j^+ + \frac{1}{2}\left[A_{ij}\rho_i\rho_j + B_{ij}\eta_i\eta_j + 2C_{ij}\rho_i\eta_j\right] \tag{3.4}$$

$$= \sum_a \mu_a^2 S_a^- S_a^+ + \frac{1}{2}\sum_b M_b^2 (S_b^0)^2, \tag{3.5}$$

where Equation (3.4) is written equal to Equation (3.3) in the flavour basis, whereas Equation (3.5) is written in the eigenbasis with the diagonal masses μ_a of the charged scalars and the diagonal masses M_b of the neutral scalars. The scalar masses in the flavour basis M_+, A, B, C of Equation (3.4) are functions of μ_{ij} and λ_{jilk} in Equation (3.3),

$$\text{for charged scalars:} \qquad M_+^2 = \tilde{\mu}^2 + \Lambda, \ \text{ with } \ \Lambda_{ij} = \sum_{kl} \lambda_{ijkl} v_k^* v_l, \ \Lambda^\dagger = \Lambda, \tag{3.6}$$

$$\begin{aligned} \text{for neutral scalars:} \qquad & A = \mathrm{Re}\left(\tilde{\mu}^2 + \Lambda + K'\right) + \mathrm{Re}K, \\ & B = \mathrm{Re}\left(\tilde{\mu}^2 + \Lambda + K'\right) - \mathrm{Re}K, \\ & C = -\mathrm{Im}\left(\tilde{\mu}^2 + \Lambda + K'\right) + \mathrm{Im}K, \end{aligned} \tag{3.7}$$

$$\text{with } \ K_{ik} = \sum_{jl} \lambda_{ijkl} v_j v_l, \quad K'_{il} = \sum_{jk} \lambda_{ijkl} v_j v_k^* \ \text{ and } \ K^T = K, \ K'^\dagger = K',$$

for further details, see [3]. Let us derive the basis change of the scalar mass terms from flavour, (3.4), into mass basis, (3.5), with the help of the orthogonal matrices $\tilde{U}$ and V in Equation (3.1), with $\varphi_k^+ = \sum_a \tilde{U}_{ka} S_a^+$ for charged scalars and $\rho_k = \sum_b \mathrm{Re}\,(V_{kb})\, S_b^0$, $\eta_k = \sum_b \mathrm{Im}\,(V_{kb})\, S_b^0$ for neutral scalars, respectively. Then the scalar mass matrices of Equation (3.4) convert into the diagonal eigenstate matrices of Equation (3.5) via

$$\tilde{U}^\dagger M_+^2 \tilde{U} = \mathrm{diag}(\mu_1^2, \ldots, \mu_{n_H}^2), \tag{3.8a}$$

$$\begin{pmatrix} \mathrm{Re}V \\ \mathrm{Im}V \end{pmatrix}^T \underbrace{\begin{pmatrix} A & C \\ C^T & B \end{pmatrix}}_{M_0^2} \underbrace{\begin{pmatrix} \mathrm{Re}V \\ \mathrm{Im}V \end{pmatrix}}_{\tilde{V}} = \mathrm{diag}\left(M_1^2 \ldots M_{2n_H}^2\right). \tag{3.8b}$$

The matrix V has a real and an imaginary part in order to rotate the real, ρ_k^0, and imaginary, η_k^0, component of the neutral scalar field $\phi_k^0 = 1/\sqrt{2}\left(v_k + \rho_k^0 + i\eta_k^0\right)$, (3.1), separately and is therefore $n_H \times 2n_H$-dimensional. In Equation (3.8b), the more convenient form for the rotation matrix is $\tilde{V} = \begin{pmatrix} \mathrm{Re}V \\ \mathrm{Im}V \end{pmatrix}$ being orthogonal, real, and $2n_H \times 2n_H$-dimensional. The orthogonality relations of the diagonalization matrices are

$$\begin{aligned} \mathrm{Re}\left(V^\dagger V\right)_{bb'} = \left(\mathrm{Re}V^T \mathrm{Re}V + \mathrm{Im}V^T \mathrm{Im}V\right)_{bb'} = \delta_{bb'}, \qquad & \mathrm{Re}V^T\,\mathrm{Im}V = 0 = \mathrm{Im}V^T\,\mathrm{Re}V, \\ \sum_k \tilde{U}_{ka}^* \tilde{U}_{ka'} = \delta_{aa'}, \qquad \sum_a \tilde{U}_{ka}^* \tilde{U}_{k'a} = 0. & \end{aligned} \tag{3.9}$$

Goldstone bosons

We will now take a closer look at the Goldstone boson fields defined in the mass basis. According to the Goldstone theorem, there are three Goldstone bosons $G^\pm$ and G^0 in the Higgs doublets as a result of the broken $SU(2)$ symmetry caused by the nonzero Higgs VEVs, v_k. The Goldstone bosons are part of the scalar mass eigenfields, to be numbered in such a way that $S_1^\pm = G^\pm$ and $S_1^0 = G^0$, see Equation (3.1). The neutral Goldstone boson is composed of shares from the imaginary components of the neutral bosons, η_k, where the share is the relation of the VEV from each Higgs doublet, v_k, to the total VEV, $v = \sqrt{v_1^2 + v_2^2 + \cdots + v_{n_H}^2}$. The same also applies to the charged Goldstone bosons. Thus the part of rotation matrices belonging to the Goldstone bosons is defined as

$$V_{k1} = i\frac{v_k}{v} = i\,\tilde{U}_{k1}. \tag{3.10}$$

If there is only one Higgs doublet, *i.e.* if $n_H = 1$, the matrix V is simply $V = (i,\ 1)$, and S_2^0 is the Higgs field of the SM. Moreover, the Goldstone bosons are massless and therefore correspond to the zero eigenvalues of the matrices M_+ and M_0 of Equation (3.8). However, in accordance with the Goldstone Boson Equivalence theorem, the Goldstone bosons correspond to the longitudinal modes of the W and Z bosons and still receive a virtual mass $m_{G^\pm} = \xi_W\, m_W$, $m_{G^0} = \xi_Z\, m_Z$ from the gauge fixing term, as explained in more detail in Chapter 3.1.2.

Higgs basis

To facilitate calculations, an advantageous basis can be found in any multi-Higgs-doublet model by a unitary transformation that is called the 'Higgs basis'. In this basis, only one Higgs doublet contains a VEV, here ϕ_1, which arises in the neutral component $\langle\varphi_1^0\rangle = v_1/\sqrt{2}$, while the other neutral components have none, $\langle\varphi_{k\neq 1}^0\rangle = 0$ [43]. Within this basis, the Goldstone bosons are necessarily components of ϕ_1 and can therefore be written independently [43], i.e. with Equation (3.10),

$$\varphi_1^\pm = \tilde{U}_{11}\, S_1^\pm = S_1^\pm = G^\pm, \qquad \eta_1^0 = -iV_{11}\, S_1^0 = S_1^0 = G^0. \tag{3.11}$$

Since in Part II of this thesis, we will work with formulas denoted in the Higgs basis, we specify further formulas, after their general presentation, whenever it makes sense, also in the Higgs basis.

3.1.2. Gauge boson masses and interactions

The gauge boson interactions with the Higgs doublets, as well as the gauge boson masses, result from the kinetic term, $\left|D_\mu \phi_k\right|^2$, of the Higgs Lagrangian, $\mathcal{L}_{higgs}$, which is according to the notation of [43] and [3].

$$\mathcal{L}_{higgs} = \textstyle\sum_k (D_\mu \phi_k)^\dagger (D_\mu \phi_k) - V_{higgs}, \tag{3.12a}$$

$$\begin{aligned} \text{with} \quad D_\mu \phi_k = &\left[\partial_\mu - i\frac{g}{\sqrt{2}}\begin{pmatrix} 0 & W_\mu^+ \\ W_\mu^- & 0 \end{pmatrix} - i\frac{g}{2c_W}\begin{pmatrix} c_W^2 - s_W^2 & 0 \\ 0 & -1 \end{pmatrix} Z_\mu \right. \\ &\left. + ie\begin{pmatrix} A_\mu & 0 \\ 0 & 0 \end{pmatrix}\right] \begin{pmatrix} \sum_a \tilde{U}_{ka} S_a^+ \\ \frac{1}{\sqrt{2}}\left(v_k + \sum_b V_{kb} S_b^0\right) \end{pmatrix}, \end{aligned} \tag{3.12b}$$

and $c_W = \cos\theta_W$, $s_W = \sin\theta_W$, where θ_W is the Weinberg angle. In Equation (3.12), the boson mass terms can be read out as well as triple and quartic couplings between gauge bosons and scalar fields. The $W^{\pm}_{\mu}$ and Z_{μ} gauge bosons receive masses from the Higgs VEV through [6]

$$\left|D_\mu \phi_k\right|^2 \supset \frac{g^2}{4} W^-_\mu W^+_\mu v^2 + \frac{g^2}{8c_W^2} Z^2_\mu v^2, \tag{3.13}$$

thus m_W and m_Z are defined as

$$v = \sqrt{\sum_k |v_k|^2} = \frac{2m_W}{g} = \frac{2m_Z c_W}{g}, \tag{3.14}$$

in case of the Higgs basis, $v = v_1$ constitutes the only VEV.

Equation (3.12) contains unphysical contributions proportional to $Z^0_\mu G^0_\mu$ and $W^{\pm}_\mu G^{\pm}_\mu$ in the kinetic part, $\left|D_\mu \phi_k\right|^2$, which are cancelled by additional gauge fixing terms after [43], here in $R\xi-$gauge,

$$\begin{aligned}
\mathcal{L}_{gauge-fix} = &-\frac{1}{2\xi_Z}\left(\partial_\mu Z^\mu - \xi_Z m_Z G^0\right)^2, &(3.15a)\\
&-\frac{1}{2\xi_W}\left(\partial^\mu W^+_\mu - \xi_W m_W G^+\right)\left(\partial^\nu W^-_\mu + \xi_W m_W G^-\right), &(3.15b)\\
&-\frac{1}{2\xi_A}\left(\partial^\mu A_\mu\right)\left(\partial^\nu A_\nu\right). &(3.15c)
\end{aligned}$$

These provide the Goldstone bosons with an additional gauge-dependent mass term, $m_{G^0} = \xi_Z m_Z$ and $m_{G^\pm} = \xi_W m_W$, which makes them virtual particles. Finally, in [6], one finds a Lagrangian, including the Faddeev–Popov ghosts, with which one can define the propagators of the gauge bosons.

All Feynman diagrams of the presented Lagrangians, which are used in the calculations in the second part of this thesis, are listed in Chapter D.

3.1.3. Yukawa interactions

In a multi-Higgs-doublet model, the Yukawa interactions with the lepton sector, as we introduced them in Equation (2.13), are extended to include n_H multi-Higgs doublets

$$\mathcal{L}_Y = -\sum_{k=1}^{n} \sum_{\ell,\ell'=e,\mu,\tau} \left[\phi_k^\dagger \bar{\ell}_R \left(\Gamma_k\right)_{\ell\ell'} + \tilde{\phi}_k^\dagger \bar{\nu}_{\ell R} \left(\Delta_k\right)_{\ell\ell'}\right] D_{\ell' L} + \text{h.c.}, \tag{3.16}$$

$$\text{with} \quad \phi_k = \begin{pmatrix} \varphi_k^+ \\ \varphi_k^0 \end{pmatrix}, \quad \tilde{\phi} = \begin{pmatrix} & 1 \\ -1 & \end{pmatrix} \phi^* = \begin{pmatrix} \varphi_k^{0*} \\ -\varphi_k^- \end{pmatrix} \quad \text{and} \quad D_{\ell L} = \begin{pmatrix} \nu_{\ell L} \\ \ell_L \end{pmatrix}. \tag{3.17}$$

So in principle, the mass matrices M_ℓ and M_D of the leptons are a sum of all VEVs with the corresponding Yukawa coupling matrices

$$M_\ell = \frac{1}{\sqrt{2}} \sum_k v_k^* \Gamma_k, \qquad M_D = \frac{1}{\sqrt{2}} \sum_k v_k \Delta_k; \tag{3.18}$$

As we mentioned in Chapter 2.3.2, without loss of generality, we assume that M_ℓ is diagonal and positive, so $M_\ell = \mathrm{diag}(m_e, m_\mu, m_\tau)$. One can turn Equation (3.16) further into the mass basis of the scalars, (3.1), and the leptons, (2.19), and break the formula down into the $S^\pm$ and S^0 part, as done in [3] to obtain the formulas for the Feynman diagrams,

$$\mathcal{L}_Y(S^\pm) = \sum_{ail}\left(S_a^-\overline{\ell}\,[(R_a)_{\ell i}\gamma_R - (L_a)_{\ell i}\gamma_L]\,\chi_i + S_a^+\overline{\chi}_i\left[(R_a^\dagger)_{i\ell}\gamma_L - (L_a^\dagger)_{i\ell}\gamma_R\right]\ell\right), \tag{3.19a}$$

$$\text{with}\quad R_a = \check{\Delta}_a^\dagger U_R, \quad \check{\Delta}_a = \sum_k \tilde{U}_{ka}\Delta_k, \tag{3.19b}$$

$$\text{and}\quad L_a = \check{\Gamma}_a^\dagger U_L, \quad \check{\Gamma}_a = \sum_k \tilde{U}_{ka}^*\Gamma_k, \tag{3.19c}$$

$$\mathcal{L}_Y(S^0) = -\frac{1}{\sqrt{2}}\sum_b S_b^0\left(\sum_{ij}\overline{\chi}_i\left[(F_b)_{ij}\gamma_L + (F_b^\dagger)_{ij}\gamma_R\right]\chi_j + \sum_{\ell\ell'}\overline{\ell}\left[(\hat{\Gamma}_b)_{\ell\ell'}\gamma_L + (\hat{\Gamma}_b^\dagger)_{\ell\ell'}\gamma_R\right]\ell'\right), \tag{3.20a}$$

$$\text{with}\quad \hat{\Gamma}_b = \sum_k V_{kb}^*\Gamma_k, \tag{3.20b}$$

$$\text{and}\quad F_b = \frac{1}{2}\left(U_R^\dagger\hat{\Delta}_a U_L + U_L^T\hat{\Delta}_b^T U_R^*\right), \quad \hat{\Delta}_b = \sum_k V_{kb}\Delta_k. \tag{3.20c}$$

3.2. Two-Higgs Doublets in the SM

In order to keep the number of parameters of this model to a minimum, let us limit ourselves to just two Higgs doublets. Therefore, from now on, we assume $n_H = 2$, *i.e.* a two-Higgs-doublet model. In addition, from now on, we will write formulas exclusively in the Higgs basis. In the Higgs basis, the VEVs of the 2HDM are then given by

$$\left\langle\varphi_1^0\right\rangle_0 = \frac{v}{\sqrt{2}}, \quad \left\langle\varphi_2^0\right\rangle_0 = 0, \tag{3.21}$$

where $v \simeq 246\,\mathrm{GeV}$ is real and positive. Thus, according to Equation (3.1),

$$\varphi_k^+ = \sum_{a=1}^{2}\tilde{U}_{ka}S_a^+ \quad \text{and} \quad \varphi_k^0 = \frac{1}{\sqrt{2}}\left(\delta_{k1}v + \sum_{b=1}^{4}V_{kb}S_b^0\right). \tag{3.22}$$

Moreover, the scalar mixing matrices $\tilde{U}$ and V, which convert the flavour states into the mass eigenstates, shall be indicated below. In the Higgs basis, we have specified $U_{11} = 1$ in Equation (3.11) as belonging to the charged Goldstone bosons, $\varphi_1^+ = S_1^+ = G^+$; and thus in a 2HDM, the charged scalars are mass eigenfields where the second charged scalar, $\varphi_2^+ = S_2^+$, is a physical scalar. Consequently, the mixing matrix $\tilde{U}$ represents the 2×2 unit matrix

$$\tilde{U} = \mathbb{1}_{2\times 2}. \tag{3.23}$$

Furthermore, in accordance with the notation of Ref. [53], V and thus the 4×4 orthogonal matrix $\tilde{V}$ of Equation (3.8b), which diagonalize the mass matrix of neutral scalar fields, can be parametrized with a 3×3 orthogonal matrix R,

$$\tilde{V} = \begin{pmatrix} 0 & R_{11} & R_{12} & R_{13} \\ 0 & R_{21} & R_{22} & R_{23} \\ 1 & 0 & 0 & 0 \\ 0 & R_{31} & R_{32} & R_{33} \end{pmatrix}, \quad i.e.\ V = \begin{pmatrix} i & R_{11} & R_{12} & R_{13} \\ 0 & R_{21} + iR_{31} & R_{22} + iR_{32} & R_{23} + iR_{33} \end{pmatrix}, \tag{3.24}$$

where, according to Section 3.11, $V_{11} = i$ and thus the third row of $\tilde{V}$ corresponds to the neutral Goldstone boson $S_1^0 = G^0$.

3.2.1. Yukawa interactions

In the Higgs basis, lepton mass matrices can be assigned to the first Yukawa coupling, after Equation (3.18), thus

$$\Delta_1 = \frac{\sqrt{2}}{v} M_D, \quad \Gamma_1 = \frac{\sqrt{2}}{v^*} M_\ell. \tag{3.25}$$

Rotating into the mass basis, the Yukawa couplings become for the charged scalars, combining (3.19b) and (3.19c) with (3.23),

$$\check{\Gamma}_1 = \sum_k \tilde{U}^*_{k1} \Gamma_k = \Gamma_1, \quad \check{\Delta}_1 = \sum_k \tilde{U}_{k1} \Delta_k = \Delta_1, \tag{3.26}$$

$$\check{\Gamma}_2 = \sum_k \tilde{U}^*_{k2} \Gamma_k = \Gamma_2, \quad \check{\Delta}_2 = \sum_k \tilde{U}_{k2} \Delta_k = \Delta_2, \tag{3.27}$$

while for the neutral scalars, combining (3.20b) and (3.20c) with (3.24), it is for $b > 1$

$$\hat{\Gamma}_b = \sum_k V^*_{kb} \Gamma_k = \Gamma_1 R_{1\,b-1} + \Gamma_2 (R_{2\,b-1} - iR_{3\,b-1}), \tag{3.28}$$

$$\hat{\Delta}_b = \sum_k V_{kb} \Delta_k = \Delta_1 R_{1\,b-1} + \Delta_2 (R_{2\,b-1} + iR_{3\,b-1}). \tag{3.29}$$

3.3. Simplifying Assumptions

In this chapter, we will define some simplifying assumptions about the Higgs sector, which are marked in italics, for the calculations in the second part, Part II, of this thesis.

The most general scalar potential V_{higgs} (see (3.3)) of a 2HDM contains 14 parameters [6]. However, since within this potential, we are only interested in the mass terms for

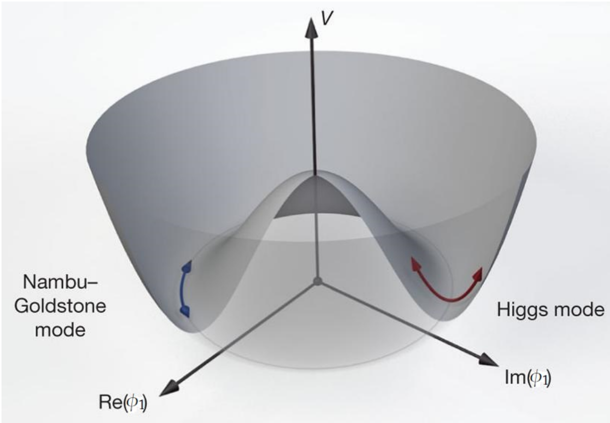

Figure 3.1.: Higgs potential for ϕ_1, source [54].

the scalars and not in interactions between them, we will not further specify the scalar potential.

For the analysis in the second part of the thesis,

we make the further assumption that ϕ_1 is just identical with the Higgs doublet of the SM;

this means that S_2^0 is exactly like the SM Higgs boson H^0, which corresponds to the radial excitations of the VEV, see Figure 3.1, i.e. $S_2^0 = H^0$. This choice relieves us from having to take into account the experimental restrictions on the couplings of the SM Higgs boson, which automatically become fulfilled. Therefore, we get with the formulas (3.1) and (3.22)

$$\phi_1 = \begin{pmatrix} \varphi_1^+ \\ \varphi_1^0 \end{pmatrix} = \begin{pmatrix} S_1^+ \\ \frac{1}{\sqrt{2}}\left(v + S_2^0 + iS_1^0\right) \end{pmatrix} = \begin{pmatrix} G^+ \\ \frac{1}{\sqrt{2}}\left(v + H^0 + iG^0\right) \end{pmatrix}, \tag{3.30}$$

and

$$\phi_2 = \begin{pmatrix} \varphi_2^+ \\ \varphi_2^0 \end{pmatrix} = \begin{pmatrix} S_2^+ \\ \frac{1}{\sqrt{2}}\left(S_3^0 + iS_4^0\right) \end{pmatrix}, \tag{3.31}$$

wherein, as already mentioned, $\varphi_1^+ = S_1^+ = G^+$ and $S_1^0 = G^0$ are the Goldstone bosons, which are to be absorbed in the longitudinal components of the Z and W bosons as part of their masses. Moreover, S_1^0 is the excitation at the bottom of the Mexican had potential, see Figure 3.1. *The choice $S_2^0 = H^0$ means that we also choose $R_{11} = 1$ in the definition of the neutral scalar mixing matrix V*, see Equation (3.24), therefore, R can be written as[4]

$$R = \begin{pmatrix} 1 & 0 & 0 \\ 0 & \cos\alpha & \sin\alpha \\ 0 & -\sin\alpha & \cos\alpha \end{pmatrix}. \tag{3.32}$$

[4]Without losing the generality, we assume that the orthogonal matrix R has determinant $+1$.

The matrix V becomes

$$V = \begin{pmatrix} i & R_{11} & R_{12} & R_{13} \\ 0 & R_{21} + iR_{31} & R_{22} + iR_{32} & R_{23} + iR_{33} \end{pmatrix} = \begin{pmatrix} i & 1 & 0 & 0 \\ 0 & 0 & e^{-i\alpha} & ie^{-i\alpha} \end{pmatrix} \tag{3.33}$$

and with the additional choice of $\alpha = 0$,

the scalar mixing matrices finally reduce to

$$S^0\text{-mixing:} \qquad V = \begin{pmatrix} i & 1 & 0 & 0 \\ 0 & 0 & 1 & i \end{pmatrix}, \tag{3.34}$$

$$S^{\pm}\text{-mixing:} \qquad \tilde{U} = \mathbb{1}_{2\times 2}. \tag{3.35}$$

This also means that the Yukawa couplings in the mass basis, according to Equations (3.26), (3.27), (3.28), and (3.29), can be simplified by Equations (3.34) and (3.35), to

$$\hat{\Gamma}_1 = -i\Gamma_1, \quad \hat{\Gamma}_2 = \Gamma_1, \quad \hat{\Gamma}_3 = i\hat{\Gamma}_4 = e^{i\alpha}\Gamma_2 = \Gamma_2, \tag{3.36a}$$

$$\hat{\Delta}_1 = i\Delta_1, \quad \hat{\Delta}_2 = \Delta_1, \quad \hat{\Delta}_3 = -i\hat{\Delta}_4 = e^{-i\alpha}\Delta_2 = \Delta_2, \tag{3.36b}$$

$$\check{\Gamma}_1 = \Gamma_1, \quad \check{\Delta}_1 = \Delta_1, \quad \check{\Gamma}_2 = \Gamma_2, \quad \check{\Delta}_2 = \Delta_2. \tag{3.36c}$$

In summary, in this setup, we get two new charged scalars $\varphi_2^{\pm} = S^{\pm}$ with mass μ_2, as well as two new neutral scalars S_3^0 and S_4^0 with mass M_3 and M_4, while the mass $M_2 = m_H$ is allocated to the Higgs particle $S_2^0 = H^0$. The scalar masses in the mass basis, after (3.5), then read

$$V_{higgs} \supset V_{mass} = \mu_2^2 S_2^- S_2^+ + \frac{1}{2} m_H^2 \left(S_2^0\right)^2 + \frac{1}{2} M_3^2 \left(S_3^0\right)^2 + \frac{1}{2} M_4^2 \left(S_4^0\right)^2. \tag{3.37}$$

4. Soft Lepton Flavour Violation

This chapter presents the realisation of the third component of our model, namely soft lepton flavour violation. After a short introduction into symmetries in Section 4.1, we will define the global symmetry of lepton flavour (also called family lepton number) and explain the connection to lepton number symmetry in Section 4.2. This is followed by a section on the concept of symmetry breaking, in particular soft symmetry breaking, in this specific case of lepton flavour, in Section 4.3. Afterwards, we implement soft lepton flavour violation in our model and provide the necessary formulas for later purposes in Section 4.4.

4.1. Introduction to symmetries

Nature has many broken and unbroken symmetries. In particle physics, symmetries are so elementary that the theoretical description of the Standard Model is constructed from them. Symmetries describe invariances of systems under symmetry transformations and are conceptualised in mathematical groups within group theory, where the transformations are the group elements. Symmetries in particle physics can be divided into space-time symmetries and *internal symmetries*. The former define symmetry operations on fields in (3+1)-dimensional space and include the Poincaré group and thus the Lorentz group as well as parity, P, and time reversal, T, whereas internal symmetries describe symmetry properties of particles and their interaction such as spin or electromagnetism, and hence acting on particle fields in a more abstract space [55]. Thus SM particles have a representation in the representation space of a symmetry group and participate in the symmetry transformations according to their quantum numbers (charges) given under this symmetry. In addition, however, local internal symmetries are space-time-dependent, although the phases from the space-time dependency should not be observable [56]; these are the known gauge symmetries. The gauge symmetries of the SM describe the strong, weak, and electromagnetic force and generate interactions between SM particles and the generators of the group, which are the force-carrying particles. A special case of the local symmetries are the *global internal symmetries*, which are not dependent on space-time; to those belong, for example, the spin and also the lepton flavour symmetry of our model.

If a symmetry is unbroken in nature, the action of the standard model remains invariant among its symmetry transformations, this also means all related quantum numbers in the terms of the action add up to zero, which is not necessarily the case anymore if they are *broken* like the flavour symmetry of this model.

New symmetries are, besides new particles, regularly used in model building to extend the SM. These symmetries often function as "hidden valley", as stated in Chapter 1, to prohibit certain tree-level characteristics of the participating fields, e.g. particle interactions such as, in our case, FCNI, etc. The Scotogenic model, for example, charges heavy right-handed neutrinos under a $\mathbb{Z}_2$ symmetry, so that these particles have no interaction terms with lighter particles, therefore cannot decay and thus become dark-matter candidates [38, 36]. In this context, a powerful tool is *accidental symmetries* that, in contrast to fundamental symmetries, are not imposed but arise from a specific particle content along with constraints from other symmetries such as gauge invariance and renormalizability [55, 56]. Accidental symmetries also restrict the physics in and beyond the SM and often explain experimental observations; prominent examples are the custodial symmetry and also the flavour symmetry [55]. In this sense, it is possible to promote an accidental symmetry to a fundamental one, as is the case in this thesis with lepton flavour symmetry as the third part of our model.

Flavour symmetries became popular in the lepton sector with the publication of neutrino data and thus have a well-established history [57]. The prior motivation to include a lepton-flavour symmetry in our model is to prohibit flavour-changing neutral interactions (FCNI) at tree-level, which are severely constrained by experimental limits, as already explained in the introduction to the previous Chapter 3. At the same time, this flavour symmetry needs to be broken since the neutrino flavour mix or, in other words, the mixing matrix U_{PMNS} is not flavour diagonal. And so, in this case, the easiest and best-justified way is to implement the breaking via an explicit soft breaking.

4.2. Lepton Flavour Symmetry

Lepton flavour symmetry, also called lepton family number symmetry, vividly predicts that the three flavours of leptons remain fixed and do not oscillate into each other. Therefore the lepton flavour symmetry group consists of three continuous and global abelian groups $U(1)_e \times U(1)_\mu \times U(1)_\tau$, each acting on a different flavour e, μ, τ. Their group elements can be written in a representation using the following symmetry transformation operators

$$U_e(\theta) = \begin{pmatrix} e^{iL_e\theta} & & \\ & 1 & \\ & & 1 \end{pmatrix}, \; U_\mu(\theta) = \begin{pmatrix} 1 & & \\ & e^{iL_\mu\theta} & \\ & & 1 \end{pmatrix}, \; U_\tau(\theta) = \begin{pmatrix} 1 & & \\ & 1 & \\ & & e^{iL_\tau\theta} \end{pmatrix}. \tag{4.1}$$

Here L_e, L_μ, L_τ represent the corresponding, preserved quantum numbers for this symmetry, and accordingly are called lepton family numbers; these are +1 for leptons and -1 for anti-leptons. The fermions transform under the group operators in Equation (4.1) as follows

$$\begin{pmatrix} \nu_\ell \\ \ell \end{pmatrix} \to U_\alpha(\theta) \begin{pmatrix} \nu_\ell \\ \ell \end{pmatrix}, \qquad \ell_R \to U_\alpha(\theta)\ell_R, \qquad \nu_R \to U_\alpha(\theta)\nu_R. \tag{4.2}$$

When the action, or Lagrangian $\mathcal{L}$, remains invariant under these transformations, the model contains a lepton flavour or L_α symmetry, as is the case in the Standard Model without neutrino masses. However, since neutrino oscillation experiments stated that lepton flavours mix, the family lepton number must be broken and hence the mass mixing matrix U_ν, and therefore also U_{PMNS} is not flavour-diagonal. The model of this work contains this breaking within an explicit softly broken lepton flavour symmetry, which is explained in the following chapter.

Connection to Lepton number symmetry

In contrast to lepton flavour symmetry, the lepton number symmetry protects the total number of leptons regardless of their flavour. The lepton number symmetry also constitutes a $U(1)_L$ group, which preserves the combined family lepton numbers $L = L_e + L_\mu + L_\tau$, so that their elements are $U(\theta) = e^{iL\theta}$. The total lepton number L, as far as is known, is not violated in the Standard Model, but will be violated by giving neutrinos a Majorana nature. A Majorana mass term $\sim \overline{(\nu_R)^c} M_R \nu_R$ violates L by two units because particles and antiparticles become the same. If the lepton number is violated, family lepton numbers are automatically violated as well.

4.3. Symmetry Breaking

Before we proceed in our description with the breaking of flavour symmetry, let us take a short excursion into the various forms of symmetry breaking. A symmetry can be broken spontaneously or explicitly, totally or partially, hard or softly. Because symmetries in particle physics are preserved within the terms of the action, symmetry breaking requires a term of the action that disobeys the symmetry on a certain level. Explicit symmetry breaking describes an action (or a Lagrangian) that contains an explicit violating term, which is an easy way to implement a symmetry breaking. On the contrary, spontaneous symmetry violation results from a first symmetry-preserving Lagrangian, whose ground-state transitions with time and/or energy into a symmetry-violating vacuum state.

Breaking a symmetry partially compared to totally is equivalent to breaking the symmetry group down to a subgroup under which the action remains invariant. (A typical example is $U(1)$ as a subgroup of the continuous groups $SU(2)$ and $SO(3)$).

Moreover, a soft broken symmetry exhibits a violating term in the action that has a dimension smaller than four in the energy dimensions of fields $dim_\varphi \leq 3$,[1] whereas a hard broken symmetry is broken by a term of $dim_\varphi = 4$.[2] This means that soft breaking terms never appear in vertices but usually in mass terms and therefore have the advantage that the symmetry breaking affects the interaction process in a softer way. For consistency reasons, all possible breaking terms of the chosen dimension and lower must be taken into account.

[1] The energy dimensions of the fields dim_φ mean that only the energy dimension of the fields are counted, no mass or length pay an impact, thus $dim_\varphi[\bar{\psi}\phi\psi] = 4$, but $dim_\varphi[\bar{\psi}m\psi] = 3$.

[2] In general, the counting of energy dimensions is based on a dimensionless action $S = \int \mathcal{L} d^4x$ of $dim[S] = 0$, therefore, the dimension of the Lagrangian $\mathcal{L}$ is $dim[\mathcal{L}] = 4$.

Due to the mentioned advantage of soft breaking and the easy implementation, the lepton flavour symmetry of this model is explicitly, totally, and softly broken.

4.4. Implementation in the Model

Our model contains the observed flavour violation of neutrinos within a soft breaking, which is solely generated by the flavour-non-diagonal, right-handed Majorana neutrino mass of the mass term in the Lagrangian (2.12), being

$$\mathcal{L}_M = -\frac{1}{2}\overline{(\nu_{\ell_1 R})^c} \underbrace{M_R^*}_{non-diag.} \nu_{\ell_2 R} + h.c., \tag{4.3}$$

which has field dimension three, $dim_\varphi\,[\mathcal{L}_M] = 3$ and is the only term with $dim_\varphi\,[\mathcal{L}_M] \leq 3$. The fact that the mass term in Equation (4.3) is not only flavour-non-diagonal because of M_R, but also of Majorana nature, additionally leads to a breaking of the total lepton number. However, flavour violation is very limited to the oscillation between left-handed neutrinos with heavy non-interacting right-handed neutrinos, which is a consequence of the soft breaking. In summary, $\mathcal{L}_M$ or M_R, in our framework, is therefore responsible for [10],

1. the smallness of the light-neutrino masses,
2. lepton mixing,
3. violation of L, and
4. violation of L_e, L_μ, and L_τ.

All other terms in the full Lagrangian remain flavour-diagonal under the flavour symmetry, such as the Yukawa couplings between scalars and leptons Γ and Δ of Equation (3.16) and thus we can parametrize them in flavour space as follows

$$\begin{array}{r} \phi_1 - \text{lepton} \\ \text{coupling:} \end{array} \quad \begin{cases} \Gamma_1 = \frac{\sqrt{2}}{v}\text{diag}(m_e, m_\mu, m_\tau) & = \frac{\sqrt{2}}{v} M_\ell \quad \text{diagonal,} \\ \Delta_1 = \text{diag}(d_e, d_\mu, d_\tau) & = \frac{\sqrt{2}}{v} M_D \quad \text{diagonal,} \end{cases} \tag{4.4a}$$

$$\begin{array}{r} \phi_2 - \text{lepton} \\ \text{coupling:} \end{array} \quad \begin{cases} \Gamma_2 = \text{diag}(\gamma_e, \gamma_\mu, \gamma_\tau), \\ \Delta_2 = \text{diag}(\delta_e, \delta_\mu, \delta_\tau), \end{cases} \tag{4.4b}$$

$$M_R \quad \text{off-diagonal.}$$

Therefore, this type of flavour violation has the desired advantage that flavour-changing processes are forbidden at tree-level and can initially occur at one-loop level, which also applies to contributions to FCNI. Furthermore, these contributions must be finite since there are no tree-level flavour-changing coupling constants and therefore there are no such renormalization constants either that could be used for a renormalization process. This is a nice circumstance for the calculations in Part II of this thesis. All of this essentially means that Yukawa couplings from the second Higgs doublet can be in the order of other SM Yukawa couplings and do not need to be suppressed to avoid high contributions from tree-level FCNI as is usually the case with multi-Higgs-doublet models.

The inclusion of a softly broken flavour symmetry holds another advantage: According to our theory, the non-diagonal structure of the U_{PMNS} matrix as part of the neutrino mixing matrix U_ν comes exclusively from the non-diagonal right-handed neutrino mass matrix M_R; this mechanism is conceptually very different from what could be realised in the quark sector with the quark-flavour mixing matrix V_{CKM} and could therefore explain the structural difference between U_{PMNS} and V_{CKM}; the different patterns of these matrices are shown in Figure 4.1.

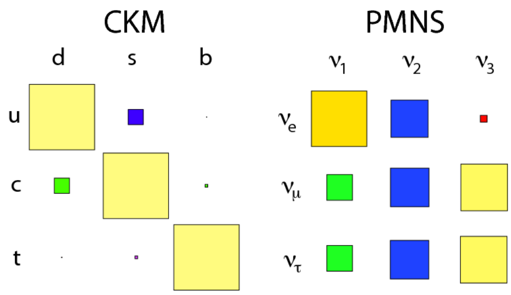

Figure 4.1.: CKM and PMNS matrices [29].

At last, another advantage in this context is that the approximately maximal atmospheric and solar mixing of the neutrinos can be generated smoothly as stated in [58].

5. Delimitation to other models

To begin with, let us again summarize our model components, which extend the standard model, these are

(A) An additional Higgs doublet, which couples to the lepton sector,

(B) Three extra right-handed neutrinos in a high-scale Type I Seesaw mechanism,

(C) A softly broken global $U(1)$ lepton flavour symmetry.

In Chapter 2 and Chapter 3 we already mentioned alternative expansions of the standard model in respectively the context of neutrino physics and a two Higgs doublet extension. Besides these, one finds the current status of research seemingly similar models as ours located in all three areas of neutrino, Higgs, and flavour physics combined. To shed light on the differences, in this chapter we briefly review a small representative collection of these other models[1] that include a 2HDM approach and some neutrino mass generation and show the delimitation to our model. All these models have to tackle lepton flavour violation and the experimental constrains on flavour changing neutral interactions (FCNI).

In this sense we start with models having the closest approach to our model: A model including only point (A) and (B) was investigated by A. Ibarra and C. Simonetto in Ref [45], which on the contrary circumvented FCNI with heavy new scalar masses instead of an extra symmetry. Furthermore, as opposed to our approach, they tried to predict the small neutrino masses and the the mild hierarchy observed between the atmospheric and the solar mass splitting. Our approach is to include light neutrino parameters in the first place to then analyse the resulting structure in the right-handed Majorana masses and mixing.

Typically also neutrino models within supersymmetry (SUSY) have a similar approach to our model. To these belong the models that include points (A) and (B), especially those that include massive neutrinos in a weak-scale SUSY. To incorporate the L-violation usually either a R-parity violation is used or a supersymmetric seesaw mechanism with an intact R-parity allowing only loop-suppressed FCNI, see [9, 59, 60, 61] and references quoted therein. However, so far SUSY models at the TeV scale suffer from a lack of experimental evidence [9].

In the last years the idea of a $U(1)$ gauge symmetry gained popularity among 2HDM, e.g. in form of the old idea of a $U(1)_{B-L}$ symmetry. The interesting features of such a model is that, first, in most cases the symmetry breaks down to a $\mathbb{Z}_2$ symmetry and thus can predict the absence of FCNI through this symmetry. Second, it exhibits a

[1] As a matter of course, we do not lay claim to completeness.

richer phenomenology that can include candidates for dark matter [62]. This type of model is especially combinable with a Type I (or II) Seesaw mechanism like examined in [62, 63, 64, 65] or with other neutrino mass generation mechanisms such as Dirac neutrino masses or radiative corrections [66, 67]. A higher symmetric model that also includes the $U(1)_{B-L}$ is the famous and well motivated left-right (LR) symmetric model. The minimal approach of the LR-symmetric model is based on the broken symmetry group $SU(2)_R \times SU(2)_L \times U(1)_{B-L}$ and can naturally realize one of the Seesaw mechanisms and gives an explanation to the electroweak parity violation [68, 69, 70].

Finally there are 2HDM with minimal extended symmetries, such as texture zero approaches for the Yukawa coupling matrices combined with a Type I Seesaw, e.g. [71, 72, 73, 74]. To these minimal symmetries belong also simple $\mathbb{Z}_2$ symmetries in form of Type I, II, X or Y 2HDM that where mentioned in the introduction of Chapter 3.2. These are combined with a Type I Seesaw [75, 76] or e.g. a neutrino mass generation via radiative corrections, such as the ones realized in [77, 78], and such as the Zee and the Scotogenic model, mentioned in Chapter 2.5. As additionally opposed to our model, the Zee model does not contain right-handed neutrinos, and the Scotogenic model contains, as pointed out, instead of a global $U(1)$ flavour symmetry a $\mathbb{Z}_2$ symmetry similar to the inert 2HDM, under which all SM particle fields are even and all new fields odd[2] [36].

Clearly, all of these models have different approaches to our model and, thus, differ also from their phenomenology. Especially the Type III 2HDM as it is in our model is seldom or not at all realised, and if realized, it has a different lepton flavour breaking approach. In general our model is generated from a bottom-up approach and belongs to the very simplistic approaches. It does not claim any pretensions to be a complete higher theory such as a GUT, but it can eventually be embedded in higher symmetric theories. Our model is one of the most general and natural models of its category which makes it interesting to investigate. It therefore has a simple phenomenology that can be well explored, and, regarding the further mentioned advantages, it has its justification among the other models.

[2] The ideal conditions for incorporating a dark matter candidate.

Part II.

Phenomenology of the Model

6. Introduction: Precision Tests and Methods

The last three chapters gave motivation and a description of the different parts of the physics of our model: An insight into neutrino physics was gained and explained why our choice of a Type I Seesaw model could be advantageous. In addition, we have derived a two-Higgs-doublet model and added new Yukawa interactions to leptons, generating interesting contributions to some lepton interaction rates as well as e.g. lepton magnetic dipole moments. Finally, it was found that a combination with an additional lepton flavour symmetry could be advantageous.

The next step is the phenomenological part, Part II of this thesis, namely the analysis of the main contributions of this model within experimentally testable phenomena. In concrete terms, this means that we will use the measurement results from experiments to provide the parameter space of the free parameters of this model defined in Section 6.2 with concrete values or limit values. To this end, in Section 6.1, we will say a few words about the three tests chosen and the reasons for their choice. Then in Section 6.2, we will list the free parameters of this model and in Section 6.3, we will continue with the description of the methods we have used to analyse our model within these tests before proceeding with the actual tests.

6.1. Precision Tests

The phenomenology of a model describes its observable consequences that can be determined in experiments. Thus, the phenomenology of a model can provide signatures of e.g. model-specific types of particles or interactions that can be searched for in experiments; this would then be referred to as **direct testing** of the model. Accordingly, experimental groups often provide different limit values from their experiments on, inter alia, particles and their masses of the most well-known theoretical models. For example, a limit value for general two-Higgs-doublet models for a new charged Higgs boson mass[1] is $M_{H^{\pm}} > 80\,\mathrm{GeV}$ [9].

The most accurately tested model in particle physics is probably the SM with its 27 parameters, and the associated tests are termed as **precision tests** of the SM [23]. These precision measurements constitute an advantage for all other models because the measurement results set quite strong constrains on physics beyond the SM; therefore, other models can be tested indirectly through them, one speaks of the **indirect testing**

[1]We will consider new scalar masses of ~ 1 TeV so the boundary is consistent with our model, as we will see in the following chapters.

of models. SM precision tests can be categorised according to the 27 SM parameters, e.g. electroweak precision tests mainly deal with three of these parameters: the two $SU(2) \times U(1)$ coupling constants, g, g', and the Higgs VEV, v; tests in flavour physics concentrate on the three mixing angles and one CP phase for quarks and leptons each as parameters, and there are further tests from QCD and other areas [23].

In this second part of the thesis, we look at the phenomenology of our model which provides signatures to the SM precision data, and thus test the model indirectly. Consequently, the parameters must be fixed or equipped with bounds so that it can be determined whether the model is realistic and feasible, where its limits lie, and where there are possibilities for further extensions. We will mainly focus on signatures of the least studied part, namely the interplay between the 2HDM, the Type I Seesaw model, and soft lepton violation. Relevant for us are electroweak precision tests, since the effects of the new neutrino and Higgs particles of this model originate from electroweak interactions between leptons, Higgs bosons, and the three gauge bosons A, Z^0 and $W^{\pm}$. That is, we will take a look at the most effective tests in this area [23], which are

1. The oblique parameters T, S, U, V, W, X, which test with precision data among others of m_Z, m_W, τ_τ, Γ_Z, whereby new physics shows up in loops from gauge boson self-energies.

2. Furthermore, the magnetic dipole moments of the electron $a_e = 115965218.091 \pm 0.026 \times 10^{-11}$ [9], and of the muon $a_\mu = 116592089 \pm 54 \pm 33 \times 10^{-11}$ [9] are well tested, in particular a_e, where a_μ still shows a discrepancy between the value from SM theory and the experiment.

Furthermore, lepton flavour physics plays an important role in this model since there is a possibility that flavour-changing currents may occur. Therefore, we will analyse

3. Flavour-changing neutral decay rates in the lepton sector, which are subject to stringent boundaries from precision experiments. While the tau-decays have an experimental boundary of $\lesssim 10^{-8}$ (e.g. $BR(\tau^- \to \mu^- e^+ e^-) < 1.8 \times 10^{-8}$ [9]), the most stringent boundaries come from muon decays with $BR(\mu^- \to e^- e^+ e^-) < 10^{-12}$ [9].

Finally, in neutrino physics

4. It is important to guarantee that the loop corrections to the light neutrino masses, $m_{1,2,3}$, remain below the experimental limits so that $\sum_{j=1}^{3} m_j < 0.17\,\text{eV}$ (CMB data [9]) or analogously $m_\nu \lesssim 0.1\,\text{eV}$ and that the experimentally determined values for U_{PMNS} and the mass differences Δm_{atm}, Δm_{sol} are kept.

There are other experimental results that could be relevant to our model and therefore serve as a test, such as in neutrino physics, the leptogenesis, the neutrinoless double beta decay; in flavour physics, the muon-electron conversion in nuclei; and the reaction and decay rates in B-physics; as well as constraints to the Higgs potential due to vacuum stability and unitarity. However, since the research field of our model is quite broad, we limit the analysis within this thesis to the main areas, namely the lepton sector and its interplay with the Higgs sector, and do not consider the quark sector and the Higgs scalar self-interactions, which limits our tests to the three selected under Points 1 to 4.

6.2. Parameters of the Model

In this section, we will collect all the parameters of the model that are added to those of the SM, and together with the assumptions that have already been made in Chapter 2.7 and 3.3 we determine the remaining degrees of freedom. This overview is helpful because the parameter space of these parameters will get additional restrictions from the experimental tests in the following chapters and will constitute the main part of our analysis.

With the new physics this model holds, we obtain an extended parameter space of 26 new parameters, in which the Higgs potential is not considered, with the exception of the scalar mass terms. These parameters together with the mentioned assumptions are:

- 3 new scalar masses: μ_2, M_3, M_4 shown in Equation (3.37),
- 2 angles from the transformation matrix V of the neutral scalars, where one was eliminated since we equate the physical scalar S_2 with the Higgs boson, and the second angle was set to $\alpha = 0$, see Equation (3.34),
- 3×3 Yukawa couplings: $\Gamma_2\left(\gamma_e, \gamma_\mu, \gamma_\tau\right)$, $\Delta_1\left(d_e, d_\mu, d_\tau\right)$, $\Delta_2\left(\delta_e, \delta_\mu, \delta_\tau\right)$ in Equation (4.4b),
- 3 heavy neutrino masses: $\hat{m}_R(m_4,\ m_5,\ m_6)$ in Equation (2.25),
- 3 mixing angles in the right-handed mixing matrix, $U_N(\theta_{12_R}, \theta_{13_R}, \theta_{23_R})$,
- 2×2 Majorana phases in the left-handed and the right-handed neutrino mixing matrix, $U_\nu(\sigma,\rho)$ and $U_N(\sigma_R,\rho_R)$ as shown in Equation (2.39), where we set $\rho = \sigma = 0$ and trivial $\sigma_R,\ \rho_R \in \{0,\ \Pi\}$ for definiteness,
- 2 CP phases for $U_\nu(\delta_{CP})$ and $U_N(\delta_{CP})$, which are trivial, i.e. $\delta_{CP} \in \{0,\ \Pi\}$, and set equal for definiteness.

Due to the assumption that all parameters are real, the phases are trivial and will not further be counted to the amount of free parameters. This leaves us with 18 undefined parameters. Five further conditions guarantee the reproducibility of the light neutrino mass-squared differences Δm_{21} and Δm_{31}, and the three neutrino mixing angles θ_{12}, θ_{13}, θ_{23}. As we will see in Chapter 9, these conditions restrict the right-handed neutrino masses and mixing angles. All in all, the 18 free parameters count therefore 13 degrees of freedom.

6.3. Analytical and Numerical Methods

Finally, we justify the choice of the order of the following tests, which is linked to the **analytical methods** used. In the case of the oblique parameters (Point 1 of the previous Section 6.1), contributions from the model contain the least amount of new parameters, namely the three scalar masses μ_2, M_3, M_4, which then can be equipped with limitations. That is the reason why we will start with this test. The test with the lowest further number of new parameters is Point 2 in Section 6.1, the lepton magnetic dipole moments, which will be our second test. Its contributions include the three scalar masses from the first test and additionally the Yukawa couplings from Γ_2 latter are γ_e showing up in the magnetic dipole moment of the electron and γ_μ showing up in the magnetic dipole moment of the muon. The formulas from the two tests just mentioned are simple enough to allow an analytic evaluation. In concrete terms, this means that we analyse the parameters in a reasonable range with 2D and 3D plots with respect to the experimental quantities, compare the results with the expected behaviour of the parameters in the formulas for consistency, and as outcome, we assign bounds and/or concrete values to the parameters an if applicable define their dependencies among each other.

Contributions to the FCNI (Point 3 in Section 6.1) are more complex. They contain the most of the new parameters, namely the three scalar masses; all nine new Yukawa couplings being $\Delta_1(d_e, d_\mu, d_\tau)$, $\Delta_2(\delta_e, \delta_\mu, \delta_\tau)$, $\Gamma_2(\gamma_e, \gamma_\mu, \gamma_\tau)$; and the masses and mixing matrix of the right-handed neutrinos, $\hat{m}_R(m_4, m_5, m_6)$ and $U_N(\theta_{R12}, \theta_{R13}, \theta_{R23}, \rho_R, \sigma_R, \delta_{CP})$. In fact, $\hat{m}_R$ and U_N can be expressed by the masses and the mixing matrix of the light neutrinos, $\hat{m}_L(m_1, m_2, m_3)$ and $U_\nu(\theta_{12}, \theta_{13}, \theta_{23}, \rho, \sigma, \delta_{CP})$, most of them are fixed by experiments, thus reducing the number of dependent free parameters. Then, according to the previous Chapter 6.2 and Point 4 of Chapter 6.1, only m_1 and δ_{CP} remain as undefined values of the mass and mixing matrix.

However, the dependence of FCNIs on neutrino parameters just described means that it is necessary to include the bounds of neutrino physics (Point 4 in Section 6.1). Therefore, as a first step in the FCNI calculation process, the right-handed neutrino mass and mixing matrix must be derived via the left-handed neutrino mass and mixing matrix. This will be done in an own chapter. In order to reproduce the experimental results for the left-handed neutrino mass and mixing matrix, vis. remaining these parameters constant, additional loop corrections to the light-neutrino masses will influence the right-handed masses and mixing matrices. Since the impact of neutrino masses on the FCNI within our model type has never been investigated before, we will also calculate the one-loop contributions to the left-handed neutrino masses and test their influence. The neutrino mass corrections at one-loop contain eight unspecified parameters, Δ_1, Δ_2, m_l, δ_{CP}, of the eleven mentioned, which are relevant to the FCNI. Both tree-level and one-loop corrections from left-handed neutrino masses turned into right-handed neutrino masses and mixing matrix can only be calculated numerically. In a second step and a following chapter, we will calculate the actual contributions to FCNIs, which will receive the corrections of the right-handed neutrino masses as numerical input, and thus the application of numerics will also be necessary for the calculation of FCNI. Furthermore, there we investigate the influence of the neutrino mass loop-corrections on FCNIs.

Since the number of parameters in the two calculation steps described is quite large, 2D and 3D analyses like before are not an option, instead we have to decide on a different method to analyse them. Either we choose a quantitative analysis, which randomly passes through a fixed parameter space. This has the advantage of a more or less full cover of the whole parameter space, but the downside that all parameters are varied constantly and the particular influence of individual parameters on the experimental quantity might not be determinable. Or we choose a **reduced systematic analysis**, which in turn has more qualitative value. A reduced systematic analysis means that a few different fixed-parameter sets[2] are chosen wisely enough to preferably cover a large variety of possible outcomes for the experimental quantity. After this a thorough analysis can be performed separately for each parameter within the set, while the other parameters of the set remain fixed. In this way parameters are analysed only in a few specific ranges of the parameter space, but the results can be more easily checked with the formulas and the role of individual parameters might become more clear. Therefore, we have decided for the method of a reduced systematic analysis and for two additional reasons. First of all, it turns out to be difficult to implement a quantitative analysis that selects random values for the calculation of right-handed neutrino masses and the mixing matrix within the numerical process required for this purpose. [3] Furthermore, the calculation of the FCNIs as described is a two-step process. Therefore, not only the implementation of randomly selected values will be complicated but also the so-called scatter plots as an outcome of this type of analysis may not represent the complex dependency of the parameters on the experimental limits and their relationships among each other in the clarity we will get from a qualitatively reduced systematic analysis.

With this knowledge, we will try to prove in the next half of this thesis that something is *possible*; we will *not* be able to perform a full scan of the parameter space of our model, which, as mentioned, is quite extensive. Nevertheless, it will be possible to investigate a certain behaviour of parameters within the respective contributions to the experimental values, to make statements about the allowed parameter space of this model analysed and the dependence between certain parameters. Moreover, we will extrapolate to other parameter ranges within the parameter space as far as possible.

Chapter organisation

In the following, we will first concentrate on the oblique parameters in Chapter 7. In the next Chapter 8, we get limits from magnetic dipole moments. In Chapter 9, one-loop corrections of the right-handed neutrino masses and mixing matrix are computed in consideration of the experimental values and bounds from neutrino physics. These one-loop corrections in turn are used for the calculation of the lepton flavour-changing neutral interactions (FCNIs) in the subsequent Chapter 10, which is the last of the precision tests presented in this thesis.

[2] By parameter sets we mean different data sets for the parameters of the model.

[3] The further concrete execution of the numerical computation is explained in the corresponding chapter.

7. Oblique Parameters

In this chapter, our model shall be tested under the bounds of electroweak precision physics in the form of the oblique parameter set. After an introduction to the oblique parameters and their origin in Section 7.1, we will calculate contributions to them from this model in the subsequent Chapter 7.2 and analyse the effects of the bounds on our parameter set.

7.1. Electroweak Precision Physics

This section will define oblique corrections as vacuum polarization diagrams of gauge boson propagators and clarify the conditions under which they dominate other corrections in electroweak precision physics. This knowledge will be relevant to classify the importance of the oblique parameters as a test of our model in the last Section 7.2.3. Moreover, in this section, the description of the oblique parameters is derived in a shortened version according to its inventors Peskin and Takeuchi, in order to obtain a better understanding of their meaning.[1] This means, we will further show that the description of the electroweak observables in the form of oblique loop corrections basically depends on six renormalized parameters, which contain the entire influence of the new physics within the oblique corrections [79]. From the formulas of these six parameters, rewritten and approximated, the three oblique parameters S, T, U or the extended six oblique parameters S, T, U, V, W, X are read out, respectively, which summarize all the information from oblique corrections in a simple, short form. S, T, U will be relevant for the new neutrino part of our model, in Section 7.2.2, and the latter six parameters, which deal with the new physics contributions around the electroweak scale m_{EW}, will be important for the new Higgs content for which calculations are made in Section 7.2.1. For a better understanding of the outcome, we will make some considerations about the meaning of the oblique parameters at the end of this chapter.

Electroweak observables

The experimental set-up for the measurement of electroweak observables usually includes light fermion scattering, with fermions in the initial and final state, as is the case in the LEP experiments [26]. Within this setup, several electroweak observables can be determined, among which the best measured and most important ones are [9, chap. 10]:

1. The tau lifetime $\tau_\tau = 290.75 \pm 0.36\,\text{fs}$,

[1] This latter part could be easily skipped with the knowledge that the important formulas of the oblique parameters we will work with in the subsequent chapter can be found in the Equations in (7.9).

2. The W-boson mass $m_W = 80.379 \pm 0.012\,\text{GeV}$,

3. The Z-boson mass $m_Z = 91.1876 \pm 0.0021\,\text{GeV}$,

4. The Z-boson decay rate $\Gamma_Z = 2.4952 \pm 0.0023\,\text{GeV}$,

5. The polarization asymmetry A^e_{LR} $(= 0.15138 \pm 0.00216)$ as an indicator of the different coupling behaviour of the electroweak theory to left- and right-handed fermions seen in $Z-$decays; it is defined as [23]

$$A^e_{LR} = \frac{\sigma_L - \sigma_R}{\sigma_L + \sigma_R} = \frac{\Gamma(e^-_L e^+_L \to Z^0) - \Gamma(e^-_R e^+_R \to Z^0)}{\Gamma(e^-_L e^+_L \to Z^0) + \Gamma(e^-_R e^+_R \to Z^0)}. \tag{7.1}$$

These data come mainly from the CERN LEP collider, but also from Tevatron, SLC, ATLAS, and others [9]. The data suggest that the relation of the gauge boson masses $m_W = m_Z \cos\theta_W$, is also well-measured; and it is indeed well-proven with an accuracy of better than 0.1% [9]. This mass relation is conserved by a global $SU(2)$ symmetry, the custodial symmetry, which is a relic of the local $SU(2)_L \times U(1)_Y$ breaking and, as we will see below, plays an important role for oblique corrections.

Oblique corrections

On the theory side, scattering amplitudes of light fermions in the initial and final state are given at tree-level by gauge-boson or Higgs particle exchange; further loop corrections are calculated in perturbation theory and may have different contributions from the new theory. To these loop corrections belong corrections to the self-energies of gauge-bosons and Higgs particles, box diagrams and vertex corrections. Some examples on the one-loop level are depicted in Figure 7.1.

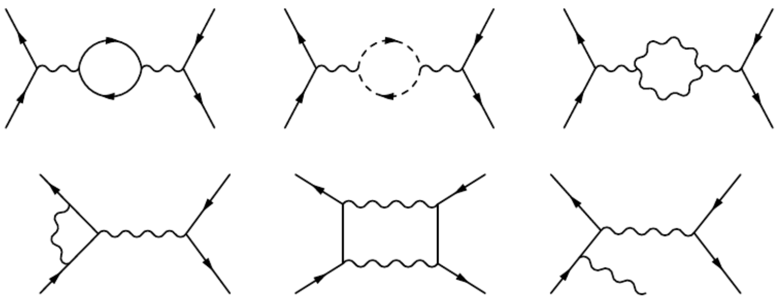

Figure 7.1.: Examples of electroweak one-loop corrections to light fermion diagrams. The dominant contributions to gauge-boson self-energies are listed above.

It will turn out that under the assumptions that [5]:

(a) The electroweak gauge group must be $SU(2)_L \times U(1)_Y$, with no new electroweak gauge bosons other than the photon, the $W^\pm$, and the Z^0,

(b) the couplings of the new physics to light fermions are suppressed compared to their couplings to the SM electroweak gauge bosons, γ, Z^0 and $W^\pm$,

the box diagrams and vertex corrections can be neglected in comparison to the gauge-boson self-energies,[2] the latter being the dominant contributions. Furthermore, couplings from the SM Higgs to the fermions are proportional to light fermion masses, which can be approximated to zero.[3] [26]. Therefore, the electroweak precision tests will focus on the new physics resulting from self-energy corrections of the gauge bosons γ, Z^0 and $W^\pm$.

Contributions to gauge-boson self-energies, Π_{XY}, with $X, Y \in \{W, Z, \gamma\}$, are referred to as **oblique corrections**, which is derived from the fact that in the case of low-energy weak interactions, the loop corrections do not couple directly to the external fermions, but indirectly (oblique) via gauge boson self-energies [26]. The involved gauge-boson self-energies are Π_{WW}, Π_{ZZ}, $\Pi_{Z\gamma}$ and $\Pi_{\gamma\gamma}$. Moreover, the gauge-boson self-energies can be written in a tensor structure and divided into two parts

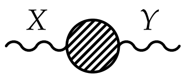

$$= \Pi^{\mu\nu}_{XY}(q^2) = g^{\mu\nu}\Pi_{XY}(q^2) + q^\mu q^\nu \Pi^{qq}_{XY}(q^2) \approx g^{\mu\nu}\Pi_{XY}(q^2), \tag{7.2}$$

the contributions to the $q^\mu q^\nu$ terms are often neglected because they are associated with a light fermion current of $\overline{f}\gamma_\mu q^\mu f \rightarrow \overline{f} m f$, where the fermion masses are set to zero [80, 81].

Electroweak parameters with oblique corrections

So, to test whether the new physics from oblique corrections fits into the experimental limits given by the Observables 1 to 5 at the beginning of this chapter, the further logical procedure is to express these observables with SM parameters in perturbative loop order, focusing on the dominant contributions from the gauge boson self-energies $\Pi_{XY}(q^2)$. To do this, one must first derive all parameters of the electroweak theory in perturbation theory with their loop corrections from the vacuum polarisation diagrams of the gauge bosons, renormalize them, and calculate their counterterms. To this end, we will continue to follow the strategy of the authors Peskin and Takeuchi [79], who achieved the most important breakthrough in the field of oblique corrections in 1992.

Thus, we start with the Lagrange densities of the fermion and the electroweak gauge boson interactions in Equations (2.37), (2.38), and (3.12), which cover all the necessary electroweak physics, including all coupling constants and gauge boson masses. From now on, one can follow the Kennedy-Lynn method and derive the running coupling

[2] Further insights can be found under [5] and the references contained therein. These authors additionally argue with the freedom of re-defining the field for the three- and four-vertex corrections to explain the dominance of gauge boson self-energies over other corrections.

[3] On the other hand, contributions from an extended Higgs sector can only be ignored if the Yukawa couplings are small or the mass of the scalars is quite high [6]. We will comment further on this in the last Section 7.2.3.

constants e_*^2 and s_{W*}^2, which determine the electric charge and the sine of the weak mixing angle

$$
\begin{aligned}
e_*^2(q^2) &= e^2\left(1+\Pi'_{QQ}(q^2)\right), \\
s_{W*}^2(q^2) &= s_W^2 - e^2\left(\Pi'_{3Q}(q^2)+s_W^2\Pi'_{QQ}(q^2)\right),
\end{aligned}
\tag{7.3}
$$

with $s_W = \sin\theta_W$, $c_W = \cos\theta_W$ and the weak mixing angle θ_W, as well as the running W and Z-boson masses m_{W*}^2, m_{Z*}^2, together with their counterterms

$$
\begin{aligned}
&Z_{W*} = 1+\frac{e^2}{s_W^2}\frac{d}{dq^2}\Pi_{11}\bigg|_{q^2=m_W^2} - \frac{e^2}{s_W^2}\Pi'_{3Q}(q^2), \\
&Z_{Z*} = \\
&1+\frac{e^2}{s_W^2c_W^2}\frac{d}{dq^2}\left(\Pi_{33}-2s_W^2\Pi_{3Q}+s_W^4\Pi_{QQ}\right)\bigg|_{q^2=m_z^2} - \frac{e^2s_W^2}{c_W^2}\Pi'_{QQ}(q^2) - \frac{e^2(c_W^2-s_W^2)}{s_W^2c_W^2}\Pi'_{3Q}(q^2),
\end{aligned}
\tag{7.4}
$$

where the star indicates the difference to the bare parameters [79]. As can be seen in Equations (7.3) and (7.4), the parameters are not defined by the self-energies of γ, Z^0 and $W^\pm$, but they are rewritten with respect to the vacuum polarization diagrams of the weak-isospin currents Π_{11}, Π_{33}, the weak-isospin-electromagnetic current Π_{3Q}, and the electromagnetic current Π_{QQ} from the gauge weak-isospin triplet (W_1, W_2, W_3^0) and the hypercharge boson B in order to obtain a simplified description; the connections to the SM gauge boson self-energies γ, Z^0 and $W^\pm$ are [82, 79]

$$
\Pi_{\gamma\gamma} = e^2\Pi_{QQ}, \qquad \Pi_{Z\gamma} = \frac{e^2}{s_Wc_W}\left(\Pi_{3Q}-s_W^2\Pi_{QQ}\right), \tag{7.5a}
$$

$$
\Pi_{WW} = \frac{e^2}{s_W^2}\Pi_{11}, \qquad \Pi_{ZZ} = \frac{e^2}{s_W^2c_W^2}\left(\Pi_{33}-2s_W^2\Pi_{3Q}+s_W^4\Pi_{QQ}\right). \tag{7.5b}
$$

Here $\Pi_{11}(q^2) = \Pi_{22}(q^2)$ applies due to the remaining $U(1)_{EM}$ symmetry after electroweak symmetry breaking. Moreover, two additional variables[4] are defined in [79],

$$
\frac{1}{4\sqrt{2}G_F} = \frac{v^2}{4}+\Pi_11(0), \qquad \frac{1}{\rho_*(0)} = 1-4\sqrt{2}G_F\left(\Pi_{11}(0)-\Pi_{33}(0)\right), \tag{7.6}
$$

for a more practical application to the experimental observables, where G_F is the Fermi constant. *The fascinating part of the Equations* (7.3), (7.4)*, and* (7.6) *is that, according to [79], all electroweak loop corrections from vacuum polarisation diagrams of the gauge bosons and also the major part of the SM corrections can be stuffed into these starred functions in Equations* (7.3), (7.4)*, and* (7.6). Thus experimental observables like those in 1 to 5 above,

[4] The parameter ρ_* is the renormalized parameter $\rho = m_W^2/(m_Z^2c_W^2)$ which, as already mentioned, is preserved by custodial symmetry and has played a significant role in the reorganization of the starred parameters of Equations (7.3), (7.4), and (7.6), so that a lean result can be obtained in the form of the parameters S, T, U, where $T = \rho - 1$ as we will see hereinafter.

τ_τ, m_W, m_Z, Γ_Z, A_{LR}, can be expressed in the form of tree-level formulas, where the coupling constants and gauge parameters are replaced by the starred, renormalized ones, which contain all orders of loop corrections from oblique parameters, that is, e.g., the observable A_{LR} is given by $A_{LR}(q^2) = 2(1-4\,s^2_{W*}(q^2))/(1+(1-4\,s^2_{W*}(q^2)))$ [79].

Oblique parameters

So now the oblique corrections became measurable by the definitions in the Equations (7.3), (7.4), and (7.6) and their connection with electroweak observables. Nevertheless, the starred parameters depend on the chosen renormalization scheme, therefore the proposal arose in the physics community to probe the new physics in the electroweak sector in a general way with finite and scheme-independent parameters. So, Peskin and Takeuchi rewrote and simplified the six parameters in Equations (7.3), (7.4), and (7.6). Among other things, they assumed that:

(c) The new physics scale, m_{new}, is far larger than the electroweak scale $m_{EW} \ll m_{new}$, with $m_{EW} \sim m_Z \approx 90\,\mathrm{GeV}$.

In this case, the gauge-boson self-energies can be extended in powers of q^2/m_{new} around the energy scale $q^2 \approx 0$, and six independent variables are obtained [81],

$$\begin{aligned}
\Pi_{\gamma\gamma}(q^2) &= q^2\Pi'_{\gamma\gamma}(0) + \mathcal{O}(q^4),\\
\Pi_{Z\gamma}(q^2) &= q^2\Pi'_{Z\gamma}(0) + \mathcal{O}(q^4),\\
\Pi_{ZZ}(q^2) &= \Pi_{ZZ}(0) + q^2\Pi'_{ZZ}(0) + \mathcal{O}(q^4),\\
\Pi_{WW}(q^2) &= \Pi_{WW}(0) + q^2\Pi'_{WW}(0) + \mathcal{O}(q^4),\\
\text{with}\quad \Pi'_{VV}(0) &\equiv \left.\frac{d\,\Pi_{VV}(q^2)}{d\,q^2}\right|_{q^2=0},
\end{aligned} \tag{7.7}$$

where $\Pi_{\gamma\gamma}(0) = \Pi_{Z\gamma}(0) = 0$ because of the Ward identity [83]. These approximations apply equivalently to the functions Π_{11}, Π_{33}, Π_{3Q}, Π_{QQ}, which in turn can be inserted into the six parameters in Equations (7.3), (7.4), and (7.6).

These six essential parameters all depend on the three main parameters g, g', v of the electroweak theory as coupling constants and the Higgs VEV or equivalently on the parameters α, G_F, m_Z and of course on the oblique corrections $\Pi_{XY}(q^2)$ approximated by Equation (7.7) [79]. In a slightly rewritten form, it is easily read from the six parameters the *three essential simple equations that must be fulfilled to reflect the full impact of the new physics of the six parameters.*

$$\begin{aligned}
\alpha S &= 4e^2\left[\Pi'_{33}(0) - \Pi'_{3Q}(0)\right] = 4s^2_W c^2_W\left[\Pi'_{ZZ} - \frac{c^2_W - s^2_W}{s_W c_W}\Pi'_{Z\gamma}(0) - \Pi'_{\gamma\gamma}(0)\right],\\
\alpha T &= \frac{e^2}{s^2_W c^2_W M^2_Z}\left[\Pi_{11}(0) - \Pi_{33}(0)\right] = \frac{\Pi_{WW}(0)}{m^2_W} - \frac{\Pi_{ZZ}(0)}{m^2_Z},\\
\alpha U &= 4e^2\left[\Pi'_{11}(0) - \Pi'_{33}(0)\right] = 4s^2_W\left[\Pi'_{WW}(0) - c^2_W\Pi'_{ZZ}(0) - 2s^2_W c^2_W\Pi'_{\gamma\gamma}(0)\right].
\end{aligned} \tag{7.8}$$

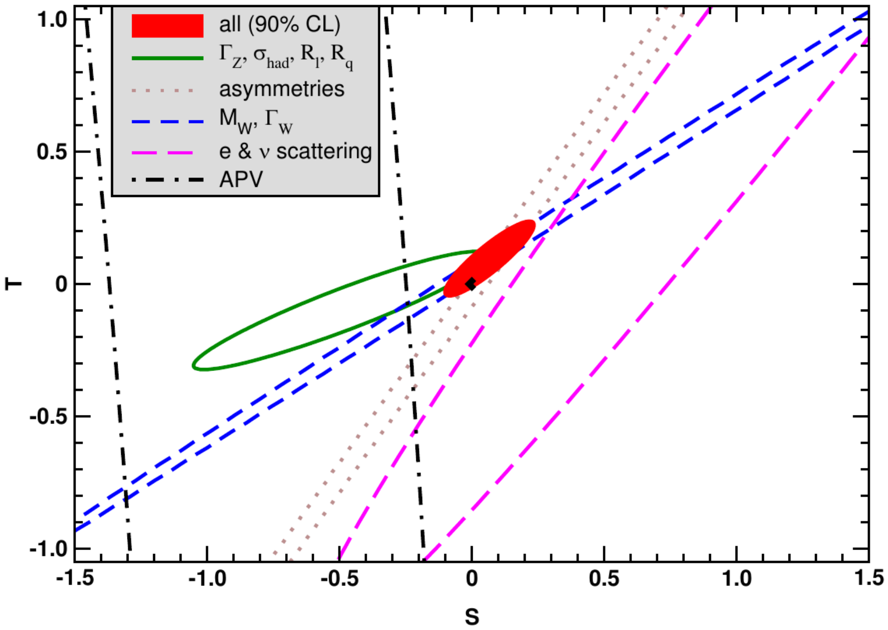

Figure 7.2.: 1 σ constraints (39.35% for the closed contours and 68% for the others) on S and T (for U=0) only from the various contributions of new physics. Datasets not involving M_W or Γ_W are insensitive to U. With the exception of the adjustment to all data, we fix $\alpha_s = 0.1182$. The black dot shows the values of the Standard Model $S = T = 0$. The graphic with text is taken from [9].

These parameters S, T, U are called **oblique parameters** or Peskin-Takeuchi parameters after their inventors (an alternative definition with ϵ parameters comes from [24]), where $\alpha = e^2/(4\pi)$ is the fine structure constant. The number of the remaining free equations, S, T, U, is three because the three other degrees of freedom are merged in the renormalization of the parameters α, G_F and m_Z, which serve as input parameters and therefore have to be fixed. Furthermore, the Peskin-Teuchari parameters are limited to a value around zero and are tested experimentally mainly by their dependence on the Observables 1 to 5 [9], as shown in Figure 7.2. The great advantage of the oblique parameters S, T, U is that they are simple, measurable, finite, and independent of the renormalization scheme [82].

Extended oblique parameters

As far as our new model is concerned, Case (c), which caused the previous approximations in Equation (7.7), applies perfectly to contributions from the neutrino Seesaw part of our model, where the new scale of physics is defined by very heavy right-handed neutrino mass $m_R \gtrsim 500\,\text{TeV}$ and thus, S, T, U are suitable parameters for a test. Case (c), however, is not fulfilled by the new Higgs physics content of our model, which has a new physics scale close to $m_{EW} \approx m_{new}$ in the form of the new scalar masses M_3, M_4, $\mu_2 \sim 1\,\text{TeV}$. On this issue, Maksymyk et al. [5] performed an analysis for new physics at $m_{new} \approx m_{EW}$ and found that three additional parameters, V, W, X, and an evaluation of the gauge-boson self-energies around $q^2 \approx m_Z^2 \approx m_W^2$ are sufficient to obtain correct electroweak precision tests. Therefore, in our analysis of the two-Higgs-doublet model (2HDM) part, we neglect the Assumption (c) and focus on the new six oblique parameters given by [84]

$$\bar{S} = \frac{\alpha}{4s_W^2 c_W^2} S = \frac{\Pi_{ZZ}(m_Z^2) - \Pi_{ZZ}(0)}{m_Z^2} - \left.\frac{\partial \Pi_{\gamma\gamma}(q^2)}{\partial q^2}\right|_{q^2=0} + \frac{c_W^2 - s_W^2}{c_W s_W} \left.\frac{\partial \Pi_{Z\gamma}(q^2)}{\partial q^2}\right|_{q^2=0}, \tag{7.9a}$$

$$\bar{T} = \alpha T = \frac{\Pi_{WW}(0)}{m_W^2} - \frac{\Pi_{ZZ}(0)}{m_Z^2}, \tag{7.9b}$$

$$\bar{U} = \frac{\alpha}{4s_W^2} U = \frac{\Pi_{WW}(m_W^2) - \Pi_{WW}(0)}{m_W^2} - c_W^2 \frac{\Pi_{ZZ}(m_Z^2) - \Pi_{ZZ}(0)}{m_Z^2} \tag{7.9c}$$

$$- s_W^2 \left.\frac{\partial \Pi_{\gamma\gamma}(q^2)}{\partial q^2}\right|_{q^2=0} + 2c_W s_W \left.\frac{\partial \Pi_{Z\gamma}(q^2)}{\partial q^2}\right|_{q^2=0}, \tag{7.9d}$$

$$\bar{V} = \alpha V = \left.\frac{\partial \Pi_{ZZ}(q^2)}{\partial q^2}\right|_{q^2=m_Z^2} - \frac{\Pi_{ZZ}(m_Z^2) - \Pi_{ZZ}(0)}{m_Z^2}, \tag{7.9e}$$

$$\bar{W} = \alpha W = \left.\frac{\partial \Pi_{WW}(q^2)}{\partial q^2}\right|_{q^2=m_W^2} - \frac{\Pi_{WW}(m_W^2) - \Pi_{WW}(0)}{m_W^2}, \tag{7.9f}$$

$$\bar{X} = \frac{\alpha}{s_W c_W} X = \left.\frac{\partial \Pi_{Z\gamma}(q^2)}{\partial q^2}\right|_{q^2=0} - \frac{\Pi_{Z\gamma}(m_Z^2)}{m_Z^2}. \tag{7.9g}$$

We can summarize that the oblique parameters, on the one hand, contain the essential equations about all new theoretical oblique corrections in a scheme-independent, simple form. On the other hand, oblique parameters are related to the electroweak observables and are therefore relatively easy to determine experimentally.

Meaning of the oblique parameters

Let us say a few more words about oblique parameters, focusing on their connection with symmetries and their meaning. The parameter T is related to the known parameter ρ of the custodial symmetry via $\alpha T = \rho - 1$. The custodial symmetry preserves the relationship

$$\frac{m_W^2}{m_Z^2} = \cos\theta_W^2 = \frac{g^2}{g^2 + g'^2}, \tag{7.10}$$

see also Appendix A.3, and thus measures the difference between charged and neutral current interaction strength, which is reflected in the difference of $\Pi_{WW}(0)$ and $\Pi_{ZZ}(0)$ in Equation (7.8). In addition, ρ describes the extent of weak-isospin breaking, namely the splitting between the members of a multiplet and their masses and couplings [82], which, e.g., can be related to scalars in a Higgs doublet. Therefore, T most likely sets limits for our scalar masses. Indeed, in the next section, we will find that assuming a degeneration of the masses of the new scalars $S_2^{\pm}$, S_4^0 in our 2HDM is advantageous since, in this case, the isospin is not broken. For a better overview of custodial symmetry, please refer to Chapter A.3.

The parameter S contains only contributions to neutral currents and is sensitive to the mixing between hypercharge and the third component of the weak isospin [83].[5] It therefore increases with the number of new doublets, especially chiral doublets such as of fermions in technicolour models [23, 82, 5]. Since we do not massively extend the sector of particles with isospin in our model, we will not expect sharp boundaries from S.

The parameter U exhibits the most varied contributions, charged currents combined with any kinds of neutral current enter only in the parameter U, which relates the energy-dependent deviation in the contribution to the three gauge-boson propagators in a complex way. In general, U tends to be small compared to S and T, which is well-reflected in the results of the following section. This circumstance results from the fact that the contributions to U can be understood as coming from a dimension-eight operator, whereas S and T are related to dimension-five operators [85, 23].

7.2. Calculation of Oblique Parameters

In this section, we calculate the new contributions of our model to the oblique parameters and derive limits for the model parameters from the experimental limits. For this purpose, we can divide the calculations into two parts: First, the contributions from the 2HDM are derived, and the limitations in Section 7.2.1 are examined. An analysis of the contributions from the new neutrino sector follows in Section 7.2.2.

All oblique parameters calculated by us are to be understood as one-loop contributions from solely new physics, so

$$\Pi_{VV}(q) = \Pi_{VV}(q)\big|_{\text{SM+new physics}} - \Pi_{VV}(q)\big|_{\text{SM}}. \tag{7.11}$$

7.2.1. Contributions to S, T, U, V, W, X from the new Higgs-doublet

In this subsection, we will determine the scalar contributions of our two-Higgs-doublet model to $\bar{S}$, $\bar{T}$, $\bar{U}$, $\bar{V}$, $\bar{W}$, $\bar{X}$. For this purpose, we will use the calculations of the oblique parameters for multi-Higgs-doublet models from [84]. The contributions from the new scalar sector to the gauge-boson self-energies, Π_{XY} with $X, Y \in \{W, Z, \gamma\}$, are of the form:

[5] One can reformulate the definition of S in Equation (7.8) with respect to the isospin-hypercharge current $\Pi_{3Y} = 2(\Pi_{3Q} - \Pi_{33})$, which results from the relation of the electromagnetic, isospin, and hypercharge currents $J_\mu^Q = j_\mu^3 - 1/2\, J_\mu^Y$ [83].

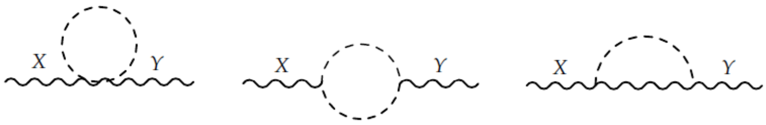

For a more detailed insight into the calculations, the reader is referred to [53]. The model contributions to the oblique parameters $\bar{S}$, $\bar{T}$, $\bar{U}$, $\bar{V}$, $\bar{W}$, $\bar{X}$ have as input, the Standard Model parameters with values from [9], namely the masses of the W, Z, and Higgs boson, $m_W \simeq 80.38\,\text{GeV}$, $m_Z \simeq 91.19\,\text{GeV}$, and $m_H \simeq 125.18\,\text{GeV}$, the weak coupling constant $g = \alpha\, 4\pi / s_W^2$ and, adhering to the definition in [9], the quantities $\alpha = \hat{\alpha}(M_Z)$ where $\hat{\alpha}(M_Z)^{-1} = 127.955$ is the weak coupling strength, and the Weinberg angle is $s_W^2 = \hat{s}_Z^2 = 0.23122$ defined in $\overline{\text{M}}\text{S}$ scheme. Furthermore, the contributions depend on the Higgs mass $M_2 = M_H$, the masses M_3, M_4 from the neutral scalars S_3^0, S_4^0, and the charged scalar mass μ_2 from $S^\pm$ of the new Higgs doublet, as well as the mixing matrix V and $\tilde{U}$ of the neutral and charged scalars from Equations (3.33) and (3.23).

This means that the parameters that will be in our focus are the masses of the new scalar particles M_3, M_4, and μ_2; on these the experimental values of the oblique parameters will set limits. Therefore, the *parameter space* of the scalar masses used in the analysis should be thought through. There are some reasons not to make the masses as small as the weak gauge boson masses. First of all, there exist experimental limits for new scalar masses from a two-Higgs-doublet model, which require that they should be higher than $m_Z \sim 80\,\text{GeV}$ the Z-boson mass [9]. Second, higher masses additionally suppress the coupling of the new Higgs doublet to the SM fermions, at least to a certain extent. This feature will be required to make the oblique parameters a valuable test. Consequently, in our analysis, we will set the scalar masses in the TeV range. As a first reference point, we will keep the mass of one of the neutral scalars at $M_3 = 1\,\text{TeV}$.

Moreover, a deeper analysis shall be limited to the three parameters S, T, and U since up to now, there are experimental limits for only these three values [9].[6] Within our parameter set, the following was found out.

Parameter T (scalar sector)

In our two-Higgs-doublet model,

$$T = \frac{1}{16\pi s_W^2 m_W^2} \left[f\left(M_3^2, \mu_2^2\right) + f\left(M_4^2, \mu_2^2\right) - f\left(M_3^2, M_4^2\right) \right],$$

where $f(x, y)$ is a function which is zero when $x = y$ [53, 6]. Thus, the result for T is zero as long as $M_3 = \mu_2$ or $M_4 = \mu_2$, as stated in our paper [10]. This is, as already mentioned, a consequence of weak isospin conservation. For $M_3 = M_4$, the discrepancy between the masses M_4 and μ_2 or M_3 and μ_2 must not be greater than $|M_{3/4} - \mu_2| \lesssim 100\,\text{GeV}$ in order to remain within the experimental limits of $T_{exp} = 0.07 \pm 0.12$ [9], as Figure 7.3

[6] For the interested reader, the authors presented in [83] a method for extracting the experimental limits of the other three parameters V, W, X.

shows.[7] The deviation must even be smaller, if the discrepancy between M_3 and M_4 is larger.

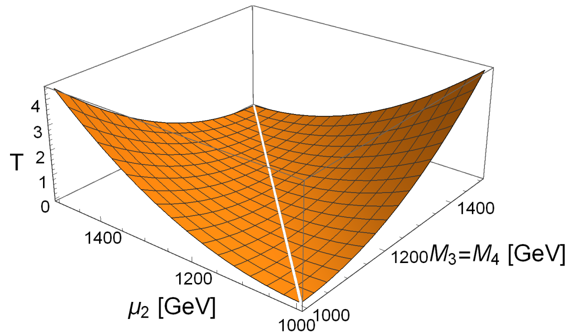

Figure 7.3.: The parameter $T(M_3, M_4, \mu_2)$ with the scalar masses $M_3 = 1\,\text{TeV}$; M_4, as well as μ_2, varies.

Parameter S (scalar sector)

Parameter S is calculated as [53]

$$S = \frac{1}{24\pi}\left[\left(2s_W^2 - 1\right)^2 G\left(\mu_2^2, \mu_2^2, m_Z^2\right) + G\left(M_3^2, M_4^2, m_Z^2\right) + \log\left(\frac{M_3^2 M_4^2}{\mu^4}\right)\right], \tag{7.12}$$

with a function $G\left(m_1^2, m_2^2, m_3^2\right)$ which goes to zero when the first two masses m_1 and m_2 are equal and become heavier, e.g. with $m = m_1 = m_2 = 500\,\text{GeV}$ $G\left(m^2, m^2, m_z^2\right) \simeq -0.007$. In general, $G\left(m_1^2, m_2^2, m_3^2\right)$ tends to give much lower values than $f(x, y)$, and therefore the largest contribution in S is the logarithm of the three masses, vis. the last term on the right-hand side of Equation (7.12). This logarithm restricts the difference between the neutral scalar masses M_3 and μ_2 or M_4 and μ_2, like T but with lower limits of $|M_{3/4} - \mu_2| \lesssim 3.4\,\text{TeV}$, when $M_3 = M_4 = 1\,\text{TeV}$, which become even less stringent when M_3, M_4 increase, as can be seen on the left graph (a) in Figure 7.4.

The oblique parameter S also sets weak limits to the discrepancy between the masses M_3 and M_4 as depicted in Figure 7.4 in the right graph (b); if $M_3 = \mu_2 = 1\,\text{TeV}$ and $M_3 = \mu_2 < M_4$, then $M_4 - M_3 \lesssim 13.1\,\text{TeV}$ must be true to stay within the experimental boundaries of $S_{exp} = 0.02 \pm 0.10$ [9], while almost nothing happens when $M_3 = \mu_2 > M_4$.

Parameter U (scalar sector)

The U parameter sets the weakest restrictions among the parameters S, T, U. In the mass range from 1-15 TeV, only the boundary $|M_{3/4} - \mu_2| \lesssim 12.6\,\text{TeV}$ are recognisable when $M_3 = M_4 = 1\,\text{TeV}$, as shown in Figure 7.5, using the experimental boundaries of

[7] The white lines in the graphs in the Figures 7.3, 7.4, and 7.5 are due to a sign change in the functions F, G, H on which the oblique parameters depend, for details, see [84].

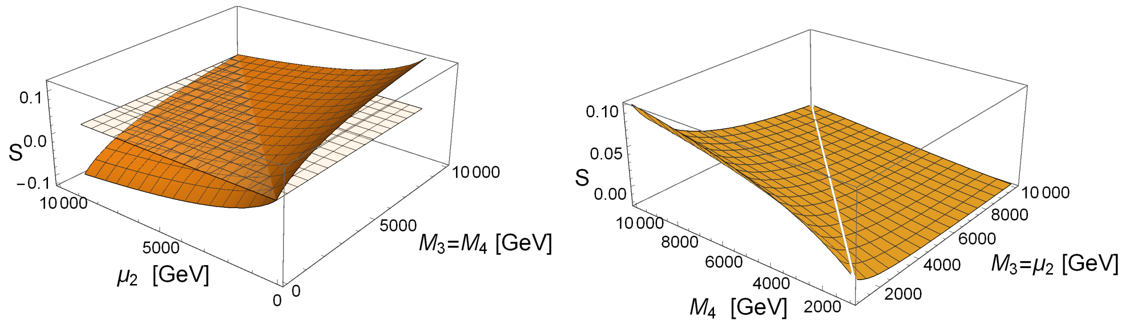

(a) $M_3 = M_4$ and μ_2 varies. The transparent layer shows where S is zero.

(b) $M_3 = \mu_2$ and M_4 varies

Figure 7.4.: The $S(M_3, M_4, \mu_2)$ parameter with the scalar masses varying.

$U_{exp} = 0.00 \pm 0.09$ [9]. This is clearly evident from the fact that U is only proportional to $G\left(m_1^2, m_2^2, m_3^2\right)$, specifically

$$U = \frac{1}{24\pi}\left[G\left(\mu_2^2, M_3^2, m_W^2\right) + G\left(\mu_2^2, M_4^2, m_W^2\right) - \left(2s_W^2 - 1\right)^2 G\left(\mu_2^2, \mu_2^2, m_3^Z\right) - G\left(M_3^2, M_4^2, m_Z^2\right)\right]. \tag{7.13}$$

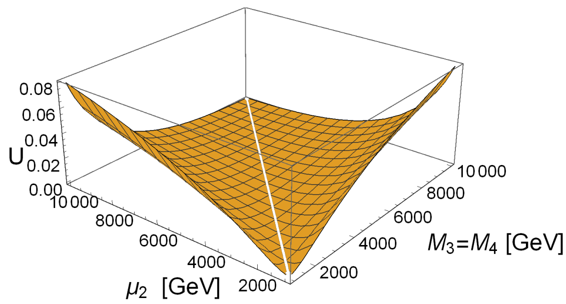

Figure 7.5.: The parameter $U(M_3, M_4, \mu_2)$ with varying scalar masses $M_3 = M_4$ and μ_2.

All oblique parameters (scalar sector)

For the same reason, the contribution to U is low, the contribution to X is also low, with

$$X = \frac{1}{48\pi}\left(2s_W - 1\right) G\left(\mu_2^2, \mu_2^2, m_Z^2\right). \tag{7.14}$$

Moreover, the other oblique parameters V and W depend on a function $H\left(m_1^2, m_2^2, m_3^2\right)$ via

$$V = \frac{1}{96\pi s_W^2 c_W^2}\left[\left(2s_W^2 - 1\right)^2 H\left(\mu_2^2, \mu_2^2, m_Z^2\right) + H\left(M_3^2, M_4^2, m_Z^2\right)\right], \tag{7.15}$$

$$W = \frac{1}{96\pi s_W^2}\left[H\left(\mu_2^2, M_3^2, m_W^2\right) + H\left(\mu_2^2, M_4^2, m_W^2\right)\right]. \tag{7.16}$$

The function $H\left(m_1^2, m_2^2, m_3^2\right)$ gives similarly low values as $G\left(m_1^2, m_2^2, m_3^2\right)$ with the difference that it goes to zero when the first two masses, m_1 and m_2, are high, where already $m = m_1 = m_2 = 500\,\text{GeV}$ leads to $H\left(m^2, m^2, m_Z^2\right) = -0.007$. Therefore, V and W do not set any discernable boundaries within the mass range of 1-15 TeV.

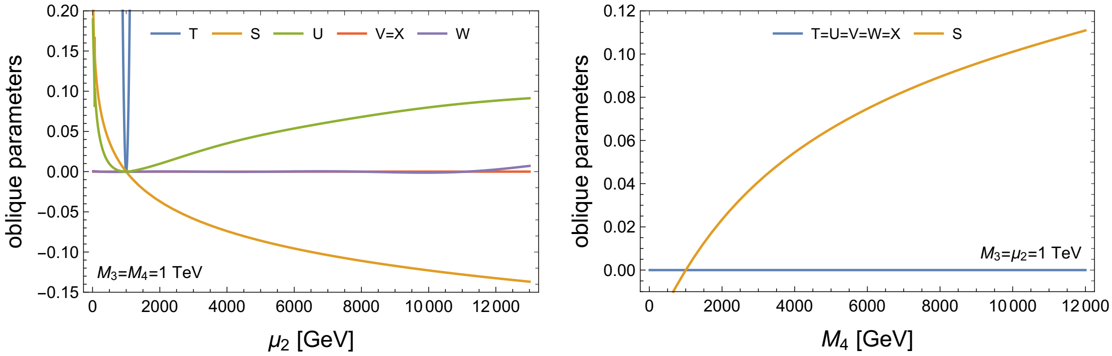

(a) The scalar mass μ_2 varies with $M_3 = M_4 = 1\,\text{TeV}$. With $M_3 = M_4 = \mu_2 = 1\,\text{TeV}$, each oblique parameter is zero.

(b) The scalar mass ΔM_4 varies with $M_3 = \mu_2 = 1\,\text{TeV}$; one gets the same picture if M_3 and M_4 are swapped.

Figure 7.6.: The behaviour of the oblique parameters on the discrepancy between the scalar masses of the new Higgs doublet.

The diagrams in Figure 7.6 show the behaviour of all oblique parameters with a certain discrepancy of the masses of the new scalars. In the left diagram, it can be seen that the contributions to T are the largest compared to the other parameters when the masses M_3, M_4 differ from μ_2 and are therefore the most restrictive. As the left diagram shows, T is followed by S and then U, latter give relatively low constraints, while the limits from the parameters V, W and X are the least stringent. As previously analysed, only the parameter S receives contributions when the discrepancy between M_4 and M_3 increases if $M_3 = \mu_2 < M_4$ or $M_4 = \mu_2 < M_3$, respectively,

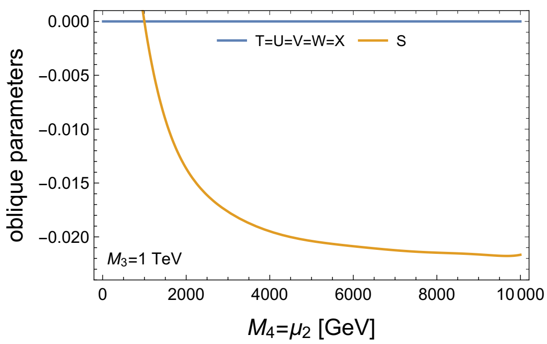

Figure 7.7.: The progression of the oblique parameters when $M_4 = \mu_2$ varies at a mass of $M_3 = 1\,\text{TeV}$.

as can be seen in the right diagram of Figure 7.6. The results from all parameters T, S, U, V, W, X are given in numbers:

	$M_3 = M_4 = 1\,\text{TeV}$, $\mu_2 =$ 1.1 TeV	4.4 TeV	12.6 TeV	$M_3 = \mu_2 = 1\,\text{TeV}$, $M_4 =$ 2.0 TeV	13.1 TeV	$M_3 = 1\,\text{TeV}$, $M_4 = 2\,\text{TeV}$, $\mu_2 = 2\,\text{TeV}$	experimental values [8] [9]
T	0.178	188.938	2002.56	0	0	0	0.07 ± 0.12
S	-0.005	-0.079	-0.135	0.023	0.120	-0.014	0.02 ± 0.10
U	0.0002	0.039	0.087	-10^{-5}	-10^{-5}	-10^{-6}	0.00 ± 0.09
V	-10^{-5}	-10^{-5}	-10^{-5}	-10^{-5}	-10^{-5}	-10^{-5}	-0.08 ± 0.13
W	-10^{-5}	-10^{-5}	0.014	-10^{-5}	-10^{-5}	-10^{-5}	-0.07 ± 0.10
X	-10^{-6}	-10^{-7}	-10^{-8}	-10^{-5}	-10^{-5}	-10^{-5}	-0.10 ± 0.10

To be save, i.e in order not to violate the experimental boundaries on oblique parameters, it is advisable to either choose a degeneracy between M_4 and μ_2 or M_3 and μ_2 and either set

$$M_3 < M_4 = \mu_2 \qquad \text{or} \qquad M_4 < M_3 = \mu_2. \tag{7.17}$$

We can see in Figure 7.7 for the former case that the contributions to the oblique parameters remain low, which equally applies to the latter case.

7.2.2. Contributions to S, T, U from right-handed neutrinos

Let us examine in this section the contributions to the oblique parameters S, T, U from the new neutrino sector of our model. Contributions to oblique parameters from heavy right-handed neutrinos in a Type I Seesaw model, as we have in our model, were derived in [31]. They comprise gauge-boson self-energies of the form:

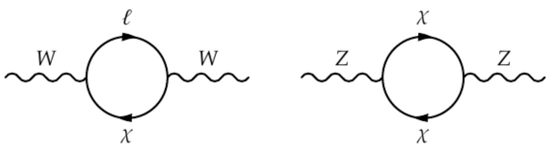

The only difference from our case is that the authors in [31] calculated these diagrams for right-handed neutrinos on the TeV scale. In general, it is believed that contributions from a much higher new physics energy scale as in our model of $m_R \gtrsim 500\,\text{TeV}$ or rather $m_R \gtrsim 10^{10}\,\text{GeV}$, are negligible [86, 87]. In our case, the reason for this becomes understandable when one considers the contribution from the right-handed neutrino propagators in the loops shown, which suppress the vacuum polarization diagrams via $1/m_R$, where m_R is in the order of the heavy neutrino masses or the seesaw scale. For comparison, the same suppression effect can be observed in flavour-changing Z boson

[8] The last three experimental values of the parameters V, W, and X in the table are calculated using the formulas presented in [83] with the experimental values from S, T, U as input.

decays, which were analysed in Equation (10.1) and [3]. Here, the flavour-changing Z boson decay also contains two propagators of right-handed neutrinos, $Z \to \chi\chi \to \ell_1\ell_2$, similar to the Z-vacuum polarization diagram above and receives a suppression factor $1/m_R^4$.

Adapting this to our case, the conclusion was drawn in [86] that loop-level corrections from sterile neutrinos are only relevant under the condition of a relatively low Seesaw scale, sizeable Yukawas, and, in addition, a large $B-L$ violation. For these reasons, contributions to oblique parameters from heavy right-handed neutrinos of our model are no longer considered.

7.2.3. Concluding remarks

Finally, a short summary can be given about the findings of the oblique corrections from a new Higgs doublet. Before we begin, let us mention briefly that the affected scalar masses that receive constraints were analysed in the lower TeV region, starting at 1 TeV, as argued at the beginning of Section 7.2.1. Coming to the results, as expected, the T parameter respects isospin and is therefore zero if the masses of the neutral, S_4^0, and charged scalar, $S_2^\pm$, degenerate, $M_4 \simeq \mu_2$ (or also the masses of S_3^0 and $S_2^\pm$), otherwise a deviation of several 10 GeV will push T out of the experimental boundaries. Compared to T, the limits of the parameter S are less restrictive, while S in addition to T requires that the neutral masses in the new Higgs doublet have a discrepancy of $M_4 - M_3 \lesssim 13.1$ TeV, if $M_3 = \mu_2 < M_4$; the same applies when M_3 and M_4 are exchanged. Parameter U specifies, as predicted in the literature, even weaker boundary conditions: In the mass range of 1-15 TeV, it sets only an upper bound to $|M_{3/4} - \mu_2| \lesssim 12.6$ TeV, if $\mu_2 = 1$ TeV with an even less strict boundary for a rising mass μ_2. Yet, the parameters V, W, and X set the weakest limits and receive an undiscernable contribution in our analysed parameter range of 1-15 TeV. All in all, the oblique parameters regarding the masses of a new Higgs doublet are not very restrictive. As an outcome of this electroweak precision test, we will, as concluded before, choose a degeneracy of the masses M_4 and μ_2 and restrict $M_3 < M_4 = \mu_2$ (or set $M_3 = \mu_2$ equal and choose $M_4 < M_3 = \mu_2$) to stay within the experimental bounds.

At last it should me mentioned, as we will see later, we will deal in our model with Yukawa couplings from the light leptons and new scalars of the order $\gamma \sim 1$ and $\delta \sim 0.01$. Thus these couplings are not necessarily suppressed compared to the gauge couplings, e.g. regarding the weak coupling constant $\alpha_W(M_Z) \sim 1/30$. Therefore, Point (b) from Section 7.1 might not be fulfilled, which is a necessary condition for the dominance of the oblique corrections. This could even be true despite relatively large scalar masses of $\gtrsim 1$ TeV, which means that not only oblique corrections might need to be considered but also couplings of the new physics to SM fermions. In other words, oblique parameters are a good reference in our case, but within the boundaries the electroweak SM parameters provide, they might not serve as a complete test. Further tests with precisely measured parameters will be necessary to check the diagrams including couplings of fermions with the new Higgs bosons. Therefore, in the next chapters, we will deal with the two remaining strongest constraints for two-Higgs doublet models [51, 52] that are relevant for our model, as mentioned in the introduction of Chapter 3. These are the magnetic dipole moments of the electron and the muon and the flavour-changing neutral interactions.

8. Magnetic and Electric Dipole Moments

As we mentioned earlier, magnetic dipole moments of the electron and muon represent powerful tests in electroweak physics for models beyond the SM, especially for those with an extended Higgs sector in the form of two or multiple Higgs doublets. Therefore, in this chapter, contributions of our model to the magnetic and electric dipole moments of leptons shall be calculated and compared with the bounds from experimental data. In this sense, we start with a pedagogical introduction in that we derive the general formulas of the magnetic and electric dipole moment in the QFT in perturbation theory for arbitrary loop order in Section 8.1. These formulas will be used to calculate the two one-loop contributions of our model to the anomalous magnetic moment (AMM) of the electron and muon and to the electric dipole moment (EDM). The known part of the calculations has been moved to Appendix B, whereas further model-specific inputs and approximations are given in Section 8.2. The result of the one-loop contributions is in turn analysed with concrete data so that parameters of the model in Section 8.3 can be provided with limits from experimental bounds. In Section 8.4, we briefly summarise the experimental status of the leptonic AMMs and EDMs in this field. In anticipation of our results concerning the muon magnetic dipole moment, we found that our model can account for the missing part between the theoretical calculations within the SM and the experimental value.

8.1. Magnetic and Electric Dipole Moments in QFT

In this chapter, we want to derive the necessary formulas to calculate the AMM and EDM contributions from our model. We could in principle start with the AMM and EDM in quantum field theory (QFT) but in order to extract the leptonic MDM and EDM in QFT from the formulas, we have to take the nonrelativistic limit and compare it with the formulas in classical mechanics. Therefore, we begin our section with a brief introduction to MDMs and EDMs in classical mechanics before proceeding to define the AMM and then derive the desired formulas in the QFT for the AMM and EDM.

8.1.1. MDM and EDM in quantum mechanics

An electric or magnetic dipole is described by its electric or magnetic moment, which gives a measure for its strength. For example, a magnetic dipole in an external B-field generates a torque with a potential energy V that is proportional to the magnetic moment $\vec{\mu}$ of the dipole,

$$V = -\vec{\mu}\,\vec{B}. \tag{8.1}$$

In classical mechanics, a magnetic dipole and its magnetic moment $\vec{\mu}$ can be caused by an orbital momentum $\vec{L}$ of a charged moving particle with charge Q, e.g., an electron spinning around a nucleus, as shown in Figure 8.1 on the left, then

$$\vec{\mu} = g\frac{eQ}{2m_e}\vec{L}. \tag{8.2}$$

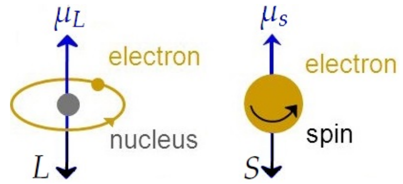

Figure 8.1.: Orbital motion (left) and spin (right) of the electron; Source [88].

The magnetic moment contains the Landé g-factor g of the spin, which is $g = 1$ in the case of a spinning electron around a nucleus (neglecting the spin of the electron). Similarly, particles and nuclei with an intrinsic spin momentum, $\vec{S} = \vec{\sigma}/2$, have a magnetic spin moment, $\vec{\mu}$, which is parallel or antiparallel to the spin, see also Figure 8.1 right. This effect can be only described in quantum mechanics. In addition, the g-factor must be taken into account with its quantum corrections resulting in a value slightly greater than $g = 2$. For the electron, for example, one has:

$$\vec{\mu} = Q\, g_e \mu_B \frac{\vec{S}}{\hbar} = g_e \frac{eQ}{2m_e}\vec{S}, \tag{8.3}$$

where the charge of the electron is Q, and $\mu_B = e\hbar/(2m_e)$ is the Bohr magneton [89].[1]

Similar to the magnetic dipole moment (MDM), the electric dipole moment (EDM) d describes the dipole strength, and e.g. it is proportional to the potential energy V when it is in an external electric field $\vec{E}$,

$$V = -\vec{d}\vec{E}. \tag{8.4}$$

Classically, the electric dipole moment is described as a charge and distance $\vec{l}$ between two attracting charges q, $\vec{d}_{class} = \vec{l}q$. An intrinsic electric dipole moment of a particle is a QFT effect and can, to put it vividly, be caused by a deviation from the spherical charge distribution, see Figure 8.2; e.g. an electron EDM, for obvious reasons, being likewise collinear to the spin,

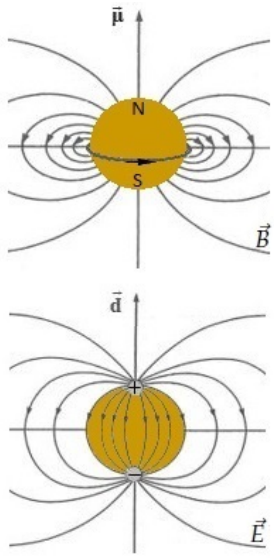

Figure 8.2.: Intrinsic MDM (top) and EDM (bottom) of a particle.

$$\vec{d} = d\,\vec{S}. \tag{8.5}$$

In the Standard Model, the intrinsic EDM for the electron is negligible and appears first in the fourth loop order [90].

[1] For the dipole moment of a nucleus, the mass changes to $m_{n,p}$, the charge is equal to the sum of its three quark constituents, and the g-factor will also be different.

The intrinsic EDM of a particle is an important measure for CP violation, which will be explained in the following. Both the electric and magnetic dipole moments of particles ($\vec{\mu}$ and $\vec{d}$) are proportional to the spin $\vec{S}$, which is an axial vector. So the EDMs and MDMs are axial-vectors too, even under parity and odds under time reflection. The same is true for the magnetic field $\vec{B}$, whereas the electric field $\vec{E}$ behaves like a vector, i.e. the opposite in terms of parity and time reflection, see also Chapter A.2.1 and [91] for details. In the Hamiltonian potentials[2] V from Equations (8.1) and (8.4), the dipole moments appear together with their corresponding fields, which is why the term with an intrinsic electric dipole moment will always violate both parity and time reversal. Therefore, the experimental values for intrinsic EDMs of particles are a measure and also a constraint for CP violation.

8.1.2. The anomalous magnetic dipole moment

In the late 1940s, experiments could for the first time only be explained by the fact that fundamental particles like the electron have an anomalous magnetic dipole moment (AMM) i.e. they show a slight deviation from the expected $g = 2$ due to quantum corrections. It therefore seemed appropriate to define the AMM, a, as the deviating part of g, *viz.* $g = 2(1 + a)$. For the electron, the AMM was experimentally determined in 1947 by Kusch and Foley and first calculated in 1948 by Schwinger in lowest order quantum corrections. This was $a \approx \frac{\alpha}{2\pi}$ [92], which was in exact agreement with the experimental data in the precision of that time. It was one of the great successes of quantum field theory and, in this respect, the most accurate verification of renormalization in quantum electrodynamics (QED) [23]. Nowadays the limits of the anomalous MDM of electrons and muons are known on the theoretical and experimental side to a fascinating accuracy: The current experimental limit regarding the AMM of the electron is $a_e^{exp} = (1159652180.91 \pm 0.26) \cdot 10^{-12}$ [9]. The theoretical value $a^{SM} = a^{QED} + a^{hadronic} + a^{EW}$ comprises the QED part with a deviation from $g = 2$, in order of percentage, as well as further contributions of strong (hadronic) and electroweak (EW) interactions, which are smaller. Experiment and theory agree up to twelve orders of magnitude, and the difference lays in the error $a_e^{err} = 2.6 \cdot 10^{-13}$ [93], whereby the theoretical value within the QED contributions additionally depends strongly on the coupling parameter, the fine-structure constant $\alpha = e^2/(4\pi)$. Compared to the theoretical value of the electron AMM, the theoretical value of the muon AMM has an amplification of the hadronic and electroweak effects that result from the higher mass of the muon $m_\mu/m_e \sim 4 \cdot 10^4$ [94]. Moreover, surprisingly, the theoretical prediction of the muon AMM is significantly smaller than the experimentally extracted AMM. The

[2]Terms proportional to the potentials also appear later in the low energy limit of the reaction amplitude when deriving the MDM and EDM.

discrepancy between the theoretical and experimental values lies within 3σ [9]:

$$a_\mu^{exp} = (1165920.91 \pm 0.63) \cdot 10^{-9}, \tag{8.6}$$
$$a_\mu^{theo} = (1165918.23 \pm 0.43) \cdot 10^{-9}, \tag{8.7}$$
$$a_\mu^{exp} - a_\mu^{theo} = 268 \pm 63(exp) \pm 43(theo) \cdot 10^{-9}. \tag{8.8}$$

The theoretical uncertainties mainly result from hadronic contributions, which are problematic due to low-energy, non-perturbative QCD effects [94]. A possible solution to overcome this discrepancy is offered by theories beyond the SM like ours, which provide additional contributions to the theory of the AMM.

Electric dipole moments of fundamental particles are predicted in the SM as very small, e.g. for the electron $|d_e| < 0.87 \cdot 10^{-28}$ e·cm [9]. The main reason for this is that a permanent dipole of a fundamental particle, as already mentioned, would violate the P and CP symmetry in an intrinsic way, whereas P and CP violation has so far only been observed in weak interactions. Therefore, several theories speculate that EDM, if observed, is one of the possible origins of such a CP violation in the quark and lepton mixing matrices V_{CKM} and U_{PMNS} and, moreover, in early baryogenesis, where CP violation is a prerequisite. For baryogenesis, the potential CP violation by the SM is too small to explain the required amount, so CP-violating models beyond the physics of the SM like ours could provide a possible source for baryogenesis, perhaps in the form of CP violation via EDMs but, more likely, in other forms as well.[3]

8.1.3. Theoretical derivation of the MDM and EDM in QFT

In quantum field theory (QFT), there is only one interaction term in the Lagrangian of the Standard Model that can cause a magnetic or electric dipole moment, namely a spinor current of a fermion $J^\mu_{em} = \overline{\psi}\gamma^\mu\psi$ interacting with the electromagnetic field represented by the photon field A^μ. The full QED Lagrange density, including the spinor-photon interaction, reads

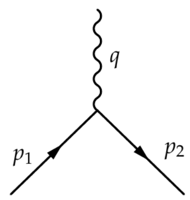

Figure 8.3.: Tree-level vertex of fermions interacting with an electromagnetic field.

$$\mathcal{L}_{QED} = \overline{\psi}(x)\left[(i\partial_\mu - e\,QA_\mu)\gamma^\mu - m_0\right]\psi(x) - \frac{1}{4}F_{\mu\nu}F^{\mu\nu}. \tag{8.9}$$

The corresponding Feynman diagram of the interaction term $e\,Q\overline{\psi}\gamma^\mu\psi A_\mu$ is shown at tree level in Figure 8.3. To extract the MDM and EDM contributions from the interaction term, we will first write the general amplitude of the interaction so that it includes all radiative corrections at any loop order in perturbation theory and then extract the terms of the desired dipole moments by comparison with low energy physics. We will need the shape of the amplitude, as well as the extracted parts, as reference for later calculations.

[3]See Outlook Chapter 12 for baryogenesis over leptogenesis within our model type.

For the estimation of the higher-order corrections to diagram 8.3, such as the one-loop contributions of $O(\alpha)$ shown in Figure 8.4, it is useful to consider the tree-level scattering amplitude of an on-shell fermion on an off-shell photon, see [23],

$$i\mathcal{A}_0 = ie\,Q\bar{u}(p_2)\gamma^\mu u(p_1)A_\mu(q). \tag{8.10}$$

One can then extend the tree-level contributions $\overline{u}(p_2)\gamma^\mu u(p_1)$ to higher orders $\overline{u}(p_2)\Gamma^\mu u(p_1)$ via the Lorentz vector Γ^μ, which is decomposed in Gordon decomposition[4] in all orders in perturbation theory

$$\Gamma^\mu = f_1\gamma^\mu + f_2 p_1^\mu + f_3 p_2^\mu + f_4 q^\mu, \tag{8.11}$$

with the fermion momenta p_1, p_2 and the photon momentum q. In the following, we can further simplify the structure of Γ^μ with some additional assumptions. Due to momentum conservation $q^\mu = p_1^\mu - p_2^\mu$, the contributions to the constant f_4 can thus be substituted into f_2 and f_3, so that we can set $f_4 = 0$. In general, f_i can contain the variables $p_1 \cdot p_2$, q^2 or $\not{p} = p_\mu\gamma^\mu$ and in the case of the parity-violating EDM also γ_5 [23]. However, factors such as $\not{p}_1$ and $\not{p}_2$ can be removed by the Dirac Equation, $\not{p}_i u(p_i) = m\,u(p_i)$, resulting in $q^2 = 2m^2 - 2p_1 \cdot p_2$; so that overall, the dependence of f_i reduces to $f_i \sim \frac{q^2}{m^2}$ and is assumed to be real. Furthermore, the Ward identity $q_\mu\overline{u}(p_2)\Gamma^\mu u(p_1) = 0$, which originates from gauge invariance[5] implies

$$\begin{aligned} q_\mu\bar{u}_2\left(f_1\gamma^\mu + f_2 p_1^\mu + f_3 p_2^\mu\right)u_1 &= f_1\bar{u}_2\,\not{q}\,u_1 + f_2\bar{u}_2\,q\cdot p_1\,u_1 + f_3\bar{u}_2\,q\cdot p_2\,u_1 = 0 \\ \Leftrightarrow \quad f_2 = f_3, &\quad \text{with} \quad qp_1 = m^2 - p_1p_2 = -qp_2, \end{aligned}$$

see also [23]. This leads to

$$\Gamma^\mu = f_1\gamma^\mu + f_2(p_1^\mu + p_2^\mu), \tag{8.12}$$

which can be further rewritten with the Gordon identity for on-shell spinors into terms of the spinor transformation operator $\sigma^{\mu\nu} = \frac{i}{2}\left[\gamma^\mu, \gamma^\nu\right]$ as

$$\bar{u}(p_2)\left(p_1^\mu + p_2^\mu\right)u(p_1) = 2m\,\bar{u}(p_2)\gamma^\mu u(p_1) + i\,\bar{u}(p_2)\sigma^{\mu\nu}q_\mu u(p_1) \tag{8.13}$$

and into the final form of the amplitude

$$i\mathcal{A} = ie\,Q\,\bar{u}(p_2)\left[F_1(q^2)\gamma^\mu + F_2(q^2)\frac{i\sigma^{\mu\nu}}{2m}q_\nu\right]u(p_1)A_\mu(q). \tag{8.14}$$

Now the way is paved to search for the AMM and afterwards the EDM contributions in the amplitude, which is best done in a non-relativistic approximation $|\vec{p}_i| << m_i$. Then

[4] For a more detailed description, see Appendix A.2.1.

[5] A quick proof of the Ward identity is given via the current conservation, valid to all orders in j_{em} $\underbrace{\partial_\nu\partial_\mu}_{symmetric}\underbrace{F^\mu}_{antisymmetric} = -e\,\partial_\nu j_{em} = 0$, which is a result of gauge invariance [91].

the components of $A^\mu(q) = (\phi(q), \vec{A}(q))^T$ can be interpreted as weak time-independent external potentials. Furthermore, the non-relativistic expansion of the spinors yields

$$u(p) = \begin{pmatrix} \sqrt{p\cdot\sigma}\xi \\ \sqrt{p\cdot\bar{\sigma}}\xi \end{pmatrix} \approx \sqrt{m}\begin{pmatrix} (1-\vec{p}\vec{\sigma}/2m)\xi \\ (1+\vec{p}\vec{\sigma}/2m)\xi \end{pmatrix}, \tag{8.15}$$

so that the terms proportional to $F_1(0)$ can be written as [26]

$$\begin{aligned} &\bar{u}(p_2)\gamma^0 u(p_1)\phi(q) = u^\dagger(p_2)u(p_1)\phi(q) \approx 2m\xi_2^\dagger\xi_1\phi(q), \\ &\bar{u}(p_2)\gamma^i u(p_1)A_i(q) \approx \xi_2^\dagger\left(p_2^j\sigma^j\sigma^i + \sigma^i p_1^j\sigma^j\right)\xi_1 A_i(q) = \xi_2^\dagger\left(-i\epsilon^{ijk}q_j\sigma_k\right)\xi_1 A_i = -\xi_2^\dagger\sigma^k B_k(q)\xi_1, \end{aligned}$$

with $\sigma^i\sigma^j = \delta^{ij} + i\epsilon^{ijk}\sigma_k$ and $B_k(q) = i\epsilon^{ijk}q_j A_i$, neglecting all contributions with $(p_2 + p_1)$. Moreover, the term proportional to $F_2(0)$ becomes

$$\bar{u}(p_2)\,\frac{i\sigma^{\mu\nu}}{2m}q_\nu\, u(p_1)A_i(q) = -\xi_2^\dagger\sigma^k B_k(q)\xi_1.$$

Finally, we obtain an $\mathcal{A}$ equivalent for the formulation of the Born approximation for electron scattering from an electric and magnetic field potential [94]:

$$i\mathcal{A} = ie\,Q\,\xi_2^\dagger\left(F_1(0)\phi(q) - \frac{1}{m}\left[F_1(0) + F_2(0)\right]\frac{\vec{\sigma}}{2}\vec{B}(q)\right)\xi_1, \tag{8.16}$$

taking into account the different normalization of states in non-relativistic quantum mechanics. In comparison with the potential in Equation (8.1) and the classical definition of the MDM in Equation (8.3), one can read out of this formula the MDM being proportionally to the Spin $\vec{S} = \vec{\sigma}/2$ and multiplied by a $\vec{B}$−field,

$$\vec{\mu} = \frac{e\,Q}{2m}\underbrace{2\left[F_1 + F_2\right]}_{g}\frac{\vec{\sigma}}{2}, \tag{8.17}$$

with a Landé factor of $g = 2\left[F_1 + F_2\right]$. Comparing Equation (8.14) with the tree-level contribution in Equation (8.10), we find that F_2 vanishes at tree level, and $F_1 = 1$ remains, thus F_1 represents the value that renormalizes the electric charge. The easiest way to compute F_i further to all orders is in the on-shell scheme,[6] where the renormalization condition requires that the renormalization constants, in our case F_1, are defined so that the one-particle irreducible vertices at all orders maintain the tree-level value at the on-shell condition $q = 0$. This means for $q = 0$ $F_1(0) = 1$ for all orders, so that according to [94],

$$F_1(0) = \underbrace{F^{tree}(0)}_{1} + F^{loops}(0) + F^{counterterms}(0) = 1. \tag{8.18}$$

[6] The on-shell scheme is presented in more detail in Chapter C.2.

Therefore, $g = 2\left[1 + F_2(0)\right]$ applies, which means

$$a = F_2(0) \equiv F_{AMM}(0) \tag{8.19}$$

is the AMM in this scheme, containing all radiative corrections with spin dependence. We also saw that F_2 does not contribute to the renormalization constants and consequently should not be divergent.

So far so good, we now also briefly mention the approach of finding the EDM contribution and extending the formula in Equation (8.14) accordingly. As we have already ascertained in Equation (8.5), the EDM is also spin-dependent like the MDM, the latter having the spin-dependence in the F_2 term the formula (8.14). In addition, we know that the EDM violates P and CP symmetry, like the γ_5 element from the underlying algebra. Accordingly, it is straightforward to add an ancillary EDM term to F_2 and rename the AMM contribution within F_2 to F_{AMM}, so $F_2(0) = F_{AMM}(0) - i\gamma_5 F_{EDM}(0)$. Then the formula for $F_2(0)$ can be included in Equation (8.14) as follows [91]

$$\begin{aligned} i\mathcal{A} &= ie\,Q\,\bar{u}(p_2)\left[F_1(0)\gamma^\mu + \left[F_{AMM}(0) - i\gamma_5 F_{EDM}(0)\right]\frac{i\sigma^{\mu\nu}}{2m}q_\nu\right]u(p_1)A_\mu(q) \\ &= ie\,Q\,\bar{u}(p_2)\left[F_1(0)\gamma^\mu + F_{AMM}(0)\frac{i\sigma^{\mu\nu}}{2m}q_\nu + F_{EDM}(0)\gamma_5\frac{\sigma^{\mu\nu}}{2m}q_\nu\right]u(p_1)A_\mu(q); \end{aligned} \tag{8.20}$$

where the EDM is

$$d = i\frac{e\,Q}{m}F_{EDM}(0), \tag{8.21}$$

according to Equation (8.5), which includes all radiative corrections and exhibits similar properties to F_{AMM} as finiteness.

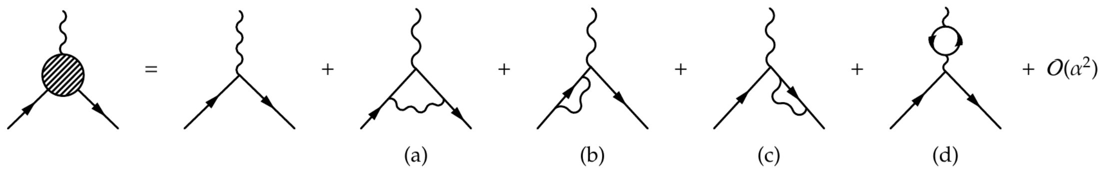

Figure 8.4.: Corrections on tree level and one-loop in the QED vertex diagram.

For further calculation, we want to make some statements about which diagrams can contribute in higher orders to the AMM or EDM. As mentioned above, the AMM receives contributions from all the different interactions $a = a^{QED} + a^{weak} + a^{strong}$, as does the EDM. The radiative vertex corrections from QED of order $O(\alpha)$ are depicted in the diagrams in Figure 8.4; all diagrams from (b) to (d) have a vertex correction, which is proportional to γ^μ and therefore only contributes to F_1. Only diagram (a) can contain a spin-dependence via $\sigma^{\mu\nu}$ and is therefore a candidate for a contribution to MDM and EDM via F_2. Thus Diagram (a) provides the first order QED correction for the AMM with $F_{AMM}(0) = \frac{\alpha}{2\pi} \approx 0.00116$, see [26] for further details.

8.2. Model Contributions to the Dipole Moments

Our theory predicts a contribution to dipole moments in the form of two Feynman diagram types for the process of a photon radiated from a fermion line $\ell \to \ell\gamma$:

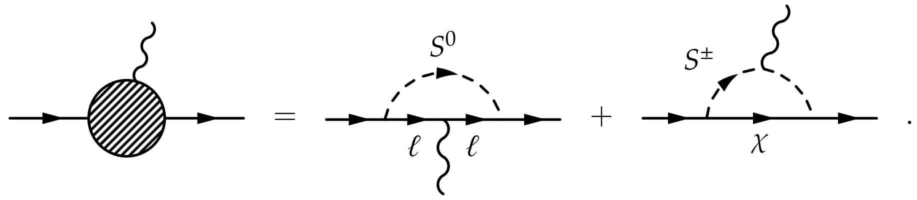

(8.22)

The contributions from (8.22) are calculated further down in Appendix B using a generalized approach to the scalar-lepton interactions, namely

$$\mathcal{L}_{\mathcal{Y}}(S) = \bar{f}'(a_L\gamma_L + a_R\gamma_R)fS + h.c. \tag{8.23}$$

In this generalised approach, the incoming and outgoing lepton ℓ has the mass m and the charge Q, while m' and Q' are the mass and charge of the leptons ℓ' or χ in the loop, the mass of the neutral scalar, and the charged scalar is denoted as M.

In the following two sections of this chapter, text is quoted and partly transcribed from the paper [10] on which this thesis is based.

We collect the results of Equations (B.35) and (B.36) in Appendix B, which are

$$\begin{aligned} F_{AMM} = -\frac{m}{(4\pi)^2}\int dz \Bigg(& Q' z^2 \frac{(1-z)m\left(|a_L|^2+|a_R|^2\right)+2m' Re(a_L^* a_R)}{zm'^2+(1-z)(M^2-zm^2)} \\ & + (Q'-Q)z(1-z)\,\frac{(1-z)\,m\left(|a_L|^2+|a_R|^2\right)+2m'^2\,Re\left(a_L^* a_R\right)}{zm'+(1-z)(M^2-zm^2)}\Bigg), \end{aligned} \tag{8.24}$$

$$F_{EDM} = -i\frac{mm'}{(4\pi)^2}\int dz \left(\frac{Q'\,z^2\,2Im(a_L^* a_R)}{zm'^2+(1-z)(M^2-zm^2)} + \frac{(Q'-Q)\,z(1-z)\,2Im\left(a_L^* a_R\right)}{zm'^2+(1-z)(M^2-zm^2)}\right), \tag{8.25}$$

The first contributions of Equations (8.24) and (8.25) proportional to Q' are contributions from the first diagram in Figure 8.22, where the photon is attached to leptons. The second contribution proportional to $(Q'-Q)$ comes from the second diagram in Figure 8.22 where the photon is attached to scalars. Note that the AMM, a, is dimensionless according to Equation (8.19) and therefore also $F_{AMM}(0) = a$; whereas the EDM, d, has the dimension $[e \cdot \text{cm}]$ but $F_{EDM}(0) = -i\frac{m}{eQ}d$ is dimensionless, after Equation (8.21), which is here the case.

Finally, one can rewrite $F_{AMM}(0)$, (8.24), and $F_{EDM}(0)$, (8.25), into the AMM, a, and the EDM, d, via Equations (8.19) and (8.21), respectively, and transfer it to a more sophisticated version with the integrals in Equation (8.28)

$$a_\ell = -\frac{2m}{(4\pi)^2}\Bigg[Q'\left(\frac{m}{2}\left(|a_L|^2+|a_R|^2\right)\frac{I_{(2,1)}}{M^2}+m'\,Re\left(a_La_R^*\right)\frac{I_{(2,0)}}{M^2}\right)$$
$$+(Q'-Q)\left(\frac{m}{2}\left(|a_L|^2+|a_R|^2\right)\frac{I_{(1,2)}}{M^2}+m'\,Re\left(a_La_R^*\right)\frac{I_{(1,1)}}{M^2}\right)\Bigg], \qquad (8.26)$$

$$d_\ell = -\frac{e\,m'}{(4\pi)^2}Im\left(a_La_R^*\right)\left[Q'\frac{I_{(2,0)}}{M^2}+(Q'-Q)\frac{I_{(1,1)}}{M^2}\right], \qquad (8.27)$$

with integrals of the form

$$I_{(p,q)}(r,s) = \int_0^1 dx\frac{x^p(1-x)^q}{1-x+xr-x(1-x)s}, \qquad r=\frac{m'^2}{M^2},\ s=\frac{m^2}{M^2}. \qquad (8.28)$$

The integrals can be calculated to yield

$$\frac{I_{(2,0)}}{M^2} = \frac{1}{m^2}+\frac{m^2+M^2-m'^2}{2m^4}\ln\frac{m'^2}{M^2}$$
$$+\frac{m'^4+m^4+M^4-2m'^2m^2-2m'^2M^2}{2m^4}f\left(m^2,m'^2,M^2\right), \qquad (8.29a)$$

$$\frac{I_{(1,1)}}{M^2} = -\frac{1}{m^2}+\frac{m'^2-M^2}{2m^4}\ln\frac{m'^2}{M^2}$$
$$+\frac{m^2M^2+m^2m'^2+2m'^2M^2-m'^4-M^4}{2m^4}f\left(m^2,m'^2,M^2\right), \qquad (8.29b)$$

$$\frac{I_{(2,1)}}{M^2} = \frac{2m'^2-2M^2-m^2}{2m^4}+\frac{m^2m'^2+2m'^2M^2-m'^4-M^4}{2m^6}\ln\frac{m'^2}{M^2}$$
$$+\frac{1}{2m^6}\left(m'^6-M^6-3m'^4M^2+3m'^2M^4+m^2M^4\right.$$
$$\left.+m^2m'^2M^2-2m^2m'^4+m^4m'^2\right)f\left(m^2,m'^2,M^2\right), \qquad (8.29c)$$

$$\frac{I_{(1,2)}}{M^2} = \frac{2M^2-2m'^2-m^2}{2m^4}+\frac{m'^4+M^4-2m'^2M^2-m^2M^2}{2m^6}\ln\frac{m'^2}{M^2}$$
$$+\frac{1}{2m^6}\left(M^6-m'^6+3m'^4M^2-3m'^2M^4+m^2m'^4\right.$$
$$\left.+m^2m'^2M^2-2m^2M^4+m^4M^2\right)f\left(m^2,m'^2,M^2\right), \qquad (8.29d)$$

where

$$f\left(m^2,m'^2,M^2\right) \equiv \frac{I_{(0,0)}}{M^2} = \begin{cases} \ln\left((t+\sqrt{\delta})/(t-\sqrt{\delta})\right)\big/\sqrt{\delta} & ,\delta>0, \\ 2/t & ,\delta=0, \\ 2\arctan\left(\sqrt{-\delta}\big/t\right)\big/\sqrt{-\delta} & ,\delta<0, \end{cases} \qquad (8.30)$$

with

$$t \equiv m'^2 + M^2 - m^2, \quad \delta \equiv t^2 - 4m'^2M^2. \tag{8.31a}$$

Let us include the parameters of our model in the AMM and EDM of Equations (8.26) and (8.27). The first diagram of (8.22) can have two neutral scalars running in the loop S_3^0, S_4^0 with mass M_b, $(b \in \{3,4\})$ so that, after Equation (3.20), we have the factors of the scalar-lepton vertex $a_L(S_b^0) = -(\hat{\Gamma}_b)_{\ell\ell}/\sqrt{2} = a_R^*(S_b^0)$; more precisely, with Equations (3.36a) and (4.4b) we obtain

$$a_L(S_3^0) = -(\Gamma_2)_{\ell\ell}/\sqrt{2} = -e^{i\alpha}\gamma_\ell/\sqrt{2} = -\gamma_\ell/\sqrt{2}, \tag{8.32a}$$
$$a_L(S_4^0) = i(\Gamma_2)_{\ell\ell}/\sqrt{2} = ie^{i\alpha}\gamma_\ell/\sqrt{2} = i\gamma_\ell/\sqrt{2}. \tag{8.32b}$$

In addition, the photon adheres to the ℓ line in the vertex, which leads to $Q' = -1$ and $m' = m = m_\ell$. In the second diagram of (8.22), the particles running in the loop are a neutrino, X, with mass $m' = m_j$ $(j \in \{1,2,\dots 6\})$ and without charge, $Q' = 0$; and a physical charged scalar $S_2^\pm$ with mass $M = \mu_2$. In this case, after Equation (3.19), we have $a_L(S_2^\pm) = (R_2^*)_{\ell j} = (U_R^*)_{\ell j}(\check{\Delta}_2)_{\ell\ell}$ and $a_R(S_2^\pm) = -(L_2^*)_{\ell j} = -(U_L^*)_{\ell j}(\check{\Gamma}_2^*)_{\ell\ell}$ and thus with (3.36c) and (4.4b) we finally get

$$a_L(S_2^\pm) = \delta_\ell(U_R^*)_{\ell j}, \tag{8.33a}$$
$$a_R(S_2^\pm) = -\gamma_\ell^*(U_L^*)_{\ell j}. \tag{8.33b}$$

With this input, Equations (8.26) and (8.27) become

$$\begin{aligned} a_\ell = \frac{2m_\ell}{(4\pi)^2}\Bigg[&\frac{m_\ell}{2}\left(|\gamma_\ell|^2\left(\frac{1}{M_3^2}+\frac{1}{M_4^2}\right)I_{(2,1)} + Re\left(e^{i2\alpha}\gamma_2^2\right)\left(\frac{1}{M_3^2}-\frac{1}{M_4^2}\right)I_{(2,0)}\right) \\ &-\left(\frac{m_\ell}{2}\left(\sum_{i=1}^{3}|\gamma_\ell(U_L)_{\ell i}|^2 + \sum_{i=4}^{6}|\delta_\ell(U_R)_{\ell i}|^2\right)\frac{I_{(1,2)}}{\mu_2^2} - m_j\,\delta_\ell\gamma_\ell\sum_{i=1}^{6}Re\left((U_R^*)_{\ell j}(U_L)_{\ell j}\right)\frac{I_{(1,1)}}{\mu_2^2}\right)\Bigg], \end{aligned} \tag{8.34}$$

$$d_\ell = \frac{e}{(4\pi)^2}\left[\frac{m_\ell}{2}Im\left(e^{i2\alpha}\gamma_2^2\right)\left(\frac{1}{M_3^2}-\frac{1}{M_4^2}\right)I_{(2,0)} + m_j\,\delta_\ell\gamma_\ell\,Im\left(U_R^*U_L\right)\frac{I_{(1,1)}}{\mu_2^2}\right]. \tag{8.35}$$

Since we choose all our parameters as real, the term $Im\left(a_La_R^*\right) \sim Im\left(U_R^*U_L\right)$ disappears in Equation (8.35) and thus $d_\ell = 0$, which means that in our parameter constitution, we will have no contributions to the electric dipole moment of any lepton. Therefore, we will further continue to approximate the contributions to the anomalous magnetic dipole moment in Equation (8.34).

One can write the first part of the calculations in Equation (8.34) with the neutral scalars in terms of $\epsilon \equiv m_\ell^2/M_b^2$, followed by an approximation in terms of ϵ under the assumption of $\epsilon \ll 1$. Then the integrals become $I_{(2,1)} = 1/3 + O(\epsilon)$ and $I_{(2,0)} =$

$-3/2 - \ln(m_\ell^2/M_b^2) + O(\epsilon)$ and

$$a_\ell^{(S^0)} \simeq \frac{m_\ell^2}{96\pi^2}\left\{2\left|\gamma_\ell\right|^2\left(\frac{1}{M_3^2}+\frac{1}{M_4^2}\right)\right.$$
$$\left. - 3\mathrm{Re}\left(e^{2i\alpha}\gamma_\ell^2\right)\left[\frac{1}{M_3^2}\left(3+2\ln\frac{m_\ell^2}{M_3^2}\right) - \frac{1}{M_4^2}\left(3+2\ln\frac{m_\ell^2}{M_4^2}\right)\right]\right\}. \tag{8.36}$$

In the following, we will deal with the second part of Equation (8.34), including the charged scalar exchange. Since the neutrino mixing matrices in the Seesaw limit $m_R \to \infty$ are approximately after (2.26),

$$U_L \approx (U_\nu, 0_{3\times 3}), \qquad U_R \approx (0_{3\times 3}, U_N),$$

where $U_\nu \sim U_{PMNS}$ and U_N are the 3×3 unitary mixing matrices of the light and heavy neutrinos, $a_L(S_2^\pm) \sim (U_R)_{\ell j} \approx 0$ for $j = 1,2,3$, with respect to Equation (8.33), and also $a_R(S_2^\pm) \sim (U_L)_{\ell j} \approx 0$ for $j = 4,5,6$, therefore, $Re(a_L a_R^*) \approx 0$, and the contribution proportional to $I_{(1,1)}$ disappears. So, it remains the contribution to $I_{(1,2)}$,

$$a_\ell^{(S^\pm)} = -\frac{m_\ell^2}{16\pi^2}\left(\sum_{j=1}^{3}|\gamma_\ell(U_L)_{\ell j}|^2\frac{I_{(1,2)}}{\mu_2} + \sum_{j=4}^{6}|\delta_\ell(U_R)_{\ell j}|^2\frac{I_{(1,2)}}{\mu_2}\right).$$

The integral $I_{(1,2)}$ must be calculated for $m = m_\ell$, the mass of the leptons, $m' = m_j$, the neutrino mass, and $M = \mu_2$, the mass of the scalars. For the case $j = 1,2,3$ $m_j \ll m_\ell \ll \mu_2$ and for $j = 4,5,6$ $m_\ell \ll \mu_2 \ll m_j$, thus in both cases, one can approximate $m_\ell \to 0$, with the solution

$$I_{(1,2)} = M^2\left(\frac{2m'^4 - M^4 + 5m'^2M^2}{6(m'^2-M^2)^3} - \frac{m'^4M^2}{(m'^2-M^2)^4}\ln\left(\frac{m'^2}{M^2}\right)\right) + O(m)$$

and then take the limits $m_j \to 0$ for $j = 1,2,3$, the light neutrinos, yielding $I_{(1,2)} \approx 1/6$ and for $j = 4,5,6$, the heavy neutrinos, yielding $\mu_2 \to 0$. This results in a suppressed integral, so $I_{(1,2)} \approx 0$, respectively. Therefore, we remain with the contribution of the light neutrinos, obtaining

$$a_\ell^{(S^\pm)} \simeq -\frac{m_\ell^2}{96\pi^2}\frac{|\gamma_\ell|^2}{\mu_2^2}. \tag{8.37}$$

Altogether, we obtain with Equations (8.36) and (8.37) the final result for $a_\ell^{(S)}$ with a good approximation

$$
\boxed{\begin{aligned}
a_\ell^{(S)} \simeq \frac{m_\ell^2}{96\pi^2} &\left\{ 2\left|\gamma_\ell\right|^2 \left(\frac{1}{M_3^2} + \frac{1}{M_4^2} \right) \right. && (8.38a)\\
&- 3\,\mathrm{Re}\left(e^{2i\alpha} \gamma_\ell^2 \right) \left[\frac{1}{M_3^2} \left(3 + 2\ln \frac{m_\ell^2}{M_3^2} \right) - \frac{1}{M_4^2} \left(3 + 2\ln \frac{m_\ell^2}{M_4^2} \right) \right] && (8.38b)\\
&\left. - \frac{\left|\gamma_\ell\right|^2}{\mu_2^2} \right\}. && (8.38c)
\end{aligned}}
$$

In summary, the lines (8.38a) and (8.38b) are derived from a loop with leptons, ℓ, with mass m_ℓ, and neutral scalars, either S_3^0 or S_4^0, with mass M_3, M_4, respectively; the photon line attaches to ℓ. Line (8.38c) comes from a loop with a charged scalar, $S_2^\pm$, and light neutrinos, χ, with the external photon attached to $S_2^\pm$; in this line, μ_2 denotes the mass of $S_2^\pm$. We have dropped all terms proportional to m_R^{-2}, especially the contributions from the loop with $S_2^\pm$ and heavy neutrinos. As a test, Equation (8.38) shows that the contributions to the AMM disappear in the decoupling limit of high scalar masses, vis. if $M_3, M_4, \mu_2 \to \infty$.

8.3. Comparison with Experimental Data

Now that we calculated the formula of the AMM, we are ready to test our model, vis. the concerned free parameters, under the limits of the muon and electron AMM given from experiments. The parameters concerned are the scalar masses M_3, M_4, and μ_2, which were analysed in the last chapter and are required to be in the TeV range or higher, i.e. $M_3, M_4, \mu_2 \gtrsim 1\,\mathrm{TeV}$, as well as $M_3 < M_4 = \mu_2$, or instead $M_4 < M_3 = \mu_2$, should be fulfilled. Furthermore, the Yukawa couplings $\Gamma_2 = \mathrm{diag}\left(\gamma_e, \gamma_\mu, \gamma_\tau\right)$ between the charged leptons and the new neutral scalars, S_3^0, S_4^0; or between the leptons and the new charged scalar, $S_2^\pm$, play a role, which is specifically γ_e in case of the electron AMM and γ_μ in the case of the muon AMM. In general, a reasonable parameter range for the Yukawa couplings would be in the order of the other couplings, i.e. $\sim 10^{-6} - 1$ since the smallest Yukawa coupling from the electron $\Gamma_1(e) = \sqrt{2}\, m_e/v \sim$ is 3×10^{-6} and the largest from the top quark $\Gamma_1(t) = \sqrt{2}\, m_t/v \sim 1$.

In the following, we start with the evaluation of the muon AMM and continue with the bound from the precisely measured electron AMM.

Model contributions to the muon anomalous magnetic dipole moment

There is a long-standing discrepancy between the experimental value of the AMM of the muon, a_μ^{exp}, and the theoretical SM value of this AMM, a_μ^{SM} [95]:[7]

$$a_\mu^{\text{exp}} - a_\mu^{\text{SM}} = \begin{cases} (287 \pm 80) \times 10^{-11} \text{ (at } 3.6\,\sigma) \text{ [97]}, \\ (261 \pm 78) \times 10^{-11} \text{ (at } 3.3\,\sigma) \text{ [98]}. \end{cases} \tag{8.39}$$

If this discrepancy indicates new physics, then the contributions of the scalars in our model to the AMM of the muon may be relevant. In this section, we want to fit our model contribution to $a_\mu^{\text{exp}} - a_\mu^{\text{SM}}$ of Equation (8.39) by using $a_\mu^{(S)}$ of Equation (8.38). In the latter equation, there are the neutral scalar masses M_3 and M_4, the charged scalar mass μ_2, the real Yukawa coupling γ_μ, and the phase α, where α is set to zero, i.e. $e^{2i\alpha} = 1$. Then one has

$$a_\mu^{(S)} \simeq -\frac{\gamma_\mu^2}{96\pi^2} \left[\frac{m_\mu^2}{M_3^2} \left(7 + 6 \ln \frac{m_\mu^2}{M_3^2} \right) - \frac{m_\mu^2}{M_4^2} \left(11 + 6 \ln \frac{m_\mu^2}{M_4^2} \right) + \frac{m_\mu^2}{\mu_2^2} \right]. \tag{8.40}$$

The right-hand side of Equation (8.40) is dominated by the two terms with logarithms. One readily sees that the terms with M_4 and μ_2 give negative contributions to $a_\mu^{(S)}$ (assuming γ_μ^2 is positive), while the term with M_3 gives a positive contribution. Since $a_\mu^{\text{exp}} - a_\mu^{\text{SM}}$ is positive, we want the term with M_3 to dominate over the other two; this is achieved with $M_3 < M_4$.

The graphs in Figure 8.5 show how the values of γ_μ have to change when the scale of the new physics, vis. the scalar masses M_3, M_4, μ_2, vary to fit within the experimental boundaries. One determines two things, first, if M_3 is taken to be larger, γ_μ has to be larger as well. Second, if the scalar masses are fully degenerated, vis. if $\Delta M = M_4 - M_3 = 0$, γ_μ must again assume larger values to compensate for the experimental and theoretical discrepancy. Since we argued earlier that we would prefer the Yukawa couplings in the order of the other couplings, this means taking M_3 relatively small, $M_3 = 1\,\text{TeV}$, and a larger discrepancy, e.g. $M_4 = \mu_2 = 2\,\text{TeV}$, as motivated by the calculations of the oblique parameters in the previous chapter. For this case, we find a suitable γ_μ with $\gamma_\mu = 1.7$ and $a_\mu^{(S)} = 261 \times 10^{-11}$, which has the correct sign and absolute value to explain the discrepancy in Equation (8.39). We conclude that our model can fill the gap between a_μ^{exp} and a_μ^{SM} by using reasonable parameters.

Model contributions to the electron anomalous magnetic dipole moment

Further on, the experimental AMM of the electron is in good agreement with the SM prediction for a_e. We must therefore ensure that the non-SM scalars of our model result in $a_e^{(S)}$ smaller than the experimental error 2.6×10^{-13} [93] of a_e. The experimental limits as a function of variations of the scalar masses are shown in Figure 8.6. Thus, even for a

[7]See also Ref. [96] for a recent review.

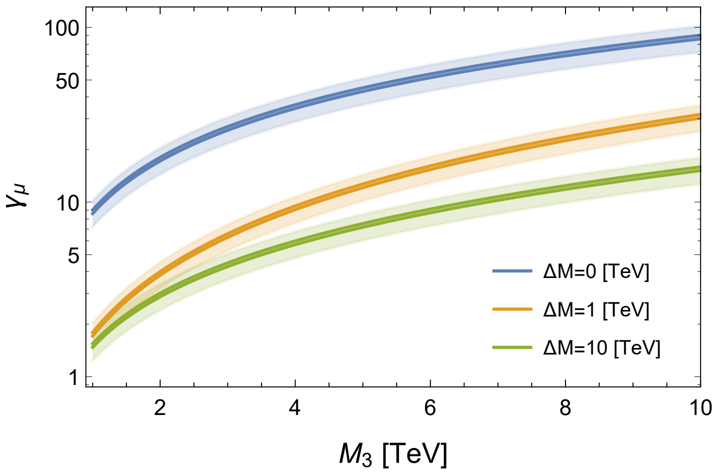

Figure 8.5.: Shown are the two slightly different best-fit values of the experimental constraints on γ_μ from Equation (8.39) fitting the discrepancy between experiment and theory. The shaded regions reflect the errors of the experimental values. The scalar mass M_3 from S_3^0 is varying together with the ones from S_4^0 and $S_2^\pm$, which take the value $M_4 = \mu_2 = M_3 + \Delta M$.

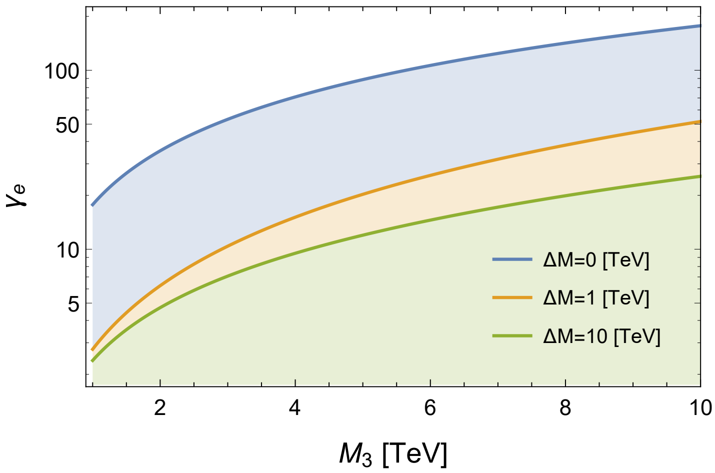

Figure 8.6.: Constraints on γ_e from exp. boundaries are depicted. The allowed region for γ_e is shaded in colour. The scalar mass M_3 of S_3^0 varies together with those of S_4^0 and $S^\pm$, where latter take the value $M_4 = \mu_2 = M_3 + \Delta M$.

relatively large γ_e, $a_e^{(S)}$ can be below the experimental error; this is naturally due to the tiny electron mass. Figure 8.6 shows that the most restrictive bound is achieved with a low mass M_3, which is $M_3 = 1\,\text{TeV}$, and a high mass difference of $\Delta M = M_4 - M_3$, e.g. $\Delta M = 10\,\text{TeV}$. In this case, we would still get an upper bound of $\gamma_e = 2.4$, laying above the preferable parameter range for our Yukawa couplings. We might of course simply take $\gamma_e = 0$, but this would eliminate the FCNI contributions to the decay $\mu^- \to e^- e^+ e^-$

(in the chapter after the next) which we would like to have close to their experimental upper limit. So, we use instead the same scalar masses as before and choose $\gamma_e = 1.7$, obtaining $a_e^{(S)} = 1.0 \times 10^{-13}$, which is below the upper limit of

$$\gamma_e \leq 2.7. \tag{8.41}$$

Concluding remarks

In this chapter, we derived a formula for the leptonic AMM, in which all contributions from right-handed neutrinos are negligible and are therefore approximated to zero. So the free parameters of the formula are reduced to the charged lepton couplings to the new scalars, $\Gamma_2 \sim \gamma_\ell$, and to their masses. This means that this formula is applicable to general 2HDMs, assuming real parameters and a flavour symmetry for the new Yukawa couplings.

To simplify the experimental tests of the next chapters, *we will fix all these parameters to the values used here in this chapter and the previous Chapter 7.2.1*, with the following consideration: Already in the previous Chapter 7.9 we have ascertained that the scalar masses of the new doublet M_3, M_4, μ_2 should be in the TeV range or higher and, additionally, $M_3 < M_4 = \mu_2$. In order to achieve both, a muon-AMM contribution fitting to the discrepancy of the theoretical and experimental value and the Yukawa coupling γ_μ in the range of the other Yukawa couplings, we prefer a small M_3, i.e. $M_3 = 1\,\text{TeV}$. We also set $M_4 = \mu_2 = 2\,\text{TeV}$. We could, of course, assume even higher values for $M_4 = \mu_2$ at $\geq 10\,\text{TeV}$, but as Figure 8.5 shows, at $M_3 = 1\,\text{TeV}$, the difference between a fitting γ_μ at $\Delta M = M_4 - M_3 = 1\,\text{TeV}$ and a fitting γ_μ at $\Delta M = 10\,\text{TeV}$ is not large. Furthermore, we decide to use smaller scalar masses to achieve some effect in the following tests on FCNIs, where we try to bring contributions close to the experimental bounds. For these mentioned scalar masses, the bound from the electron AMM is $\gamma_e \leq 2.7\,\text{TeV}$. In light of this information, we set out the values at

$$M_3 = 1\,\text{TeV}, \quad M_4 = \mu_2 = 2\,\text{TeV}, \tag{8.42a}$$

$$\gamma_\mu = 1.7. \tag{8.42b}$$

Note in Equation (8.42b) that γ_μ is assumed to be real.

8.4. Experimental Status

Finally, let us take a look at the ongoing experiments that detect lepton dipole moments. The electron AMM belongs to the the most precise measurements in electroweak physics, where $a_e = 11596521809.1 \pm 2.6 \times 10^{-13}$ has an accuracy in the order of 10^{-12} [99]. The most accurate value was measured by a group in Cambridge who used a Penning trap to extract the electron AMM from the spin level and frequency of excited electron states [100].

The currently most precise experimental value for the muon AMM of $a_\mu = (g_\mu - 2)/2 = 11659208.9 \pm 5.4 \pm 3.3$ [9] comes from the muon (g-2) experiment, which ran at the Brookhaven National Laboratory until 2001 and worked with the E821 storage ring [101]. This experiment was then transferred to Fermilab, where it got refurbished, and started taking its first data at the end of May 2017. In the experiment, protons from the Tevatron collide with a heavy target and create pions that decay further in a delivery ring. Their decay products, the muons, arrive shortly afterwards in a beam in the Muon g-2 storage ring called E821. In the E821 storage ring, ultracold magnets are used to store the muons until they decay into a positron and two electrons, which are detected by electromagnetic calorimeter detectors. The muon AMM is calculated from the energy and time of the detected positron relative to the injected muon beam, source [102]. The entire procedure just described is shown in Figure 8.7.

Another promising new experiment is the Muon g-2/EDM experiment at JPAC in Japan, which is looking for the muon EDM. It works with ultracold muons, which are accelerated in a linear accelerator. The Muon g-2/EDM group began collecting its first data in October 2017 [103].

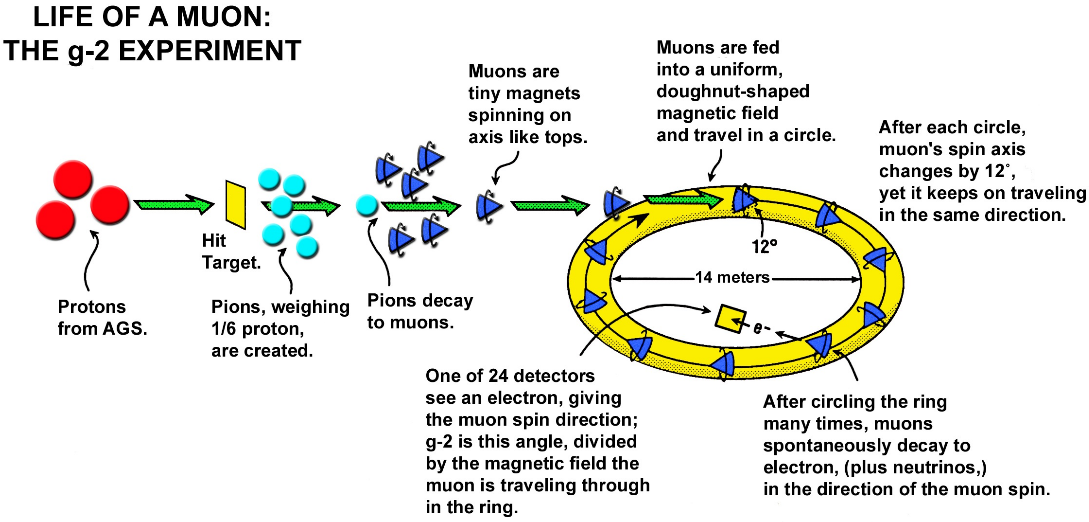

Figure 8.7.: Muon (g-2) experiment at Fermilab [104]

9. Corrections to Neutrino Masses

A characteristic of our model is that it contributes to the experimentally restricted branching rations of lepton FCNIs at one-loop. As stated in Chapter 10, these contributions are strongly determined by heavy right-handed neutrino masses, the latter obviously being related to the light neutrino masses. When calculating these model contributions to the FCNIs, the questions therefore arise: What effects do corrections to the light-neutrino masses have on lepton FCNIs at one-loop? Do these one-loop corrections already impose certain additional restrictions on our parameters? The importance of one-loop corrections to neutrino seesaw models was already pointed out in [105, 106]. In the following we show that one-loop corrections to masses of the light neutrinos within our model shift into corrections to the masses of the heavy right-handed neutrinos, m_4, m_5, m_6, when we fix the masses of light neutrinos, m_1, m_2, m_3, and the mixing matrix $U_\nu \sim U_{PMNS}$ by the given experimental values.[1] These corrections to right-handed neutrino masses in turn have a significant impact on contributions to the FCNIs under certain conditions.

In this Chapter 9, the aim is to calculate and compute one-loop corrections to the light neutrino masses and to analyse their influence on the right-handed neutrino masses. After that, we will continue in Chapter 10 with computing the branching ratios of lepton FCNIs and include both tree-level and one-loop neutrino masses and finally discuss the results. In order to pursue our goal, we need to clarify some points that lead to the following organisation of this chapter: To simplify our calculations of the one-loop corrections to light neutrino masses, we first need to find a way to extract the dominant corrections and neglect the subleading ones, which is done in Section 9.1. With these findings, we are able to perform the actual calculation of this dominant one-loop correction, being δM_L, in the following Section 9.2, which comprises three self-energy diagrams. In the last Section 9.3, the result for δM_L is transformed into corrections of the right-handed neutrino mass, $\hat{m}_R$, and mixing matrix when the light neutrino masses and mixing matrix are fixed to their experimental values. Therefore, δM_L is converted into a formula for $\hat{m}_R$, which then is computed numerically. During the computation, the remaining free parameters are varied and analysed, namely the Yukawa couplings δ_ℓ, d_ℓ, with $\ell \in \{e, \mu, \tau\}$, the light neutrino mass m_1, and $\delta_{CP} \in \{0, \pi\}$.

[1] With a given order of neutrino masses, the light neutrino mass $m_1 \lesssim 0.1\,\mathrm{eV}$ [9] remains as a free parameter.

9.1. Deriving the Relevant Contributions

It is generally known that neutrino masses can also arise from loop corrections to the self-energies, as we mentioned in Chapter 2.5, where various concepts of neutrino mass generation were presented, and so they are do arise in this model framework. To simplify the calculation of these one-loop corrections, we concentrate in this Section 9.1 only on the derivation of the dominant contributions to the neutrino masses. The derivation of these contributions proves to be complicated, so each step in the process is carefully explained.

The determination of dominant and negligible one-loop corrections of the neutrino masses is best done in the flavour space, where the one-loop neutrino mass contributions are written as δM_L, δM_D, and δM_R. We discuss this procedure in the next Section 9.1.1. In Section 9.1.2, we transform these mass corrections into the mass basis to find the relationship to the light neutrino masses, which are the masses we are interested in. As a result, in Section 9.1.3, we obtain an expression for δM_L, δM_D, and δM_R, which allows us to extract them from self-energy diagrams. With these findings, we show in Section 9.1.4 that δM_R and δM_D can be neglected compared to δM_L. Furthermore, Section 9.2 provides another useful approximation for δM_L, being $\delta M_L = U_L^* B_L(0) U_L^\dagger$.

9.1.1. Corrections to neutrino masses in flavour basis

In the analysis of contributions to neutrino masses, a clever approach is to go into the flavour space and later perform a rotation of the masses and their loop contributions into the mass basis, as has been done in [107]. The reason for this is that it is possible in the flavour space to identify the dominant and suppressed contributions and neglect the latter. In this way, we can simplify calculations. Let us therefore follow this approach.

In the flavour space, the neutrino Majorana mass matrix for a Type I Seesaw, M_{D+M}^{tree}, can be retrieved at tree-level from Equation (2.15),

$$\mathcal{L}_{M+D} = -\frac{1}{2}\left(\overline{(\nu_L)^c}, \overline{\nu_R}\right)\underbrace{\begin{pmatrix} 0 & M_D^T \\ M_D & M_R \end{pmatrix}}_{M_{D+M}^{tree}}\begin{pmatrix} \nu_L \\ (\nu_R)^c \end{pmatrix}. \tag{9.1}$$

According to Ref. [107], which extends the work of [108] (and [109]), one-loop corrections on this neutrino mass matrix δM_{D+M} are defined as follows

$$M_{D+M} = \underbrace{\overbrace{\begin{pmatrix} 0 & M_D^T \\ M_D & M_R \end{pmatrix}}^{tree-level}}_{M_{D+M}^{tree}} + \underbrace{\overbrace{\begin{pmatrix} \delta M_L & \delta M_D^T \\ \delta M_D & \delta M_R \end{pmatrix}}^{one-loop}}_{\delta M_{D+M}} \simeq \begin{pmatrix} \delta M_L & M_D^T \\ M_D & M_R \end{pmatrix}. \tag{9.2}$$

We adhere to the notation that each one-loop contribution is marked with δ, i.e. M_D, M_R are tree-level matrices. To avoid lengthy formulas, each mass not marked as tree-level, besides M_D and M_R, contains both tree-level and one-loop contributions. The left-handed Majorana neutrino mass, M_L, at tree-level is zero,[2] as can be seen in the upper left corner of M_{D+M}^{tree}, but receives a non-zero contribution at one-loop level, namely δM_L. A nice side effect of the condition $M_L^{tree} = 0$ is that one cannot assign counterterms for this mass and therefore the one-loop correction δM_L should be finite.

At this point, we have already indirectly revealed in Equation (9.2) one of the main outcomes of this whole Section 9.1, namely that the dominant one-loop correction is δM_L.

9.1.2. Rotation of the flavour mass matrix into a mass basis

Let us find out how these one-loop corrections in Equation (9.2) are related to the light or heavy masses by diagonalizing M_{M+D}, i.e. by rotating them into the mass basis. From Section 2.3.3, it should be remembered that this rotation is carried out in two steps [28]. The first step is the block diagonalization according to Equation (2.23) with a separation into the small, M_ν, and large mass matrix, M_N, followed by a separate diagonalization of M_ν and M_N in a second step. For our purposes, the first transformation step will be sufficient. This is performed using the transformation matrix

$$D \simeq \begin{pmatrix} \mathbb{1} & (M_R^{-1} M_D)^\dagger \\ -M_R^{-1} M_D & \mathbb{1} \end{pmatrix}, \quad \text{i.e.} \quad D^T M_{D+M} D = \begin{pmatrix} M_\nu & 0 \\ 0 & M_N \end{pmatrix}. \tag{9.3}$$

With Equations (9.3) and (9.2), we get the complete form for the small and large mass matrix, including tree-level and one-loop contributions,

$$M_N \simeq M_R - M_\nu^{tree} - \delta M_\nu \simeq M_R, \tag{9.4}$$

$$M_\nu \simeq \underbrace{-M_D^T M_R^{-1} M_D}_{M_\nu^{tree}} + \underbrace{\delta M_L - \delta M_D^T M_R^{-1} M_D - M_D^T M_R^{-1} \delta M_D + M_D^T M_R^{-1} \delta M_R M_R^{-1} M_D}_{\delta M_\nu}. \tag{9.5}$$

Since we know that right-handed neutrino masses are not experimentally limited and therefore their parameters are adjustable, it is clear that corrections to $\hat{m}_R$ and thus to M_N are irrelevant. *For this reason, in the following, we will concentrate only on corrections of the light neutrino masses, i.e. on corrections to* M_ν. In Equation (9.5), M_ν consists of a tree-level contribution and one-loop corrections proportional to δM_L, δM_D, and δM_R. Let us therefore examine these last three contributions in more detail in order to make statements about their significance.

The mass corrections in the flavour basis δM_L, δM_D, and δM_R are part of neutrino self-energy diagrams, $\Sigma(p)$ and can be calculated through them. The self-energy diagrams include all one-loop contributions in the mass basis. The relationship between δM_L, δM_D, and $\Sigma(p)$ is simply defined by rotating the former, vis. δM_{D+M} from Equation (9.2), into the mass basis. This is done with the full two-step rotation via the unitary

[2] M_L is prohibited at tree level due to gauge invariance.

matrix U; according to Equations (2.25) and (2.26), it is then

$$U^T \delta M_{D+M} U = \Sigma(p), \quad \text{with} \quad U = \begin{pmatrix} U_L \\ U_R^* \end{pmatrix}. \tag{9.6}$$

Therefore, the one-loop corrections can be written as part of the self-energy [107]:

$$\delta M_L = U_L^* \, \Sigma(p) \, U_L^\dagger, \qquad \delta M_D = U_R \, \Sigma(p) \, U_L^\dagger, \qquad \delta M_R = U_R \, \Sigma(p) \, U_R^T. \tag{9.7}$$

In the following, we will continue to derive all possible one-loop Feynman diagrams of the neutrino self-energy within this model, using the results from the self-energies of [107] and [110] to determine δM_L, δM_D, and δM_R.

9.1.3. Mass contributions from Feynman diagrams

Neutrino interactions with SM particles are mediated by the weak interacting $W^\pm$ and Z bosons as well as by the Higgs boson. In our model adds additionally the new scalars S_b^0 and $S_a^\pm$, which can interact with neutrinos. Therefore, the one-loop contributions δM_L, δM_D, and δM_R can only be generated from neutrino self-energies under consideration of these interactions. The corresponding Feynman diagrams[3] contain a Z^0 and S_b^0 loop with $b \in \{2, 3, 4\}$ (remember $S_2^0 = H^0$),

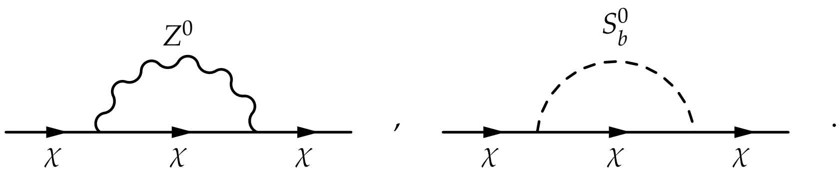

(9.8)

Both diagrams lead to corrections of δM_L (after a thorough analysis of [107]), while the diagram with the neutral scalars also contributes to δM_D.[4] Further Feynman diagrams are the following two self-energies

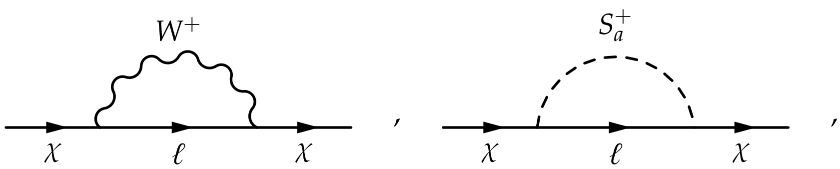

(9.9)

where the W^+ boson loop contributes to δM_L. The diagram with a charged scalar running in the loop exhibits only contributions to δM_D [107]. As we will conclude in the next Subsection 9.1.4, the first two Feynman diagrams in Equation (9.8) are the dominant corrections of the light neutrino mass matrix M_ν, while the other two diagrams lead to negligible corrections.

[3] The Feynman diagrams of this model can be found in the Appendix, Chapter D.

[4] The Z–boson does not lead to a contribution to δM_D as it does not have a $U_R^\dagger U_L$ combination, according to Equation (9.7).

9.1.4. Dominating neutrino mass corrections

Now the way is paved for arguing about subdominant corrections of the neutrino masses. As we have already explained in Subsection 9.1.2, we are interested in one-loop contributions to the light neutrino masses, M_ν. Furthermore, we can see in Equation (9.5) that contributions to M_ν that are proportional to δM_R are suppressed by the square of the Seesaw scale, m_R^{-2}, and are therefore negligible. However, one-loop corrections to δM_R are zero anyway [110]. Moreover, when calculating the contributions of δM_D via the self-energy diagrams with S_b^0 and $S_a^\pm$ (the diagrams on the right in Equations (9.8) and (9.9)), it turns out that δM_D is proportional to a Yukawa coupling $Y \in \{\Gamma, \Delta\}$ and the lepton mass m_ℓ, i.e. $\delta M_D \sim Y^2 m_\ell$, see [107]. The lepton mass is proportional to the scale of the Dirac particles $m_\ell \sim m_D$, which is below the electroweak scale m_{EW}. Therefore, the corrections to δM_D of M_ν given in Equation (9.5) are in the order of magnitude $\sim Y^2 m_D^2/m_R$, which is also suppressed by the large seesaw scale m_R, unlike the remaining δM_L contributions. All in all, M_ν consists mainly of the tree-level contributions with a small corrections at one-loop, where latter is to a good approximation dominated by δM_L. Thus the corrections are

$$\boxed{M_\nu = M_\nu^{tree} + \delta M_L} \,. \tag{9.10}$$

Let us therefore only focus on δM_L which is determined from the self-energy using the formula $\delta M_L = U_L^* \Sigma(p) U_L^\dagger$. The self-energy, $\Sigma(p)$, can in turn be specified as follows. Corrections to neutrino masses by means of self-energy diagrams, as we depicted them in Equations (9.8) and (9.9), are corrections of the neutrino propagator; whereby the latter consists of the sum over all one-particle irreducible diagrams with two external lines [26] and can be summarized with the aid of the geometric series,

$$\begin{aligned}\int d^4x\, \langle|\nu(x)\nu(0)|\rangle e^{ipx} &= \frac{i}{\not{p} - m_0} + \frac{i}{\not{p} - m_0}\left(\frac{\Sigma(p)}{\not{p} - m_0}\right) + \frac{i}{\not{p} - m_0}\left(\frac{\Sigma(p)}{\not{p} - m_0}\right)^2 + \ldots \\ &= \frac{i}{\not{p} - m_0 - \Sigma(p)},\end{aligned}$$

Thus, the self-energy $\Sigma(p)$ can include parts that are proportional to $\not{p}$ and m. Moreover, $\Sigma(p)$ for Seesaw masses can be divided into chiral parts [107], which leads to the following decomposition,

$$\Sigma(p) = A_L(p)\not{p}\gamma_L + A_R(p)\not{p}\gamma_R + B_L(p)\gamma_L + B_R(p)\gamma_R. \tag{9.11}$$

At this point, we can once again make some statements about negligible contributions to Σ and thus to δM_L. First of all, notice that due to the unitarity of $\Sigma(p)$, $A_{L/R}^\dagger = A_{L/R}$ and $B_L^\dagger = B_R$. Furthermore, all neutrino self-energies are contributions to the neutrino Majorana masses, therefore, they have to obey the laws set by the Majorana condition $\chi = \chi^c$, which are[5] $\Sigma(p) = C\left[\Sigma(-p)\right]^T C^T$ [107] and thus $A_L = A_R^T$ and $B_{L/R} = B_{L/R}^T$.

[5] For a self-energy $\Sigma(p) = \overline{\chi} M(p)\chi$, it is with (A.7) and (A.9) $\overline{\chi} M(p)\chi = \overline{(\chi^c)} M(-p)\chi^c = -\chi^T C^{-1} M(-p)\, C\left(\overline{\chi}\right)^T = \overline{\chi} C\left[M(-p)\right]^T C^{-1}\chi$ and thus $M(p) = C\left[M(-p)\right]^T C^{-1}$, which applies equivalent to $\Sigma(p)$.

From this, we conclude that B_L contains the same information as B_R, as well as A_L as A_R. Thus, Equation (9.11) reduces to $\Sigma(p) = \not{p} A_L(p)\gamma_L + B_L(p)\gamma_L$. Furthermore, we know that the self-energy has the largest value at the pole mass, $p \sim m_\nu \lesssim m_D^2/m_R$, which can be approximated to $p \simeq 0$. Therefore, contributions to $\not{p} A_{L/R}$ are suppressed with the scale of the right-handed neutrino mass m_R and are thus negligible. This condition is certainly valid for the self-energy diagram with the $W^{\pm}$-boson exchange, which contains an additional momentum factor, and therefore has the form $\not{p} A_{L/R} \sim 0$, see the explicit formula in [107]. This leaves us with $\Sigma(0) = B_L(0)\gamma_L$ and hence we finally get the desired formula for δM_L,

$$\boxed{\delta M_L = U_L^* B_L(0) U_L^\dagger}\,, \tag{9.12}$$

comprising contributions from the two self-energy diagrams with neutral scalar S_b^0 and Z^0-boson exchange, as shown in (9.8).

9.2. Calculating Neutrino One-Loop Mass Corrections

The aim of the following sections is to determine the full form of M_ν, i.e. in particular to derive the one-loop contribution δM_L from self-energy diagrams with the help of Equation (9.12).

As mentioned above, the calculation of the finite one-loop neutrino mass correction δM_L includes contributions from the Z^0 boson, the Goldstone boson G^0, and the scalars S_b^0,

$$\delta M_L = \delta M_L^{(Z^0)} + \delta M_L^{(G^0)} + \delta M_L^{(S_b^0)}\,. \tag{9.13}$$

These are explicitly derived in R_ξ gauge in [111], [110], and [107] and shall therefore only be briefly presented here in Feynman gauge,[6] where the following applies:

$$\xi_A = \xi_Z = \xi_W = 1\,.$$

For all further calculations in this section, the following points will be considered:

- On the basis of Equations (9.12) and (9.11), we consider only contributions that are proportional to $B_L(0)$ and thus to γ_L, and leave all other terms out of account.
- The dominant contribution of the neutrino propagator in the loop with momentum k occurs at the on-shell limit when $k = m_\nu \simeq 0$, so we neglect all terms proportional to $\not{k}$. Thus, the neutrino momentum of the external neutrinos p on the mass-shell is also approximately zero, $p = m_\nu \simeq 0$ and contributions proportional to $\not{p} A_{L/R}$ can be neglected, see Section 9.1.4.

[6] The Feynman diagrams to this model can be found in Appendix D.

- The calculation of each of the three parts in Equation (9.13) is straightforward and encounters similar integration. Therefore, let us calculate it here beforehand and refer to it later. The common form of integrals is rewritten with Feynman parameters,

$$
\begin{aligned}
&\frac{d^d k}{(2\pi)^d}\frac{1}{(k^2-m_\ell^2)((k-p)^2-m_Z^2)} \\
&\quad = \frac{d^d k}{(2\pi)^d}\int dx\,\frac{1}{[x(k^2-m_\ell^2)+(1-x)((p-k)^2-m_Z^2)]^2} = \frac{d^d k}{(2\pi)^d}\int dx\,\frac{1}{[l^2-\Delta]^2}, \\
&\quad \text{with}\quad l = k-(1-x)p,\ \Delta_\ell = (1-x)(m_Z^2-xp^2)+xm_\ell^2. \qquad (9.14)
\end{aligned}
$$

Using a Wick rotation, Equations (C.3) and (C.5), we obtain for the integral

$$
\begin{aligned}
\int \frac{d^d\ell}{(2\pi)^d}\int dx\,\frac{1}{\left[\ell^2-\Delta\right]^2} &= i\int \frac{d^d\ell}{(2\pi)^d}\int dx\,\frac{1}{\left[\ell^2+\Delta\right]^2} \\
&= \int dx\,\frac{i}{(4\pi)^2}\left(\frac{2}{\epsilon}-\gamma_E+\ln\left(\frac{4\pi}{\Delta}\right)\right) = -\int dx\,\frac{i}{(4\pi)^2}\left(\ln\Delta+\eta+1\right), \qquad (9.15)
\end{aligned}
$$

and the like

$$
\begin{aligned}
\int \frac{d^d\ell}{(2\pi)^d}\int dx\frac{d}{\left[\ell^2-\Delta\right]^2} &= \int dx\frac{i}{4\pi^2}\left(\frac{2}{\epsilon}-\gamma_E-\frac{1}{2}+\ln\left(\frac{4\pi}{\Delta}\right)\right) \\
&= -\int dx\frac{i}{4\pi^2}\left(\ln\Delta+\eta+\frac{3}{2}\right), \qquad (9.16)
\end{aligned}
$$

where we call the infinite part $\eta = -\frac{2}{\epsilon}+\gamma_E-\ln(4\pi)-1$, where γ_E is the Euler-Mascheroni constant.

- Due to a leaner notation, we will write the equations leading to the next step above the equal sign, e.g. $\overset{(9.12)}{=}$.

- Further, it is $m_W^2 = c_W^2 m_Z^2$, Equation (3.14), with $c_W = \cos(\theta_W)$, the weak mixing angle.

- From
$$\int_0^1 dx\ln(ax+b) = \ln(a+b)+\frac{b}{a}\ln\left(\frac{a+b}{b}\right)-1, \qquad (9.17)$$
follows
$$\int dx\ \ln\Delta = \ln(m_\ell^2)+\frac{m_Z^2}{m_\ell^2-m_Z^2}\ln\left(\frac{m_\ell^2}{m_Z^2}\right)-1. \qquad (9.18)$$

- The relationships of the mixing matrices from Equations (2.27c) and (2.27b) are very useful, in particular

$$
\begin{aligned}
&U_L U_L^\dagger = \mathbb{1}_{3\times 3} = U_R U_R^\dagger, \quad U_L U_R^T = 0, && \text{(9.19a)}\\
&U_L^* \hat{m} U_L^\dagger = 0\,(= M_L), && \text{(9.19b)}\\
&U_R \hat{m} U_R^T = M_R, && \text{(9.19c)}\\
&U_R \hat{m} U_L^\dagger = M_D \;\Leftrightarrow\; U_R \hat{m} = M_D U_L. && \text{(9.19d)}
\end{aligned}
$$

9.2.1. Z^0 boson contribution

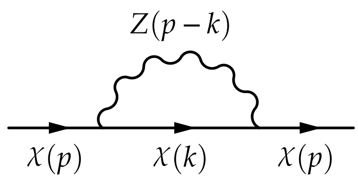

(9.20)

The one-loop contribution to the light neutrino masses from the Z^0-boson exchange is

$$
\begin{aligned}
-i\Sigma^{(Z^0)}(p^2=0) = &-\frac{g^2}{4c_W^2}\int\frac{d^dk}{(2\pi)^d}\sum_\ell\left[\gamma_R(U_L^\dagger U_L)_{i\ell}-\gamma_L(U_L^T U_L^*)_{i\ell}\right]\frac{\gamma^\mu(\not{k}+m_\ell)g_{\mu\nu}\gamma^\nu}{(k^2-m_\ell^2)((k-p)^2-m_Z^2)}\\
&\times\left[\gamma_L(U_L^\dagger U_L)_{\ell j}-\gamma_R(U_L^T U_L^*)_{\ell j}\right]\\
=&\frac{g^2\gamma_L}{4c_W^2}\sum_\ell(U_L^T U_L^*)_{i\ell}\,m_\ell\left(\int\frac{d^dk}{(2\pi)^d}\frac{d}{(k^2-m_\ell^2)(k^2-m_Z^2)}\right)(U_L^\dagger U_L)_{\ell j}, \quad \text{(9.21)}
\end{aligned}
$$

where m_ℓ is the mass of the neutrino in the loop. From this, we can determine the corresponding contribution to δM_L via Equation (9.12). After applying Equation (9.14), where $\Delta_\ell = m_Z^2 + x(m_\ell^2 - m_Z^2)$, we obtain the following

$$
\begin{aligned}
\delta M_L^{(Z^0)} &\stackrel{(9.12)}{=} -\frac{g^2}{4c_W^2}\sum_\ell (U_L^*)_{i\ell}\,m_\ell\left(\int dx\int\frac{d^dl}{(2\pi)^d}\frac{d}{[l^2+\Delta_\ell]^2}\right)(U_L^\dagger)_{\ell j}\\
&\stackrel{(9.16)}{=} -\frac{g^2 m_Z^2}{(4\pi)^2 m_W^2}\sum_\ell (U_L^*)_{i\ell}\,m_\ell\left(\frac{2}{\epsilon}-\gamma_E-\frac{1}{2}+\ln(4\pi)-\int x\ln(\Delta_\ell)\right)(U_L^\dagger)_{\ell j}\\
&\stackrel{(9.18)}{=} \frac{g^2 m_Z^2}{16\pi^2 m_W^2}U_L^*\,\hat{m}\left(\eta+\frac{1}{2}+\ln(\hat{m}^2)+\frac{m_Z^2}{\hat{m}^2-m_Z^2}\ln\left(\frac{\hat{m}^2}{m_Z^2}\right)\right)U_L^\dagger\\
&\stackrel{(9.19b)}{=} \frac{g^2 m_Z^2}{16\pi^2 m_W^2}U_L^*\,\hat{m}\left(\ln(\hat{m}^2)+\frac{m_Z^2}{\hat{m}^2-m_Z^2}\ln\left(\frac{\hat{m}^2}{m_Z^2}\right)\right)U_L^\dagger\\
&\stackrel{7}{=} \frac{g^2}{16\pi^2 m_W^2}U_L^*\,\frac{\hat{m}^3 m_Z^2}{\hat{m}^2-m_Z^2}\ln\left(\frac{\hat{m}^2}{m_Z^2}\right)U_L^\dagger. \qquad \text{(9.22)}
\end{aligned}
$$

The final result for $\delta M_L^{(Z^0)}$ reads

$$\boxed{\delta M_L^{(Z^0)} = \frac{g^2}{16\pi^2 m_W^2} U_L^* \frac{\hat{m}^3 m_Z^2}{\hat{m}^2 - m_Z^2} \ln\left(\frac{\hat{m}^2}{m_Z^2}\right) U_L^\dagger} \,. \tag{9.23}$$

9.2.2. G^0 Goldstone boson contribution

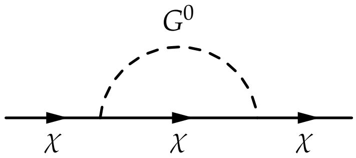

(9.24)

The self-energy with a Goldstone boson in the loop is given by

$$-i\Sigma^{(G^0)} = -\frac{g^2\gamma_L}{4m_W^2} \sum_\ell \underbrace{(U_R^\dagger M_D U_L + U_L^T M_D^T U_R^*)}_{\tilde{F}_1}{}_{i\ell}\, m_\ell \left(\int \frac{d^dk}{(2\pi)^d} \frac{1}{(k^2 - m_\ell^2)(k^2 - m_Z^2)} \right) (\tilde{F}_1)_{\ell j}. \tag{9.25}$$

To receive the part belonging to δM_L via Equation (9.12), one can contract $U_L^* \tilde{F}_1 = M_D^T U_R^*$ and $\tilde{F}_1 U_L^\dagger = U_R^\dagger M_D$ using Equation (9.19a). Now by employing Equations (9.14),(9.15), and (9.18), we get

$$\begin{aligned} \delta M_L^{(G^0)} &= -\frac{g^2}{64\pi^2 m_W^2} M_D^T U_R^* \hat{m} \left(k + \ln(\hat{m}^2) + \frac{m_Z^2}{\hat{m}^2 - m_Z^2} \ln\left(\frac{\hat{m}^2}{m_Z^2}\right) \right) U_R^\dagger M_D \\ &\overset{(9.19d)}{=} \underbrace{-\frac{g^2}{64\pi^2 m_W^2} U_L^* \left(\frac{\hat{m}^3 m_Z^2}{\hat{m}^2 - m_Z^2} \ln\left(\frac{\hat{m}^2}{m_Z^2}\right) \right) U_L^\dagger}_{\delta M_L'^{(G^0)}} \underbrace{- \frac{g^2}{64\pi^2 m_W^2} M_D^T U_R^* \hat{m} \left(\eta + \ln(\hat{m}^2) \right) U_R^\dagger M_D}_{\delta M_L''^{(G^0)}} . \end{aligned} \tag{9.26}$$

---

[7] Since relation (9.19b) holds, each term with $U_L^* \hat{m} U_L^\dagger = 0$ can be added or subtracted, see [111]

$$\begin{aligned} \hat{m}\left(\ln(\hat{m}^2) + \frac{m_Z^2}{\hat{m}^2 - m_Z^2} \ln\left(\frac{\hat{m}^2}{m_Z^2}\right) \right) &= \frac{\hat{m}}{\hat{m}^2 - m_Z^2} \left(\hat{m}^2 \ln(\hat{m}^2) - m_Z^2 \ln(m_Z^2) + \underbrace{m_Z^2 \ln(m_Z^2) - \hat{m}^2 \ln(m_Z^2)}_{\text{added terms}} \right) \\ &= \frac{\hat{m}^3}{\hat{m}^2 - m_Z^2} \ln\left(\frac{\hat{m}^2}{m_Z^2}\right). \end{aligned}$$

.

The result is,

$$\boxed{\delta M_L'^{(G^0)} = -\frac{g^2}{64\pi^2 m_W^2} U_L^* \left(\frac{\hat{m}^3 m_Z^2}{\hat{m}^2 - m_Z^2} \ln\left(\frac{\hat{m}^2}{m_Z^2}\right)\right) U_L^\dagger} \,. \tag{9.27}$$

One can see that $\delta M_L^{(Z^0)} = -4\,\delta M_L'^{(G^0)}$.

9.2.3. S^0 scalar contribution

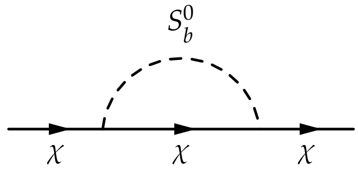

(9.28)

The last contribution is due to the self-energy with the neutral scalar in the loop, for which we receive

$$-i\Sigma^{(S^0)} = \frac{\gamma_L}{2} \sum_\ell \underbrace{(U_R^\dagger \hat{\Delta}_b U_L + U_L^T \hat{\Delta}_b^T U_R^*)_{i\ell}}_{\tilde{F}_b} m_\ell \left(\int \frac{d^d k}{(2\pi)^d} \frac{1}{(k^2 - m_\ell^2)(k^2 - M_b^2)} \right) (\tilde{F}_b)_{\ell j}.$$

To extract δM_L with Equation (9.12), we can use a similar contraction as before for the self-energy with the Goldstone boson, $U_L^* F_b = \hat{\Delta}_b^T U_R^*$ and $F_b U_L^\dagger = U_R^\dagger \hat{\Delta}_b$ with Equation (9.19a). After applying Equations (9.14), (9.15), and (9.18), we obtain

$$\begin{aligned}
\delta M_L^{(S^0)} =& \frac{1}{32\pi^2} \hat{\Delta}_b^T U_R^* \hat{m} \left(k + \ln(\hat{m}^2) + \frac{M_b^2}{\hat{m}^2 - M_b^2} \ln\left(\frac{\hat{m}^2}{M_b^2}\right)\right) U_R^\dagger \hat{\Delta}_b \\
=& \underbrace{\frac{1}{32\pi^2} \hat{\Delta}_b^T U_R^* \left(\frac{M_b^2\, \hat{m}}{\hat{m}^2 - M_b^2} \ln\left(\frac{\hat{m}^2}{M_b^2}\right)\right) U_R^\dagger \hat{\Delta}_b}_{\delta M_L'^{(S^0)}} + \underbrace{\frac{1}{32\pi^2} \hat{\Delta}_b^T U_R^* \hat{m} \left(\eta + \ln(\hat{m}^2)\right) U_R^\dagger \hat{\Delta}_b}_{\delta M_L''^{(S^0)}} .
\end{aligned} \tag{9.29}$$

The final result is,

$$\boxed{\delta M_L'^{(S^0)} = \frac{1}{32\pi^2} \hat{\Delta}_b^T U_R^* \left(\frac{M_b^2\, \hat{m}}{\hat{m}^2 - M_b^2} \ln\left(\frac{\hat{m}^2}{M_b^2}\right)\right) U_R^\dagger \hat{\Delta}_b} \,. \tag{9.30}$$

9.2.4. Adding all one-loop mass corrections

The sum of all diagrams in *Feynman gauge* finally results in

$$\delta M_L = \delta M_L'^{(S^0)} + \delta M_L^{(Z^0)} + \delta M_L'^{(G^0)}. \tag{9.31}$$

Note that the second term of the scalar contribution $\delta M_L''^{(S^0)}$ in Equation (9.29) is cancelled with the second term of the Goldstone boson $\delta M_L''^{(G^0)}$ in Equation (9.26). To see that $\delta M_L''^{(S^0)} = -\delta M_L''^{(G^0)}$, one has to rewrite the terms using the orthogonality relation $\sum_{b\neq 1} V_{ib} V_{bj} + V_{i1} V_{1j} = 0$. If we also apply Equations (3.20c), (3.10), together with Equations (3.14) and (3.18), which are listed here once again sequentially

$$\hat{\Delta}_b = \sum_i V_{kb} \Delta_k, \tag{9.32a}$$

$$V_{k1} = i g v_k/(2 m_W), \tag{9.32b}$$

$$M_D = \frac{1}{\sqrt{2}} \sum_k v_k \Delta_k, \tag{9.32c}$$

we can see that the neutrino Yukawa couplings to the neural scalars $\hat{\Delta}_b$ can be rewritten in terms of the neutrino Yukawa coupling to the neutral Goldstone boson $\hat{\Delta}_1$, which can be expressed by the Dirac mass M_D:

$$\hat{\Delta}_1 \overset{(9.32a)}{=} \sum_k V_{1k}\, \Delta_k \overset{(9.32b)}{=} \sum_k \frac{ig}{2\, m_W} v_k\, \Delta_k \overset{(9.32c)}{=} \frac{ig}{\sqrt{2}\, m_W} M_D, \tag{9.33}$$

$$\begin{aligned}\sum_{b\neq 1} \hat{\Delta}_b^T\, \mathcal{M}\, \hat{\Delta}_b &= \sum_{b\neq 1} \sum_{ij} \Delta_i V_{ib}\, \mathcal{M}\, V_{bj} \Delta_j = \sum_{1} \sum_{ij} \Delta_i V_{i1}\, \mathcal{M}\, V_{1j} \Delta_j \\ &= \sum_1 \hat{\Delta}_1^T\, \mathcal{M}\, \hat{\Delta}_1 = \frac{g^2}{2 m_W^2} M_D^T\, \mathcal{M}\, M_D. \end{aligned} \tag{9.34}$$

Finally, $\delta M_L''^{(S^0)}$ can be reworded as follows

$$\begin{aligned}\delta M_L''^{(S^0)} &= \frac{1}{32\pi^2} \hat{\Delta}_b^T U_R^* \hat{m} \left(\eta + \ln(\hat{m}^2)\right) U_R^\dagger \hat{\Delta}_b \\ &\overset{(9.34)}{=} \frac{g^2}{64\pi^2 m_W^2} M_D^T U_R^* \hat{m} \left(\eta + \ln(\hat{m}^2)\right) U_R^\dagger M_D = -\delta M_L''^{(G^0)}.\end{aligned}$$

On the other hand, for δM_L using Equations (9.23), (9.27), and (9.30), we get

$$\delta M_L = \sum_{b\neq 1} \frac{M_b^2}{32\pi^2} \hat{\Delta}_b^T U_R^* \left(\frac{\hat{m}}{\hat{m}^2 - M_b^2} \ln \frac{\hat{m}^2}{M_b^2} \right) U_R^\dagger \hat{\Delta}_b + \frac{3g^2}{64\pi^2 m_W^2} U_L^* \left(\frac{\hat{m}^3 m_Z^2}{\hat{m}^2 - m_Z^2} \ln \left(\frac{\hat{m}^2}{m_Z^2} \right) \right) U_L^\dagger.$$

This equation can be further brought into a form that is more appropriate for later computations. We would like to express the neutrino mixing matrices U_L and U_R in the form of the mixing matrix U_N of right-handed neutrinos, and $\hat{m}$ with $\hat{m}_R$. This can be achieved by approximating $U_R^* \simeq (0, U_N)$ on the basis of Equation (2.26). If we now use Equation (9.19c) and $\hat{m} = \text{diag}(\hat{m}_\nu, \hat{m}_R)$, we obtain $M_R = U_R \hat{m} U_R^T \simeq U_N^* \hat{m}_R U_N^\dagger$. Moreover, considering Equation (9.19d), which leads to $\hat{m}\, U_L^\dagger = U_R^\dagger M_D$ ($m_W = gv/2$ through Equation (3.14)), we finally get

$$\boxed{\delta M_L = \sum_{b\neq 1} \frac{M_b^2}{32\pi^2} \hat{\Delta}_b^T U_N \left(\frac{\hat{m}_R}{\hat{m}_R^2 - M_b^2} \ln \frac{\hat{m}_R^2}{M_b^2} \right) U_N^T \hat{\Delta}_b + \frac{3\, m_Z^2}{16\pi^2 v^2} M_D^T U_N \left(\frac{\hat{m}_R}{\hat{m}_R^2 - m_Z^2} \ln \frac{\hat{m}_R^2}{m_Z^2} \right) U_N^T M_D} \,. \tag{9.35}$$

To verify this formula, we want to perform a short dimensional analysis: If the Standard Model is treated as an effective theory with a new physics sector, the decoupling theorem [112, 113] states that the new physics has to decouple as soon as the scale of the new physics goes to infinity. In our framework, this is achieved by setting the Seesaw scale m_R and the new scalar masses M_3, M_4 to infinity.

- The case $m_R \to \infty$ means $\hat{m}_R \to \infty$ and consequently, both the first and the second terms of Equation (9.35) disappear.
- If $M_{3,4} \to \infty$, the sum in the first term on the right-hand side of Equation (9.35) totals over the physical neutral scalars $b \in \{2, 3, 4\}$, where $M_2 = m_H$ is the SM Higgs mass. The other two terms with M_3 and M_4 are the scalars of the second doublet, therefore, they have the same Yukawa couplings in the scalar mass basis, but differ by an imaginary number i: $\hat{\Delta}_3 = \Delta_2$, $\hat{\Delta}_4 = i\Delta_2$. Since $\delta M_L \propto \hat{\Delta}_b^2$, the two terms cancel each other out when $M_3 = M_4$, which is a good approximation in the limit $M_{3,4} \to \infty$. Consequently, as expected, only the terms with the SM Higgs and the second term of Equation (9.35) remain.

9.3. Analysing Loop Contributions to Neutrino Masses with Concrete Data

Now we are ready to perform an analysis of the neutrino masses with concrete data input. For this purpose, we will use input data from neutrino experiments, namely the light neutrino mass matrix $\hat{m}_\nu = \text{diag}(m_1, m_2, m_3)$ (with m_1 as a free parameter) and the neutrino mixing matrix $U_\nu \sim U_{PMNS}$. Since the masses of the light neutrinos are fixed, δM_L introduces corrections to the *right-handed* neutrino masses $\hat{m}_R = \text{diag}(m_4, m_5, m_6)$ and the mixing matrix U_N, which are the remaining free parameters, receiving in this way indirect corrections. Therefore, right-handed neutrino masses will be the focus of our interest from now on.

The organisation of this section is as follows. We have to solve the formulas of mass corrections for the right-handed neutrino masses $\hat{m}_R$. This will be done in the next two sections, at tree-level in Section 9.3.1 and at one-loop level in Section 9.3.2. In this course, we will also describe the numerical computation process in the latter section, which uses the tree-level data as starting values. Subsequently, we search in Section 9.3.3 for suitable parameter ranges of the remaining free model parameters, in order to proceed according to the qualitative method presented in Chapter 6.3 and in Section 9.3.4 to perform a parameter analysis of the right-handed neutrino masses with one-loop corrections.

9.3.1. Right-handed neutrino masses at tree-level

In this section, the aim is to obtain a formula for the masses of the right-handed neutrinos at tree-level. The resulting tree-level values for $\hat{m}_R$ and the corresponding mixing matrix U_N are used as starting values for the numerical determination of the one-loop values of $\hat{m}_R$ and U_N described in the next section.

The tree-level mass matrix of the light neutrinos is obtained by the Seesaw formula. In our notation, using Formula (9.5), it reads reads

$$M_\nu^{tree} = -M_D^T M_R^{-1} M_D = -\frac{v^2}{2}\,\Delta_1 M_R^{-1}\Delta_1, \tag{9.36}$$

where $\Delta_1 = \mathrm{diag}\left(d_e, d_\mu, d_\tau\right)$ is diagonal according to Equation (4.4a). By inverting Equation (9.36), we obtain an expression for the right-handed matrix

$$M_R = -\frac{v^2}{2}\,\Delta_1 \left(M_\nu^{tree}\right)^{-1}\Delta_1. \tag{9.37}$$

The matrix M_ν^{tree} is diagonalized further

$$U_\nu^T M_\nu^{tree} U_\nu = \mathrm{diag}\left(m_1, m_2, m_3\right) \equiv \hat{m}_\nu, \tag{9.38}$$

see Equation (2.24), where $m_{1,2,3}$ are the light-neutrino masses, remember $U_\nu = e^{i\hat{\alpha}}\,U_{\mathrm{PMNS}}\,e^{i\hat{\beta}}$, (2.17). Using Equations (9.37) and (9.38) together with the fact that the matrices Δ_1, $\hat{m}_\nu$, $e^{i\hat{\alpha}}$ and $e^{i\hat{\beta}}$ are diagonal, we obtain the final formula for the right-handed neutrinos at tree-level

$$M_R = -\frac{v^2}{2}\,e^{i\hat{\alpha}}\Delta_1\,U_{\mathrm{PMNS}}\left(e^{2i\hat{\beta}}\hat{m}_\nu^{-1}\right)U_{\mathrm{PMNS}}^T\,\Delta_1 e^{i\hat{\alpha}}. \tag{9.39}$$

M_R can be further diagonalized with the mixing matrices U_N, according to[8]

$$U_N^T M_R U_N = \hat{m}_R. \tag{9.40}$$

A dimensional analysis of the right-handed mass yields

$$m_R \sim -d_\ell^2 \frac{v^2}{2\,m_\nu}. \tag{9.41}$$

Based on this formula, we get a lower limit for m_R, e.g. for $d_\ell \sim 0.01$, we get $m_R \gtrsim 10^{10}\,\mathrm{GeV}$, and for $d_\ell \sim 0.1$, we have $m_R \gtrsim 10^{12}\,\mathrm{GeV}$. Note that here we use an estimate for the light neutrino, i.e. $m_\nu \sim 0.05\,\mathrm{eV}$.

[8] For this, we estimated Equation (2.27c) on $M_R = U_R \hat{m} U_R^T$ with $U_R \simeq (0, U_N^*)$, according to Equation (2.26) and reached $M_R \simeq U_N^* \hat{m}_R U_N^\dagger$.

9.3.2. Right-handed neutrino masses at one-loop

Similar to the previous section, in the following, we intend to achieve a formula for the right-handed neutrino masses in one-loop.

Including the one-loop mass corrections δM_L given in Equation (9.35) into the light neutrino masses, using Equation (9.10), we obtain

$$M_\nu = \delta M_L(\hat{m}_R, U_N) \underbrace{-M_D^T M_R^{-1}(\hat{m}_R, U_N) M_D}_{M_\nu^{tree}}, \tag{9.42}$$

where here, instead of M_ν^{tree}, M_ν is diagonalized according to Equation (9.38). Now the right-handed masses $\hat{m}_R(m_4, m_5, m_6)$, together with the right-handed mixing matrix U_N, need to be extracted from the far more complicated Equation (9.42), which will be done numerically.

A dimensional analysis of Equation (9.35) yields for δM_L

$$\begin{aligned}\delta m_L \sim \frac{1}{32\pi^2}\frac{1}{m_R}\Bigg[&\delta_\ell^2\left(M_3^2 \ln\left(\frac{m_R^2}{M_3^2}\right) - M_4^2 \ln\left(\frac{m_R^2}{M_4^2}\right)\right) \\ &+d_\ell^2\left(m_H^2 \ln\left(\frac{m_R^2}{m_H^2}\right) + 3\, m_Z^2 \ln\left(\frac{m_R^2}{m_Z^2}\right)\right)\Bigg],\end{aligned} \tag{9.43}$$

which can be used to estimate m_R from formula (9.42),

$$m_R \sim \frac{1}{m_\nu}\Bigg[\delta_\ell^2 \frac{1}{32\pi^2}\left(M_3^2 \ln\left(\frac{m_R^2}{M_3^2}\right) - M_4^2 \ln\left(\frac{m_R^2}{M_4^2}\right)\right) \tag{9.44a}$$

$$+d_\ell^2 \frac{1}{32\pi^2}\left(m_H^2 \ln\left(\frac{m_R^2}{m_H^2}\right) + 3\, m_Z^2 \ln\left(\frac{m_R^2}{m_Z^2}\right)\right) + d_\ell^2 \frac{v^2}{2}\Bigg]. \tag{9.44b}$$

Here m_H, m_Z are the masses of the Higgs and $Z-$bosons, and M_3, M_4 are the masses of the new scalars S_3 and S_4, respectively. The parameters marked in red in Equation (9.44) are free parameters.[9] One can see the contributions to m_R from the new scalars S_3 and S_4 scale with the Yukawa couplings δ_ℓ, while they are in the order of

$$\frac{M_4^2 - M_3^2}{32\pi^2\, m_\nu} \sim 10^{14}\,\text{GeV} \quad (M_3 = 1\,\text{GeV},\, M_4 = 2\,\text{GeV},\, m_\nu \sim 0.1\,\text{eV}), \tag{9.45}$$

whereas the Higgs and $Z-$Boson contributions scale with d_ℓ couplings and are of the order of

$$\frac{m_{EW}^2}{32\pi^2\, m_\nu} \sim 10^{12}\,\text{GeV} \quad (m_{H/Z} \sim m_{EW} \sim 100\,\text{GeV},\, m_\nu \sim 0.1\,\text{eV}). \tag{9.46}$$

[9] For m_ν, the absolute value is still not known, nor is the hierarchy of the masses.

The last term in Equation (9.44b) results from the tree-level contribution, which also scales with d_ℓ. In a dimensional analysis, ignoring the couplings δ_ℓ and d_ℓ, this tree-level contribution,

$$\frac{v^2}{2\,m_\nu} \sim 10^{14}\,\mathrm{GeV} \quad (m_\nu \sim 0.1\,\mathrm{eV}), \tag{9.47}$$

dominates over the one-loop contributions if the mass-squared differences $M_4^2 - M_3^2$ are small. Thus, one can see in Equation (9.45) that the effect of the new scalars S_3^0, S_4^0 not only depends on the Yukawa couplings δ_ℓ but also depends strongly on the mass difference $\Delta M^2 = M_4^2 - M_3^2$. Note that by setting $\Delta M^2 \sim \mathcal{O}(\mathrm{TeV}^2)$ and considering $\delta_\ell = d_\ell$, the relationship changes in such a way that the contributions from the new scalars dominate over the SM contributions.

Unfortunately, the dominating contributions of the new scalars seem to be problematic to find numerical solutions for the parameters $\hat{m}_R$ and U_N via formula (9.42). To shed light on this fact, it is easier to examine a simplified formula; in fact, the main characteristics of the solution of m_R can be approximated by the solution of $x_{m_R} \sim m_R/\mathrm{GeV}$, given by the following formula,

$$c\,x_{m_R} + \ln\left(x_{m_R}^2\right)(a-b) = a\ln a + b\,(10 - \ln b)\,, \tag{9.48}$$

with $c \sim m_\nu/\mathrm{GeV}$, $a \sim \delta_\ell^2\left(M_4^2 - M_3^2\right)/\mathrm{GeV}^2$ and $b \sim d_\ell^2 m_{EW}^2/\mathrm{GeV}^2$, which is an intricate Lambert W function. The solution of Equation (9.48) exhibits singularities; in the case that (I) the size of the one-loop contribution of the new scalars is equal to the size of the tree-level ones, i.e. when $a = b$ or, in other words, if (9.45) times δ_ℓ^2 equals (9.46) times d_ℓ^2, as shown in Figure 9.1, and (II), additionally, if near this region $c = m_\nu/\mathrm{GeV}$ assumes low values, e.g. $m_\nu \leq 0.01\,\mathrm{eV}$. This behaviour is illustrated in the diagrams shown in the following Section 9.3.4 and can be the cause of the lack of numerical results.

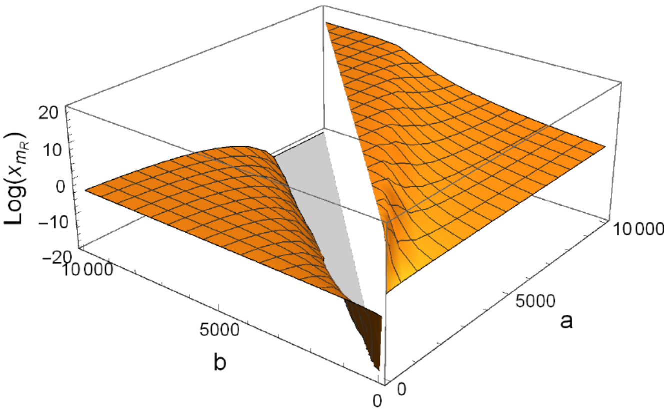

Figure 9.1.: Shown is $x_{m_R} \sim m_R/\mathrm{GeV}$, the solution to Equation (9.48) as a function of $a \sim \delta^2\left(M_4^2 - M_3^2\right)/\mathrm{GeV}^2$ and $b \sim d^2\,m_{EW}^2/\mathrm{GeV}^2$ and with $m_\nu = 0.05\,\mathrm{eV}$. One can recognize a singularity when $a = b$.

Numerical calculation method

Let us explain how we have dealt with this numerically problematic behaviour.

Here we list the numerical calculation steps for $\hat{m}_R$ and U_N:

- We start with the calculation of M_ν, which is determined by experimental values by $M_\nu^{fixed} = U_\nu^* \hat{m}_\nu U_\nu^\dagger$, (9.38). Here U_ν is parametrized after Equation (2.39), where the Majorana phases are $\rho = \sigma = 0$.

- Then we determine the right-handed neutrino masses $\hat{m}_R = \mathrm{diag}\,(m_4, m_5, m_6)$ and the mixing matrix U_N at tree-level according to Section 9.3.1 and employing the eigenvalue equation in (9.40).

- To extract the mixing angles θ_{R12}, θ_{R13}, and θ_{R23} from the mixing matrix for the right-handed neutrinos U_N, we define U_N in the same parametrization as U_ν, namely

$$U_N = \begin{pmatrix} c_{R12}\, c_{R13} & s_{R12}\, c_{R13} & \epsilon^* \\ -s_{R12}\, c_{R23} - c_{R12}\, s_{R23}\, \epsilon & c_{R12}\, c_{R23} - s_{R12}\, s_{R23}\, \epsilon & s_{R23}\, c_{R23} \\ s_{R12}\, s_{R23} - c_{R12}\, c_{R23}\, \epsilon & -c_{R12}\, s_{R23} - s_{R12}\, c_{R23}\, \epsilon & c_{R23}\, c_{R13} \end{pmatrix} \begin{pmatrix} 1 & & \\ & e^{i\rho_R} & \\ & & e^{i\sigma_R} \end{pmatrix}, \tag{9.49}$$

where $s = \sin\theta$, $c = \cos\theta$, and $\epsilon = \sin\theta_{R13}\exp(i\delta_{CP})$, where the CP phase is δ_{CP}, and the Majorana phases are ρ_R and σ_R. The result for U_N determined above is adapted to this parametrization by varying the Majorana angles ρ_R and σ_R either by 0 or π. The resulting tree-level values for $m_{4,5,6}$ and θ_{R12}, θ_{R13}, θ_{R23} are the initial values for the computation of the one-loop corrections for $m_{4,5,6}$.

- Finally, we use Equation (9.42) to evaluate the one-loop correction,

$$M_\nu\left(\hat{m}_R, \theta_R\right) = M_\nu^{tree}\left(\hat{m}_R, \theta_R\right) + \delta M_L\left(\hat{m}_R, \theta_R\right), \tag{9.50}$$

and M_ν^{fixed} from the first bullet point and take the root of $\left(M_\nu^{fixed} - M_\nu\right)$. Now using the initial values from above we can determine the one-loop corrections for $m_{4,5,6}$ and θ_{R12}, θ_{R13}, and θ_{R23}.

- The problematic part in the computation is the one-loop contribution from the new scalar masses proportional to δ_ℓ. To deal with this problem, we start with the initial values given by the tree-level contribution and slowly turn on the one-loop level contributions with a pre-factor. Then, in each run, we use the results of the previous run as new inputs for the initial values. Using this iterative procedure, we found numerical solutions for the respective parameters in certain small steps.

- As a test, we first reinsert the solutions found for θ_{R12}, θ_{R13}, θ_{R23} back into the U_N parametrization given in Equation (9.49), then the U_N was put back into Equation (9.50) together with $m_{4,5,6}$ and finally it was tested whether $\left(M_\nu^{fixed} - M_\nu\right)$ is equal to zero. In general, we only allowed solutions in Mathematica for data points that had an accuracy in the order of the machine precision of $< 10^{-14}$.

9.3.3. The corresponding parameter space

Now after we have described the numerical solutions for $\hat{m}_R$ and θ_{R12}, θ_{R13}, θ_{R23}, including one-loop corrections, we want to provide a parameter analysis for the right-handed neutrino masses with the remaining free model parameters. As the first step in this section, we will look at suitable parameter spaces.

As explained in Section 6.3, we will apply the following strategy for our qualitative analysis: After we have determined reasonable parameters spaces for the corresponding free parameters of the model, we select two parameter sets where all parameters are fixed. In the best case, these sets cover most of the possible effects in the outcomes. Before we dive into the process of searching for thorough parameters spaces, let us define the parameters that we will not investigate further in order to have a simplified analysis.

In general, we include all the simplifying assumptions mentioned in Chapter 2.7: We chose the normal mass order for the light neutrino masses $\hat{m}_\nu$, see Equation (2.5). We have adapted the neutrino parameters Δm^2_{21}, Δm^2_{31}, and θ_{12}, θ_{13}, θ_{23} to their best-fit values defined by Ref. [18] in Chapter 2.7. In addition, we have chosen the neutrino mixing matrices U_ν and U_N as real, then the Majorana angles are $e^{i\hat{\alpha}} = e^{i\hat{\beta}} = \mathbb{1}$ and thus ρ_R, $\sigma_R \in \{0, \pi\}$, while $\rho = \sigma = 0$. Thereby we have fixed the two CP mixing angles in U_ν and U_N at $\delta_{CP} = \pi$. Alternatively, we could have chosen $\delta_{CP} = 0$; we have verified that there is no qualitative difference between the two cases, neither in this chapter nor in the calculations of the following chapter. Although it would be interesting to have results for e.g. $\delta_{CP} = \pi/2$, it has not been possible in the context of this thesis to perform calculations with $\delta_{CP} \neq \{0, \pi\}$. It seems that when terms become imaginary, numerics collapse, so this problem will require further thorough analysis in the future. Furthermore, it was argued in Chapter (8.3) that the new scalar masses M_3, M_4 must be fixed by Equation (8.42a) in the lower TeV range at $M_3 = 1\,\text{TeV}$ and $M_4 = 2\,\text{TeV}$ in order to obtain higher contributions for branching ratios of FCNIs. Additionally, a lower mass split is much easier to adapt because already at $\Delta M^2 = M_4^2 - M_3^2 = 3\ \text{TeV}^2$, as we used it here, the numerics requires massive CPU power and, therefore, this is time-consuming, which is another reason not to opt for larger masses.

The new Yukawa couplings

With regard to the new Yukawa couplings of the neutrinos to the Higgs boson $\Delta_1 = \text{diag}(d_e, d_\mu, d_\tau)$ and to the new scalars $\Delta_2 = \text{diag}\left(\delta_e,\, \delta_\mu,\, \delta_\tau\right)$, we consider a similar approach to γ_ℓ in the previous chapter in Section 8.3, i.e. we want them to be in the parameter range of the other SM Yukawa couplings, which is in the order of $10^{-6} - 1$.

Let us deduce what could be a good scale for the input parameter d_ℓ, vis. the Yukawa couplings corresponding to the Dirac neutrino masses $M_D = v/\sqrt{2}\,\Delta_1$, see Equation (4.4a). If we average over all SM masses, we get a value in the lower GeV range, so let us for instance take $m_D \sim 1\,\text{GeV}$ for the Dirac mass scale. The corresponding Yukawa coupling would then be roughly estimated as $\Delta_1 = \sqrt{2}/v\, m_D \sim 0.01$. Therefore, the Yukawa couplings d_e, d_μ, d_τ are considered to be of the same size and should be set to the values

$$d_e = 0.07, \quad d_\mu = d_\tau = 0.01. \quad \text{(Set B)} \tag{9.51}$$

We are going to call this parameter set "Set B". Another analysed parameter set "Set A" for comparison will be

$$d_e = 0.4, \quad d_\mu = d_\tau = 0.1, \quad \text{(Set A)} \tag{9.52}$$

which belong to Dirac masses of the order $m_D \sim 10\,\text{GeV}$.

For further analysis, the Yukawa couplings to the new scalars $\Delta_2 = \text{diag}(\delta_e, \delta_\mu, \delta_\tau)$ shall also be fixed in these two sets. The values were found after a careful study of the relevant contributions to FCNIs, with the aim of reaching flavour-changing branching ratios close to but below the experimental limits. For the reasons given in the following chapter we therefore set them to

$$\delta_e = 0.003, \quad \delta_\mu = 0.0001, \quad \delta_\tau = 0.7, \quad \text{(Set B)} \tag{9.53}$$

and

$$\delta_e = 0.002, \quad \delta_\mu = 0.0002, \quad \delta_\tau = 0.07, \quad \text{(Set A).} \tag{9.54}$$

The light neutrino mass

The remaining parameter is the light neutrino mass m_1. This has a strong upper limit from cosmology, which is $m_1 \lesssim 0.1\,\text{eV}$ [9]. On the other hand, it should correspond to the Seesaw condition $m_\nu = m_D^2/m_R$, i.e. lower values for m_1 increase the Seesaw scale m_R even further, so we rate m_1 in the range of $0.001 - 0.1$ and select $m_1 = 0.05\,\text{eV}$ for the analysis.

Evaluation of the two parameter sets

The two full parameter sets that we will use for our qualitative analysis are listed again in Table 9.1. These two parameter sets are not the only working sets, they only serve to illustrate what is possible under the constraints set by the experimental precision tests discussed in this thesis.

Set A	Set B
$m_1 = 0.05\,\text{eV}$ $(\delta_{CP} = \pi)$	
$d_e = 0.4$	$d_e = 0.07$
$d_\mu = d_\tau = 0.1$	$d_\mu = d_\tau = 0.01$
$\delta_e = 0.002$	$\delta_e = 0.003$
$\delta_\mu = 0.0002$	$\delta_\mu = 0.0001$
$\delta_\tau = 0.07$	$\delta_\tau = 0.7$

Table 9.1.: Full parameter sets of "Set A" and "Set B" of the model.

For the two parameter sets in Table 9.1, we obtain heavy right-handed neutrino masses, which are listed in Table 9.2. These masses represent the Seesaw scale.[10]

	Set A		Set B	
	$m_R[10^{12}\,\text{GeV}]$		$m_R[10^{10}\,\text{GeV}]$	
	(tree-level)	(one-loop)	(tree-level)	(one-loop)
m_4	4.32	3.93	4.32	4.24
m_5	5.99	50.95	5.99	240.50
m_6	95.80	77.56	293.37	24674.19

Table 9.2.: Right-handed masses, calculated from tree-level (Equation (9.39)) and one-loop (Equation (9.42)) light neutrino masses, taking into account the parameter set of Table 9.1.

In addition, we obtain for our two sets the right-handed mixing matrices U_N, which are visualized in Figure 9.2 with the mixing angles $\theta_{R12} = 1.543(1.567)$, $\theta_{R13} = -1.242(-0.004)$, and $\theta_{R23} = -0.144(-0.017)$ for Set A (Set B) with U_N defined in Equation (9.49). The Majorana phases were found to be $\rho_R = \pi$ and $\sigma_R = 0$. Figure 9.2 shows that right-handed neutrino mixing follows a different pattern in each set with large off-diagonal entries.

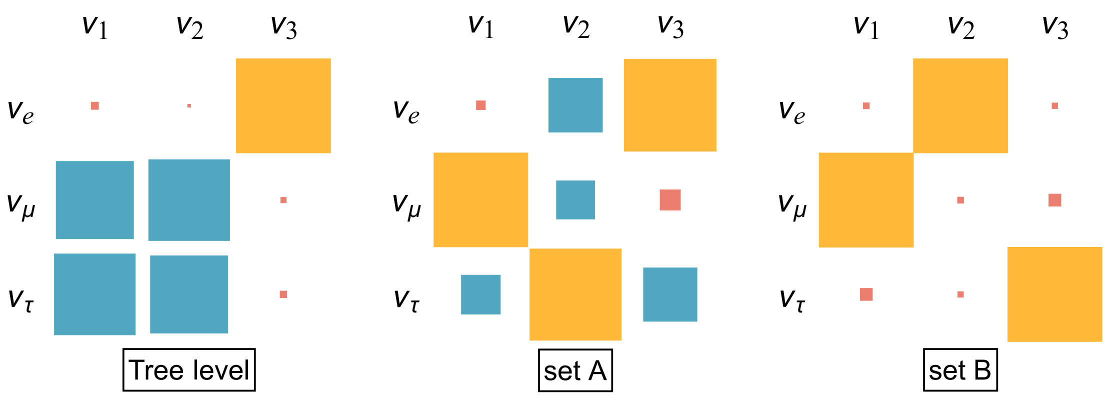

Figure 9.2.: A visualization of the entries in the mixing matrices of the right-handed neutrinos U_N with one-loop corrections. The mixing matrices are calculated numerically with the parameters taken from Table 9.1. U_N is shown in the middle for parameter Set A and on the right, for Set B. The corresponding tree-level mixing matrices for both sets have the shape of the left picture.

[10] In fact, the right-handed masses m_4, m_5, m_6 differ by several orders of magnitude, and therefore there is no precisely defined Seesaw scale, but this is not relevant for our purposes.

9.3.4. Parameter analysis of the right-handed neutrino mass from one-loop contributions

Finally, the purpose of this section is to analyse the remaining free parameter space spanned by d_ℓ, δ_ℓ, and m_1 in connection with the one-loop corrections for right-handed neutrino masses m_R, in order to find good fixation ranges and potential limits for the parameters.

In anticipation of the next chapter on FCNIs, we will not only analyse m_R but also the parameter $X_{\ell_1\ell_2}$, i.e. $|X_{\ell_1\ell_2}|^2$. $X_{\ell_1\ell_2}$ is the special part of the FCNI branching ratio, in which the right-handed neutrino masses $\hat{m}_R$ and the mixing matrix U_N enter. The parameter $X_{\ell_1\ell_2}$ is defined as

$$X_{\ell_1\ell_2} = 1/\left(16\sqrt{2}\pi^2\right)\sum_{i=4}^{6}\left((U_N^*)_{\ell_1 i}(U_N)_{\ell_2 i}\ln(m_i^2/\mu^2)\right). \tag{9.55}$$

Here, $\ell_1 \neq \ell_2$, where $\ell_{1/2}$ are the participating leptons in the FCNIs, while μ is an arbitrary mass parameter. Note that $X_{\ell_1\ell_2}$ is independent of μ due to the orthogonality relation $(U_N^*)_{\ell_1 i}(U_N)_{\ell_2 i} = 0$.

To find good parameter regions in this analysis means to avoid the regions of parameter spaces where m_R and $|X_{\ell_1\ell_2}|^2$ are not well-defined or very unstable to avoid fine-tuning problems in the next chapter. As mentioned in section 9.3.2 and illustrated in Equation (9.44), the value of m_R, and thus also $|X_{\ell_1\ell_2}|^2$ results from a delicate interplay between the tree-level mass contribution regulated by $d_\ell \cdot m_{EW}$ and the new scalar masses S_3 and S_4, which are regulated by $\delta_\ell \cdot \sqrt{M_4^2 - M_3^2}$ in the one-loop contributions, while the contributions of the Higgs and Z boson are negligible. As we will observe, this main determination is also reflected in the following parameter analysis.

Parameters δ_ℓ

The diagrams of Figure 9.3 show m_R and $|X_{\ell_1\ell_2}|^2$ as a function of the parameter δ_τ. It can be seen that if $\delta_\ell < d_\ell$, the one-loop mass contributions of the new scalars S_3 and S_4 proportional to δ_ℓ are subdominant and have an impact on m_R or $|X_{\ell_1\ell_2}|^2$ only if $\delta_\ell \sim d_\ell$, for which m_R and $|X_{\ell_1\ell_2}|^2$ show irregularities. Due to the smaller d_ℓ in Set B, this effect also occurs at lower δ_ℓ. In fact, δ_τ is chosen here because it has the biggest impact in the region where $\delta_\ell \gtrsim d_\ell$; varying δ_μ and δ_e show only slight changes at high δ_ℓ values. Overall, this means that choosing lower values of δ_ℓ with $\delta_\ell < d_\ell$ results in more stable regions for m_R and $|X_{\ell_1\ell_2}|^2$ and avoids fine-tuning problems.

Parameters d_ℓ

The quantities m_R and $|X_{\ell_1\ell_2}|^2$ generally are very sensitive to the couplings d_ℓ since they regulate the dominance and the suppression of the tree-level contribution. The diagrams in Figure 9.5 show for one-loop values a jump in the course of the curves with a gap in between, surrounded by an unsteady course. This numerical instability in the

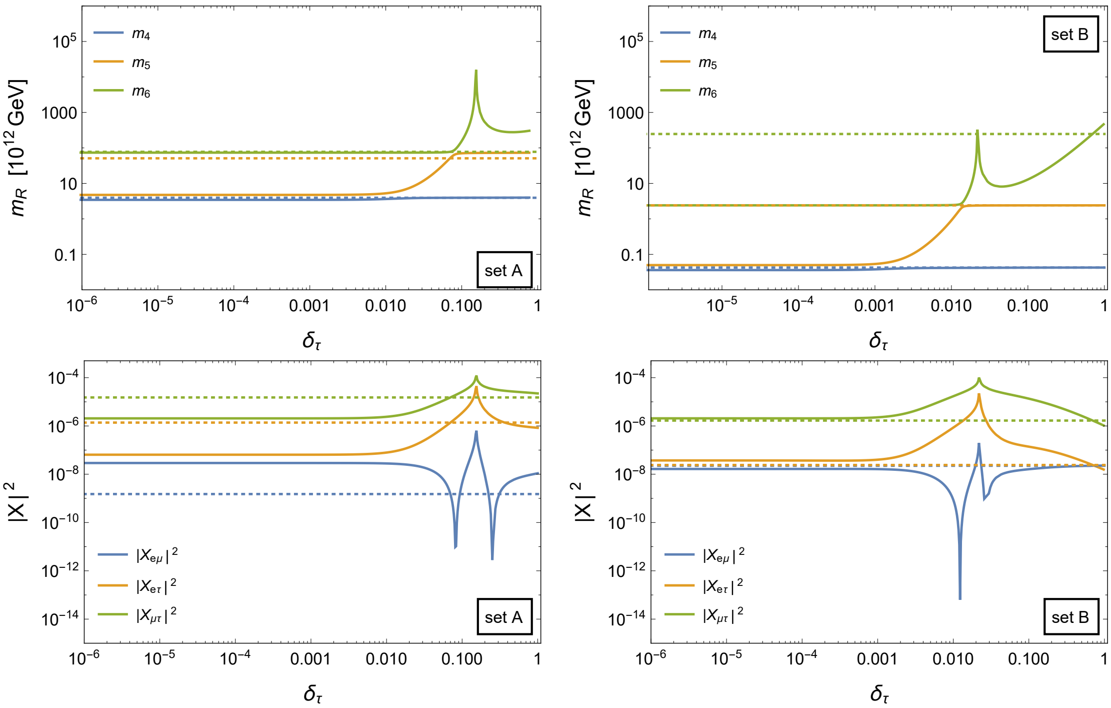

Figure 9.3.: Depicted are the right-handed neutrino masses m_R and the corresponding quantity $|X|^2$, which is relevant for FCNI. All parameters except δ_τ remain fixed with the values of the two sets taken from Table 9.1. The dotted lines reflect the values at tree-level, the solid lines at one-loop. Contributions that are proportional to δ_ℓ have only an influence on the right-handed masses m_R and the value $|X|^2$ if their value is close to d_ℓ. At δ_μ and δ_e, the effect is equivalent but even smaller.

solutions can be explained by the formula for m_R, whereby a rough approximation of this formula by Equation (9.48) in Section 9.3.2 illustrates the problem: As shown in Figure 9.5, this approximate solution shows singularities with jumps if $a = b$, vis. if $m'_\delta\,\delta_\ell = d_\ell$, with $m'_\delta = \sqrt{M_4^2 - M_3^2}/m_{EW}$ or rather if the one-loop contributions from the new scalar masses equal those at tree-level. We observe for this case that irregularities begin to appear in the course of m_R and $|X_{\ell_1\ell_2}|^2$ when

$$\sqrt{M_4^2 - M_3^2}/m_{EW}\,\delta_\ell \gtrsim d_\ell, \tag{9.56}$$

which is consistent with the previous diagrams in Figure 9.3, where we have already observed this effect when d_ℓ comes close to δ_ℓ. From this, we derived heuristically a rule of thumb when singularities occur, i.e. when

$$m_\delta\,\delta_\ell \sim d_\ell, \quad \text{with } m_\delta \sim \frac{\sqrt{M_4^2 - M_3^2}}{m_{EW}} \times \frac{10^{-3}}{2}\,, \tag{9.57}$$

and thus for the case $M_3 = 1\,\text{TeV}$ and $M_4 = 2\,\text{TeV}$, if

$$\delta_\ell \sim 100\, d_\ell. \tag{9.58}$$

As a reference for the definition of Equation (9.57), we have taken the values for the singularities shown in the diagrams in Figure 9.5 and two different parameter sets not presented here with $M_4 = 1.1\,\text{TeV}$. Therefore, Equation (9.57) should be taken as a rough guideline for the search for singularities and could slightly differ for each individual varying parameter since the equation is derived from the behaviour of the approximate solution for m_R given by Equation (9.48) and does not take mixing effects into account.

In order to compute the diagrams of Set B with the progressions of a varying d_ℓ, we had to take a hundred times the precision in terms of decimal places and $1/100$ of the step size compared to those of Set A. The numerics become unstable around the singularity and at lower d_ℓ values if $m_\delta\, \delta_\ell > d_\ell$, i.e. the one-loop contributions exceed the tree-level contributions so that not many valid points were found in this region. The reason for this is that with the parameter Set B with $(\delta_\ell/d_\ell)_{max} = \delta_\tau/d_\tau = 70 \lesssim 1/m_\delta$, m_R is very close to the singularity where the one-loop terms are equal to the tree-level terms.

All in all, it seems better for our parameter sets to take larger d_ℓ, e.g. $d_\ell \gtrsim 0.01$ to avoid singularities and unsteady regions and at the same time to approach the experimental limits of the τ-decaying branching ratios $BR(\tau \to \ell_1 \ell_2 \bar{\ell}_2)$, which will be discussed in the next chapter.

Parameter m_1

As depicted in the diagrams in Figure 9.4 on the right, it is not possible to find solutions for m_R and thus also not for $|X_{\ell_1\ell_2}|^2$ using the parameters of Set B with smaller m_1 values. It is strongly suspected that this is caused by the problem just mentioned, namely that the parameter Set B locates m_R near the unstable region. Corresponding to this observation, the approximate solution for m_R derived from Equation (9.48) predicts a further critical region for the case $m_\delta \cdot \delta_\ell$, which is close to d_ℓ with a simultaneously small light neutrino mass as in the present case.

Furthermore, we see in the diagrams for Set A in Figure 9.4 that m_R and m_1 are antiproportional if one decreases, the other increases, as predicted by the Formula (9.44b); thus, the same effect also applies to $|X_{\ell_1\ell_2}|^2$. Moreover, one can see cancellations in $|X_{e\mu}|^2$. These become useful for the calculation of the branching ratio $BR(\mu \to eee)$ in the next chapter, where $BR(\mu \to eee)$ has a rather restrictive low experimental limit of $BR(\mu \to eee) < 10^{-12}$.

Summing up this information, we conclude that a light neutrino mass, m_1, of higher value seems more appropriate. This applies in particular to the parameter Set B for bypassing problematic regions. This leads us to take $m_1 = 0.05\,\text{eV}$ for the two parameter sets.

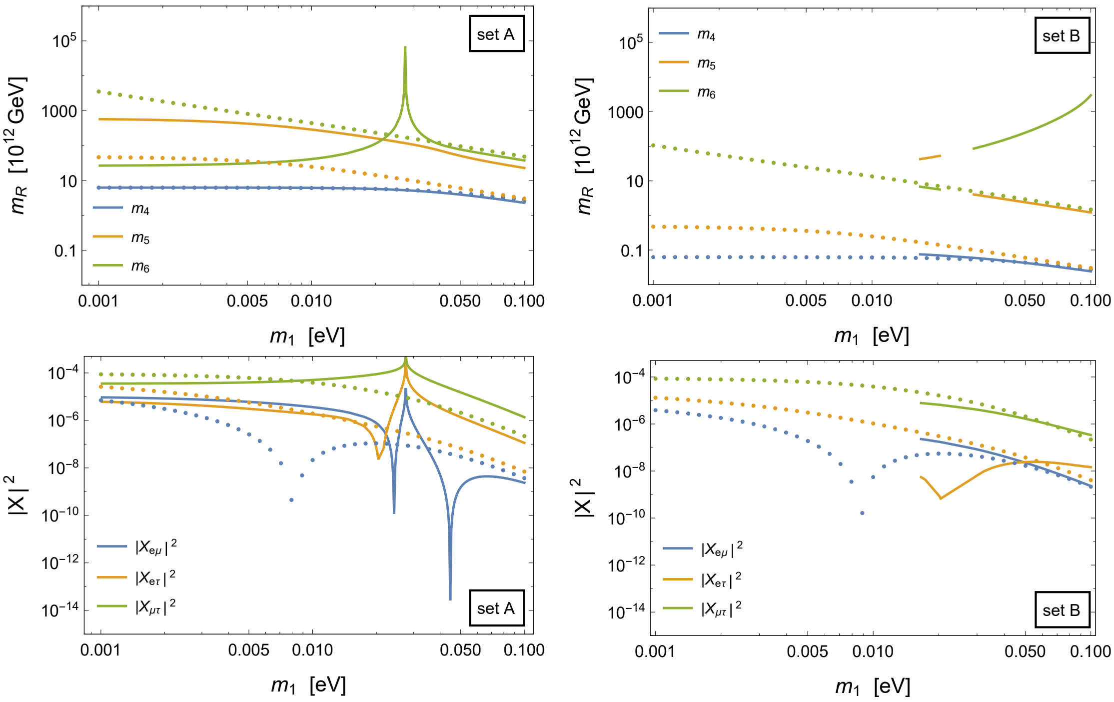

Figure 9.4.: Depicted are the right-handed neutrino masses m_R and the corresponding quantity $|X|^2$ relevant for FCNIs. All parameters except m_1 remain fixed with the values of the two sets taken from Table 9.1. The dotted lines reflect the values at tree-level, the solid lines at one-loop. The large regions for parameter Set B, where there are no one-loop solutions for m_R and $|X|^2$, very likely result from the fact that the parameter Set B is close to the region of a singularity, i.e. if the one-loop contributions of the new scalar masses dominate over the tree-level contributions, thus the numerics breaks down. Furthermore, the anti-proportional behaviour between m_R and m_1 can be seen.

Concluding remarks

In this chapter, we have derived a formula for the dominant one-loop correction δM_L for the light neutrino masses within the settings of this model. Interestingly, when the light neutrino masses are fixed, this correction shifts and becomes a non-negligible contribution to the right-handed neutrino masses.

As could be gained from the study in this section, there is a critical contribution to the right-handed neutrino masses, m_R, and thus to the quantity[11] $|X_{\ell_1 \ell_2}|^2$, it is the one-loop contribution, which is proportional to the Yukawa couplings δ_ℓ and the new scalar masses. Specifically, if the one-loop contributions are close to the contributions at tree-level, i.e. if our derived rule of thumb $\delta_\ell \sqrt{M_4^2 - M_3^2} \times 10^{-3}/2 \sim d_\ell \cdot m_{EW}$ in Equation (9.57) applies (where m_{EW} is the electroweak scale), the courses of m_R and

[11] The quantity $|X_{\ell_1 \ell_2}|^2$ is the part of the FCNI branching rations that contain the neutrino parameters.

thereby $|X_{\ell_1\ell_2}|^2$ exhibit a jump with a gap in the solution of the formula for m_R (9.42), interpreted as a singularity. Consequently, the parameter space should in any case avoid regions where singularities for m_R and $|X_{\ell_1\ell_2}|^2$ occur since, for the latter, no physical solution exists in these regions. The preferred parameter range is in a region where irregularities are additionally avoided, given by Equation (9.56), vis. where the one-loop contributions are smaller than those at tree-level and thus where $\delta_\ell \sqrt{M_4^2 - M_3^2} < d_\ell\, m_{EW}$.

As a side note: We also investigated the case of a smaller discrepancy between the masses squared of the new scalars, namely where $M_3 = 1\,\text{TeV}$, but $M_4 = 1.1\,\text{TeV}$, and otherwise for similar parameter Sets A and B. In this case, the one-loop contributions proportional to $\delta_\ell \sqrt{M_4^2 - M_3^2}$ are more suppressed compared to the examined case with $M_4 = 2\,\text{TeV}$; consequently, with Equation (9.57), the singularity is at $\delta_\ell \sim 440\, d_\ell$ (instead of $\delta_\ell \sim 100\, d_\ell$) and thus outside the examined regions of the parameter spaces. The course of the parameters δ_ℓ, d_ℓ, and m_1 for Set A ($d_\ell \sim 0.1$, $\delta_\ell \lesssim 0.01$) with such suppressed one-loop contributions naturally equals the tree-level contribution, whereas for the same small mass $M_4 = 1.1\,\text{TeV}$ and the parameters of Set B ($d_\ell \sim 0.01$, $\delta_\ell \lesssim 0.01$), the courses of m_R and $|X_{\ell_1\,\ell_2}|^2$ already show similar behaviour as the just presented case with $M_4 = 2\,\text{TeV}$ and Set A. Thus, this investigation confirms our results.

The solution of the neutrino mass correction (9.42) seems to be non-trivial and therefore needs further research, whereby a rough guideline in this direction represent the heuristically derived Equation (9.57), which defines the position of the singularities, and Equation (9.56), which defines the area where irregularities begin.

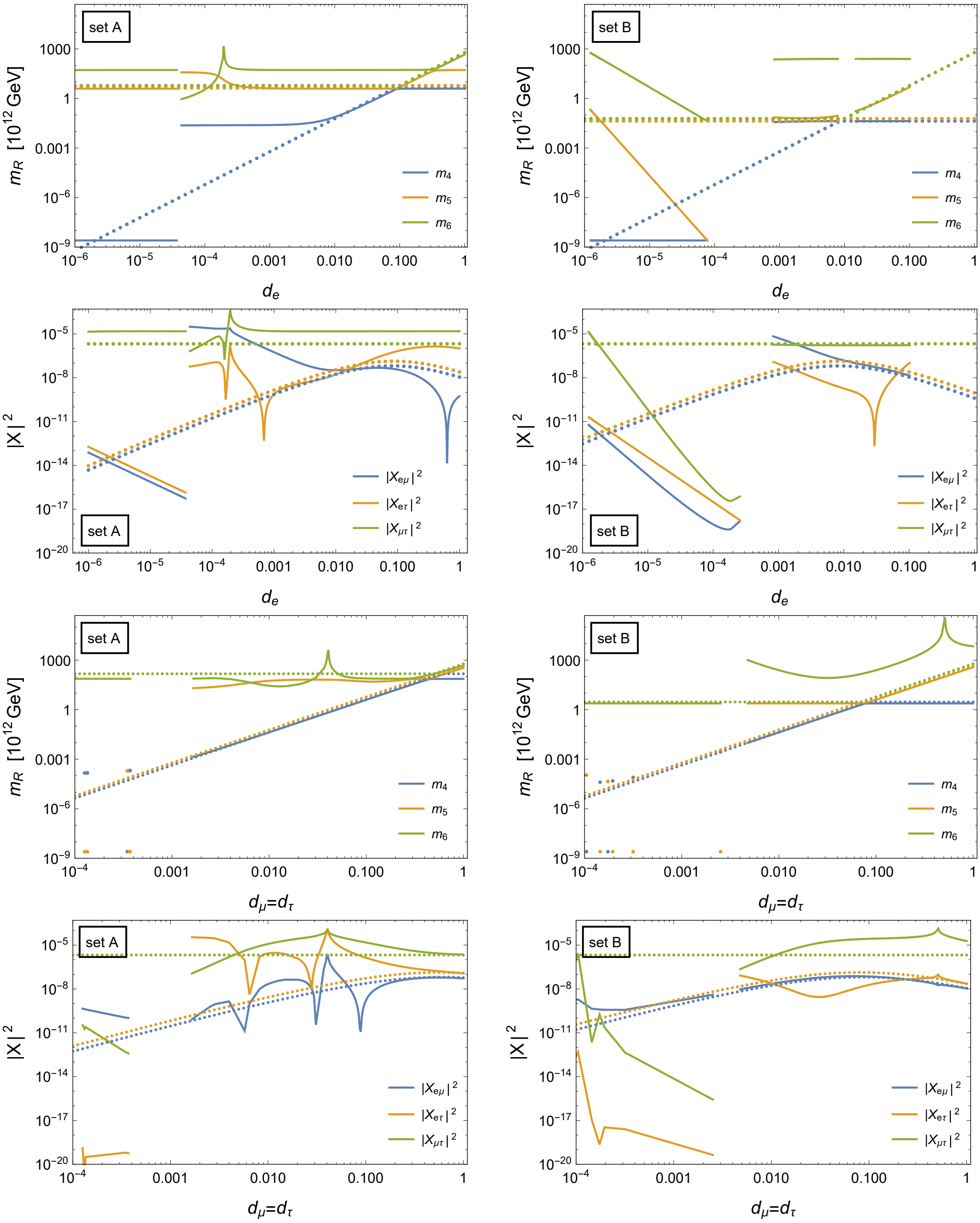

Figure 9.5.: Shown are the right-handed neutrino masses m_R and the corresponding quantity $|X|^2$ relevant for FCNIs. All parameters except the varied d_e, d_μ, and d_τ, respectively, remain unchanged with the values of the two sets taken from Table 9.1. The dotted lines reflect the values at tree-level, the solid lines at one-loop. Values for $d_\mu = d_\tau < 10^{-4}$ are not displayed because the numerics in this range becomes unstable, especially due to a changing d_τ. The right-handed masses m_R and the quantity $|X|^2$ are sensitive to d_ℓ in the regions shown: At lower d_ℓ scales, the interplay between the one-loop and tree-level terms, shown in Equation (9.44b), causes singularities surrounded by irregularities in $|X|^2$.

10. Lepton Flavour-Changing Neutral Interactions (FCNIs)

As we learned at the beginning of Part II, flavour-changing processes are sensitive to new physics in the electroweak sector. This is especially true for theories that include multi-Higgs doublets since new Yukawa couplings are imposed between leptons and scalars, which are generally not flavour-diagonal. To be able to realise these models nevertheless, they often suffer from the unnaturally small Yukawa couplings of the new Higgs doublets compared to the Yukawa couplings of the SM Higgs[1], or these models are provided with another symmetry to suppress FCNI. In our case, the latter is true, the model is equipped with a softly broken lepton-flavour symmetry, which prevents the occurrence of FCNIs at tree-level. Since the soft breaking is realised through the Majorana mass term of the right-handed neutrinos, any new possible one-loop contributions to FCNIs from the framework of this model must have a right-handed neutrino exchange to generate flavour violation.

Parts of the following text are quoted and partially rewritten from the paper to this thesis, [10].

To give meaning to the structure of this chapter, we want to anticipate a discussion of the relevant processes of lepton FCNIs for our model.

In models of our kind, the processes that violate lepton flavour were explicitly studied in one-loop order in Ref. [3], and the following property of a framework like ours was discovered. Let m_R denote the Seesaw scale – the scale of the square roots of the eigenvalues of $M_R M_R^*$ – and n_H denote the number of Higgs doublets; it was found in Ref. [3] that

i. The amplitudes of the lepton flavour-violating processes involving gauge bosons, like $\mu^- \to e^-\gamma$ and $Z^0 \to e^-\mu^+$, scale down as $1\big/m_R^2$ if $m_R \to \infty$; this holds even when in those processes the gauge bosons γ and Z^0 are virtual, *i.e.* they are off-mass shell, so

$$\mathcal{A}(\mu \to e\gamma),\ \mathcal{A}(Z^0 \to e^-\mu^+) \propto \frac{1}{m_R^2}; \tag{10.1}$$

ii. The amplitudes of the box diagrams for lepton flavour-violating processes like $\tau^- \to \mu^-\mu^-e^+$ and $\tau^- \to e^-e^-\mu^+$ also scale down as $1\big/m_R^2$ for a large Seesaw scale,

[1] E.g. the smallest Yukawa coupling in the SM comes from the electron $Y_e \sim 2\cdot 10^{-6}$ ($m_e = Y_e v/\sqrt{2} \sim$ 511 keV)

e.g.

$$\mathcal{A}(\tau^- \to \mu^-\mu^-e^+) \propto \frac{1}{m_R^2}.$$

iii. However, if $n_H \geq 2$, the amplitudes for lepton flavour-violating processes $\ell_1^- \to \ell_2^- \left(S_b^0\right)^*$, where $\left(S_b^0\right)^*$ is a virtual (off-mass shell) neutral scalar, approaching a nonzero limit when $m_R \to \infty$. The non-decoupling of the Seesaw scale in $\ell_1^- \to \ell_2^- \left(S_b^0\right)^*$ is an effect of the one-loop diagrams with neutrinos and charged scalars in the loop, which are shown in Figure 10.1.

Consequently, in our framework, the amplitude of the process $\mu^- \to e^-e^+e^-$, which is derived from $\mu^- \to e^- \left(S_b^0\right)^*$ followed by $\left(S_b^0\right)^* \to e^+e^-$, is *unsuppressed* in the limit $m_R \to \infty$. The same happens with the amplitudes of the four τ^-decays of the same type,[2] *viz.* with [3]

$$\mathcal{A}(\ell_1^- \to \ell_2^-\ell_3^+\ell_3^+) \propto \text{constant}, \quad \text{for } n_H \geq 2. \tag{10.2}$$

It is important to stress that, as pointed out in (iii) mentioned above, in our model, the amplitude for $\mu^- \to e^-e^+e^-$ is unsuppressed because of the penguin diagrams for the neutral-scalar emission in the $\mu^- \to e^-$ conversion; in fact, the penguin diagrams for either γ or Z^0 emission vanish in the limit value $m_R \to \infty$. Therefore, our model for lepton flavour violation differs from, for instance, the scotogenic model discussed in Ref. [114], in which it is precisely the γ and Z^0 penguins that are instrumental in $\mu^- \to e^-e^+e^-$ and in muon–electron conversion in nuclei.[3]

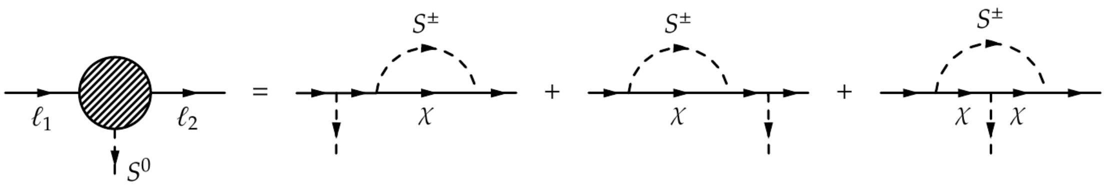

Figure 10.1.: Dominant one-loop corrections to the FCNI subprocess $\ell_1 \to \ell_2 S^0$, further decaying into $S^0 \to \ell_3\bar{\ell}_3$.

It is the purpose of this chapter to investigate the dominant contributions to FCNI decays numerically in the framework of Ref. [3], *whereby it is assumed that the m_R is so large that the radiative charged-lepton decays are invisible.*

[2] The reason for these unsuppressed diagrams is vividly illustrated by the fact that the scalars in them do not only connect through the Yukawa couplings to left-handed neutrinos, such as the W and Z bosons do, but also directly to right-handed neutrinos, and therefore these diagrams avoid a further suppression factor of $1/m_R$ coming from converting left to right-handed neutrinos and back. Remember that in our model, flavour-violating processes require a right-handed neutrino exchange.

[3] In this paper, we do not address muon–electron conversion in nuclei because this would require us to specify the Yukawa couplings of the extra Higgs doublets to the quarks by making *additional assumptions*. This is because, in our model, muon–electron conversion in nuclei occurs – in the limit $m_R \to \infty$ – through $\mu^- \to e^- \left(S_b^0\right)^*$ followed by the $\left(S_b^0\right)^*$ coupling to quarks.

$\mathrm{BR}\left(\mu^{+} \to e^{+}\gamma\right)$	$<$	4.2×10^{-13}
$\mathrm{BR}\left(\tau^{-} \to e^{-}\gamma\right)$	$<$	3.3×10^{-8}
$\mathrm{BR}\left(\tau^{-} \to \mu^{-}\gamma\right)$	$<$	4.4×10^{-8}
$\mathrm{BR}\left(\mu^{-} \to e^{-}e^{+}e^{-}\right)$	$<$	1.0×10^{-12}
$\mathrm{BR}\left(\tau^{-} \to e^{-}e^{+}e^{-}\right)$	$<$	2.7×10^{-8}
$\mathrm{BR}\left(\tau^{-} \to e^{-}\mu^{+}\mu^{-}\right)$	$<$	2.7×10^{-8}
$\mathrm{BR}\left(\tau^{-} \to \mu^{-}\mu^{+}\mu^{-}\right)$	$<$	2.1×10^{-8}
$\mathrm{BR}\left(\tau^{-} \to \mu^{-}e^{+}e^{-}\right)$	$<$	1.8×10^{-8}

Table 10.1.: The experimental bounds of the branching ratios of some lepton flavour-changing decays. All the bounds are at the 90% CL. The first bound is from Ref. [115], all the other bounds are from Ref. [93].

This chapter is structured as follows: To properly suppress these radiative decays, we must first derive the corresponding lower limit on the Seesaw scale m_R. For this purpose, we estimate in Section 10.1 the m_R-suppressed flavour-changing processes of charged leptons with photon radiation $\ell_2^{\pm} \to \gamma\ell_2^{\pm}$ and thus equip the heavy Seesaw scale m_R with a lower bound. Then, in Section 10.2, we analyse the promising branching ratios from FCNIs of the form $\ell_1^- \to \ell_2^-\ell_3^+\ell_3^-$ and $\ell_1^- \to \ell_2^-\ell_2^+\ell_2^-$ and calculate the formulas of the unsuppressed branching ratios, closely following the calculations in the papers [3] and [10]. These branching ratios shall be further analysed on a numerical basis by concrete data input and compared with experimental bounds in order to make assumptions about the remaining, not-fixed parameters in Section 10.3. Thereby we will have to consider the results of the tree-level and one-loop corrections of the neutrino masses from the previous Chapter 9 as input for the branching ratios. Here we demonstrate that it may well be to have *all* five decays $\ell_1 \to \ell_2\ell_3^+\ell_3^-$ just around the corner. Furthermore, we will be able to make a statement about the relevance of one-loop corrections from neutrino masses in FCNIs. Finally, the last Section 10.4 contains the experimental status of lepton FCNIs to get a taste of the current status of this field.

10.1. The Lepton Flavour-Violating Decays $\ell_1 \to \ell_2\gamma$

Let us estimate a lower limit for m_R by using the experimental bounds for radiative decays $\ell_1 \to \ell_2\gamma$ given in Table 10.1.

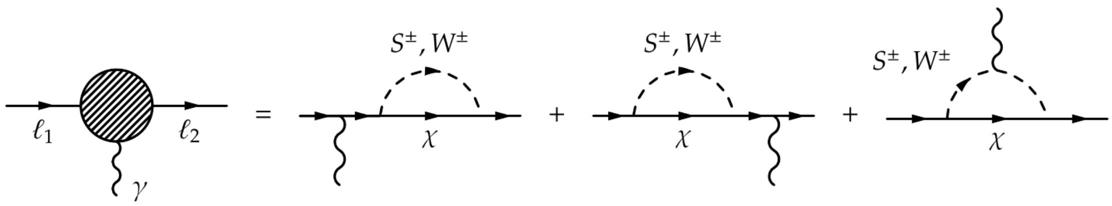

Figure 10.2.: One-loop corrections to FCNIs from radiative decays $\ell_1 \to \ell_2\gamma$.

The amplitude for any such decay has the form

$$\mathcal{A}\left(\ell_1^{\pm} \to \ell_2^{\pm}\gamma\right) = e\,\varepsilon_\rho^*\,\bar{u}_2\left(i\sigma^{\rho\lambda}q_\lambda\right)(A_L\gamma_L + A_R\gamma_R)\,u_1, \tag{10.3}$$

consisting of the Feynman diagrams shown in Figure 10.2, where ε_ρ is the polarization vector of the photon, u_1 and u_2 are the spinors of $\ell_1^{\pm}$ and $\ell_2^{\pm}$, respectively, and γ_L and γ_R are the projectors of chirality. The decay rate is given in the limit $m_{\ell_2} = 0$, by

$$\Gamma\left(\ell_1^{\pm} \to \ell_2^{\pm}\gamma\right) = \frac{\alpha m_{\ell_1}^3}{4}\left(|A_L|^2 + |A_R|^2\right). \tag{10.4}$$

Knowing that A_L and A_R are suppressed by m_R^{-2}, one may estimate on dimensional grounds alone that

$$A_{L,R} \sim \frac{1}{16\pi^2}\frac{m_{\ell_1}}{m_R^2}. \tag{10.5}$$

Using the first two bounds of Table 10.1 together with the experimental values for the masses and widths of the μ and τ, one may then derive the lower limits $m_R \gtrsim 50\,\text{TeV}$ from $\mu^+ \to e^+\gamma$ and $m_R \gtrsim 2\,\text{TeV}$ from $\tau^- \to e^-\gamma$.

Thus, if we take $m_R \gtrsim 500\,\text{TeV}$ in the framework of Ref. [3], then the radiative decays $\ell_1 \to \ell_2\gamma$ are invisible in the foreseeable future. On the other hand, because of the nonzero limit of the amplitudes for $\ell_1 \to \ell_2\left(S_b^0\right)^*$, the charged-lepton decays $\ell_1 \to \ell_2\ell_3^+\ell_3^-$ are unsuppressed when $m_R \to \infty$. Then, m_R is also much larger than the masses of the scalars in the model, which we assume to be between one and a few TeV. This is in agreement with the estimates of the right-handed neutrino masses m_R from the previous chapter, Section 9.3.2, for which we obtained realistic masses in the order of $m_R \gtrsim 10^{10}\,\text{GeV}$, see Table 9.1. So this masses are in fact so large that all the radiative charged lepton decays will be completely invisible for a very long time.

10.2. The Lepton Flavour-Violating Decays $\ell_1^- \to \ell_2^-\ell_3^+\ell_3^-$

Let us get a more detailed picture of the FCNI of three-particle decays. In general, three-particle decay into leptons can be generated through different types of mechanisms:

A. $\Gamma(\ell_1 \to \ell_2\gamma^* \to \ell_2\ell_3\ell_3) \sim \dfrac{1}{16\pi^2}\dfrac{\alpha^2}{G_F^2 m_R^4}\left(\dfrac{m_D}{m_{EW}}\right)^4,$

B. $\Gamma(\ell_1 \to \ell_2 Z^{0*} \to \ell_2\ell_3\ell_3) \sim \dfrac{\alpha_W^4}{G_F^2 m_R^4}\left(\dfrac{m_D}{m_Z}\right)^4,$

C. $\Gamma(\ell_1 \to \ell_2 S^{0*} \to \ell_2\ell_3\ell_3),$

D. $\Gamma(\ell_1 \to \ell_2\ell_3\ell_3)$ in box diagrams, where m_{EW} and m_D is the electroweak scale and the scale for the Dirac masses, respectively, whereby the formulas were taken from [3]. Thus, this decay can either be generated by means of penguin diagrams – a combination of two subprocesses (Types A, B, and C) – as shown in Figure 10.3 in the first two diagrams on the right (with the subprocesses depicted in Figure 10.4), or by means of four box diagrams of Type D, which have the shape of the last diagram outlined in Figure 10.3. It can be clearly seen

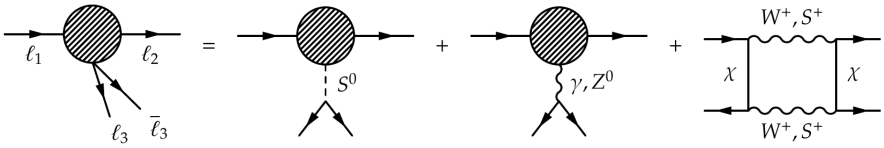

Figure 10.3.: One-loop corrections at the FCNI.

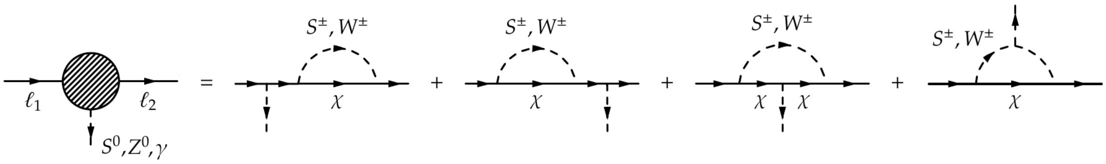

Figure 10.4.: One-loop corrections at the FCNI.

that the branching ratios of Types A and B decrease with the Seesaw scale m_R^{-4}. The authors of [3] further state that a similar suppression was found in the amplitudes of the box diagrams, where $\mathcal{A} \propto m_R^{-2}$ and thus also the branching ratios are suppressed by at least a factor m_R^{-4}. Therefore, the dominant contributions are of Type C, in particular, these are the contributions of the form depicted in Figure 10.1, including two scalars, where a charged scalar runs in the loop and a neutral off-shell scalar decays further into leptons, $S^{0*} \to \ell^- \ell^+$.

The further calculations concentrate exclusively on the dominant contributions of Type C. Since the amplitudes for Type C decays are already derived in [3], we deduce the effective Lagrangian for the subprocess $\ell_1 \to \ell_2 (S_b^0)^*$ in the following Section 10.2.1 on the basis of these results. Afterwards these formulas are simplified with assumptions about the parameter space of this model, the latter being given at the end of the Sections 2 and 3. We continue with the determination of the amplitude of the flavour-changing processes in order to define the formulas for the decay rate in Section 10.2.2.

10.2.1. The effective lepton flavour-violating interaction

Let us start with the calculation of the relevant flavour-violating branching ratios by defining the effective Lagrangian of the subprocess $\ell_1 \to \ell_2 (S_b^0)^*$. As ascertained in the previous section, this subprocess describes FCNIs between leptons and the physical neutral scalars S_b^0, which include loops with charged scalars and neutrinos as they are shown in Figure 10.1. According to Ref. [3], this subprocess is given in the limit $m_R \to \infty$ by

$$\mathcal{L}_{\text{eff}}\left(S^0\right) = \sum_{b\geq 2} S_b^0 \sum_{\ell_1\neq\ell_2} \bar{\ell}_1 \left[\left(A_L^b\right)_{\ell_1\ell_2} \gamma_L + \left(A_R^b\right)_{\ell_1\ell_2} \gamma_R\right] \ell_2. \tag{10.6}$$

Note that the summation over b starts with $b = 2$, i.e. it excludes the Goldstone boson S_1^0. The coefficients $\left(A_{L,R}^b\right)_{\ell_1\ell_2}$ were calculated in Ref. [3] and contain the contributions depicted in Figure 10.1.

Let us further define the variables $(A_L^b)_{\ell_1\ell_2}$ and $(A_R^b)_{\ell_1\ell_2}$, which are given in Formula (10.7) with their parts $X_{\ell_1\ell_2}$ and $A^b_{\ell_1\ell_2}(A_1, A_2, A_3)$ specified below,

$$\left(A_L^b\right)_{\ell_1\ell_2} = \frac{X_{\ell_1\ell_2} A^b_{\ell_1\ell_2}}{m_{\ell_1}^2 - m_{\ell_2}^2} \quad \text{and} \quad \left(A_R^b\right)_{\ell_1\ell_2} = \frac{X^*_{\ell_2\ell_1}\left(A^b_{\ell_2\ell_1}\right)^*}{m_{\ell_2}^2 - m_{\ell_1}^2}, \tag{10.7}$$

where m_{ℓ_i} is the mass of the charged lepton ℓ_i and

$$X_{\ell_1\ell_2} \equiv \frac{1}{16\sqrt{2}\pi^2} \sum_{i=4}^{6} \left[(U_R)_{\ell_1 i}\left(U_R^*\right)_{\ell_2 i} \ln\frac{m_i^2}{\mu^2}\right] = X^*_{\ell_2\ell_1}, \tag{10.8}$$

where μ is a mass scale which is arbitrary due to the unitarity of U_R.

$$\begin{aligned} A^b_{\ell_1\ell_2} \quad = \quad & \sum_{k=1}^{n} V^*_{kb} \Big\{ \left(\Delta_k^*\right)_{\ell_1\ell_1} \left(m_{\ell_1}^2 - m_{\ell_2}^2\right)(A_1)_{\ell_1\ell_2} \\ & + (\Gamma_k)_{\ell_1\ell_1}\left[-m_{\ell_1}\left(M_D^*\right)_{\ell_1\ell_1}(A_1)_{\ell_1\ell_2} + \frac{m_{\ell_2}^2}{2}(A_2)_{\ell_1\ell_2} - m_{\ell_2}(M_D)_{\ell_2\ell_2}(A_3)_{\ell_1\ell_2}\right] \\ & + (\Gamma_k)_{\ell_2\ell_2}\left[m_{\ell_2}\left(M_D^*\right)_{\ell_1\ell_1}(A_1)_{\ell_1\ell_2} - \frac{m_{\ell_1}m_{\ell_2}}{2}(A_2)_{\ell_1\ell_2} + m_{\ell_1}(M_D)_{\ell_2\ell_2}(A_3)_{\ell_1\ell_2}\right]\Big\}. \end{aligned} \tag{10.9}$$

Finally, we define the flavour-space matrices $A_{1,2,3}$ as part of $A^b_{\ell_1\ell_2}$, which are given in Formula (10.9),

$$(A_1)_{\ell_1\ell_2} \equiv \sum_{k=1}^{n} (\Gamma_k)_{\ell_1\ell_1}(\Delta_k)_{\ell_2\ell_2}, \tag{10.10a}$$

$$(A_2)_{\ell_1\ell_2} \equiv \sum_{k=1}^{n} \left(\Delta_k^*\right)_{\ell_1\ell_1}(\Delta_k)_{\ell_2\ell_2}, \tag{10.10b}$$

$$(A_3)_{\ell_1\ell_2} \equiv \sum_{k=1}^{n} \left(\Delta_k^*\right)_{\ell_1\ell_1}\left(\Gamma_k^*\right)_{\ell_2\ell_2}. \tag{10.10c}$$

Note that $A_3 = A_1^\dagger$ and $A_2 = A_2^\dagger$. With the equations[4] in (3.25), we find that in the sum over k in Equation (10.9), the term with $k = 1$ gives a null contribution. So, *in the Higgs*

[4] As a reminder of Formula (3.25): $(\Delta_1^*)_{\ell_1\ell_1} = \frac{\sqrt{2}}{v^*}(M_D^*)_{\ell_1\ell_1}$, $(\Gamma_1)_{\ell_1\ell_1} = \frac{\sqrt{2}}{v^*}m_{\ell_1}$.

basis, the contribution to $A^b_{\ell_1\ell_2}$ proportional to V^*_{1b} is identical to zero. Especially, if only one Higgs doublet is present, i.e. in the SM, $A^b_{\ell_1\ell_2} = 0$, viz. if $n_H = 1$, there are no effective lepton flavour-violating interactions of the neutral scalar in the limit $m_R \to \infty$.

10.2.2. The decay rate

If $\ell_2 \neq \ell_3$, then $\ell_1^- \to \ell_2^- \ell_3^+ \ell_3^-$ may be either $\tau^- \to \mu^- e^+ e^-$ or $\tau^- \to e^- \mu^+ \mu^-$. Equation (10.6) supplies the amplitude of the subprocess $\ell_1^- \to \ell_2^- \left(S^0_b\right)^*$. For the following $\left(S^0_b\right)^* \to \ell_3^+ \ell_3^-$, we revise the Lagrangian of Equation (3.20a)

$$\mathcal{L}^{(\ell^\pm)}_{\rm Y}\left(S^0\right) = -\frac{1}{\sqrt{2}} \sum_{b=2}^{2n} S^0_b \sum_{\ell=e,\mu\tau} \bar{\ell}\left[\left(\hat{\Gamma}_b\right)_{\ell\ell}\gamma_L + \left(\hat{\Gamma}^\dagger_b\right)_{\ell\ell}\gamma_R\right]\ell, \tag{10.11}$$

where according to Equation (3.20b)

$$\hat{\Gamma}_b \equiv \sum_{k=1}^{n} V^*_{kb}\Gamma_k. \tag{10.12}$$

We write the decay amplitude for $\ell_1^- \to \ell_2^- \ell_3^+ \ell_3^-$ as

$$\mathcal{A} = \sum_{b=2}^{2n} \bar{u}_2\left[(\lambda_b)_{\ell_2\ell_1}\gamma_L + (\rho_b)_{\ell_2\ell_1}\gamma_R\right]u_1\, \bar{u}_3\left[\left(\hat{\Gamma}_b\right)_{\ell_3\ell_3}\gamma_L + \left(\hat{\Gamma}^\dagger_b\right)_{\ell_3\ell_3}\gamma_R\right]v_3, \tag{10.13}$$

where, from Equations (10.6) and (10.11),

$$(\lambda_b)_{\ell_2\ell_1} = -\frac{\left(A^b_L\right)_{\ell_2\ell_1}}{\sqrt{2}\,M_b^2} \quad \text{and} \quad (\rho_b)_{\ell_2\ell_1} = -\frac{\left(A^b_R\right)_{\ell_2\ell_1}}{\sqrt{2}\,M_b^2}. \tag{10.14}$$

In Equations (10.14), M_b is the mass of S^0_b. In the scalar propagators, we have neglected the four-momentum of the $\ell_3^+\ell_3^-$ subsystem. With the amplitude in Equation (10.13), the decay rate is given by

$$\Gamma = \left(\ell_1^- \to \ell_2^-\ell_3^+\ell_3^-\right) = |\mathcal{A}|^2 \frac{1}{2m}\int\frac{d^3p_2}{2E_2}\int\frac{d^3p_3}{2E_3}\int\frac{d^3p_3'}{2E_3'}\,\delta^{(4)}\left(p_1 - p_2 - p_3 - p_3'\right), \tag{10.15}$$

which, after some calculations in which we neglected the masses of the final charged leptons in the kinematics, leads to

$$\begin{aligned}\Gamma\left(\ell_1^- \to \ell_2^-\ell_3^+\ell_3^-\right) \;=\; & \frac{m^5_{\ell_1}}{6144\pi^3}\left[\left|\sum_{b=2}^{2n}(\lambda_b)_{\ell_2\ell_1}\left(\hat{\Gamma}_b\right)_{\ell_3\ell_3}\right|^2 + \left|\sum_{b=2}^{2n}(\lambda_b)_{\ell_2\ell_1}\left(\hat{\Gamma}^*_b\right)_{\ell_3\ell_3}\right|^2\right. \\ & \left. + \left|\sum_{b=2}^{2n}(\rho_b)_{\ell_2\ell_1}\left(\hat{\Gamma}_b\right)_{\ell_3\ell_3}\right|^2 + \left|\sum_{b=2}^{2n}(\rho_b)_{\ell_2\ell_1}\left(\hat{\Gamma}^*_b\right)_{\ell_3\ell_3}\right|^2\right].\end{aligned} \tag{10.16}$$

If $\ell_2 = \ell_3$, then $\ell_1^- \to \ell_2^- \ell_2^+ \ell_2^-$ may be either $\mu^- \to e^- e^+ e^-$ or $\tau^- \to e^- e^+ e^-$ or $\tau^- \to \mu^- \mu^+ \mu^-$. In Equation (10.13), the amplitude must be antisymmetrical with respect to ℓ_2^-, and an additional factor 1/2 must be added to the kinematics. The final result is

$$\begin{aligned}\Gamma\left(\ell_1^- \to \ell_2^- \ell_2^+ \ell_2^-\right) &= \frac{m_{\ell_1}^5}{6144\pi^3} \left[\frac{1}{2} \left| \sum_{b=2}^{2n} (\lambda_b)_{\ell_2 \ell_1} \left(\hat{\Gamma}_b\right)_{\ell_2 \ell_2} \right|^2 + \frac{1}{2} \left| \sum_{b=2}^{2n} (\rho_b)_{\ell_2 \ell_1} \left(\hat{\Gamma}_b^*\right)_{\ell_2 \ell_2} \right|^2 \right. \\ &\left. + \left| \sum_{b=2}^{2n} (\lambda_b)_{\ell_2 \ell_1} \left(\hat{\Gamma}_b^*\right)_{\ell_2 \ell_2} \right|^2 + \left| \sum_{b=2}^{2n} (\rho_b)_{\ell_2 \ell_1} \left(\hat{\Gamma}_b\right)_{\ell_2 \ell_2} \right|^2 \right]. \qquad (10.17)\end{aligned}$$

Assuming Γ, Δ in the diagonal notation of Equation (4.4), Equations (10.10) and (10.9) yield

$$A_{\ell_1 \ell_2}^b = V_{2b}^* A_{\ell_1 \ell_2}, \qquad (10.18a)$$

$$\begin{aligned}A_{\ell_1 \ell_2} &= \frac{\sqrt{2}\left(m_{\ell_1}^2 - m_{\ell_2}^2\right) m_{\ell_1} \delta_{\ell_1}^* d_{\ell_2}}{v} \\ &- \left(m_{\ell_1}^2 + \frac{m_{\ell_2}^2}{2}\right) \gamma_{\ell_1} d_{\ell_1}^* d_{\ell_2} + \frac{3 m_{\ell_1} m_{\ell_2}}{2} d_{\ell_1}^* \gamma_{\ell_2} d_{\ell_2} \\ &+ \left(m_{\ell_1}^2 - \frac{m_{\ell_2}^2}{2}\right) \gamma_{\ell_1} \delta_{\ell_1}^* \delta_{\ell_2} - \frac{m_{\ell_1} m_{\ell_2}}{2} \delta_{\ell_1}^* \gamma_{\ell_2} \delta_{\ell_2} \\ &+ \frac{v m_{\ell_2}}{\sqrt{2}} \left(\gamma_{\ell_1} d_{\ell_1}^* \gamma_{\ell_2} \delta_{\ell_2} - \gamma_{\ell_1} \delta_{\ell_1}^* \gamma_{\ell_2}^* d_{\ell_2}\right) + \frac{v m_{\ell_1}}{\sqrt{2}} \left(\delta_{\ell_1}^* \left|\gamma_{\ell_2}\right|^2 d_{\ell_2} - \gamma_{\ell_1}^2 d_{\ell_1}^* \delta_{\ell_2}\right) \qquad (10.18b)\end{aligned}$$

As demonstrated at the end of Section 10.2.1, in $A_{\ell_1 \ell_2}^b$, the term proportional to V_{1b}^* disappears. With the assumption for the scalar mixing matrix V, (3.34), and the lepton-Yukawa coupling $\hat{\Gamma}_b$, (3.36a), we obtain from Equation (10.18a),

$$A_{\ell_1 \ell_2}^2 = 0, \quad A_{\ell_1 \ell_2}^3 = e^{i\alpha} A_{\ell_1 \ell_2}, \quad A_{\ell_1 \ell_2}^4 = -i e^{i\alpha} A_{\ell_1 \ell_2}. \qquad (10.19)$$

The decay rates are then

$$\Gamma\left(\ell_1^- \to \ell_2^- \ell_3^+ \ell_3^-\right) = \frac{m_{\ell_1}^5}{6144\pi^3} \left|X_{\ell_2 \ell_1}\right|^2 \left|\gamma_{\ell_3}\right|^2 \frac{\left|A_{\ell_2 \ell_1}\right|^2 + \left|A_{\ell_1 \ell_2}\right|^2}{\left(m_{\ell_2}^2 - m_{\ell_1}^2\right)^2} \left(\frac{1}{M_3^4} + \frac{1}{M_4^4}\right), \qquad (10.20a)$$

$$\begin{aligned}\Gamma\left(\ell_1^- \to \ell_2^- \ell_2^+ \ell_2^-\right) &= \frac{m_{\ell_1}^5}{6144\pi^3} \left|X_{\ell_2 \ell_1}\right|^2 \left|\gamma_{\ell_2}\right|^2 \frac{\left|A_{\ell_2 \ell_1}\right|^2 + \left|A_{\ell_1 \ell_2}\right|^2}{\left(m_{\ell_2}^2 - m_{\ell_1}^2\right)^2} \\ &\times \left[\frac{3}{4}\left(\frac{1}{M_3^4} + \frac{1}{M_4^4}\right) + \frac{1}{2 M_3^2 M_4^2}\right]. \qquad (10.20b)\end{aligned}$$

The decay rates depend on the masses M_3 and M_4 of the non-SM-neutral scalar fields S_3^0 and S_4^0, respectively. There is no dependence on the phase α. In Equation (10.20a), $\ell_2 \neq \ell_3$ is understood.

We stated before in Equation (10.2) that according to the results of [3], the amplitudes of FCNIs such as $\ell_1^- \to \ell_2^- \ell_3^+ \ell_3^-$ remain constant even if the Seesaw scale m_R goes to infinity. This is consistent with our result in Equation (10.20). Moreover, this means that although the only flavour-violating part, the right-handed neutrinos, decouple with $m_R \to \infty$, effective flavour-violating Yukawa couplings arise from one-loops and are non-zero, non-decoupling, and therefore not m_R-suppressed. The model in the limit $m_R \to \infty$ develops into a normal two-Higgs-doublet model, however, with loop-suppressed flavour-changing Yukawa couplings of the order $\sim m_D/M_{EW}$ as indicated in [3]. This non-decoupling phenomenon just appears at $n_H \geq 2$, so the non-vanishing contributions must also include processes with new scalars, as we have just seen.

10.3. Parameter Analysis of FCNI Branching Ratios

In this section, we want to show that in the two-Higgs-doublet version of the framework of Ref. [3], *there is not only a parameter space that respects the experimental limits of the flavour-violating branching ratios, but there are also regions in the parameter space where the branching ratios of all five decays $\ell_1^- \to \ell_2^- \ell_3^+ \ell_3^-$ are close to their current experimental upper bounds,* displayed in Table 10.1, where the branching ratios are defined as

$$\mathrm{BR}\left(\ell_1^- \to \ell_2^- \ell_3^+ \ell_3^-\right) = \frac{\Gamma\left(\ell_1^- \to \ell_2^- \ell_3^+ \ell_3^-\right)}{\Gamma_{\text{tot}}(\ell_1)}, \tag{10.21}$$

where $\Gamma_{\text{tot}}(\ell_1)$ is the inverse lifetime of ℓ_1.

We will further analyse the parameters within the branching ratios and search for fitting parameter spaces by means of the reduced qualitative method, as introduced and justified in Chapter 6.3, and as we did in the previous Chapter 9. In concrete terms, this means that we stick to the chosen parameter Sets A and B in Table 9.1 and analyse the space of each free parameter by varying it while the other parameters remain fixed at the given values. In addition, we will analyse the emerging relationships between the parameters resulting from the constraints imposed by the experimental limits of the branching ratios, as far as it is possible.

Furthermore, in each graph, we will plot the branching ratios, including the tree-level neutrino masses, in dotted lines, together with the one-loop masses in solid lines. In this way we can show the difference between them and investigate the relevance of the one-loop corrections for the neutrino masses in FCNIs at the end, which in turn contain the neutrino masses via the quantities $|X_{\ell_1\ell_2}|^2$ calculated in the last Chapter 9.1.1. In the course of the computations, in that last chapter, the values for $\left|X_{\ell_2\ell_1}\right|^2$ were saved, together with the values of all relevant parameters. This list of parameters is in turn plugged into the formulas of the decay rates and thus the branching ratios and was used to create the desired diagrams in this section.

The lepton flavour-changing branching ratios, Equation (10.21), including the decay rates in Equation (10.20), contain the parameters

1. M_3, M_4, μ_2, which we have defined in Equation (8.42a) in Chapter 8.3,

2. The masses and mixing matrix of the right-handed neutrinos via $\left|X_{\ell_2\ell_1}\right|^2$ and thus the light neutrino mass m_1, all of which were calculated in the previous Chapter 2.3 and analysed in Section 9.3.4,

3. The Yukawa coupling constants d_ℓ ($\sim \Delta_1$) proportional to the neutrino Dirac mass M_D, which connects neutrinos with the Higgs boson,

4. The couplings between leptons and the new scalars γ_ℓ ($\sim \Gamma_2$) and δ_ℓ ($\sim \Delta_2$), respectively.

Among this parameters, Points 2-4 include those that can still be varied, these are analysed and defined below by the objectives we set at the beginning of this chapter, namely to set all branching ratios lower than but close to the experimental bounds. As we will see in the further analysis of the parameter space, the outcome of the branching ratios is essentially dependent on the parameter interplay within the value $A^b_{\ell_1\ell_2}$, given in Equation (10.18b), besides the value $\left|X_{\ell_2\ell_1}\right|^2$ from Equation (10.8).

In general, it can be stated for all investigated parameters that the branching ratio progressions shown in the following quite accurately reflect the patterns of the $\left|X_{\ell_2\ell_1}\right|^2$ progressions investigated in the previous chapter, including the singularities and irregularities around the area where one-loop contributions within the formula of the neutrino masses are equal to the contributions at tree-level, i.e. if Equation (9.57) applies.

The organization of this section follows a line of argumentation. The analysis for each parameter is based on a mixture of the expected behaviour read from the formula, which is compared with the numerical outcome shown in the diagrams, leading to the conclusions regarding our objectives as indicated at the beginning of this chapter.

Parameter γ_ℓ

Among the Yukawa couplings γ_ℓ mentioned in Point 4, γ_μ is set to $\gamma_\mu = 1.7$ by the μ-MDM in Equation (8.42b). We now focus on finding a parameter range for the remaining γ_e and γ_τ-Yukawa couplings, taking into account that the upper limit on γ_e is $\gamma_e < 2.7$ from Equation (8.41).

All experimental upper bounds of the branching ratios of the τ decays in Table 10.1 are quite similar. So if we want both $\tau^- \to \ell^- e^+ e^-$ and $\tau^- \to \ell^- \mu^+ \mu^-$ to be close to their experimental upper bounds, then γ_e and γ_μ must be similar – see the explicit factors γ_{ℓ_3} and γ_{ℓ_2} in the decay rates of Equations (10.20a) and (10.20b), respectively. Furthermore, the branching ratios scale with BR $\sim \gamma^6$ (taking $\gamma = \gamma_{\ell_1} = \gamma_{\ell_2} = \gamma_{\ell_3}$)

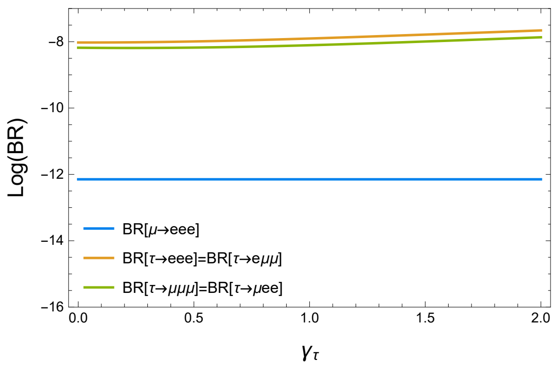

Figure 10.5.: The FCNI branching ratios as functions of γ_τ, where all variables except γ_τ are given by Set A of Table 9.1. The course of γ_τ for Set B looks similar.

and are therefore strongly suppressed for lower $\gamma < 1$. The approximate symmetry between γ_e and γ_μ and the strong dependence on γ_ℓ is reflected in the diagrams in Figure 10.6, where we show the way the five branching ratios vary as functions of γ_e and γ_μ, γ_τ: The branching ratios increase to the power of two, four, or six, respectively.

Since, in addition, the variation of γ_τ has almost no influence on the branching ratios, see Figure 10.5, and it does not matter what value it takes, we choose all three γ_ℓ the same for our parameter sets,

$$\gamma_e = \gamma_\mu = \gamma_\tau = 1.7. \tag{10.22}$$

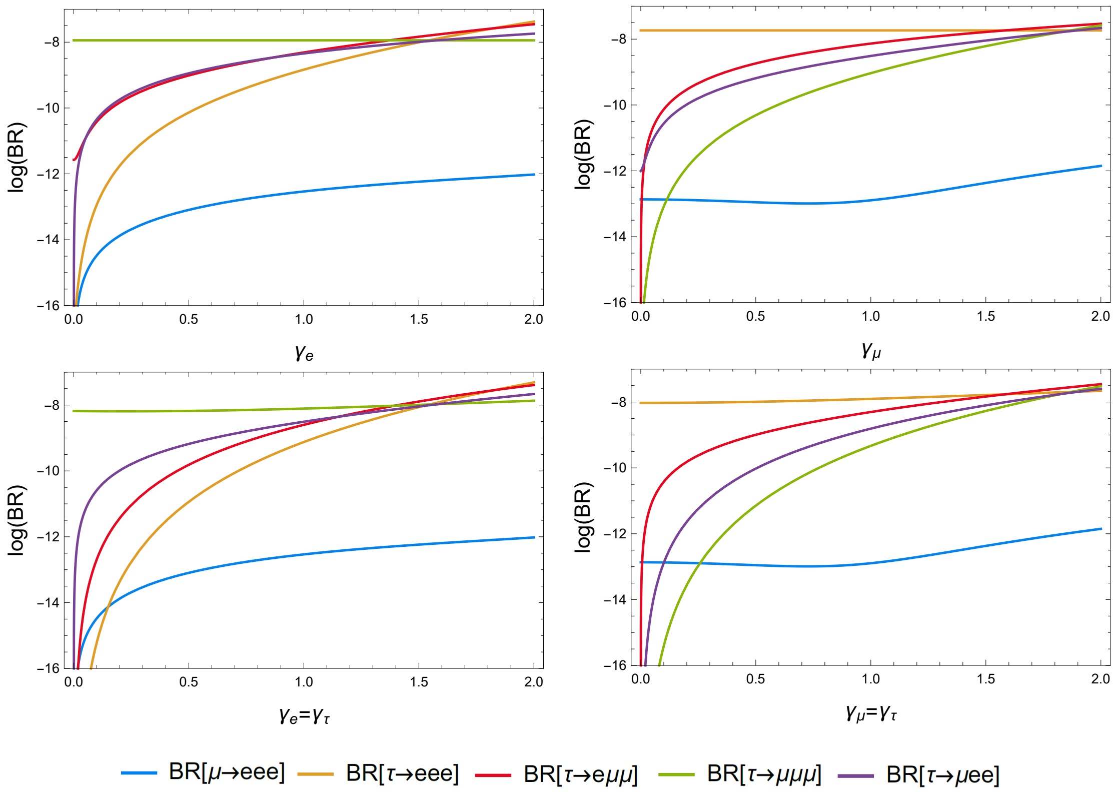

Figure 10.6.: The branching ratios of the FCNIs as functions of various Yukawa couplings. In the figure above left, γ_e varies between 0 and 2. In the figure on the top right, γ_μ varies. At the bottom left, γ_e and γ_τ change but with γ_τ remaining equal to γ_e. In the bottom right, $\gamma_\mu = \gamma_\tau$ varies. In all figures, all Yukawa couplings which do not vary take the values of Set A from Table 9.1. The course of the varying γ_ℓ is the same for Set B.

Parameter m_1

The mass of the lightest neutrino m_1 is only indirectly contained in the factors $\left|X_{\ell_2\ell_1}\right|^2$ by the right-handed neutrino masses $\hat{m}_R(m_1)$ and the mixing matrices $U_N(m_1)$ computed in the previous chapter, see Figure 9.4.

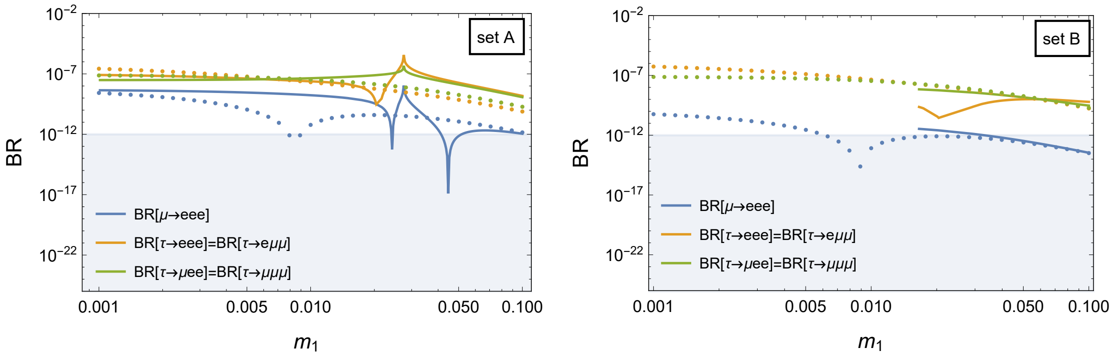

Figure 10.7.: The branching ratios as a function of m_1. The dotted lines reflect the branching ratios with contributions from the right-handed neutrino masses at tree-level, the solid lines ones at the one-loop level. The experimental allowed range for $\mathrm{BR}\left(\mu^- \to e^- e^+ e^-\right)$ with the bound $\mathrm{BR}\left(\mu^- \to e^- e^+ e^-\right) < 10^{-12}$ is shown via the blue-shaded region. The region without one-loop solutions for the branching ratios within Set B is highly likely to result from the fact that parameter Set B is close to the critical range, i.e. Equation (9.57) applies, see previous Chapter 9.3.4.

Comparing the diagrams in Figure 9.4 with those representing the branching ratios of the lepton decays in Figure 10.7, one can see, as predicted, that the patterns of $\left|X_{\ell_2\ell_1}\right|^2$ are directly reflected in the branching ratios. E.g. one finds the critical regions without solutions for lower values of m_1, which, as mentioned in Section 9.3.4 come from Set B being close to a singularity where Equation (9.57) applies. Also, an antiproportional behaviour between m_1 and the leptonic branching ratios can be recognized. Consequently, and with regard to the experimental limit value for $\mathrm{BR}\left(\mu^- \to e^- e^+ e^-\right) < 10^{-12}$, it can be observed in Figure 10.7 that larger values for m_1 not only avoid critical ranges but are also advantageous to suppress $\mathrm{BR}\left(\mu^- \to e^- e^+ e^-\right)$. This, and the fact that a lower m_1 leads to an even higher m_R, makes a relatively high m_1 a good choice so that for our parameter sets, we take

$$m_1 = 0.05\,\mathrm{eV}. \tag{10.23}$$

Parameters δ_e and δ_μ

The δ_ℓ Yukawa couplings of the new scalars influence only the contributions $A_{\ell_1\ell_2}$ of the decay rates. In $A_{\ell_1\ell_2}$, the dominant terms in Equation (10.18b) have $v \simeq 246\,\mathrm{GeV}$ in the numerator; if we assume all γ_ℓ to be equal and real $\gamma_e = \gamma_\mu = \gamma_\tau = \gamma$ as previously suggested, these become

$$A_{\ell_1\ell_2} \approx \frac{vm_{\ell_2}}{\sqrt{2}}\gamma^2\left(d^*_{\ell_1}\delta_{\ell_2} - \delta^*_{\ell_1}d_{\ell_2}\right) + \frac{vm_{\ell_1}}{\sqrt{2}}\gamma^2\left(\delta^*_{\ell_1}d_{\ell_2} - d^*_{\ell_1}\delta_{\ell_2}\right), \quad \text{vis.} \tag{10.24a}$$

$$A_{\ell_1\ell_2} \approx \frac{v}{\sqrt{2}}\gamma^2\left(m_{\ell_1} - m_{\ell_2}\right)\left(\delta_{\ell_1}d_{\ell_2} - d_{\ell_1}\delta_{\ell_2}\right), \qquad \text{for } \delta_\ell,\ d_\ell \text{ real.} \tag{10.24b}$$

These dominant terms for $A_{\mu e}$ (and equally for $A_{e\mu}$) will contribute far too much to $\mathrm{BR}\left(\mu^- \to e^-e^+e^-\right)$ for large $\gamma_e = \gamma_\mu = 1.7$ and large $d_e \sim d_\mu \geq 0.01$ unless there is a delicate cancellation between the terms proportional to δ_e and the terms proportional to δ_μ. This is achieved with the condition derived from Equation (10.24b)

$$\frac{d_e}{d_\mu} \simeq \frac{\delta_e}{\delta_\mu}. \tag{10.25}$$

This equation and the cancellation are illustrated in Figure 10.8 for given $d_e/d_\mu = 4$ of the Set A. If Equation (10.25) had an equal sign, $A_{\mu e}$ would almost completely disappear.

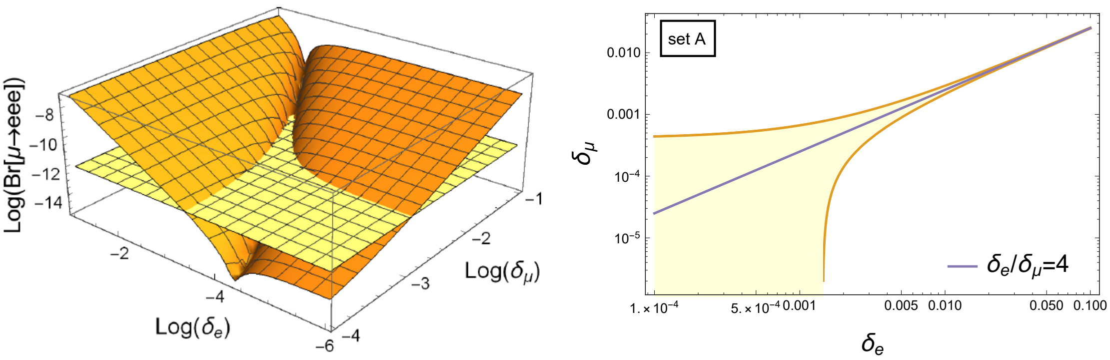

Figure 10.8.: On the left side, $\mathrm{BR}\left(\mu^- \to e^-e^+e^-\right)$ is plotted as functions of δ_e and δ_μ for Set A, the light yellow area shows the experimental boundary of $\mathrm{BR}\left(\mu^- \to e^-e^+e^-\right) < 10^{-12}$. Therefore, the blue area between the orange areas indicates the allowed range for the parameters δ_e and δ_μ. This area is shown again in the diagram on the right. In the two diagrams, all variables except the varied δ are taken from Table 9.1. The behaviour of Set B is identical.

This case is illustrated by the purple line in the right diagram in Figure 10.8. Since we want the branching ratio to be near the experimental boundary rather than disappearing, there must be an offset $\Delta\delta$ in the $\delta_e - \delta_\mu$ relation of

$$\delta_e = \frac{d_e}{d_\mu}\delta_\mu \pm \Delta\delta, \tag{10.26}$$

represented by the orange borders in the right diagram in Figure 10.8. The lower orange line remains for small $\delta_\mu < 0.0007$ with the offset of $\Delta\delta = 0.0015$. The same applies to Set B with even less strict limits of $\delta_\mu < 0.0005$ and $\Delta\delta = 0.004$. Thus, lower values for $\delta_{e,\mu}$ and even more in combination with a lower $d_{e,\mu}$ require less fine-tuning to stay below the experimental limit of $\mathrm{BR}\left(\mu^- \to e^- e^+ e^-\right) < 10^{-12}$, probably because the other terms in $A_{\mu e}$ besides the one considered dominant are suppressed as well. Using the formula in Equation (10.26), one can now choose any number of combinations for δ_e and δ_μ that would fit.

Since we concluded in the previous Chapter 9 that smaller δ_ℓ couplings $\delta_\ell < d$ would be advantageous, we chose $\delta_\mu = 0.0002(0.0001)$ and $\delta_e = 0.002(0.003)$ as illustrations for Sets A and B.

Parameter d_e and δ_τ

In contrast to the previous chapter, where we concentrated more on the cancellation of $\mathrm{BR}\left(\mu^- \to e^- e^+ e^-\right) < 10^{-12}$, we would like to have large branching ratios of the τ decays near the boundaries and therefore we try to achieve high values for the factor $\delta_\tau d_{e/\mu} - d_\tau \delta_{e/\mu}$ in Equation (10.24b), from which follows

$$\delta_\tau \, d_{e/\mu} \gg d_\tau \, \delta_{e/\mu} \qquad \text{or} \qquad d_\tau \, \delta_{e/\mu} \gg \delta_\tau \, d_{e/\mu}. \tag{10.27}$$

If $d_e \simeq d_\mu = d_\tau$ as in our parameter sets, Equation (10.27) leads to either

$$\delta_\tau \gg \delta_e, \delta_\mu \qquad \text{or} \qquad \delta_e, \delta_\mu \gg \delta_\tau. \tag{10.28}$$

Since we have found in the previous subsection that, in order to stay below the experimental boundary of $\mathrm{BR}\left(\mu^- \to e^- e^+ e^-\right) < 10^{-12}$, low values for δ_e, δ_μ are beneficial for less fine-tuning, we decide for the case

$$\delta_\tau \gg \delta_e, \delta_\mu \qquad \text{and thus} \qquad \delta_\tau \, d_{e/\mu} \gg d_\tau \, \delta_{e/\mu}, \tag{10.29}$$

e.g. for Sets A(Set B), it is a factor of $\delta_\tau/\delta_e \sim 35(233)$. As assumed, the diagrams in Figure 10.9 show that δ_τ needs to have a larger value > 0.01 to keep the τ-branching ratios close to the boundary, so we choose for Sets A(Set B)

$$\delta_\tau = 0.07(0.7). \tag{10.30}$$

However, condition (10.29) is not sufficient to obtain the reaction rates at the level of experimental boundaries. For this, it needs

$$d_e > d_\mu \geq d_\tau \tag{10.31}$$

to compensate the factor $1/(m_\tau^2 - m_e^2)$ in the decay rates, Equation (10.20), which is much smaller compared to $1/(m_\tau^2 - m_\mu^2)$. Therefore, $d_e = 0.4$ is chosen in Set A and $d_e = 0.07$ in Set B.

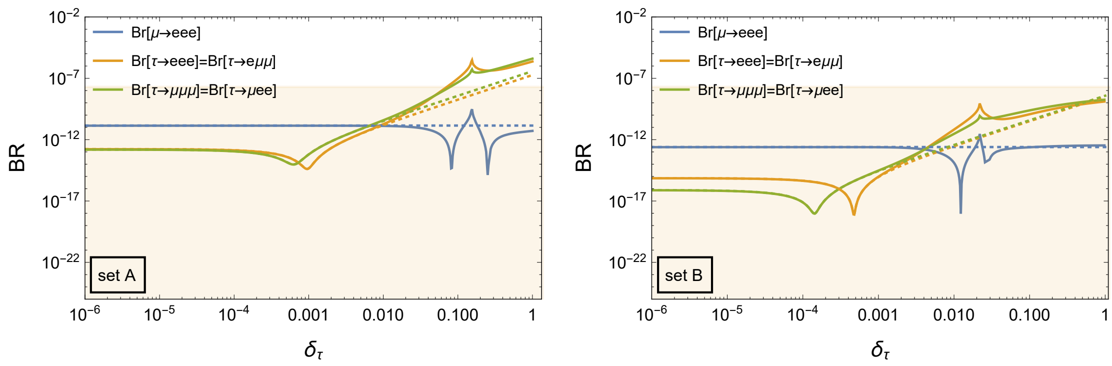

Figure 10.9.: The branching ratios of the τ-decays are plotted as a function of δ_τ for Set B and Set A. The dotted lines reflect the branching ratios with contributions of the right-handed neutrino masses at tree-level and the solid lines for those at the one-loop level. The upper edge of the orange area represents the experimental boundary for the branching ratios of the τ decays. Parameters that are not varied parameters are taken from Table 9.1.

Parameter d_ℓ

Summarizing the preliminary results for the coupling d_ℓ in Chapter 9.3.3, we derived a plausible scale for the Dirac masses m_D with Equations (9.51) and (9.52), which are proportional to the Yukawa couplings d_ℓ. We found that reasonable ranges are from $d = 0.01 - 0.1$. In Chapter 9.3.4, we have analysed that unproblematic parameter spaces are located in the regions where $\delta_\ell \sqrt{M_4^2 - M_3^2} < d_\ell \, m_{EW}$, i.e. where $\delta_\ell < 100\, d_\ell$ for the scalar masses $M_3 = 1\,\text{TeV}$ and $M_4 = 2\,\text{TeV}$. For our parameter sets, considering a high value δ_τ in Equation (10.30) requires $d \gtrsim 0.01$.

Furthermore, we find that as d_e, d_μ, d_τ increases, the leptonic branching ratios increase due to BR$\sim |A_{\ell_1\ell_2}|^2 \sim d^2_{\ell_{1/2}}$, (10.20), as also shown in Figure 10.10: An increase in d_e also increases BR$\,(\tau^- \to e^-\ell^+\ell^-)$ (if like here, $\delta_\tau > \delta_e$), and an increase in d_μ also increases BR$\,(\tau^- \to \mu^-\ell^+\ell^-)$ and BR$\,(\mu^- \to e^-e^+e^-)$ (if like here, $\delta_e > \delta_\mu$). This could become problematic since the leptonic branching ratios also increase with a decreasing light neutrino mass m_1 by an increase of $|X_{\ell_1\ell_2}|^2$. Therefore, these two quantities $|X_{\ell_1\ell_2}|^2$ and $A_{\ell_1\ell_2}$ must be in equilibrium within the branching ratios, (10.20), in order to respect the experimental boundaries[5]. This thus means also the parameters d_ℓ and m_1 must compensate each other; from a big m_1 follows a big d_ℓ. In particular, an upper limit on $m_1 \lesssim 0.1\,\text{eV}$ sets an upper limit on the d_ℓ couplings of $d \lesssim 1$. To achieve relatively large τ-decay rates and at the same time keep d_ℓ and $m_1 = 0.05\,\text{eV}$ greater,[6] as recommended in the previous sections and in Chapter 9.3.4, we set the two parameters to $d_\mu = d_\tau =$

[5] This only applies if the branching ratio is not suppressed by small $\gamma_\ell < 1$ or large M_b. Remember that $\gamma_\ell \sim 1$ and $M_3 \sim 1\,\text{TeV}$ were the preferred parameter values within the solutions of a suitable muon AMM in Chapter 8.3.

[6] Note that if one uses $d_e = d_\mu = d_\tau = 0$ in the $A_{\ell_1\ell_2}$ of Equation (10.18b), then only two subdominant terms, i.e. terms without v in the numerator, survive.

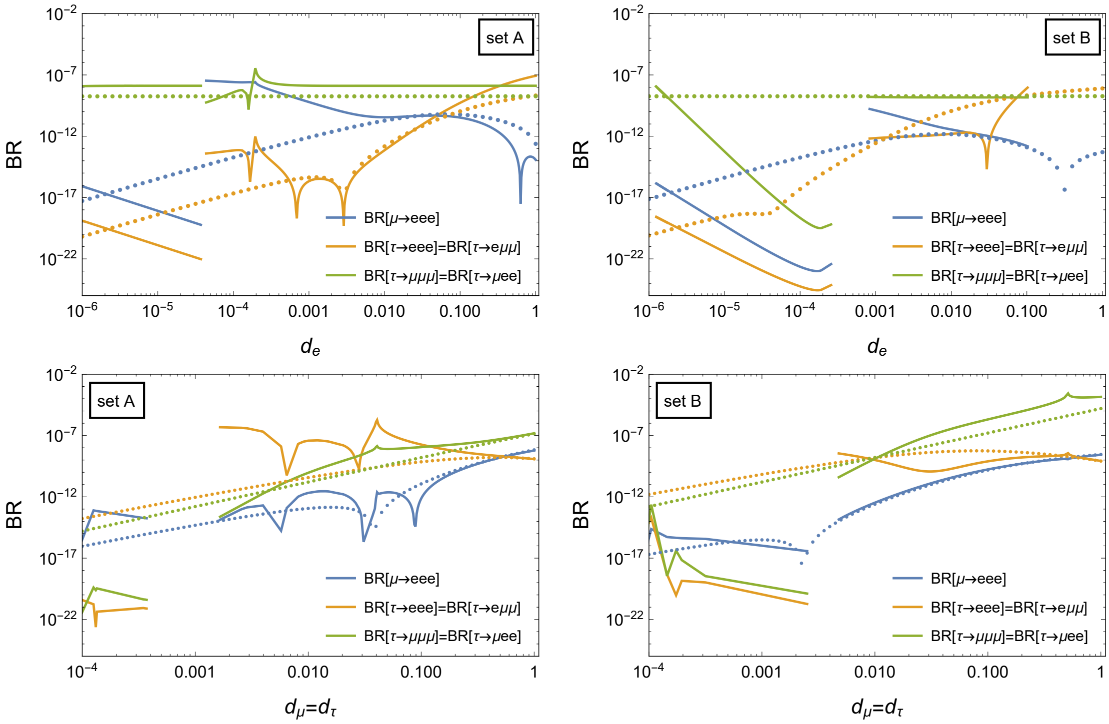

Figure 10.10.: The branching ratios of the τ decays are shown as a function of d_e and $d_\mu = d_\tau$ for Set B and Set A. The dotted lines reflect the branching ratios with contributions of the right-handed neutrino masses at tree-level, the solid lines those at one-loop level. Parameters that are not varied are taken from Table 9.1. Values for $d_\mu = d_\tau < 10^{-4}$ are not shown because the numerics in this range become unstable, especially due to a changing d_τ. On lower d-scales, the interplay between the one-loop and tree-level neutrino mass terms, (9.44b), causes singularities surrounded by irregularities in $|X|^2$.

$0.1(0.01)$ for Sets A(Set B).

In addition, the upper bound on m_1 and the lower bound on $d_\ell > 0.01$ gives some limited freedom to the Seesaw scale m_R, its scale at tree-level is essentially dependent on these two parameters; specifically, these two bounds set a lower bound on m_R, which is $m_R \gtrsim 10^{10}$ GeV. *Thus, the effect we want to create in our model can only occur for a large Seesaw scale ($m_R \gtrsim 10^{10}$).*

Concluding remarks

The results from [107] showed that our model has non-vanishing contributions to the branching ratios of FCNIs in form of lepton decays like $\ell_1^\pm \to \ell_2^\pm \ell_3^- \ell_3^+$, with $\ell_1 \neq \ell_2$. In this chapter and in the accompanying paper [10], we have defined a lower limit of the Seesaw scale, which is $m_R \geq 500$ GeV, in order to suppress all other types of FCNIs. We then derived the formulas for the relevant decay rates and thus the branching ratios of the FCNIs with the help of [107] and analysed their behaviour on the basis of a concrete parameter input in this section.

With the knowledge from this section, we can get various parameter sets that keep the branching ratios below the experimental limits. This applies even with our requirement to simultaneously have the branching ratios close to the experimental limit, where the parameters d_ℓ and δ_ℓ are particularly dependent on each other as shown by the conditions in (10.26) to (10.31). We may thus say that the branching ratios obtained by these input variables in Table 10.2 for Sets A and B involve some fine-tuning. One

	Set A		Set B	
	tree-level	1-loop corr.	tree-level	1-loop corr.
BR $(\mu^- \to e^- e^+ e^-)$	1.404×10^{-11}	7.109×10^{-13}	2.493×10^{-13}	3.334×10^{-13}
BR $(\tau^- \to e^- e^+ e^-)$	8.770×10^{-10}	1.837×10^{-8}	1.574×10^{-9}	1.010×10^{-9}
BR $(\tau^- \to e^- \mu^+ \mu^-)$	1.011×10^{-9}	2.118×10^{-8}	1.814×10^{-9}	1.164×10^{-9}
BR $(\tau^- \to \mu^- \mu^+ \mu^-)$	1.579×10^{-9}	1.138×10^{-8}	1.609×10^{-9}	1.277×10^{-9}
BR $(\tau^- \to \mu^- e^+ e^-)$	1.820×10^{-9}	1.311×10^{-8}	1.854×10^{-9}	1.471×10^{-9}

Table 10.2.: Branching ratios for set B and set A with tree-level as well as one-loop corrections from the right-handed neutrino mass compared to each other; the input variables are taken from table 9.1.

further recognizes that all these branching ratios in Table 10.2, which contain one-loop corrections from right-handed neutrino masses, are less than a factor of ten away from the upper bounds of Table 10.1. *We have thus demonstrated that in our model, it is possible to suppress the radiative decays of the muon and tau lepton, while keeping the branching ratios of their decays into charged leptons very close to the experimental upper bound.*

In addition, it can be concluded from Table 10.2 and the diagrams in Figures 10.7, 10.9, and 10.10, that one-loop contributions of the right-handed neutrino masses are not negligible in the final values of the investigated branching ratios from FCNIs if the parameters d_ℓ, from the neutrino Dirac masses m_D; and δ_ℓ, the Yukawa couplings to the new Higgs doublet; as well as the scalar mass-squared differenced $M_4^2 - M_3^2$ are defined in a way that the size of one-loop corrections are in the same order as the size of the tree-level corrections, i.e. if $\sqrt{M_4^2 - M_3^2}\,\delta_\ell > d_\ell\, m_{EW}$, Equation (9.56). However, to obtain calculable one-loop neutrino corrections, it is sufficient if $\sqrt{M_4^2 - M_3^2}\,\delta_\ell < d_\ell\, m_{EW} \times 2 \cdot 10^3$ and near this limit, $m_1 \geq 0.01$ is fulfilled.

In contrast to the neutrino mass corrections, the branching ratios of FCNIs are sensitive to the size of the new scalar masses M_3, M_4, and not to the mass squared difference. The leptonic branching ratios are BR$\sim 1/M_{3/4}^4$ and therefore decrease rapidly for large scalar masses. This cannot be achieved by an increase in the neutrino mass contributions due to a higher discrepancy of the scalar masses since m_R only occurs via a logarithm, vis. BR $\sim \log(m_R)$. To keep the branching ratios close to the experimental limits, at least one of the scalar masses M_3 or M_4 must therefore be $M_{3/4} \sim 1\,\text{TeV}$.

The same suppression effect within the FCNIs as with the scalar masses applies with lower γ, since BR$\sim \gamma^6$ with $\gamma = \gamma_{\ell_1} = \gamma_{\ell_2}\gamma_{\ell_3}$.

10.4. Experimental Status

The experiments that achieved the most precise experimental values from Table 10.1 can be categorized into experiments measuring tau decays and those for measuring muon decays.

The tau-decay measurements with the most precise limits are performed at the BELLE II experiments in Japan using the $e^{-}e^{+}$-SuperKEKB accelerator, and the BaBar experiment in California at SLAC National Accelerator Laboratory analysing $e^{-}e^{+}$ collisions from a linear collider, and there are LHCb and ATLAS from the LHC and the CLEO experiment in New York [9]. Improving the precision on the FCNIs is usually difficult to achieve because of a large QCD background e.g. from B-meson decays or $q\bar{q}$ processes [116].

Lepton flavour-changing measurements from the muon decays achieve a much higher precision compared to tau decays. The most precise limit value for $\mu \to e\gamma$ comes from the MEG experiment located at the Swiss Paul-Scherrer Institute (PSI). The experiment works with π^{+} decays producing a muon beam that hits a plastic target, with the decay products detected as a back-to-back reaction, see Figure 10.11 [117]. Moreover, the current best value for $\mu \to eee$ still comes from the data taken in 1988 in the SINDIUM I experiment [9]. Two new experiments are planned at the Paul-Scherrer Institute in the search for lepton-flavour violations. The MEG II experiment [118], the successor of the MEG experiment, started already in 2017 and plans to improve the sensitivity by one order of magnitude for $\mu^{+} \to e^{+}\gamma$ after three years data acquisition. The *Mu3e* experiment [119], which was in the construction phase until autumn of last year 2019, carried out the first run in November 2019 [120] and aims at a sensitivity for $\mathrm{BR}\left(\mu^{+} \to e^{+}e^{-}e^{+}\right)$ of order 10^{-16}. The latter two experiments give rise to the hope that flavour-violating processes in lepton decay will soon be detected and thus improve the constrains of our model.

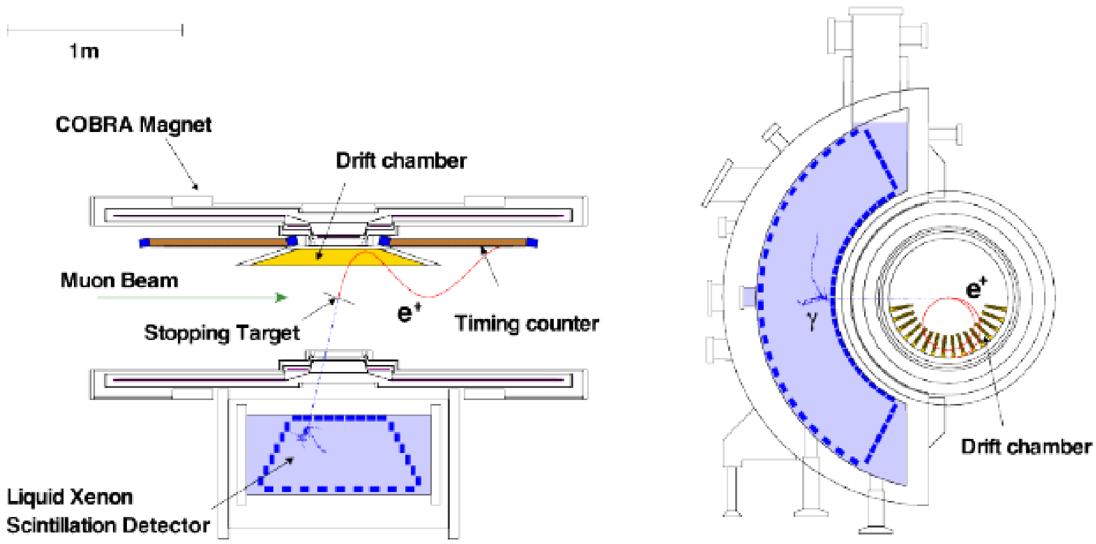

Figure 10.11.: Schematic representation of the MEG experiment [117].

11. Results and Conclusion

In this chapter, we will first present a detailed list of the results obtained from the tests we conducted on the model, specifically the parameter analyses of the last four chapters in Part II of this thesis will be given in the following result Section, 11.1. From this we can make a statement on the characteristics of this model in the second Section 11.2, the conclusion. The conclusion presents moreover the outcomes and impacts of the analyses in a more general context and presents the characteristics of the tests. In the end, the limits and further research potential are shown.

11.1. Summary of the Parameter Analysis

In this thesis, our model was verified by various tests in the phenomenological part. These were tests under the constraints from

(a) electroweak precision tests in form of the oblique parameters S, T, U, V, W, X,

(b) measurements of the anomalous magnetic moments (AMM) of electrons and muons,

(c) neutrino data from neutrino oscillation experiments applied on neutrino mass corrections,

(d) the lack of experimental observation of flavour-changing neutral interactions (FCNIs).

The results of these tests restrict the parameter space from 18 free parameters[1] of the model. These parameters consist of the new scalar masses μ_2, M_3, M_4, the heavy neutrino masses m_4, m_5, m_6, the three mixing angles of the heavy neutrinos, θ_{12_R}, θ_{13_R}, θ_{23_R}, and the nine Yukawa couplings: Three couplings from the new scalars to neutrinos, δ_ℓ, and three from the new scalars to the charged leptons, γ_ℓ, as well as three neutrino-Higgs couplings,[2] d_ℓ, with $\ell \in \{e, \mu, \tau\}$. Additional to this we get five more conditions preserving the experimental values of the mass-squared differences of the light neutrinos as well as their mixing angles. All in all, we arrive at 13 degrees of freedom, which were analysed in the phenomenological part of this thesis, as concluded in Chapter 6.2.

[1] The whole new parameter space counts 26 parameters, from which eight were eliminated by previous assumptions to simplify the analysis. The not listed parameters are angles and phases. These are concretely the angles of the scalar transformation matrix, furthermore, the Majorana and CP phases of the neutrino mixing matrices for light and heavy neutrinos. Due to the assumption of all parameters being real, these angles were either found to be zero or π or, for simplicity, set to zero or π.

[2] Remember that the couplings d are proportional to the neutrino Dirac masses m_D.

In order to estimate the size and location of the free parameter space, a detailed summary of these parameter constraints will be given in this section. These constraints are only occasionally quantitative, vis. with concrete ranges for each parameter, and mainly of a qualitative nature, which means that mostly only relations between parameters with approximate limits could be derived. Furthermore, as expected, the number of tests was not sufficient to completely restrict the entire parameter space of 18 parameters with 13 degrees of freedom. Therefore, we often cannot specify concrete parameter ranges, but only qualitative parameter dependencies. Nevertheless, we can derive statements about the feasibility, naturalness, and testability of the model as well as make suggestions for further experimental and theoretical tests.

The constraints can be divided into *necessary constraints* and rather *advantageous constraints*. Necessary constraints are those which result from the parameter limits set by experimental data and are thus mandatory for a realistic model. Advantageous constraints are constraints that are not essential, but which give our model an advantage in certain aspects. For example, with regard to the muon magnetic dipole moment, one advantage of this model is that it compensates for the discrepancy between the experimental and theoretical values. Additional advantageous constraints would be if the FCNI branching ratios were close to the experimental limits to demonstrate the potential testability of this model. In the following, we will list the constraints according to the chronology in which they appeared in this thesis.

Necessary constraints on the parameter set of the model

Necessary constraints are given by the experimental limits on oblique parameters; the limits of the AMM of the electron; singularity regions without solutions within the neutrino mass corrections, which directly enter into the branching ratios of the FCNIs; and the experimental bounds of the FCNI branching ratios. The latter includes the bounds of the FCNIs that emit a photon (e.g. $\mu \to e\gamma$) and in particular the strong bounds on $\mathrm{BR}\left(\mu^- \to e^- e^+ e^-\right)$. From these constraints, the model gets the following characteristic additions:

1. As expected, the oblique parameters under Point (a) do not set sharp limits on the scalar masses except from the T-parameter. The T-parameter conserves weak isospin[3] and therefore requires a degeneracy of the new scalar masses $M_3 = \mu_2$ or $M_4 = \mu_2$ with little margin $M_{3/4} - \mu_2 < 100\,\mathrm{GeV}$. In addition, the parameter S relates the neutral scalar masses M_3 and M_4 to each other: For the cases M_3, $\mu_2 < M_4$ or M_4, $\mu_2 < M_3$, limits appear for the deviation of the scalar masses, if S remains within the experimental limits, $|M_3 - M_4| < 13.1\,\mathrm{TeV}$; whereas for the cases M_3, $\mu_2 > M_4$ or M_4, $\mu_2 > M_3$, there is no relevant limit on $|M_3 - M_4|$. Altogether, one plays in a safe range with $M_3 < M_4 = \mu_3$ or $M_4 < M_3 = \mu_2$.

[3] The T-parameter is directly proportional to ρ, the parameter of custodial symmetry, which preserved weak isospin, see Appendix A.3. Of course the weak isospin is broken by the masses, i.e. Yukawa couplings, of the particles within a $SU(2)$ doublet, but this breaking is small compared to the experimental uncertainty of T or ρ.

2. Furthermore, the electron AMM sets an upper limit on the Yukawa coupling γ_e of the electron to the new scalars. Assuming that the scalar masses[4] are $M_3 = 1\,\text{TeV}$ and $M_4 = 2\,\text{TeV}$, the coupling has an upper limit of $\gamma_e < 2.7$. A lower degeneracy of these new scalar masses increases the limit, whereas a higher degeneracy does not lower the limit noticeably if the scalar masses are retained $M_{3/4} \geq 1\,\text{TeV}$. This means, the Yukawa coupling can always be located in the natural region of the other SM couplings, namely $10^{-6} - 1$, which in turn makes the limit not very restrictive.

3. One-loop corrections to light-neutrinos directly enter in the formula for right-handed neutrino masses, $\hat{m}_R$, and thus influence them heavily, where the latter in turn are input parameters for lepton FCNIs. In the course of the investigation of these right-handed neutrino masses, we have determined a region in the parameter space where the numerics are unstable and do not find a solution for these masses that most likely results from a mathematical singularity in the formula. This singularity occurs, if the one-loop terms of the light-neutrino masses are in the same order or larger then their tree level term, for details be refereed to chapter 9.3.2 and 9.3.4. It is necessary to bypass this region defined by[5] $\sqrt{M_4^2 - M_3^2}\,\delta_\ell < d_\ell\, m_{EW} \times 2 \cdot 10^3$, as indicated in Equation (9.57). An additional condition for bypassing the singularity is that a larger light neutrino mass of $m_1 > 0.01\,\text{eV}$ is required near the region defined by Equation (9.57).

4. The upper bound on the FCNI branching ratios of the form $\text{BR}(\ell_1 \to \ell_2\gamma)$ set a lower limit on the Seesaw scale $m_R \gtrsim 50\,\text{TeV}$, the scale of the right-handed neutrino masses. In order to make radiative flavour-changing decays invisible in the foreseeable future, a Seesaw scale of $m_R \gtrsim 500\,\text{TeV}$ is preferable.[6]

5. Finally, the strong experimental bound on the branching ratio $\text{BR}\,(\mu^- \to e^-e^+e^-) < 10^{-12}$ requires a dependence of d_e, d_μ, the neutrino Yukawa couplings to the Higgs, on δ_e and δ_μ, the neutrino Yukawa coupling to the new scalars, given by Equation (10.25), being $d_e/d_\mu \simeq \delta_e/\delta_\mu$. A suppression of $\text{BR}\,(\mu^- \to e^-e^+e^-)$ and of all other electron-inhibiting flavour-changing branching ratios of the form $\text{BR}\left(\ell_1^\pm \to \ell_2^\pm \ell_3^\pm \ell_3^\mp\right)$ can, however, still be achieved alternatively with higher scalar masses $M_b > 2\,\text{TeV}$ or with a lower coupling γ_e, the coupling between electrons and new scalars.

[4] The scalar masses were analysed in the lower TeV region, starting at 1 TeV. As argued at the beginning of section 7.2.1 one of the main reasons for the lower mass limit of 1 TeV is given by experimental boundaries [9].

[5] Here, m_{EW} is the electroweak scale.

[6] This stronger limit can be derived from the Seesaw formula $m_R \sim d_\ell^2 v^2/(2\,m_1) \gtrsim d_\ell^2/m_1\,10^{14}\,\text{GeV}$. This takes into account the upper limit of the neutrino mass $m_1 \leq 0.1\,\text{eV}$ and $d_\ell \sim 10^{-6}$, which is in the lower range of the SM Yukawa couplings, assuming in general $m_R \gtrsim$TeV.

Advantageous constraints on the parameter set of the model

Advantageous constraints arise from naturalness arguments to have all Yukawa couplings in the region of the SM couplings. They also arise from our wish to set all flavour-changing branching ratios close to the experimental limits. It is further advantageous to resolve the experimental and theoretical discrepancy of the muon AMM. The following conclusions can be drawn here:

6. As a solution to the discrepancy in the muon AMM, the model can provide the necessary theoretical contribution if $M_3 < M_4$. In addition, the Yukawa coupling of the muon to the new scalars, γ_μ, is depended on the difference of the new scalar masses squared, $M_4^2 - M_3^2$. As an example, a suitable value is $\gamma_\mu = 1.7$, which belongs to $M_4^2 - M_3^2 = 3\,\text{TeV}^2$. For a suitable higher (lower) γ_μ, the mass-squared differences must be accordingly lower (higher). To keep γ_μ in the same order as the other Yukawa couplings ($10^{-6} - 1$), a small mass $M_3 = 1\,\text{TeV}$ and a larger mass deviation from M_4 is required, e.g. $M_4 = 2\,\text{TeV}$, like in the example above; much higher mass deviations do show no greater effect on γ_μ.

7. In the numerical calculation of the one-loop neutrino mass corrections to $\hat{m}_R$, there appear irregularities in the solutions to $\hat{m}_R$ before the singularity, discussed under Point 3, as shown in the diagrams of $\hat{m}_R$ as a function of the relevant model parameters. Irregularities in $\hat{m}_R$ can lead to fine-tuning effects in FCNIs. Therefore, the preferred parameter space is in a region where the irregularities are avoided, given by Equation (9.56), $\delta_\ell \sqrt{M_4^2 - M_3^2} \gtrsim d_\ell\, m_{EW}$.

8. To bring the branching ratios from the τ decays of the form $\tau^- \to \ell_1^- \ell_2^+ \ell_3^-$ close to the experimental limit, the scalar masses must be small, $M_b \sim 1\,\text{TeV}$, and the Yukawa couplings γ_ℓ must be relatively large, $\gamma_\ell \sim 1$ since the branching ratios scale with BR $\sim \gamma_\ell^6 / M_b^4$. In addition, further conditions between the neutrino couplings to the Higgs, d_ℓ, and to the new scalars, δ_ℓ, are required to bring the branching ratios close to the experimental bounds. These conditions are given in Equations (10.27) and (10.31). Taking into account Point 7, a relation $d_\ell \gtrsim \delta_\ell$ with $d_\ell \gtrsim 0.01$ is preferable.

9. The previous Point 8 proposed larger Yukawa couplings γ_ℓ, d_ℓ and scalar masses. A combination of a larger d_ℓ and the neutrino mass m_1, which is experimentally bound from above $m_1 \lesssim 0.1\,\text{eV}$, causes a large Seesaw scale, i.e. at tree-level $m_R \sim (v\, d_\ell)^2 / m_1 \gtrsim 10^{10}\,\text{GeV}$. Therefore, a large Seesaw scale of $m_R \sim 10^{10}\,\text{TeV} \gg 500\,\text{TeV}$ is not necessary but advantageous for the experimental detection of the τ-branching ratios.

10. Finally, fine-tuning with respect to the stringent limitation to BR $(\mu^+ \to e^+ e^- e^+) < 10^{-12}$ is more easily avoided if the Yukawa couplings $\delta_{e/\mu}$ and the neutrino-Higgs couplings d_ℓ are low, e.g. $d_\ell = 0.01$, $\delta_\ell \leq 0.001$.

There is no restriction on γ_τ, the tau coupling to new scalars, nor does this model show a significant difference in changing the CP-violating angle δ_{CP} of the neutrino mixing matrices from π to 0 among the tests performed.

Short discussion

In order to obtain the results just listed under Points 1 to 10, we have used the reduced qualitative method described in Chapter 6.3 for our parameter analysis. According to the method, we carefully picked two suitable parameter sets[7] and analysed each parameter within a set separately, while the others of the set remained fixed. This method was sufficient to obtain the desired relationships between the model parameters and their limits; for further research, however, a combination with a quantitative method could be interesting, e.g. a method in which random parameter values are chosen, and scatter plots are generated from them.

In the analyses of our Type-I-Seesaw-2HDM, we used the experimental data of light neutrinos as an input and obtained in this setup right-handed neutrino masses of the order $10^{10} - 10^{14}$ GeV, taking into account the one-loop contributions to light neutrino masses. The three right-handed masses have a factor of 10-100 distance to each other comparable to the mass ratios observed at the other SM fermion masses within a family. Furthermore, we observed that the pattern of the right-handed mixing matrix, U_N, varies massively with the parameter input, especially with the values of the Yukawa couplings, and thus can be completely different from the mixing matrix of the light neutrinos ($\sim U_{PMNS}$).

All in all, including all necessary and advantageous constraints from the precision tests of Points (a), (b), (c), and (d), various parameter sets are still possible in this model, i.e. a considerable part of the parameter space is still unconstrained. This means that the parameter space of the model is not subject to strong restrictions, it can have parameters in natural parameter scales, e.g. the Yukawa couplings can be of the order of SM couplings. This makes the model feasible and realistic, while it can at the same time compensate for the muon AMM discrepancy, and have the lepton flavour-changing branching ratios close to the experimental limits, which are thus on the doorstep for future experiments.

11.2. Conclusion

This section contains a few parts quoted and partially rewritten from the paper to this thesis, [10]. In the following, we summarize the investigated model and the tests performed in the chronology given in the thesis. The advantages of the model should be presented in detail. Furthermore, we will mention the relevance of each test, its feasibility (if important), and its results in a general context, with an emphasis on the findings for the model.

[7] By parameter sets we mean different data sets for the parameters of the model.

Our model, first considered in Ref. [121, 58, 122], has three right-handed neutrino singlets within a high-scale Seesaw mechanism of Type I and two Higgs doublets. It contains a softly broken flavour symmetry, which has as its main crucial consequence that lepton flavours are conserved in the Yukawa couplings and are only broken in the Majorana mass terms of the right-handed neutrinos; this assumption is field-theoretically consistent since these mass terms have field dimension three, while the Yukawa couplings have field dimension four, which means that the lepton-flavour breaking is *soft*.

From the theoretical point of view, **our model combines several advantages** of right-handed Seesaw Type I neutrinos, the additional Higgs doublets, and soft-flavour violation:

i. It is a relatively simple, economical minimal SM extension,

ii. Neutrino masses are generated,

iii. It can explain the smallness of the neutrino masses compared to the masses of other SM particles,

iv. As a natural extension, it includes right-handed neutrinos without destroying charge quantization, and it expands the Higgs sector with additional non-suppressed Yukawa couplings,

v. It offers the possibility of smooth leptogenesis, as is can be seen from [4], where the lepton number is violated by right-handed Majorana neutrinos of mass $m_R > 10^9$ GeV and the possibility of CP violation from the neutrino mixing matrices and the Higgs potential,

vi. It can explain the difference between U_{PMNS} and V_{CKM},

vii. And finally, within this model, the approximately maximal atmospheric and solar mixing of neutrinos can be generated [58].

We applied several tests to this model, assuming that the first Higgs-doublet ϕ_1 coincides with the Higgs-doublet of the SM, vis. it does not mix with the second doublet. In addition, we have employed several further **simplifying assumptions** to reduce the parameter space of the model: We have opted for normal neutrino mass ordering; as well as the Higgs basis, i.e. the basis for the Higgs doublets, where only one of the doublets has a nonzero VEV; and we have set all parameters of the model to be real. The last assumption leads to Majorana angles and CP angles being $\in [0, \pi]$, which also applies to the mixing angles from the scalar sector.

Under these preconditions, we have successfully tested the two-Higgs-doublet-model (2HDM) part of this model using **oblique parameters**. We found that a certain degree of degeneracy is required for the scalar masses to fit within the experimental limits of the oblique parameters, as mentioned in Point 1 of the previous section. The S- and T-parameters are the relevant quantities that preserve isospin but allow a generous mass difference between the neutral scalar masses of several TeV.

For the next test, we explicitly calculated the one-loop contributions to the **anomalous magnetic moment** (AMM) of the electron and muon and derived a formula in which the right-handed neutrino contributions are negligible. The only free parameters thus left in this formula are the new scalar masses and the charged-lepton Yukawa couplings to the new scalars, γ_ℓ. We adjusted these findings to the experimental limits (as mentioned in Point 6 of the last section) and proved

viii. The possibility of compensating for the discrepancy between the experimental and theoretical values for the muon AMM.

The explanation of the muon-AMM requires a relatively large Yukawa coupling between the muon and the new scalars of $\gamma_\mu = 1.7$. On the other hand, the limits for the electron AMM proved not to be very restrictive as pointed out under Point 2 in the previous section.

We also saw that **one-loop contributions to the light neutrino mass matrix** strongly affect right-handed neutrino masses and mixing because these parameters have to be adjusted—compared to their tree level values—in order to comply with the experimental constraints on the masses and mixing of the light neutrinos. These corrections to the light neutrino mass matrix can increase right-handed neutrino masses, $\hat{m}_R$, by several orders of magnitude, as well as create very different right-handed-neutrino mixing patterns, depending on the assumptions about scalar masses and Yukawa couplings. The formula for the one-loop corrections to $\hat{m}_R$ is involved: An interplay between tree-level and one-loop terms creates singularities, i.e. points without solution, that are surrounded by irregularities in diagrams showing $\hat{m}_R$ as a function of the concerned model parameters, see Points 3 and 7 from the previous section. Due to the complexity of the formula and within the numeric approach, it was not possible to test the model for values of the CP phase and Majorana angles beyond 0 and π within the scope of this thesis. Further research would be required for this extension of the test. Our work demonstrated the need to take into account one-loop corrections of neutrino masses in lepton flavour-changing branching ratios[8] when our rule, elaborated in Point 7 of the previous section 11.1, applies. This rule basically suggests a consideration of neutrino one-loop corrections, if the above mentioned one-loop terms in the formula for $\hat{m}_R$ are equal or larger then the tree-level term.

Finally, we investigated **flavour-changing leptonic decays**, specifically, radiative decays and three-lepton decays. Using two explicit numerical examples, we have demonstrated that in our class of models, the radiative decays $\ell_1^\pm \to \ell_2^\pm \gamma$ may so be suppressed as to be utterly invisible (see Point 4 of the last section). Yet

ix. any of the five three-lepton decays of the form $\ell_1^\pm \to \ell_2^\pm \ell_3^\pm \ell_3^\mp$, or even – if one assumes a certain fine-tuning – all these five decays at the same time may be just around the corner.

[8] We have not considered corrections to the new scalar masses since the new scalar masses are included as free parameters anyway.

Specifically, we have noted that some fine-tuning is required to keep the branching ratio BR $(\mu^- \to e^-e^+e^-)$ small when all five branching ratios are simultaneously close to their experimental limits, as described in detail in Point 8 and 9 of the last section. But even including this fine-tuning together with all other results from the tests

x. The parameter space of the model is realistic and can have parameters in natural parameter ranges, i.e. on scales of other SM parameters of similar type,

as concluded in the last section.

Point ix could be an interesting fact for the following reason: Since the experimental observation of neutrino oscillations [123, 124, 125],[9] it is known that there is lepton flavour violation. However, this violation has not yet been observed in the charged-lepton sector, and it is not entirely certain where it is most likely to be observed first. Considering the promised sensitivity improvements on the branching ratios of the processes $\mu \to eee$ [119] and $\mu \to e\gamma$ [118], the decays of the form $\ell_1^\pm \to \ell_2^\pm \ell_2^\pm \ell_3^\mp$ seem the best guess, and radiative decays $\ell_1^\pm \to \ell_2^\pm \gamma$ may be an option as well, although not within our model.

As demonstrated in Ref. [3], the effect mentioned in the penultimate paragraph under Point ix and before occurs if the Seesaw scale is much larger than all other scales in this model class (see also Point 9 of the last section). In this context, we have shown that there is a relevant simplification of the effective flavour-violating couplings to the neutral scalars that emerges at the one-loop level when using the Higgs basis.

Moreover, since this model is, interestingly, a good candidate for smooth leptogenesis, as is apparent from [4], further studies should examine the connection with this area.

This model holds further potential for extensions: So far, the model contains neither the quark sector nor a concrete realisation of the Higgs potential. When considering the inclusion of the quark sector, several points need to be borne in mind. First of all, the flavour-symmetry breaking cannot be adopted in the same way as in the lepton sector[10] as there is no soft breaking term. However, the flavour symmetry is slightly broken in the quark sector, as can be seen on the nearly diagonal V_{CKM} matrix. It is therefore necessary to allow non-diagonal Yukawa couplings for the quarks and eventually avoid excessive flavour-changing neutral interactions by fine-tuning.[11] As further tests for this addition, one would have to consider the limits from the precision data of quark physics, such as electron-muon conversion in nuclei, neutrinoless double beta decay, scalar decays, B-physics, possibly Kaon physics, and other constraints from meson physics, etc. If the model is extended by defining the Higgs potential, decisive limits result from the stability and unitarity of the Higgs vacuum [51, 52]. The fine-tuning in the quark sector may seem not elegant, but, as pointed out in this thesis, the intriguing consequences for

[9] For reviews on the phenomenology of neutrino oscillations, see, for instance, Ref. [126, 127, 128].

[10] For an attempt in this direction, however, see Ref. [129].

[11] One option would be, for example, the old idea of including left-right symmetric models with a local $(B-L)$ symmetry, as indicated in the review [130], which could explain the $V_{CKM} \simeq \mathbb{1}$ and the generation of right-handed Majorana masses. Another possibility is shown in Ref. [46], where a 2HDM with a heavy Scalar mass scale and without an added symmetry was proposed, which can reproduce the quark masses and mixing angles without fine-tuning.

charged-lepton decays, together with all the other advantages mentioned under Points i to x, make a consideration of such a framework worthwhile.

12. Outlook

There are more important experimental and theoretical constraints against which this model should be tested in its current state. As explained in the corresponding chapters in Part I of this thesis, it would be interesting in neutrino physics to investigate the model under leptogenesis and neutrinoless double beta decay, the latter in relation to the Majorana nature of neutrinos. Furthermore, an extension of the model in the quark sector would inevitably lead to an investigation of the muon-electron conversion in nuclei. In our model, this occurs in the limit $m_R \to \infty$ through $\mu^- \to e^-(S_b^0)^*$, followed by the $(S_b^0)^*$ coupling to quarks [10]. In addition, the experimental limits of reaction and decay rates in B-physics will further restrict the Yukawa couplings to the quark sector [51]. In the Higgs sector, the Higgs potential would have to be specified and is in this case subject to the constraints of vacuum stability and unitarity and will eventually also concern the hierarchy problem.

In the following, we will give a short insight into some tests and their importance for this model as considerations for further research, starting with the neutrinoless double beta decay, followed by leptogenesis, Higgs vacuum stability, and the hierarchy problem.

Contribution to neutrinoless double beta decay

The double beta decay is a nucleus (Z,A) of charge Z and atomic number A, which decays to its isobar (Z+2,A) via the transition (Z,A)→(Z+2,A)+$2e^- + 2\bar{\nu}$. This normally only happens when the single beta decay into (Z+1,A) would lead to a higher energy state and is therefore disadvantaged, as shown in Figure 12.1.

An even more interesting decay can occur if neutrinos are of Majorana nature, which means that the particle is its own antiparticle. In this case, one neutrino in double beta decay can be interchanged instead of radiated; this decay is then called neutrinoless double beta decay ($0\nu\beta\beta$), see Figure 12.2. Among the most commonly used isotopes in experiments that exhibit the correct structure for $0\nu\beta\beta$ are ^{76}Ge, ^{100}Mo, ^{130}Te, ^{136}Xe, which are the core material of recent experiments like COURE, EXO-200, GERDA, KamLAND-Zen, and NEMO-3 [9]. The half-lives of these isotope decays via $0\nu\beta\beta$ have been measured to date at more than 10^{23} years.

If $0\nu\beta\beta$ was measured, we would not only know the information about the Majorana nature of neutrinos, but we would also receive additional information, e.g. about neutrino masses, their hierarchy, and the Majorana phases [132]. One can understand this connection if one examines the formula for the decay rate $\Gamma_{0\nu\beta\beta}$ or equally the

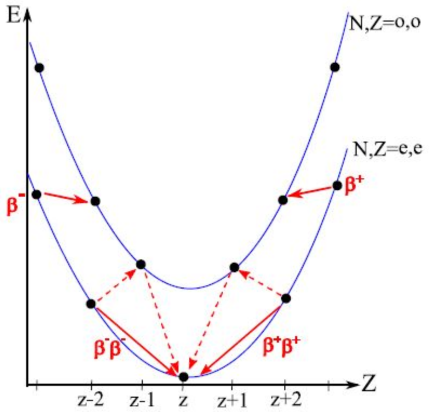

Figure 12.1.: When single beta decay leads to a higher energy state than that of the mother nuclei (dashed lines), double beta decay is possible [131].

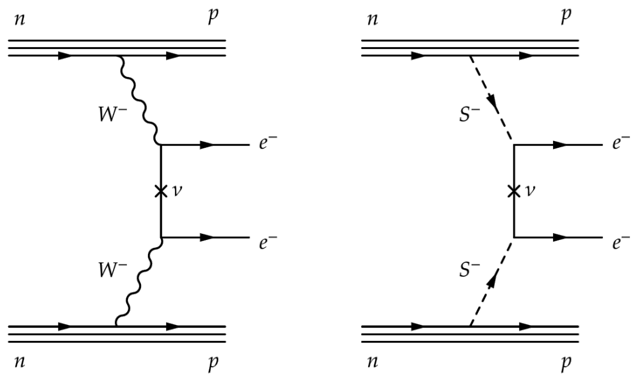

Figure 12.2.: The process of neutrinoless double beta decay, with left, the standard contribution, and right, the additional contribution from the charged scalar of a second Higgs doublet.

inverted half-life $[\tau^{1/2}]^{-1}$ of $0\nu\beta\beta$ [133, 134, 7],

$$\frac{\Gamma_{0\nu\beta\beta}}{\ln 2} = \left[\tau^{1/2}\right]^{-1} \simeq G_{0\nu} \left| \sum_{i=1}^{3} U_{ei}^2 \frac{m_i}{m_e} M^{0\nu\beta\beta}(m_i) + \sum_{I=4}^{6} U_{eI}^2 \frac{m_p}{m_I} M^{0\nu\beta\beta}(m_I) \right|^2 , \tag{12.1}$$

where $G_{0\nu}$ is the well-known phase space factor, m_p is the proton mass, and $M^{0\nu\beta\beta}$ is the less-known nuclear matrix element (NME). The second factor on the right-hand side of Equation (12.1) corresponds to the sum over the eigenstates of the heavy neutrino masses, which are $m_I \gtrsim 100\,\text{MeV}$. In our model having $m_R \gtrsim 10^{10}$, this heavy neutrino factor is suppressed, and the exchange of light neutrinos dominates. In this situation, one often renders an approximation in which the nuclear matrix element is factorized from the neutrino part, which leads to the effective Majorana mass[1] $m_{\beta\beta}$ [7],

$$\frac{\Gamma_{0\nu\beta\beta}}{\ln 2} \approx G_{ov} \left| M^{0\nu\beta\beta}(0) \right|^2 \left| \frac{m_{\beta\beta}}{m_e} \right|^2 , \qquad m_{\beta\beta} = \left| \sum_i U_{ei}^2\, m_i \right| . \tag{12.2}$$

Regarding the decay rate of $0\nu\beta\beta$ in conjunction with our model, one would have to consider another diagram, shown in Figure 12.2 on the right; thus for this the quark-scalar interactions would need to be specified. Normally, the one-loop contribution to the light neutrino masses δM_L might play a not inconsiderable role as contribution to $m_{\beta\beta}$ as stated in [133]. However, this is not relevant in our model since we have fixed the light neutrino masses with the experimental limits. All in all, the experimental values for Equation (12.2) could provide interesting limits for this model, e.g. by limit values for the Yukawa couplings of quarks and leptons to the new scalars.

[1] Notice that the Majorana mass, $m_{\beta\beta}$, differs from the neutrino mass in flavour space $m_{\nu_\ell} = \left(\sum_i |U_{\ell i}|^2 m_i^2\right)^{1/2}$.

Leptogenesis

The predominant abundance of matter over antimatter in the universe – the baryon asymmetry η_B, defined as the amount of baryons minus anti-baryons divided by the number of photons, $\eta_B = (n_B - n_{\bar{B}})/n_\gamma \simeq 6 \times 10^{-10}$ – represents one of the known unsolved problems of cosmology. However, baryon asymmetry is commonly believed as being dynamically generated in the early universe after inflation. The generation of baryon asymmetry is referred to as baryogenesis and requires three conditions known as the Sakharov conditions: Baryon asymmetry (or rather the breaking of $B - L$ [34]), C violation, and CP violation, and a deviation from thermal equilibrium, for an overview, see e.g. [135, 7]. Since the SM does not provides neither a sufficient CP violation nor a sufficient deviation from thermal equilibrium, theories beyond the SM try to explain this problem. A promising approach is leptogenesis, which creates baryon asymmetry via lepton asymmetry, which in turn can be created by decaying right-handed Majorana neutrinos.

In the simplest model of leptogenesis, which contains right-handed neutrino masses of $m_R \gtrsim 10^9$ GeV, the time evolution begins with the thermal production of right-handed Majorana neutrinos directly after inflation and continuous with their decay at their freeze-out temperature $T \sim m_R$. The freeze-out is the time when the right-handed neutrinos, ν_R, go out of equilibrium, so their decay rate, Γ, becomes smaller than the expansion of the universe, whereby the latter is specified by the Hubble rate, H, so $\Gamma < H$. The decays[2] of the lepton number-violating Majorana neutrinos into leptons and Higgs scalars, $\Gamma(\nu_R \to \ell\, S)$, can provide the necessary CP violation, ϵ, through CP violating Yukawa couplings[3] [4]; ϵ is written as

$$\epsilon = \frac{\Gamma(\nu_R \to \ell\, S) - \overline{\Gamma}(\nu_R \to \ell\, S)}{\Gamma(\nu_R \to \ell\, S) + \overline{\Gamma}(\nu_R \to \ell\, S)}.$$

The out-of-equilibrium condition prevents the so generated lepton asymmetry, η_L, which is proportional to the CP violation ($\eta_L \sim \epsilon$), from being further washed out by lepton number-violating inverse and scattering processes. In the last step of leptogenesis, sphaleron processes turn lepton asymmetry into baryon asymmetry, i.e. $\eta_L \sim \eta_B$, before electroweak symmetry breaking, vis. if $T \gtrsim m_{EW}$. Sphalerons are non-perturbative solutions of the electroweak field equations, i.e. hypothetical excitations of the vacuum, which convert leptons into antibaryons, baryons into antileptons, and vice versa [135]. In [4], it was found out that for successful leptogenesis as described here to occur, the right-handed masses are subject to a bound from below $m_R \gtrsim 4 \times 10^8$ GeV, called the Davidson-Ibarra bound. There are other mechanisms that enable leptogenesis even with $m_R \lesssim m_{EW}$, such as special flavour-oscillation mechanisms or resonant leptogenesis, whereby the latter has two nearly degenerate masses $m_4 \simeq m_5$, see [7] and the references therein.

[2] Lepton number violating processes can not only be decays but also inverse decays, scattering processes and flavour oscillation, depending on the model. The Majorana nature is what breaks lepton number.

[3] Part of these phases can, after electroweak symmetry breaking, be translated into CP-violation in the neutrino mixing matrices.

This model includes the high-scale Type I Seesaw mechanism and therefore contains the necessary Majorana neutrinos with sufficiently high mass $m_R \gtrsim 10^{10}\,\mathrm{GeV}$. CP-violating phases are located in the neutrino mixing matrices and can additionally be introduced into the Yukawa couplings and in the diagonalization matrix of the scalar masses. The decay rate of the heavy neutrinos would be extended by additional lepton number-violating decays into the new scalars. All in all, this could lead to a worthwhile, successful leptogenesis within this model.

Higgs vacuum stability

A vacuum state will always assume the minimum energy state of a potential. If the Higgs vacuum is not stable, i.e. it has a lower energy state, then at the time of the transition to a lower vacuum state, the present constitution of our universe would be destroyed and restructured.

In the standard model with one Higgs doublet $\phi = (0, \varphi)^T$, including a physical boson φ, the potential of the Higgs boson is

$$V(\varphi) = -\frac{1}{2}\mu^2(\varphi)\varphi^2 + \frac{1}{4}\lambda(\varphi)\varphi^4,$$
$$\text{with } v^2 = \frac{\mu^2}{\lambda},\; m_H^2 = 2\lambda v^2.$$

The first term of the potential with μ can be neglected in a discussion of vacuum stability as long as $\varphi \gg v$ [136]. What is more crucial is the evolution of the second term. So, if one evolves λ in first-order loop correction, it gets contributions from self-interactions, and fermions, as well as gauge boson loops. The most critical contribution comes from the Yukawa coupling of the heavy top quark y_t, which adds a negative value, as can be seen from the beta function $\beta_\lambda \sim \left[6\lambda^2 - 6y_t^4 + \dots\right]$, with $\beta_\lambda = (4\pi)^2 \frac{d\lambda}{d\ln\mu}$, according to [137]. The running of λ goes down and even to negative values at higher energy scales $\sim 10^{10}\,\mathrm{GeV}$, see Figure 12.3. This leads to a lower negative vacuum state in the potential for various λ and thus to another vacuum state that could lay right next to our present vacuum, as depicted in Figure 12.4.

This becomes problematic if the new vacuum is equally high (metastable) or lower (unstable) than the present vacuum. Since then the possibility of tunnelling into the new vacuum state increases, which would have dramatic effects on our universe. The calculations for the SM suggest that we live in a metastable Higgs vacuum, see [136] for a pedagogical introduction and [139] for a recent review.

The situation for two or more Higgs doublets is rather intricate: there are more Higgs vacua, and couplings between the scalars have to be considered in the stability calculations; the literature is full of works that search for stationary points [85].

In our case, we have chosen the scalar mixing matrices in such a way that the first Higgs behaves like the SM Higgs and is decoupled from the second Higgs doublet. That means we are only dealing with one Higgs vacuum and the scenario is relatively simple. Furthermore, the 2HDM potential has limitations in the scalar mass terms,

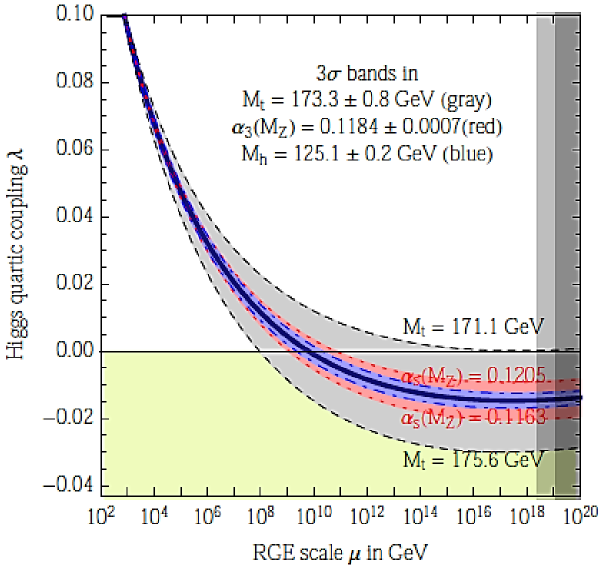

Figure 12.3.: Renormalisation group evolution of λ, varying M_t, $\alpha(M_Z)$ and M_h by $\pm 3\sigma$, [138].

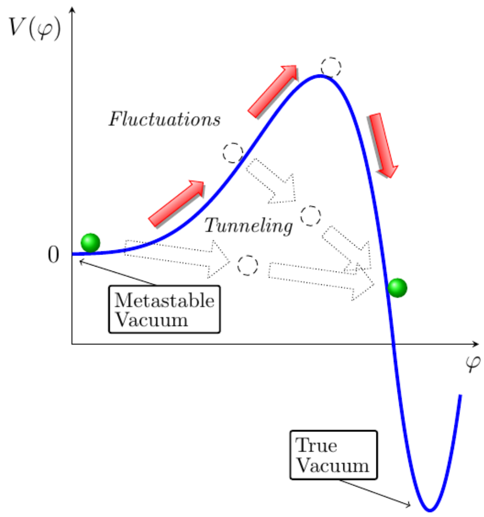

Figure 12.4.: Image of a metastable vacuum at the origin, source [139].

the new scalar masses are defined at $M_2 = 1\,\mathrm{TeV}$ and $M_4 = \mu_2 = 2\,\mathrm{TeV}$. However, a thorough analysis of the vacuum stability can only be performed by imposing further constraints on the couplings in between the scalars. Therefore, so far, we cannot make any predictions about the stability of the vacuum from the scalar side.

A more interesting situation arises for the vacuum stability with regard to the extended right-handed neutrino sector. Additional contributions to the quartic coupling λ come from the neutrino masses $m_\nu = m_D/m_R^2 = \Delta_1 v/m_R^2$ where the Yukawa coupling Δ_1 enters the renormalization group evolution of λ in the following way $\Delta\beta_\lambda = 4\lambda\,\mathrm{tr}(\Delta_1^\dagger\Delta_1) - 8\,\mathrm{tr}((\Delta_1\Delta_1)^2)$, according to [137] and the references contained therein. Here, one can see that for Yukawa couplings $\Delta_1 = \mathrm{diag}(d_e, d_\mu, d_\tau)$ close to but lower than one ($d_\ell \lesssim 1$), as is the case in our model $d_\ell \sim 0.1(0.01)$ for Set A (Set B), one might shift the evolution of the Higgs quartic coupling to higher values and thus to a more stable Higgs potential.

However, the problem of the stability of the Higgs vacuum is a regular theme of the Grand Unified Theory (GUT), and since we are not proposing that our model is close to a GUT model, there will be room for any expansion with various potential particle candidates that can contribute to the running of λ. It is therefore questionable whether it is useful to make a statement at this point about the contributions to vacuum stability from our model.

The hierarchy problem

The hierarchy problem considers the large discrepancy between the weak gravitational force at the Planck scale $\Lambda \sim 10^{19}\,\mathrm{GeV}$ and the electroweak force at $m_{EW} \sim 100\,\mathrm{GeV}$

as unnatural. This problem is reflected in the relation between the Higgs mass $m_H \sim 125\,\text{GeV}$ and its potentially large quantum contributions on higher scales. If the Higgs mass is much smaller than its quantum corrections, a delicate fine-tuning must be made to achieve the observed Higgs mass; this is equally considered unnatural. This circumstance might pose a problem especially with regard to the new physics, as in our model. When specifying the scalar self-interactions, additional Higgs scalars as well as heavy right-handed neutrinos can contribute to the Higgs mass in loop processes, and thus, these models would be considered unnatural.

However, analyses have been carried out on this topic, which reason that within the evolution of the Higgs potential, the Higgs mass $m_H^2 = 2\lambda v^2$ remains protected and is therefore scale-independent, so that the hierarchy problem as a whole might not be a problem, see [140, 141] for a detailed discussion.

A. Model-Relevant Global Symmetry Groups

This chapter will focus on specific global symmetry groups in QFT that are important in the subject area of this thesis.

Throughout history, group theory has been a powerful tool for describing and explaining various phenomena in physics. This includes the structure of crystals, phase transitions in superconductors, and also fundamental properties of particles, forces, and their interactions in particle physics. In particle physics, group theory is the intrinsic foundation of the mathematical description of the Standard Model. Groups define the broken or unbroken symmetries of the nature to which the particles and their interactions are subject. Concretely, there are the global symmetry groups, which are the Lorentz or Poincaré, spin, C, P, and T symmetries, and the local gauge symmetry groups, which describe the weak, the electromagnetic, and the strong force. If a symmetry in nature is unbroken, the action of the Standard Model remains invariant among its symmetry transformations. When a particle field obeys the laws of a symmetry, it can be represented as part of this symmetry group as shown in the next chapter with fermions and the Lorentz symmetry. When, on the other hand, a particle field is just interacting with a group element of local symmetry, a gauge boson, it can be represented as an element in the underlying Lie algebra of this group and receives charges (quantum numbers) corresponding to the interaction strength.

A short introduction is given to the application of some special symmetry groups in the QFT which are used in this thesis. In Section A.1 we will start with the group concept of the spinors, including the spin and Lorentz groups to better understand the implementation of the fermionic property spin 1/2, which is important, among other things, to understand electric and magnetic dipole moments. Furthermore, in Section A.2 we will focus on charge conjugation C, which is important for neutrino Majorana masses. This is followed by parity P, time-reversal T, and CP-violation and in Section A.3 custodial symmetry, all of which are particularly relevant for oblique parameters and in Higgs physics. The references used in these chapters are [142, 143, 144, 145].

A.1. Spinors, the Lorentz Group, Chirality, and Helicity

The standard model in the QFT is, as already mentioned, build out of local and global symmetry groups. The latter ones include the spin and Lorentz groups, under which each type of particle has a specific representation. In this chapter, we want to address the question of how fermions, which are spin 1/2 particles, are implemented in the SM, especially with regard to the Lorentz symmetry, and how it is related to their fundamental properties, chirality and helicity. These properties will be important, for example, to understand charge conjugation and thus also the concept of Majorana neutrinos. In addition, embedding the fermion attribute spin 1/2 is an important step towards understanding how the magnetic dipole moment (MDM) of a fermion is implemented in quantum field theory (QFT). Since the MDM is caused by the spin in combination with the electromagnetic force. Consequently, in the first Section A.1.1, we discuss how the properties of the fermions under the spin and Lorentz group can form spinors with chiral components. Further, in Section A.1.2, fermion fields are derived from the spinors under consideration of the equations of motion. The following section shows the differences between chirality as an attribute of fermion fields and helicity as an attribute of fermion states. Finally, chiral symmetry is to be defined, which is associated with the chiral components of the fermions. To chiral symmetries belong especially weak interactions.

A.1.1. Spinors and the Lorentz group

Before we dive into the subject, let us say a few words about the Lorentz group. The Lorentz group is referred to as $SO(1,3)^+$, sometimes written as $\mathcal{L}_+^\uparrow$, the proper orthochronous Lorentz group, which maintains the direction of time ($\Lambda^0_0 \geq 1$) and space ($\det \Lambda = 1$), where Λ is a group element. Space and time reflections change the Lorentz transformation into an improper and non-orthochronous one and can be performed with transformations of the discrete parity, P, and time-reversal, T, groups [26]. The representation space of the algebra of the $SO(1,3)^+$ group, the Dirac algebra, has the gamma matrices as elements γ_0, γ_1, γ_2, γ_3, where $\gamma^\mu = \begin{pmatrix} & \sigma^\mu \\ \bar{\sigma}^\mu & \end{pmatrix}$ in Weyl representation, and $\sigma^\mu = (\mathbb{1}, \sigma^i)$, $\bar{\sigma}^\mu = (\mathbb{1}, -\sigma^i)$, where σ^i, with $i \in \{1,2,3\}$, are the Pauli matrices. As we will later see, these gamma-matrices often come together with fermion fields that live in this space.

Now the way is paved for the main topic, the representation of the fermion fields. Fermion states obey the Lorentz symmetry operations such as rotations and boosts from the Lorentz group $SO(1,3)^+$ and, simultaneously, the spin 1/2 rotations from the $SU(2)_{1/2}$ group. Accordingly, the states of the fermions must lie in a vector space in which both the operator representations for the $SO(1,3)^+$ Lorentz group and those for the $SU(2)$ spin groups operate. The solution is the two-fold overlapping of the isomorphic groups $SU(2)$ on $SO(1,3)^+$, which is $SO(1,3)^+ \simeq SU(2) \otimes SU(2)$,[1] see [144]. Consequently, the fermion representation, ψ, is described by $\left(0, \frac{1}{2}\right) \otimes \left(\frac{1}{2}, 0\right)$ states[2] of this new group having two $SU(2)$ components: The left-handed *chiral* spinor, ψ_L,

[1] Instead of $SO(1,3)^+ \simeq SU(2) \otimes SU(2)$, it is also often referred to the Lie algebra $\mathfrak{su}(2) \oplus \mathfrak{su}(2)$ generating the universal cover of the Lorentz group $SL(2,\mathbb{C})$ [23].

[2] For completeness, the $\left(\frac{1}{2}, \frac{1}{2}\right) \otimes \left(\frac{1}{2}, \frac{1}{2}\right)$ representation represents the normal 4-vector in spacetime, whereas the $(0,0) \otimes (0,0)$ representation describes a scalar under spacetime rotations.

which belongs to the $\left(\frac{1}{2},0\right)$ representation and the right-handed *chiral* spinor, ψ_R, which belongs to the $\left(0,\frac{1}{2}\right)$ representation. Together, the chiral representations are written in the Dirac notation as bispinors, $\psi = \psi_L + \psi_R = \begin{pmatrix}\chi_R\\ \chi_L\end{pmatrix}$, where $\psi_R = \begin{pmatrix}\chi_R\\ 0\end{pmatrix}$, $\psi_R = \begin{pmatrix}0\\ \chi_L\end{pmatrix}$ and $\chi_{R/L}$ are two-component spinors. The affiliation of a spinor to one of these two Lorentz representations is called *chirality*, from which the adjunct chiral is derived. The chiral states of a bispinor are eigenvectors of the chiral operator $\gamma_5 = i\gamma_0\gamma_1\gamma_2\gamma_3$, therefore, the projection operators for left- and right-handed fields include γ_5 and are $\gamma_{L/R} = (1 \pm \gamma_5)/2$ with $\gamma_L\, \psi = \psi_L$, $\gamma_R\, \psi = \psi_R$ and $\gamma_{L/R}\, \psi_{R/L} = 0$.

As already mentioned, the left-handed, ψ_L, and right-handed, ψ_R, states are different representations of the Lorentz group, and therefore transform differently under the Lorentz transformation, more specifically under Lorentz boosts [23]. The representation of the Lorentz transformation operators for spinors, $\Lambda_{1/2}$, is, such as the better-known four-vector representation, Λ^{μ}_{ν}, divided into rotations with the parameter $\vec{\theta}$ and boosts with $\vec{\eta}$

$$\Lambda^{\mu}_{\nu} = \exp\left(i\theta_i\,(J_i)^{\mu}_{\nu} + i\eta_i\,(K_i)^{\mu}_{\nu}\right), \tag{A.1}$$

$$\Lambda_{1/2} = \exp\begin{pmatrix}-i(\vec{\theta}-\vec{\eta})\frac{\vec{\sigma}}{2} & \\ & -i(\vec{\theta}+\vec{\eta})\frac{\vec{\sigma}}{2}\end{pmatrix} = e^{\frac{i}{4}\sigma_{\mu\nu}\omega^{\mu\nu}}, \text{ with } \omega^{\mu\nu} = \begin{pmatrix}0 & -\vec{\eta}_x & -\vec{\eta}_y & -\vec{\eta}_z\\ \vec{\eta}_x & 0 & \theta_z & -\theta_y\\ \vec{\eta}_y & -\theta_z & 0 & \theta_x\\ \vec{\eta}_z & \theta_y & -\theta_x & 0\end{pmatrix}, \tag{A.2}$$

J_i and K_i are the generators in the four-vector representation (for explicit formulas, see [26]) and $\sigma_{\mu\nu} = \frac{i}{2}\left[\gamma_\mu, \gamma_\nu\right]$. Thus, the transformation of a bispinor is $\psi(x_\mu) \to \Lambda_{1/2}\psi(\Lambda^{\mu}_{\nu}x_\mu)$.

A.1.2. Spinors as fermion fields

If a bispinor, ψ, is to describe a fermion field, it must also satisfy the equations of motion, the Dirac equations, i.e. as a result, states with negative energy are obtained. These states are interpreted using the Feynman-Stückelberg[3] interpretation, which requires that the full bispinor is additionally divided into particle $u^{\pm} \sim \begin{pmatrix}\xi^{\pm}\\ \xi^{\pm}\end{pmatrix}$ and antiparticle spinors $v^{\pm} \sim \begin{pmatrix}\xi^{\pm}\\ -\xi^{\pm}\end{pmatrix}$, where $\xi^{\pm}$ are spin states. The upper and lower entries in $u_{\pm}$ and $v_{\pm}$ are still the left- and right-handed chiral states resulting from the Lorentz symmetry, but their property of the spin 1/2 group can now be explicitly recognized by $\xi^{\pm}$. Consequently, a

[3]Particles with negative energy moving backwards in time equal antiparticles of positive energy moving forwards in time, based on the CPT-symmetry.

bispinor is written as a fermion field, ψ, via

$$\psi(x) = \int \frac{d^3p}{(2\pi)^3} \frac{1}{\sqrt{2E}} \sum_{h=1,2} \left(a_p^h u^h(p) e^{-ipx} + b_p^{h\dagger} v^h(p) e^{ixp} \right), \tag{A.3a}$$

$$u^h = \begin{pmatrix} \sqrt{p_\mu \sigma^\mu} \xi^h \\ \sqrt{p_\mu \bar{\sigma}^\mu} \xi^h \end{pmatrix}, \; v^h = \begin{pmatrix} \sqrt{p_\mu \sigma^\mu} \xi^{-h} \\ -\sqrt{p_\mu \bar{\sigma}^\mu} \xi^{-h} \end{pmatrix}, \tag{A.3b}$$

where $a^\dagger$ and a are the creation and annihilation operator of particles from the vacuum state, as well as $b^\dagger$ and b for antiparticles, derived from the second quantisation in QFT [26]. In low-energy physics, the spin states can be specified as $\xi^+ = (1,0)^T$, which is the spin-up projected on the z-axis ($\sigma^3 \xi = +\xi$) and $\xi^- = (0,1)^T$ as the spin-down projection ($\sigma^3 \xi = -\xi$), [26]. In high-energy physics with high relativistic momenta, it makes more sense to talk about $\xi^\pm$ as being the spin projection on the particle momentum, which is called negative $\xi^- = (0,1)^T$ and positive $\xi^+ = (1,0)^T$ helicity [23]. These helicity states are often described in the literature as left- and right-handed helicity states, which in many cases, lead to confusion with the chirality eigenstates of the same name. Therefore, we will stick here to the terms of negative and positive helicity states.

It is important to note that chirality is a property of the particle fields ψ, while spin and helicity are properties of the excited states produced by the field acting on the vacuum.[4]

A.1.3. Helicity and Chirality

Similar to the chiral fields, the helicity states can be projected out using the helicity operator $\hat{h}$. If we apply the helicity operator $\hat{h}$ on the quantized field ψ in Equation (A.3) with $u^\pm$ and $v^\pm$, we find that the fields $u^\pm$ and $v^\pm$ are eigenstates of $\hat{h}$ with eigenvalue h but with opposite sign because of the anticommutation relation of the fermion fields [17], so

$$\hat{h}\, u^h = h\, u^h, \qquad \hat{h}\, v^h = -h\, v^h, \quad \text{with} \quad \hat{h} = \frac{\vec{p}\,\vec{s}}{|\vec{p}|} \quad \text{and} \quad \vec{s} = \int d^3x \psi^\dagger \vec{\sigma} \psi. \tag{A.4}$$

Moreover, since the helicity state is the projection of the spin $\vec{s}$ on the momentum $\vec{p}$ of the particle, it is not a fundamental property of massive fermions, one can flip the direction of the momentum by a boost into a system that is faster than the particle.

Helicity, however, becomes a fundamental property for fermions in the ultra-relativistic limit $E \gg m$ or for particles without mass. In addition, the chiral fields ψ_L and ψ_R decouple in this limit, which can easily be seen in the Dirac equations. Furthermore, one can see that the eigenstates of the chiral operator $\gamma_{L/R}$ and the helicity operator $\hat{h}$ become equal[5] [26, 17]. That means that spin eigenstates of fermions also become the helicity

[4] More precisely, the particles correspond to states in the Fock space, the space created in perturbation theory by applying the creation operators of the free field to the vacuum state.

[5] Written in the Dirac basis, it is $(E - \vec{\sigma}\vec{p})\,\psi_R = m\,\psi_L$ and $(E + \vec{\sigma}\vec{p})\,\psi_L = m\,\psi_R$, so for $E \gg m$, it applies that $\vec{\sigma}\vec{p}/E\,\psi_R = \psi_R$ and $\vec{\sigma}\vec{p}/E\,\psi_L = -\psi_L$.

eigenstates and chirality eigenstates [23]. Note that the correlation between helicity and chirality is inverse for antifermions due to Equation (A.4). Thus, the left-handed field $\psi_L \sim u_L^-$ describes particles with negative helicity, and $\psi_L^\dagger \sim v_L^+$ antiparticles with positive helicity, and the right-handed field $\psi_R \sim u_R^+$ describes particles with positive helicity and $\psi_R^\dagger \sim v_L^-$ antiparticles with negative helicity [17]. One can see this nicely in the chiral representation, where $u^\pm$ and $v^\pm$ in the limit $E \gg m$ reduce to [17]

$$u^+ = \sqrt{2E}\begin{pmatrix}0\\0\\1\\0\end{pmatrix} = u_R^+,\; u^- = \sqrt{2E}\begin{pmatrix}0\\1\\0\\0\end{pmatrix} = u_L^-,\; v^- = -\sqrt{2E}\begin{pmatrix}0\\0\\0\\1\end{pmatrix} = v_R^-,\; v^+ = \sqrt{2E}\begin{pmatrix}1\\0\\0\\0\end{pmatrix} = v_L^+. \tag{A.5}$$

The inverse correlation between chirality and helicity of antifermions as opposed to fermions naturally often leads to confusion, especially when it comes to charge-conjugation (which turns a particle into its antiparticle) and chiral symmetries such as the weak force.

A.1.4. Chiral symmetries

Apart from the $SU(2)$ symmetry of weak interaction, which is a chiral symmetry, all SM-gauge symmetries are non-chiral theories . Chiral theories behave asymmetrically in relation to chirality, e.g. weak interactions only couple to left-handed fermion fields. This means that for particles and antiparticles that interact only via the weak force (such as nearly massless neutrinos and antineutrinos), only their left-handed fields can be detected. Moreover, due to this property, chiral theories such as the weak interactions also break C and P symmetry as will be shown in the next Chapter A.2.

A.2. C, P, T Symmetry

This chapter is dedicated to the three discrete $\mathbb{Z}_2$ symmetry groups parity, P, charge conjugation, C, and time-reversal, T. The $\mathbb{Z}_2$ eigenvalues of the representations are the quantum numbers (QN) of C, P, T, which are normally {1, -1}. CP and especially C play an important role in neutrino physics. More specifically, the CP violation, which is measured in the quark sector, is actively searched for in the lepton sector and can be Moreover, C is an important component for the description of Majorana neutrinos. Therefore, the following sections focus on the C, P, T transformation properties of fermion fields.

A.2.1. Parity

Parity is a point reflection of the Euclidean space, it flips all coordinates $\vec{x}$ via $P\vec{x} = -\vec{x}$, where P is the parity operator. Applied to a fermion field ψ, it reverses the momentum of the fermion without flipping the spin [17, 26], but therefore flips the spin projection on the momentum, the helicity; in Dirac space, the transformation is $P\psi(\vec{p}) = \gamma_0\psi(-\vec{p})$ with $P = \gamma_0$. Parity is maintained in QED and QCD, but it is broken by weak interactions. The weak symmetry group $SU(2)_L$ breaks parity because it only acts on left-handed fields and thus, for a massless fermion $SU(2)_L$, acts on the negative helicity component of that particle (and the positive part of an antiparticle) and not on the parity-transformed positive helicity component (or the negative one for an antiparticle), see Table A.1; this is proven e.g. by the Wu-experiment.

Change of...	**P**	**C**	**T**	**CP**	**CPT**
Direction $\vec{x}$	yes	no	no	yes	yes
Elec. dipole moment $\vec{d}$	yes	no	no	yes	yes
Momentum $\vec{p}$	yes	no	yes	yes	no
Spin $\vec{s}$	no	no	yes	no	yes
Helicity $\vec{h}$	yes	no	no	yes	yes
Charge q	no	yes	no	yes	yes

examples

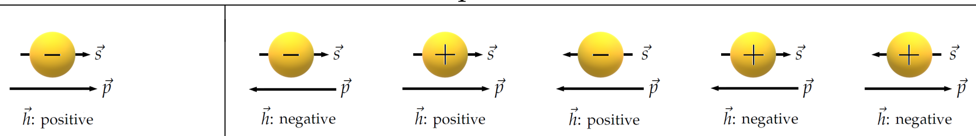

e^-_R	e^-_L	$(e^-)^c_L$	e^-_R	$(e^-)^c_R$	$(e^-)^c_R$

Table A.1.: Transformation of a fermion state under C, P, T and CP, CPT. Chirality is a property of the fermion field, and changes under C, e.g. with e^-_R; in the examples, a right-handed electron field is meant, which changes into a left-handed field under P and C.

Furthermore, P-transformation properties of Dirac bilinears, $\overline{\psi}\Gamma\psi$, are often quite useful, e.g. in the calculation of lepton magnetic dipole moments in Chapter 8. Dirac bilinears are a combination of fermion fields, ψ, and an element of the Clifford algebra, Γ. The vector space of the $SO(1,3)^+$ Lorentz group, the Dirac algebra, is a special case of the Clifford algebra $C\ell_{1,3}(\mathbb{C})$, the latter is spanned by the set of gamma matrices $\Gamma \in \{\mathbb{1}, \gamma^5, \gamma^\mu, \gamma^\mu\gamma^5, \sigma^{\mu\nu}\}$ with $\sigma^{\mu\nu} = \frac{i}{2}[\gamma^\mu, \gamma^\nu]$. Dirac bilinears $\overline{\psi}\Gamma\psi$, which are partly found in the Lagrange density, transform as a vector, scalar, or tensor under Lorentz transformation and, interestingly, behave differently under parity transformations. Depending on their transformation behaviour, these elements are called scalar, pseudo-scalar, vector, axial-vector or tensor [43], see Table A.2.

	Scalar	Pseudo-scalar	Vector	Axial-vector	Tensor
P	+	-	-	+	-
Dirac bilinears[6]	$\overline{\psi}\mathbb{1}\psi$	$\overline{\psi}\gamma^5\psi$	$\overline{\psi}\gamma^\mu\psi$	$\overline{\psi}\gamma^\mu\gamma^5\psi$	$\overline{\psi}\sigma^{\mu\nu}\psi$
Physical parameters	$E,\ \mu$	d	$\vec{x},\ \vec{E}$	$\vec{s},\ \vec{B}$	$F^{\mu\nu}$

Table A.2.: Parity transformation of Dirac bilinears and physical parameters. E is the Energy, μ and d the magnetic and electric dipole moment, $\vec{s}$ the spin, $\vec{E}$ and $\vec{B}$ the electric and magnetic field, and $F^{\mu\nu}$ a field tensor [43].

Vectors transform odd under parity and even under time reflection, whereas axial-vectors do the opposite.

A.2.2. Charge conjugation

An antiparticle differs from a particle by the conjugation of all $U(1)$ charges (quantum numbers), such as the electric charge, baryon and lepton number, and flavour-quantum numbers such as strangeness; while mass, lifetime, spin, and momentum are the same [43]. Therefore, charge conjugation transforms a particle into an antiparticle and vice versa. A charge-conjugated fermion field is defined as $\psi^c = C\overline{\psi}^T$, where C is the charge conjugation operator. As can be deduced from the above, C does not change the helicity of a fermion, but it changes the chirality of the fermion field [24, 17, 26], which means C maps the $\left(\frac{1}{2}, 0\right)$ Lorentz representation to the $\left(0, \frac{1}{2}\right)$ representation [23]; With Equation (A.9), it is

$$(\psi_L)^c = (\psi^c)_R\,. \tag{A.6}$$

Without loss of generality, the charge conjugation operator obeys the following rules,

$$C^T = -C,\ C^\dagger = C^{-1},\ C^{-1}\gamma_\mu C = -\gamma_\mu^T,\ C^{-1}\gamma_5 C = \gamma_5^T \tag{A.7}$$

$$\Lambda^T C^{-1}\Lambda = C^{-1},\ \text{with}\quad C\sigma_{\mu\nu}^T C^{-1} = -\sigma_{\mu\nu}\quad \text{(Lorentz-invariance)} \tag{A.8}$$

$$\psi^c = C\overline{\psi}^T = C\gamma_0^T\psi^*,\ \text{and}\quad \psi^T C^{-1} = -\overline{\psi^c}, \tag{A.9}$$

where Λ is the operator for Lorentz transformations from Equation (A.2); in Dirac space, $C = i\gamma^2\gamma^0$. Thus, for a massless particle, C changes e.g. a left-handed fermion field into a right-handed antifermion, where, by definition, only the first field couples to the charge current of the weak interactions [26]. Therefore, C and P are found to be maximally violated by the $SU(2)_L$ symmetry [24, 17], in the same way that any chiral symmetry would violate C and P [26]. Consequently, also the quantum numbers: the third component of the weak isospin, I_3, and weak hypercharge, Y, are different for particles and antiparticles, e.g. for electrons and positrons $I_3(e^-) = 1/2$, $Y(e^-) = -1$ and $I_3(e^+) = 0$, $Y(e^+) = +2$.

Moreover, charge conjugation by itself only changes the sign of the weak charge, e.g. a right-handed weak-isospin singlet, ψ_R, remains a singlet after charge conjugation, $(\psi_R)^c$ [123] for the same reason that a left-handed field ψ_L, as part of a weak-isospin doublet, remains charged under weak-isospin when charge-conjugated, $(\psi_L)^c$. For this reason, charge conjugation is very interesting for Majorana neutrino theorists, it introduces two new fields to the SM: A charge conjugated $(\nu_L)^c$ as part of a weak-isospin doublet and the $(\nu_R)^c$ singlet, as analysed in more detail in Chapter 2.2.

[6] The P transformation for relativistic four-component vectors results in a minus in the spatial coordinates and for pseudo-vectors in the time coordinates.

A.2.3. Time reversal

Time reversal changes the direction of the propagation of particles, $(\psi_\alpha \to \psi_\beta) \xrightarrow{T} (\psi_\beta \to \psi_\alpha)$, see [17], and the spin of a particle, therefore, the helicity remains invariant. The transformation of time-reversal applied to a fermion field is in the Dirac space $T\psi(t,x) = (\gamma^1\gamma^3)\psi(-t,x)$, where T is the time-reversal operator. T is conserved by all standard model gauge symmetries; nevertheless, since CPT is an unbroken symmetry in the Standard Model, but CP is found to be violated, also T must be violated. CP violation is found in weak decays in the quark sector and is represented, within the mass terms, via a complex phase, δ_{CP}, in the *CKM*-matrix. For the violation in the lepton sector, it can be represented equivalently in the *PMNS*-matrix. In general, a CP violation is necessary because it is one of the Sakharov conditions for successful baryogenesis in the early universe, but for this, the known SM-CP violation is not sufficient, so additional sources of CP violation are searched for.

A.3. Custodial Symmetry

Since custodial symmetry is relevant for a new Higgs sector and is directly related to the oblique parameters, it will be explained in more detail below.

Custodial symmetry is a global $SU(2)$ symmetry and a remnant of the local $SU(2)_L \times U(1)_Y$ gauge symmetry [23]. Accordingly, it maintains weak isospin, i.e. all charged particles transform within multiplets, mostly $SU(2)_L$ doublets, via $U(\theta) = \exp(igQ\theta^a\tau^a)$, with the coupling constant g, the charge Q, the transformation angle θ^a, and the generators τ^a, with $a \in \{1,2,3\}$. That means, the symmetry treats the members within a multiplet equally, such as up- and down-quarks or neutrinos and electrons from an $SU(2)_L$ doublet, or the Goldstone bosons in the Higgs doublet [26]. It therefore generally also preserves the splitting between the masses of the members within a multiplet and their couplings [82]. Nevertheless, we know e.g. $Y_u \neq Y_d$ or $m_e \neq m_\nu$, so from this follows that custodial symmetry must be broken by the differing Yukawa couplings, Y, or the fermion masses, m. This breaking is small, however, because fermion masses are small apart from the mass of the top quark, m_{top} [23]. The top quark mass is, therefore, also the dominant SM contribution to the well-measured oblique parameter $T = \rho - 1$ being a measure for custodial symmetry breaking. The parameter T, or rather ρ, reflects the relation between the masses of the gauge bosons $\rho = m_W^2/(m_Z^2 \cos\theta_W^2) = 1$, which in turn is preserved by the custodial symmetry.

A reasonable question now is how custodial symmetry is related to the masses of the weak-isospin gauge bosons W and Z. This will be examined in more detail below. After electroweak symmetry breaking (EWSB), a rotational symmetry remains within the Higgs doublet between three of the four scalars, namely between the Goldstone bosons, whereas the Higgs scalar receives a VEV. This symmetry is an O(3), or rather an SU(2) symmetry, which is in fact the custodial symmetry. The Goldstone boson equivalence theorem states that each Goldstone boson corresponds to a longitudinal mode of the weak gauge bosons W and Z, in accordance with the statement that in unitary gauge, the gauge bosons absorb the Goldstone bosons to gain mass [26]. So it is clear that Goldstone bosons are connected to the mass of gauge bosons, and thus it is not surprising that custodial symmetry preserves the relation $m_W = m_Z \cos\theta_W$, ensuring that the gauge boson masses lay close together.

B. Model Contributions to Dipole Moments of Leptons

Our theory predicts contributions to the dipole moments of leptons in the form of two Feynman diagrams, specifically for the process of a photon emitted from a fermion line $\ell \to \ell\gamma$:

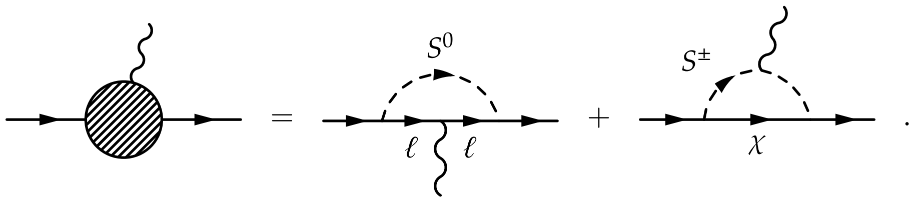

(B.1)

In this chapter, we calculate the contributions from (B.1) using a general approach for the scalar-lepton vertex, being

$$\mathcal{L}_{\mathcal{Y}}(S) = \bar{f}'(a_L\gamma_L + a_R\gamma_R)fS + h.c. \tag{B.2}$$

The notation is as follows: The incoming and outgoing lepton ℓ has mass m and charge Q, while m' and Q' are the mass and charge of the leptons ℓ' or χ in the loop, while the mass of the neutral scalar S^0 and the charged scalar is designated as M. Feynman diagrams for the calculations can be found in Appendix D.

B.1. First Diagram: Photon Attaches to Leptons

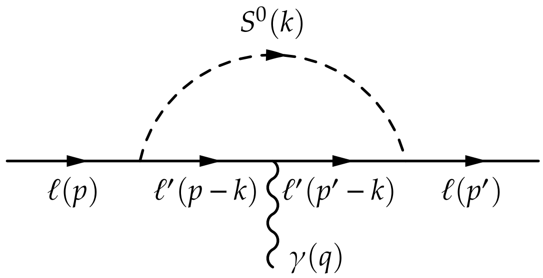

The amplitude of the first diagram, including a neutral scalar in the loop, is calculated as

$$i\mathcal{A}^{(S^0)} = \int \frac{d^4k}{(2\pi)^4} \bar{u}(p')\, \underbrace{i\left(a_L^* \gamma_R + a_R^* \gamma_L\right)}_{\ell'\ell S^0-vertex} \underbrace{i\frac{\not{q}_2 + m'}{q_2^2 - m'^2 + i\epsilon}}_{\ell'-prop} \underbrace{iQ'e\gamma^\mu}_{\ell'\ell'\gamma-vertex} \underbrace{i\frac{\not{q}_1 + m'}{q_1^2 - m'^2 + i\epsilon}}_{\ell'-prop}$$
$$\times \underbrace{i\left(a_L \gamma_L + a_R \gamma_R\right)}_{\ell\ell' S^0-vertex} \underbrace{\frac{i}{k^2 - M^2 + i\epsilon}}_{S^0-prop} u(p)$$
$$= -eQ' \int \frac{d^4k}{(2\pi)^4} \bar{u}(p') \frac{\left(a_L^* \gamma_R + a_R^* \gamma_L\right)(\not{q}_2 + m')\gamma^\mu(\not{q}_1 + m')\left(a_L \gamma_L + a_R \gamma_R\right)}{(q_2^2 - m'^2 + i\epsilon)(q_1^2 - m'^2 + i\epsilon)(k^2 - M^2 + i\epsilon)} u(p), \tag{B.3}$$

with $q_1 = p - k$ and $q_2 = p' - k = p + q - k$ the momenta in the loops.

Denominator

We will first concentrate on the denominator of Equation (B.3), which can be rewritten using Feynman parameters[1], Equation (C.1), into

$$\frac{1}{(q_2^2 - m'^2)(q_1^2 - m'^2)(k^2 - M^2)}$$
$$= \int dxdy \frac{2}{[x(q_2^2 - m'^2) + y(q_1^2 - m'^2) + (1 - x - y)(k^2 - M^2)]^3} \tag{B.4}$$
$$= \int dxdy \frac{2}{[l^2 - \Delta]^3}, \tag{B.5}$$

with

$$l = k - [xp' + yp], \quad \Delta = (1 - x - y)(M^2 - xp'^2 - yp^2) + (x + y)m'^2 - xy(p'^\mu - p^\mu)^2 + i\epsilon. \tag{B.6}$$

To get from Equation (B.4) to Equation (B.5), we calculated

$$\begin{aligned} x(q_2^2 - m'^2) &+ y(q_1^2 - m'^2) + (1 - x - y)(k^2 - M^2) \\ &= x((p' - k)^2 - m'^2) + y((p - k)^2 - m'^2) + (1 - x - y)(k^2 - M^2) \\ &= k^2 - 2k(xp' + yp) + xp'^2 + yp^2 - m'^2(x + y) - M^2(1 - x - y) \\ &= l^2 - \Delta. \end{aligned} \tag{B.7}$$

[1] See Appendix C.1 for details of regularization.

Moreover, the parameters x and y are symmetrical in the denominator and the integral, so we can exchange $x, y \to 1/2(x+y)$ and Equation (B.5) becomes

$$\frac{1}{(\not{q}_2^2 - m'^2)(\not{q}_1^2 - m'^2)(k^2 - M^2)} = \int dz(1-z)\,\frac{2}{[l^2-\Delta]^3}, \tag{B.8}$$

$$\text{with} \quad \Delta = zM^2 + (1-z)m'^2 - \frac{(1-z)z}{2}(p'^2+p^2) - \frac{(1-z)^2}{4}(p'^\mu - p^\mu)^2 + i\epsilon \tag{B.9}$$

and $x+y+z=1$ as well as $\int_0^1 dz \int_0^{1-z} dy f(z) = \int dz(1-z)f(z)$.

Numerator

The numerator of Equation (B.3), which we call β^μ, on the other hand, can be arranged in two parts, according to the chiral projection operators,

$$\begin{aligned}\beta^\mu &= \left(a_L^*\,\gamma_R + a_R^*\,\gamma_L\right)(\not{q}_2 + m')\gamma^\mu(\not{q}_1 + m')\,(a_L\,\gamma_L + a_R\,\gamma_R)\\ &= \left(|a_L|^2\,\gamma_R + |a_R|^2\,\gamma_L\right)\left(\not{q}_2\gamma^\mu\not{q}_1 + m'^2\gamma^\mu\right) + m'\left(a_L^* a_R\,\gamma_R + a_R^* a_L\,\gamma_L\right)\left(\not{q}_2\gamma^\mu + \gamma^\mu\not{q}_1\right).\end{aligned} \tag{B.10}$$

Let us briefly list the inputs we will use to calculate the terms in Equation (B.10). As we found in Equation (8.20), the contributions to AMM and EDM have a spin-dependence and are proportional to $\sigma^{\mu\nu}$, or rather $(p^\mu + p'^\mu)$, whereas all other terms, which are only proportional to the four-component γ^μ, belong to the contributions of $F_1(0)$, vis. to the renormalization of the electric charge. Therefore,

- We will omit any term $\sim \gamma^\mu$ in the following calculations,

e.g. that in the first term of Equation (B.10). Also, remember that the Dirac matrices follow the anti-commutation relation $\{\gamma^\mu, \gamma^\nu\} = 2g^{\mu\nu}$ and therefore,

- A useful relation is $\not{p}\gamma^\mu = 2p^\mu - \gamma^\mu\not{p}$ (and also $\not{p}p'^\mu = p'^\mu\not{p}$).
- Since everything is calculated on-shell, we can use the Dirac equation, i.e. $\bar{u}(p')\not{p}' = \bar{u}(p')\,m$ and $\not{p}u(p) = m\,u(p)$.
- In addition, terms with the momentum k will be rewritten to l with $k = l + [xp' + yp]$, from Equation (B.6).
- In the further course, we will neglect all contributions that are single-proportional to l since $\int dl\, l = 0$.
- The magnetic or electric dipole moment is evaluated under on-shell condition, i.e. $q^2 = 0$ (note $q \neq 0$). Therefore, $q^2 = (p'^\mu - p^\mu)^2 = 2m^2 - 2p'p = 0$ and thus $p'p = m^2$.

We will continue with calculating terms in Equation (B.10). The second term in Equation (B.10) includes

$$\begin{aligned} \not{q}_2\gamma^\mu &= \left(\not{p}' - \not{k}\right)\gamma^\mu = m\gamma^\mu - \not{k}\gamma^\mu = -\not{k}\gamma^\mu = -\left(\not{l} + x\not{p}' + y\not{p}\right)\gamma^\mu \\ &= -\left(xm + y\not{p}\right)\gamma^\mu = -y\not{p}\gamma^\mu = -y\left(2p^\mu - \gamma^\mu\not{p}^\mu\right) = ym\gamma^\mu - y2p^\mu = -2yp^\mu \end{aligned} \tag{B.11}$$

and, accordingly, it is

$$\gamma^\mu\not{q}_1 = \gamma^\mu\left(\not{p} - \not{k}\right) = m\gamma^\mu - \gamma^\mu\not{k} = -\gamma^\mu\not{k} = -\gamma^\mu\left(x\not{p}' + y\not{p}\right) = -x\gamma^\mu\not{p}' = -2xp'^\mu. \tag{B.12}$$

When using the Dirac equation with $\bar{u}(p')\not{p}' = \bar{u}(p')\,m$, caution is required because prefactors such as $|a_L|^2\gamma_R$, which are between $\bar{u}(p')$ and $\not{p}$ in formula (B.10) are provided with chiral operators $\gamma_{R/L}$, which will invert the sign and thus the chirality, for example, $\bar{u}(p')\,|a_L|^2\,\gamma_R\,\not{p}'\,\gamma^\mu = \bar{u}(p')\,|a_L|^2\,\gamma_L\,m\,\gamma^\mu$. Therefore, in the following, we will mark all terms that invert the sign of the chiral operators with blue colour, as it was done in the previous example. In this sense, the first term in Equation (B.10) contains

$$\begin{aligned} \not{q}_2\gamma^\mu\not{q}_1 &= \left(\not{p}' - \not{k}\right)\gamma^\mu\left(\not{p} - \not{k}\right) = m^2\gamma^\mu - m\left(\gamma^\mu\not{k} + \not{k}\gamma^\mu\right) + \not{k}\gamma^\mu\not{k} \\ &= -2m\left(x\,p'^\mu + y\,p^\mu\right) + \not{k}\gamma^\mu\not{k} \\ &= 2m\left(-x\,p'^\mu - y\,p^\mu + x^2\,p'^\mu + y^2\,p^\mu + xy\,p'^\mu + xy\,p^\mu\right), \end{aligned} \tag{B.13}$$

using

$$\begin{aligned} \not{k}\gamma^\mu\not{k} &= \left(\not{l} + x\not{p}' + y\not{p}\right)\gamma^\mu\left(\not{l} + x\not{p}' + y\not{p}\right) \\ &= \not{l}\gamma^\mu\not{l} + x^2\not{p}'\gamma^\mu\not{p}' + y^2\not{p}\gamma^\mu\not{p} + xy\left(\not{p}'\gamma^\mu\not{p} + \not{p}\gamma^\mu\not{p}'\right) \\ &= x^2m\gamma^\mu\not{p}' + y^2m\not{p}\gamma^\mu + xy\not{p}\gamma^\mu\not{p}' = 2m\left(x^2p'^\mu + y^2p^\mu\right) + xy\not{p}\gamma^\mu\not{p}' \\ &= 2m\left(x^2p'^\mu + y^2p^\mu + xy\,p'^\mu + xy\,p^\mu\right), \end{aligned} \tag{B.14}$$

with

$$\begin{aligned} &\not{p}\gamma^\mu\not{p}' = \not{p}\left(2p'^\mu - \not{p}'^\mu\gamma^\mu\right) = 2\not{p}p'^\mu - \not{p}\not{p}'\gamma^\mu = 2mp'^\mu + m\left(2p^\mu - \gamma^\mu\not{p}^\mu\right) = 2m\left(p'^\mu + p^\mu\right), \\ &\text{with} \qquad \not{p}\not{p}' = p_\mu\gamma^\mu\not{p}' = p_\mu\left(2p'^\mu - \not{p}'\gamma^\mu\right) = 2pp' - \not{p}'\not{p} = 2m^2 - \not{p}'\not{p}. \end{aligned} \tag{B.15}$$

Finally, for the numerator in Equation (B.10), using Equations (B.11), (B.12), and (B.13), we obtain

$$\begin{aligned} \beta^\mu &= \left(a_L^*\,\gamma_R + a_R^*\,\gamma_L\right)\left(\not{q}_2 + m'\right)\gamma^\mu\left(\not{q}_1 + m'\right)\left(a_L\,\gamma_L + a_R\,\gamma_R\right) \\ &= 2m\left(|a_L|^2\,\gamma_R + |a_R|^2\,\gamma_L\right)\left(-y\,p^\mu + y^2\,p^\mu + xy\,p'^\mu\right) \\ &\quad + 2m\left(|a_L|^2\,\gamma_L + |a_R|^2\,\gamma_R\right)\left(-x\,p'^\mu + x^2\,p'^\mu + xy\,p^\mu\right) \\ &\quad - 2m'\left(a_L^*a_R\,\gamma_R + a_R^*a_L\,\gamma_L\right)\left(xp'^\mu + yp^\mu\right). \end{aligned} \tag{B.16}$$

Denominator & numerator:

Combining the results of the denominator of Equation (B.8), and the numerator of Equation (B.16), the amplitude in Equation (B.3) gives

$$i\mathcal{A}^{(S^0)} = -eQ'\,\bar{u}(p')\int\frac{d^4l}{(2\pi)^4}\int dz(1-z)\frac{2\beta^\mu}{[l^2-\Delta]^3}u(p). \tag{B.17}$$

We use dimensional regularization to solve the integral over l in terms of $d = 4-\epsilon$. Thus, after Wick rotation, (C.3) (where we get an extra factor of $-i$) we solve the integral with Equation (C.5) and obtain

$$\begin{aligned} i\mathcal{A}^{(S^0)} &= ieQ'\,\bar{u}(p')\int dz(1-z)\int\frac{d^dl}{(2\pi)^d}\frac{2\beta^\mu}{[l^2+\Delta]^3}u(p) \\ &= \frac{ieQ'}{(4\pi)^2}\bar{u}(p')\int dz(1-z)\,\frac{\beta^\mu}{\Delta}\,u(p) \end{aligned} \tag{B.18}$$

with $\Delta = zM^2 + (1-z)(m'^2 - zm^2)$ on the mass shell.

Determining the AMM and EDM:

Now we will extract the AMM and EDM contributions from this amplitude in Equation (B.18). The contributions of AMM and EDM are proportional to $\sigma^{\mu\nu}q_\nu$, i.e. using the Gordon identity, (8.13),

$$\bar{u}(p')\gamma^\mu u(p) = \bar{u}(p')\left[\frac{p'^\mu + p^\mu}{2m} + \frac{i\sigma^{\mu\nu}q_\nu}{2m}\right]u(p), \tag{B.19}$$

we will rewrite terms proportional to $(p'^\mu + p^\mu)$ into terms proportional to $i\sigma^{\mu\nu}q_\nu$ (whereby all terms proportional to γ^μ will be neglected, like before when calculating the numerator). Furthermore, due to the Ward-identity, the contributions with $q^\mu = p^\mu - p'^\mu$ are zero.

According to Equation (8.20),

$$i\mathcal{A} \supset \frac{ieQ}{2m}\left(F_{AMM}(0)\,i\sigma^{\mu\nu}q_\nu + F_{EDM}(0)\,\gamma_5\,\sigma^{\mu\nu}q_\nu\right) \tag{B.20}$$

and thus, the contribution to the AMM in the amplitude is not scaling like those to the EDM with γ_5, but with the factor $\frac{ieQ}{2m}i\sigma^{\mu\nu}q_\nu$. So we omit the γ_5 contributions of the chiral projectors γ_L, γ_R. Moreover, we can use the fact that the parameters x and y are symmetrical in the denominator and the integral to exchange $x, y \to 1/2(x+y)$ and $x + y = 1-z$, the numerator of Equation (B.16) then becomes

$$\begin{aligned} \beta^\mu_{AMM} &= -(1-z)\frac{1}{2}\left(zm\left(|a_L|^2 + |a_R|^2\right) + 2m'Re(a_L^* a_R)\right)(p'^\mu + p^\mu) \\ &= (1-z)\frac{1}{2}\left(zm\left(|a_L|^2 + |a_R|^2\right) + 2m'Re(a_L^* a_R)\right)i\sigma^{\mu\nu}q_\nu. \end{aligned} \tag{B.21}$$

With this input, by comparing Equation (B.20) with Equation (B.18), we can extract the AMM as

$$F^{(S^0)}_{AMM}(0) = \frac{Q'm}{(4\pi)^2}\int dz(1-z)^2 \frac{zm\left(|a_L|^2+|a_R|^2\right)+2m'Re(a_L^* a_R)}{zM^2+(1-z)(m'^2-zm^2)}. \tag{B.22}$$

According to Equation (B.20), the contribution to the EDM scales with the factor $\frac{ieQ}{2m}\gamma_5\,\sigma^{\mu\nu}q_\nu$. So we collect the γ_5 contributions from the projectors $\gamma_{R/L} = (1\pm\gamma_5)/2$ and write Equation (B.16) as before with symmetrical x and y, via $x, y \to 1/2(x+y)$,

$$\begin{aligned}\beta^\mu_{EDM} &= -(1-z)\,\frac{1}{2}\left[m\left(|a_L|^2-|a_R|^2\right)(p'^\mu-p^\mu)+2m'Im(a_L^* a_R)\,(p'^\mu+p^\mu)\right]\gamma_5\\ &= (1-z)\,m'\,Im(a_L^* a_R)\gamma_5\,i\sigma^{\mu\nu}q_\nu.\end{aligned} \tag{B.23}$$

The factor $(p'^\mu - p^\mu)$ does not contribute, so when comparing Equation (B.20) with Equation (B.18), it is

$$F^{(S^0)}_{EDM}(0) = i\frac{Q'mm'}{(4\pi)^2}\int dz(1-z)^2\frac{2Im(a_L^* a_R)}{zM^2+(1-z)(m'^2-zm^2)}. \tag{B.24}$$

B.2. Second Diagram: Photon Attaches to Scalars

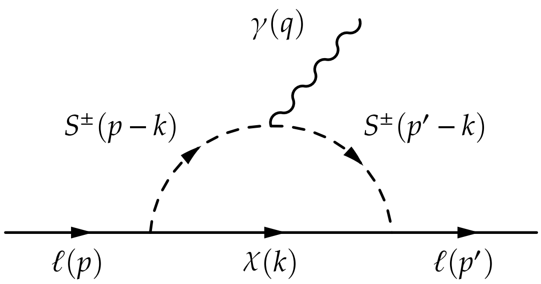

The amplitude of this second diagram, including charged scalars in the loop, is denoted as

$$\begin{aligned} i\mathcal{A}^{(S^\pm)} &= \int \frac{d^4k}{(2\pi)^4}\bar{u}(p')\,\underbrace{i\left(a_L^*\,\gamma_R + a_R^*\,\gamma_L\right)}_{\ell\chi\,S^- -vertex}\underbrace{i\frac{\not{k}+m'}{k^2-m'^2+i\epsilon}}_{\chi-prop}\underbrace{i\left(a_L\,\gamma_L + a_R\,\gamma_R\right)}_{\chi\,\ell S^- -vertex}\\ &\quad\times \underbrace{\frac{i}{q_2^2-M^2+i\epsilon}}_{S^- -prop}\underbrace{ie(Q'-Q)(q_1+q_2)^\mu}_{S^\pm\gamma-vertex}\underbrace{\frac{i}{q_1^2-M^2+i\epsilon}}_{S^- -prop}u(p)\\ &= -e(Q'-Q)\bar{u}(p')\int\frac{d^4k}{(2\pi)^4}\frac{\left(a_L^*\,\gamma_R+a_R^*\,\gamma_L\right)(\not{k}+m'^2)\,(a_L\,\gamma_L+a_R\,\gamma_R)\,(q_1^\mu+q_2^\mu)}{(k^2-m'^2+i\epsilon)(q_2^2-M^2+i\epsilon)(q_1^2-M^2+i\epsilon)}u(p), \end{aligned} \tag{B.25}$$

where $q_1 = p - k$ and $q_2 = p' - k = p - q - k$ are the momenta in the loops. As before, m and Q are the mass and charge of the incoming and outgoing lepton ℓ, and m' and Q' are mass and charge of the lepton in the loop, here a neutrino; finally, M denotes the mass of the charged scalar $S^{\pm}$.

In the further calculation, we will proceed with a similar strategy as before for the first diagram in Section B.1, therefore, we will not mention the steps in the detail as before and refer the reader to the procedure in the first calculation in case of questions. In the following, we will calculate first the denominator and second the numerator of the amplitude in Equation (B.25). Then we will collect both results and write down the amplitude with the relevant contributions and finally extract the AMM and EDM from them.

Denominator

When using the Feynman parameters with $x + y + z = 1$, the denominator of the amplitude of Equation (B.25) becomes

$$\frac{1}{(q_2^2 - M^2)(q_1^2 - M^2)(k^2 - m'^2)} = \int dz (1-z) \frac{2}{[l^2 - \Delta]^3}, \tag{B.26}$$

with $l = k - [xp' + yp]$ and

$$\Delta = zm'^2 + (1-z)M^2 - \frac{(1-z)z}{2}(p'^2 + p^2) - \frac{(1-z)^2}{4}(p'^{\mu} - p^{\mu})^2 + i\epsilon. \tag{B.27}$$

Numerator

The numerator of Equation (B.25) gives

$$\begin{aligned}
\beta^{\mu} &= \left(a_L^* \gamma_R + a_R^* \gamma_L\right) (\not{k} + m') \left(a_L \gamma_L + a_R \gamma_R\right) (q_1^{\mu} + q_2^{\mu}) \\
&= \left[\left(|a_L|^2 \gamma_R + |a_R|^2 \gamma_L\right) \not{k} + m' \left(a_L^* a_R \gamma_R + a_R^* a_L \gamma_L\right)\right] (p^{\mu} + p'^{\mu} - 2k^{\mu}) \\
&= \Big[m \left(|a_L|^2 \gamma_L + |a_R|^2 \gamma_R\right) x + m \left(|a_L|^2 \gamma_R + |a_R|^2 \gamma_L\right) y \\
&\quad + m' \left(a_L^* a_R \gamma_R + a_R^* a_L \gamma_L\right)\Big] (p^{\mu}(1-2y) + p'^{\mu}(1-2x)) \\
&= \left[m \left(|a_L|^2 + |a_R|^2\right) \frac{\gamma_R + \gamma_L}{2} (1-z) + m' \left(a_L^* a_R \gamma_R + a_R^* a_L \gamma_L\right)\right] z (p^{\mu} + p'^{\mu}),
\end{aligned} \tag{B.28}$$

using $l = k - [xp' + yp]$ and $x + y + z = 1$, symmetrising β^{μ} in x and y, and omitting all terms that are single-proportional to γ^{μ} or l.

Amplitude and AMM & EDM

Taking Equations (B.25), (B.26), and (B.28) gives an amplitude of the shape (B.29). To obtain Equation (B.30), we use dimensional regularization with $d = 4 - \epsilon$, perform a wick rotation, (C.3) (which brings an additional factor of $-i$), and then solve the integral using Equation (C.5), i.e.

$$i\mathcal{A}^{(S^\pm)} = -e(Q'-Q)\bar{u}(p')\int dz(1-z)\int \frac{d^dl}{(2\pi)^d}\frac{2\beta^\mu}{[l^2-\Delta]^3}u(p) \tag{B.29}$$

$$= \frac{ie(Q'-Q)}{(4\pi)^2}\bar{u}(p')\int dz(1-z)\frac{\beta^\mu}{\Delta}u(p), \tag{B.30}$$

with $\Delta = zm'^2 + (1-z)(M^2 - zm^2)$ on the mass shell.

In addition, we can obtain the AMM and EDM contribution as in the previous section with a comparison to the terms in Equation (B.20) and use the Gordon Identity in (B.19). Then, we get for the AMM and EDM, with Equation (B.28) and

$$\beta^\mu_{AMM} = -\frac{1}{2}\left[m\left(|a_L|^2+|a_R|^2\right)(1-z) + 2m'\,Re\left(a_L^*a_R\right)\right]z\,i\sigma^{\mu\nu}q_\nu, \tag{B.31}$$

$$\beta^\mu_{EDM} = -m'\,Im\left(a_L^*a_R\right)z\,i\sigma^{\mu\nu}q_\nu, \tag{B.32}$$

finally, the contributions

$$F^{(S^\pm)}_{AMM}(0) = -\frac{m(Q'-Q)}{(4\pi)^2}\int dz\,(1-z)z\,\frac{m\left(|a_L|^2+|a_R|^2\right)(1-z)+2m'^2\,Re\left(a_L^*a_R\right)}{zm'+(1-z)(M^2-zm^2)}, \tag{B.33}$$

$$F^{(S^\pm)}_{EDM}(0) = -i\frac{mm'(Q'-Q)}{(4\pi)^2}\int dz\,(1-z)z\,\frac{2Im\left(a_L^*a_R\right)}{zm'^2+(1-z)(M^2-zm^2)}. \tag{B.34}$$

B.3. All Contributions Summarized

Here we collect the results of $F_{AMM}(0)$ and $F_{EDM}(0)$ from both diagrams in (B.1), thus Equations (B.22), (B.33), and (B.24), (B.34) together yield

$$\begin{aligned} F_{AMM} = -\frac{m}{(4\pi)^2}\int dz\Bigg(&Q'z^2\frac{(1-z)m\left(|a_L|^2+|a_R|^2\right)+2m'Re(a_L^*a_R)}{zm'^2+(1-z)(M^2-zm^2)} \\ &+(Q'-Q)z(1-z)\,\frac{(1-z)\,m\left(|a_L|^2+|a_R|^2\right)+2m'^2\,Re\left(a_L^*a_R\right)}{zm'+(1-z)(M^2-zm^2)}\Bigg), \end{aligned} \tag{B.35}$$

$$F_{EDM} = -i\frac{mm'}{(4\pi)^2}\int dz\left(\frac{Q'\,z^2\,2Im(a_L^*a_R)}{zm'^2+(1-z)(M^2-zm^2)}+\frac{(Q'-Q)\,z(1-z)\,2Im\left(a_L^*a_R\right)}{zm'^2+(1-z)(M^2-zm^2)}\right), \tag{B.36}$$

where m is the mass of the incoming and outgoing fermion with charge Q, and m' and Q' are the mass and charge of the fermions running in the loop and M is the mass of the neutral and charged scalar in the integral. Note that $F_{AMM}(0)$ and $F_{EDM}(0)$ must be dimensionless, which is the case here. $F_{EDM}(0)$ is connected to the EDM via Equation (8.21), where $d = i\frac{e}{m}F_{EDM}(0)$, so that the EDM is real as expected.

C. Renormalization and Regularization

In this chapter, the basic steps of the renormalization procedure in $\overline{MS}$ and the on-shell scheme will be very briefly recapitulated at the example of QED together with the treatment of dimensional regularization with the help of [146] and [94].

QFT calculations are in most cases successfully treated within the framework of perturbation theory: Calculations or reaction rates, cross-sections, masses, and other physical values are derived in loop corrections of Feynman diagrams, whereby higher-order corrections are suppressed by the powers of the coupling constant,[1] here e.g. in QED in the order of $\frac{e^2}{16\pi^4} = \frac{\alpha}{4\pi} \sim 5{,}8 \cdot 10^{-4}$ for low energies. In QED, higher-order radiative corrections become more relevant at higher energies, in contrast to QCD and weak interactions, see Figure C.1 describing the running couplings. Within this perturbative calculations, one often finds loop calculations that diverge in the ultraviolet region, i.e. at infinitely large momenta. The infinity part of these divergent loop contributions can be extracted very nicely using the tool of regularization and absorbed in the charges and parameters within the interpretation of renormalization.

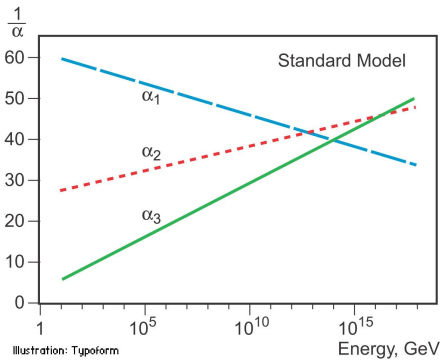

Figure C.1.: Running couplings, where α_1 is the electromagnetic coupling, α_2 the weak coupling, and α_3 the strong coupling [147]

C.1. Regularization

As described above, regularization is a tool to extract the infinity part of divergent integrals. There are different parts of regularization, like cut-off, or Pauli-Villard, and dimensional regularization. Dimensional regularisation is probably the most widely used regularization today due to its advantages: It does not introduce an additional energy scale and therefore preserves power-counting, it preserves gauge invariance and chiral symmetry and is technically much simpler and more transparent. In the calculation processes in Part II of this thesis, we regularly use dimensional regularization.

The basic idea of dimensional regularization is to perform all integrals in $d \neq 4$

[1] At low-energy, the QCD perturbation theory breaks down because the coupling constant becomes too high.

space-time dimensions, more precisely, $d = 4 - \epsilon$, with poles at $d = 4$. In this way, the integrals are brought into a form in which can be calculated with their divergences in a regular manner [146]. The basic steps of the procedure for a d-dimensional integral are described as follows.

- **Feynman parameters**:

  The idea of introducing Feynman parameters is to rewrite the numerator as an integral in a form that can be better integrated. The general formula is

$$\left[\frac{1}{A_1 ... A_n} = \int_0^1 dx_1 ... dx_n \, \delta\Big(\sum_i x_i - 1\Big) \frac{(n-1)!}{[x_1 A_1 + ... + x_n A_n]^n}\right], \tag{C.1}$$

  which will be followed by a small example

$$\begin{aligned}
&\frac{1}{((p-k)^2 - m_p^2)((q-k)^2 - m_q^2)(k^2 - m_k^2)}) \\
&= \int dxdydz \frac{2\delta(x+y+z-1)}{\left[x((p-k)^2 - m_p^2) + y((q-k)^2 - m_q^2) + z(k^2 - m_k^2)\right]^3} \\
&= \int dxdy \frac{2}{\left[x((p-k)^2 - m_p^2) + y((q-k)^2 - m_q^2) + (1-x-y)(k^2 - m_k^2)\right]^3} \\
&= \int dxdy \frac{2}{[l^2 - \Delta]^3},
\end{aligned} \tag{C.2}$$

  with

$$\begin{aligned}
&x((p-k)^2 - m_p^2) + y((q-k)^2 - m_q^2) + (1-x-y)(k^2 - m_k^2) \\
&= k^2 - 2k(px+qy) \pm (px+qy)^2 + x(p^2 - m_p^2) + y(q^2 - m_q^2) - (1-x-y)m_k^2 \\
&= \underbrace{[k - (px+qy)]}_{l}{}^2 + \underbrace{(1-x-y)(xp^2 + yq^2 - m_k^2) - xm_p^2 - ym_q^2 + xy(p^2 - q^2)}_{-\Delta}.
\end{aligned}$$

- **Wick rotation**:

  The next step is to deal with an integration in Minkowski space, where time and the three spatial coordinates have different signs. In the Wick rotation, the time coordinate l_0 is rotated into imaginary space so that the integral can be treated as being in an Euclidean space,

$$l^\mu = \begin{pmatrix} l_0 \\ \vec{l} \end{pmatrix} \rightarrow \begin{pmatrix} -l_0 \\ \vec{l} \end{pmatrix} \quad \Rightarrow \quad -l^2 = -(il_0^2 - \vec{l}^{\,2}) = l_0^2 + \vec{l}^{\,2} \quad \text{and} \quad d^d l = i\, dl_0\, d^i l_i,$$

  so

$$\int d^d l \frac{1}{[l^2 - \Delta]^n} \rightarrow i(-1)^n \int d^d l \frac{1}{[l^2 + \Delta]^n}. \tag{C.3}$$

- **Beta functions**:

  Beta functions always occur when it comes to the calculation of loop integrals, they have the form

$$\left[B(\alpha,\beta) = \frac{\Gamma(\alpha)\Gamma(\beta)}{\Gamma(\alpha+\beta)} = \int_0^\infty dx \frac{x^{\alpha-1}}{(1+x)^{\alpha+\beta}}, \quad \text{with } Re(\alpha,\beta) > 0 \right],$$

$$\text{gamma fct.:} \qquad \Gamma\left(\frac{1}{2}\right) = \sqrt{\pi},\ \Gamma(1) = 1,\ \Gamma(1+x) = x\Gamma(x),$$

  and, according to [26], are generally used in this way.

$$\begin{aligned}
\int \frac{d^d l}{(2\pi)^d} \frac{1}{(l^2-\Delta)^n} &= \frac{(-1)^n i}{(4\pi)^{d/2}} \frac{\Gamma(n-\frac{d}{2})}{\Gamma(n)} \left(\frac{1}{\Delta}\right)^{n-\frac{d}{2}} \\
\int \frac{d^d l}{(2\pi)^d} \frac{l^2}{(l^2-\Delta)^n} &= \frac{(-1)^{n-1} i}{(4\pi)^{d/2}} \frac{d}{2} \frac{\Gamma(n-\frac{d}{2}-1)}{\Gamma(n)} \left(\frac{1}{\Delta}\right)^{n-\frac{d}{2}-1} \\
\int \frac{d^d l}{(2\pi)^d} \frac{l^\mu l^\nu}{(l^2-\Delta)^n} &= \frac{(-1)^{n-1} i}{(4\pi)^{d/2}} \frac{g^{\mu\nu}}{2} \frac{\Gamma(n-\frac{d}{2}-1)}{\Gamma(n)} \left(\frac{1}{\Delta}\right)^{n-\frac{d}{2}-1} .
\end{aligned}$$

- **Expansion in epsilon**:

  The expansion of the integrals around the pole is the heart-piece of dimensional regularization, where the infinities are extracted. This means that everything is expanded in orders of ϵ, with $d = 4 - \epsilon$, one gets, with γ as the Euler-Mascheroni constant and

$$e^x = \sum_{n=0}^\infty \frac{x^n}{n!} = 1 + x + \frac{x^2}{2} + ..., \qquad \Gamma(z) = \frac{1}{z} - \gamma + \frac{1}{2}\left(\gamma^2 + \frac{\pi^2}{6}\right) z + ...,$$

$$\begin{aligned}
(4\pi)^{-d/2} &= (4\pi)^{-2}(4\pi)^{\epsilon/2} = (4\pi)^{-2}\, e^{\epsilon/2\,\ln(4\pi)} = \frac{1}{(4\pi)^2}\left(1 + \frac{\epsilon}{2}\ln(4\pi) + O(\epsilon^2)\right), \\
\Delta^{d/2-n} &= \Delta^{2-n}\Delta^{-\epsilon/2} = \Delta^{2-n}\, e^{-\epsilon/2\ln(\Delta)} = \Delta^{2-n}\left(1 - \frac{\epsilon}{2}\ln\Delta + O(\epsilon^2)\right), \\
\Gamma(2-d/2) &= \Gamma(\epsilon/2) = \frac{\Gamma(\epsilon/2)}{(\epsilon/2-1)} = \frac{2}{\epsilon} - \gamma + O(\epsilon), \\
\Gamma(1-d/2) &= \Gamma(\epsilon/2-1) = -\frac{2}{\epsilon} + (\gamma-1) + O(\epsilon), \\
\Gamma(3-d/2) &= \Gamma(\epsilon/2+1) = \frac{\epsilon}{2}\Gamma(\epsilon/2) = 1 - \gamma\frac{\epsilon}{2} + O(\epsilon^2), \\
\Gamma(n+2-d/2) &= \Gamma(\epsilon/2+n) = \prod_{m=1}^{n}\left(\frac{\epsilon}{2} + m\right)\Gamma(\epsilon/2).
\end{aligned}$$

The formulas are then

$$
\begin{aligned}
\int \frac{d^d l}{(2\pi)^d}\,\frac{1}{[l^2+\Delta]^2} &= \frac{\Delta^{d/2-2}}{(4\pi)^{d/2}}\frac{\Gamma(2-d/2)}{\Gamma(2)} \\
&= \frac{1}{(4\pi)^2}\Big(1+\frac{\epsilon}{2}\ln(4\pi)\Big)\Big(1-\frac{\epsilon}{2}\ln\Delta\Big)\Big(\frac{2}{\epsilon}-\gamma\Big)+\mathcal{O}(\epsilon) \\
&= \frac{1}{(4\pi)^2}\left(\frac{2}{\epsilon}-\gamma+\ln\left(\frac{4\pi}{\Delta}\right)\right)+\mathcal{O}(\epsilon), \qquad \text{(C.4)}
\end{aligned}
$$

$$
\begin{aligned}
\int \frac{d^d l}{(2\pi)^d}\,\frac{1}{[l^2+\Delta]^3} &= \frac{\Delta^{d/2-3}}{(4\pi)^{d/2}}\frac{\Gamma(3-d/2)}{\Gamma(3)} \\
&= \frac{1}{2(4\pi)^2}\Big(1+\frac{\epsilon}{2}\ln(4\pi)\Big)\frac{1}{\Delta}\Big(1-\frac{\epsilon}{2}\ln\Delta\Big)\Big(1-\gamma\frac{\epsilon}{2}\Big)+\mathcal{O}(\epsilon) \\
&= \frac{1}{2\Delta(4\pi)^2}+\mathcal{O}(\epsilon), \qquad \text{(C.5)}
\end{aligned}
$$

$$
\begin{aligned}
\int \frac{d^d l}{(2\pi)^d}\,\frac{l^2}{[l^2+\Delta]^2} &= \frac{\Delta^{d/2-1}}{(4\pi)^{d/2}}\frac{d}{2}\frac{\Gamma(1-d/2)}{\Gamma(2)} \\
&= \frac{1}{2(4\pi)^2}\Big(1+\frac{\epsilon}{2}\ln(4\pi)\Big)\Delta\Big(1-\frac{\epsilon}{2}\ln\Delta\Big)(4-\epsilon)\Big(-\frac{2}{\epsilon}+(\gamma-1)\Big)+\mathcal{O}(\epsilon) \\
&= \frac{2\Delta}{(4\pi)^2}\left(-\frac{2}{\epsilon}+\gamma-\frac{1}{2}+\ln\left(\frac{\Delta}{4\pi}\right)\right)+\mathcal{O}(\epsilon), \qquad \text{(C.6)}
\end{aligned}
$$

$$
\begin{aligned}
\int \frac{d^d l}{(2\pi)^d}\,\frac{l^2}{[l^2+\Delta]^3} &= \frac{\Delta^{d/2-2}}{(4\pi)^{d/2}}\frac{d}{2}\frac{\Gamma(2-d/2)}{\Gamma(3)} \\
&= \frac{1}{4(4\pi)^2}\Big(1+\frac{\epsilon}{2}\ln(4\pi)\Big)\Big(1-\frac{\epsilon}{2}\ln\Delta\Big)(4-\epsilon)\Big(\frac{2}{\epsilon}-\gamma\Big)+\mathcal{O}(\epsilon) \\
&= \frac{1}{(4\pi)^2}\left(\frac{2}{\epsilon}-\gamma-\frac{1}{2}+\ln\left(\frac{4\pi}{\Delta}\right)\right)+\mathcal{O}(\epsilon). \qquad \text{(C.7)}
\end{aligned}
$$

This step is often followed by the results of the Passarino-Veltman functions defined in [148], where one deals with the remaining integrals over x, y, which is quite tricky.

- **Tricks**:

  There are some useful tricks for calculating the loop integrals, which shall be listed here briefly.

  - $\int_{-\infty}^{\infty} dl\, l = 0$.
  - On-shell condition (Dirac equation fulfilled):

    $\not{p}\,u(p) = m\,u(p)$ and $\bar{u}(p)\not{p} = m\,\bar{u}(p)$.
  - Relations for γ-matrices:

    $g^{\mu\nu}g_{\mu\nu} = d, \quad \{\gamma^\mu,\gamma^\nu\} = 2g^{\mu\nu}, \quad \not{p}\gamma^\mu = 2p^\mu - \gamma^\mu\not{p}.$

C.2. Renormalization

In renormalizable QFT, the UV-divergences that originate from loop integrals (and can be regularized) are interpreted as the result of an underlying, local, effective approximative theory. This means that they originate from a too naive choice of couplings and parameters that encode the high-energy information in the formulation of the effective Lagrangian [146]. Renormalization is thus a tool to rescale these bare couplings and parameters in such a way that the UV-divergences are absorbed into them, more specifically, into their renormalization constants in the counterterms, and one is left with finite renormalized couplings and parameters and finite radiative corrections. A theory is renormalizable if the mass dimension of all operators O_i is $[O_i] \lesssim 4$ and of all couplings g_i $[g_i] \gtrsim 0$, $\forall i$.

In the following, the QED Lagrangian is renormalized as an example.

$$\mathcal{L}_{QED} = \overline{\psi}_0 \left[(i\partial_\mu + e_0 A^0_\mu)\gamma^\mu - m_0 \right] \psi_0 - \frac{1}{4} F^{(0)}_{\mu\nu} F^{\mu\nu(0)} - \frac{1}{2\xi_0} (\partial_\mu A^\mu_0)(\partial_\nu A^\nu_0) \tag{C.8}$$

C.2.1. Renormalization steps

- The first step towards renormalization is a dimensional analysis of couplings and parameters;

$$\left[\int d^d x \mathcal{L} \right] = 0, \quad [\mathcal{L}] = d, \quad [m_0] = [\partial] = 1, \quad [\psi_0] = \frac{1}{2}(d-1) = \frac{3}{2} - \epsilon,$$
$$\left[A^0_\mu \right] = \frac{1}{2}(d-2) = 1 - \epsilon, \quad [e_0] = \epsilon, \quad [\xi] = 1.$$

- Then, the couplings and parameters are redefined.

  Within renormalization, the infinite bare charge e_0, the bare mass m_0 and the bare gauge parameter ξ_0, as well as the bare fermion ψ_0 and gauge boson A^0_μ fields, are redefined to finite, renormalized parameters e, m,ξ, ψ, and A^μ, and renormalization constants Z_i,

$$\psi_0 = Z^{1/2}_\psi \psi, \quad A^0_\mu = Z^{1/2}_A A_\mu, \quad m_0 = Z_m m, \quad e_0 = \tilde{\mu}^\epsilon Z_e e, \quad \xi_0 = Z_\xi \xi.$$

- The renormalization constants are perturbatively expanded to the applied loop order,

$$Z_i = 1 + \delta Z^1_i + \delta Z^2_i \cdots + \delta Z^k_i, \qquad i \in \{\psi, A, m, e, \xi\}, \tag{C.9}$$

  where k is the specific loop order, so $\delta Z^k_i \sim \mathcal{O}(\alpha^k) \sim 1/\epsilon^m$.

- The Lagrangian is redefined into a renormalized part and a counterterm part

$$
\begin{aligned}
\mathcal{L}_{QED} =& Z_\psi \overline{\psi} \Big[(i\partial_\mu + \underbrace{Z_e Z_A^{1/2}}_{1} eA_\mu)\gamma^\mu - Z_m m \Big] \psi - \frac{1}{4} Z_A F_{\mu\nu} F^{\mu\nu} - \frac{Z_A}{2\, Z_\xi \xi} (\partial_\mu A^\mu)(\partial_\nu A^\nu) \\
=& \overline{\psi} \Big[(i\partial_\mu + eA_\mu)\gamma^\mu - m \Big] \psi - \frac{1}{4} F_{\mu\nu} F^\mu - \frac{1}{2\xi} (\partial_\mu A^\mu)(\partial_\nu A^\nu) \\
& + \delta Z_\psi \overline{\psi} \Big[\underbrace{(\delta Z_e + 1/2 \delta Z_A)}_{0} eA_\mu \gamma^\mu - \delta Z_m m \Big] \psi - \frac{1}{4} \delta Z_A F_{\mu\nu} F^{\mu\nu} \\
& - (\delta Z_A - \delta Z_\xi) \frac{1}{2\xi} (\partial_\mu A^\mu)(\partial_\nu A^\nu), \qquad \text{(C.10)} \\
=& \overline{\psi} \Big[(i\partial_\mu + eA_\mu)\gamma^\mu - m \Big] \psi - \frac{1}{4} F_{\mu\nu} F^\mu - \frac{1}{2\xi} (\partial_\mu A^\mu)(\partial_\nu A^\nu) + \mathcal{L}_{couterterms} \qquad \text{(C.11)}
\end{aligned}
$$

with $Z_e Z_A^{1/2} = 1 \;\Rightarrow\; \delta Z_e + 1/2 \delta Z_A = 0$, when QED gauge invariance is expected.

- New Feynman rules for the counterterms are derived.

- A renormalization scheme must be chosen to define the method for determining the renormalization constants Z_i.

  The renormalization constants Z_i^k are determined in the way that the $1/\epsilon$ singularities of one-particle irreducible Feynman diagrams are absorbed; these can be of k-order in perturbation theory. Nevertheless, some freedom remains for adding additional finite terms to the Z_i. In a renormalization scheme, one chooses a certain way of determining the renormalization constants. There are two frequently used schemes: the on-shell scheme and the minimal subtraction $\overline{MS}$ scheme; see the next subsection for more information.

- The renormalization constants Z_i are determined from one-particle irreducible diagrams (1PI) within the particular scheme.

  All 1PI diagrams should be finite, moreover, the results for physical values such as masses or cross-sections or decay rates shall be independent of the renormalization scheme, e.g.

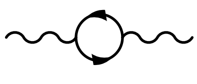 $+$  $=$ finite, (C.12)

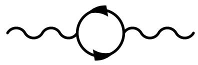

$$= -i\left(g^{\mu\nu} - \frac{p^\mu p^\nu}{p^2}\right)\underbrace{p^2 \frac{4}{3}\frac{e^2}{16\pi^2}\left(\frac{1}{\epsilon} + \ln(\mu^2) + \dots\right)}_{\Sigma_T^A(p^2)}, \tag{C.13}$$

$$= -i\left(p^2 g^{\mu\nu} - p^\mu p^\nu\right)\delta Z_A. \tag{C.14}$$

In the $\overline{MS}$ scheme $\delta Z_A^{\overline{MS}} = -\frac{4}{3\epsilon}\frac{e^2}{16\pi} = -\frac{\alpha}{3\pi\epsilon}$ and in the on-shell scheme $\delta Z_A^{on-shell} = -\frac{\partial}{\partial p^2}\Sigma_T^A(p^2)\Big|_{p^2=0} = -2\delta Z_e$, with $\delta Z_e\Big|_{p^2=0} = 0$ [146].

C.2.2. Renormalization schemes

There are two commonly used schemes: the on-shell scheme and the minimal subtraction $\overline{MS}$ scheme.

The basic idea of the **on-shell scheme** is that the renormalized masses, m, and charges, e, remain physical under the on-shell condition, which is $p^2 \to m^2$. Therefore, in this scheme couplings, masses and fields are not dependent on the renormalization scale μ, while the renormalization constants, $Z_i(\mu)^{on-shell}$, are. The condition for on-shell renormalization states that all corrections to propagators, e.g. the loop in Equation (C.12), disappear with any loop-order in the on-shell limit, so $Z_m^{on-shell} = 1$. Thus, the on-shell mass of e.g. the electron, m_e, is the rest mass of the particle, called the pole mass, $m_e^{pole} = Z_e^{-1} m_e^0 = m_0$. Furthermore, the on-shell scheme requires that all corrections to the charges disappear in the Thomson limit, thus $Z_e(q^2 = 0) = 1$. The Thomson limit is the low-energy limit of Compton scattering ($e^-\gamma \to e^-\gamma$) where $q^2 = 0$ is the momentum of the photon. The cross-section of Compton scattering is then given to all orders in perturbation theory by the Thomson formula, which ensures that the renormalized charge, e, corresponds to the physical charge, e_0, and is equivalent to the electric charge involved in the interaction between an electron and an electric field in classical electrodynamics, i.e. $\alpha^{on-shell} = \alpha_{em} = e^2/(4\pi) \simeq 1/137.036$ is the fine structure constant. This scheme is widely used in calculations of QED corrections to collider physics observables.

On the other hand, in QCD, the mass of a quark is unphysical due to confinement, so the physical on-shell mass interpretation makes no sense here. For the same reason, in QCD, one also often struggles with large logarithms in the loop corrections. Therefore, both problems in QCD can be better treated in the **minimal subtraction scheme** or also called $\overline{MS}$ **scheme**. The renormalization conditions in the $\overline{MS}$ scheme state that the counterterms only contain the part with the $1/\epsilon_{UV}^n$ singularities. The consequence is that the renormalization constants, Z_i, in contrast to the on-shell scheme, are not directly μ-dependent, $\delta Z^k \sim (\alpha/\pi)^k 1/\epsilon^n$, whereas the renormalized parameters in general are, e.g. $e(\mu)$, $m(\mu)$. Thus, masses and couplings do have no direct physical meaning. The advantage is that this scheme is better suited to deal with large logarithms.

C.2.3. Comment on the renormalization group equation

As already mentioned, in the $\overline{MS}$ scheme, the renormalized parameters are scale-dependent and are therefore "running" with the chosen energy-scale μ, e.g. $e_0 = Z_e^{\overline{MS}} e(\mu)$, $m_0 = Z_m^{\overline{MS}} m(\mu)$. For deriving a general formula for this "running" process of the renormalized parameters in loop precision, e.g. as shown in Figure C.1, the renormalization group equations (RGE) are used. RGEs obtained from one-loop renormalization constants are called RGEs in the "leading-logarithmic (LL) approximation" [146]. For example, for the QED coupling α, one calculates at one-loop,

$$\frac{d}{d\ln\mu^2}\alpha_0 = 0 = \frac{d}{d\ln\mu^2}\left(\tilde{\mu}^{2\epsilon} Z_e^2 \alpha\right) = \frac{d}{d\ln\mu^2}\left[\tilde{\mu}^{2\epsilon}\left(1 + \frac{\alpha}{3\pi\epsilon^2} + \dots\right)\alpha\right],$$

with the beta function β_α, one gets

$$\Leftrightarrow \quad \left.\frac{d\alpha}{d\ln\mu^2}\right|_{\epsilon=0} = \frac{\alpha^2}{4\pi}\cdot\frac{4}{3} \stackrel{!}{=} \frac{\alpha^2}{4\pi}\beta_\alpha^{\epsilon=0} \quad \Leftrightarrow \quad \alpha(\mu) = \frac{\alpha(\mu_0)}{1 + \frac{\alpha(\mu_0)}{4\pi}\beta_\alpha \ln\frac{\mu^2}{\mu_0^2}}. \tag{C.15}$$

D. Feynman Diagrams in the Rξ Gauge

The Feynman rules for the leptons, scalars, and gauge bosons are derived from the Lagrangians of the Equations (2.37), (2.38), (3.19), (3.20), (3.12), (3.15), and[1] $\mathcal{L}_{ghost}$ from Equation (D.1).

Therefore, the total Lagrange density of our model is composed of[2]

$$\mathcal{L} = \mathcal{L}_{cc}(W^{\pm}) + \mathcal{L}_{nc}(Z, A) + \mathcal{L}_{Y}(S^{\pm}) + \mathcal{L}_{Y}(S^{0}) + \mathcal{L}_{higgs} + \mathcal{L}_{gauge-fix} + \mathcal{L}_{ghost}. \tag{D.2}$$

From this, one can read out the Feynman diagrams, which were calculated according to the conventions in [3]. A special case in the derivation is the case of the Majorana particles, which receive an additional factor two in e.g. Equations (D.5), (D.10), and (D.11). This results from the contraction possibilities in any calculation since in the case of Majorana particles, not only particle and antiparticle contract, but also particles with particles and antiparticles with antiparticles.

In the following, the Higgs particle is designated $S_1^0 = H$, while the Goldstone bosons are designated $S_1^0 = G^0$, $S_1^{\pm} = G^{\pm}$. The Yukawa coupling of H and G^0 to leptons can be rewritten with Equations (3.18) and (3.14) into[3] $\hat{\Delta}_1 = \sum_k V_{1k}\Delta_k = i\sqrt{2}M_D/v = \frac{ig}{\sqrt{2}m_W}M_D$, according to [3]. Furthermore, with Equation (2.27c), $U_L M_D U_R^{\dagger} = m_j$ ($j \in \{1, 2, \ldots 6\}$) where m_j are the eigenmasses of the neutrinos. Ghosts are not listed here because they come from gauge fixing terms and therefore only appear in vertices with scalars and gauge bosons but not together with fermions.

---

[1] Fadev-Popov ghosts arise from the gauge-fixing procedure of the non-Abelian $SU(2) \times U(1)$ groups. The term for the Fadev-Popov ghosts of the broken symmetry reads

$$\mathcal{L}_{ghost} = \bar{c}^a \left[-(\partial_\mu D^\mu)^{ab} - \xi_A g^2 \left(T^a v\right) T^b \left(v + G_A\right) \right] c^b. \tag{D.1}$$

Ghosts get their interaction terms with both the gauge bosons and scalars, for a detailed description, see [43].

[2] For a more detailed set of Lagrangians of the multi-Higgs-doublet model part be refereed to [53].

[3] Here, the convention is $V_{1k} = \frac{i}{v} v_k$, where $v = \sqrt{\sum_k v_k}$ and with Equation (3.14), $v = \frac{2}{g} m_W$ and further with Equation (3.18), $M_D = \frac{1}{\sqrt{2}} \sum_k v_k \Delta_k$.

<u>The SM gauge boson vertices are</u>:

llA :

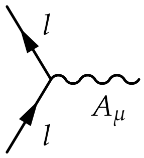

$$= ieQ_f\gamma^\mu = -ie\gamma^\mu, \tag{D.3}$$

llZ :

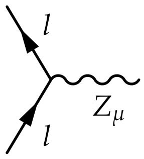

$$= i\frac{g}{c_W}\gamma^\mu\left(I_3\gamma_L - Q_f s_W^2\right) = \quad i\frac{g}{c_W}\gamma^\mu\left(s_W^2\frac{1}{2}\gamma_L\right), \tag{D.4}$$

$\chi\chi Z$:

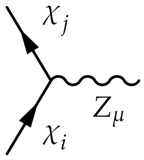

$$= i\frac{g}{2\,c_W}\gamma^\mu\left[\gamma_L(U_L^\dagger U_L)_{ij} - \gamma_R(U_L^T U_L^*)_{ij}\right], \tag{D.5}$$

udW^+ :

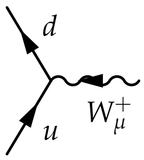

$$= i\frac{g}{\sqrt{2}}\gamma^\mu\gamma_L V_{du}, \tag{D.6}$$

duW^- :

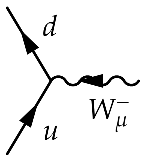

$$= i\frac{g}{\sqrt{2}}\gamma^\mu\gamma_L V_{du}^\dagger, \tag{D.7}$$

$l\chi W^+$:

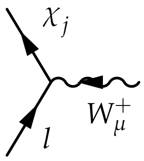

$$= i\frac{g}{\sqrt{2}}\gamma^\mu\gamma_L(U_L^\dagger)_{jl}, \tag{D.8}$$

$\chi l W^-$:

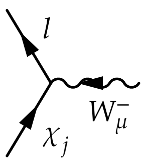

$$= i\frac{g}{\sqrt{2}}\gamma^\mu\gamma_L(U_L)_{jl}. \tag{D.9}$$

<u>The scalar vertices are</u>:

$\chi\chi S_b^0$:

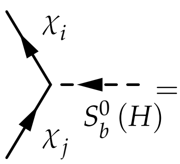

$$= -i\sqrt{2}\left(\underbrace{\frac{1}{2}\left[U_R^\dagger\Delta_b U_L + U_L^T\Delta_b^T U_R^*\right]_{ij}}_{F_b}\gamma_L + (F_b)_{ij}^\dagger\gamma_R\right) \quad ,\chi\chi H:\ -\frac{igm_j}{2m_W}, \tag{D.10}$$

$\chi\chi G^0$:

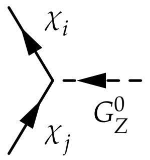

$$= -i\sqrt{2}\Big((F_{b_Z})_{ij}\gamma_L + (F_{b_Z})^\dagger_{ij}\,\gamma_R\Big)$$

$$= \frac{g}{m_W}\Bigg(\underbrace{\frac{1}{2}\Big[U_R^\dagger M_D U_L + U_L^T M_D^T U_R^*\Big]_{ij}}_{\tilde{F}_{b_Z}}\gamma_L + (\tilde{F}_{b_Z})^\dagger_{ij}\,\gamma_R\Bigg), \tag{D.11}$$

llS_b^0 :

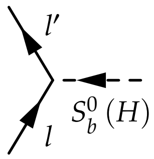

$$= -\frac{i}{\sqrt{2}}\Big((\Gamma_b)_{ll'}\,\gamma_L + (\Gamma_b^\dagger)_{ll'}\,\gamma_R\Big) \qquad ,llH:\; -\frac{igm_l}{2m_W}, \tag{D.12}$$

llG^0 :

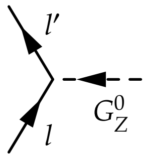

$$= -\frac{i}{\sqrt{2}}\Big((\Gamma_1)_{ll'}\,\gamma_L + (\Gamma_1^\dagger)_{ll'}\,\gamma_R\Big) \;=\; -\frac{i\,g}{2m_W}\Big((M_l)_{ll'}\,\gamma_L + (M_l^\dagger)_{ll'}\,\gamma_R\Big), \tag{D.13}$$

$l\chi S_a^-$:

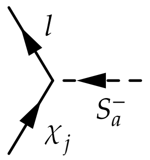

$$= i\Big[(\underbrace{\Delta_a^\dagger U_R}_{R_a})_{lj}\,\gamma_R - (\underbrace{\Gamma_a U_L}_{L_a})_{lj}\,\gamma_L\Big], \tag{D.14}$$

$l\chi G^-$:

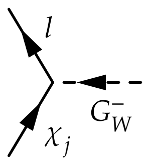

$$= i\Big[(R_{a_W})_{lj}\,\gamma_R - (L_{a_W})_{lj}\,\gamma_L\Big] = \frac{ig}{\sqrt{2}\,m_W}\underbrace{\Big((M_D^\dagger U_R)_{lj}\gamma_R - (M_l U_L)_{lj}\gamma_L\Big)}_{\left(m_j\gamma_R - m_l\gamma_L\right)U_{lj}}, \tag{D.15}$$

$\chi l S_a^+$:

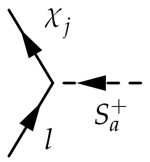

$$= i\Big[(R_a^\dagger)_{jl}\gamma_L - (L_a^\dagger)_{jl}\gamma_R\Big], \tag{D.16}$$

$\chi l G^+$:

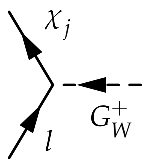

$$= i\Big[(R_{a_W}^\dagger)_{jl}\gamma_L - (L_{a_W}^\dagger)_{jl}\gamma_R\Big] = \frac{ig}{\sqrt{2}\,m_W}\underbrace{\Big((U_R^\dagger M_D)_{jl}\gamma_L - (U_L^\dagger M_l^\dagger)_{jl}\gamma_R\Big)}_{\left(m_l\gamma_L - m_j\gamma_R\right)U^*_{jl}}. \tag{D.17}$$

<u>The propagators are</u>:

$$f : \underset{f}{\longrightarrow} \quad = \quad i\frac{\not{k} + m_f}{k^2 - m_f^2}, \tag{D.18}$$

$$A_\mu : \underset{\gamma}{\sim\!\sim\!\sim} \quad = \quad \frac{-ig_{\mu\nu}}{k^2} + (1 - \xi_A)\frac{ik_\mu k_\nu}{k^4}, \tag{D.19}$$

$$Z_\mu : \underset{Z_\mu}{\sim\!\sim\!\sim} \quad = \quad \frac{-ig_{\mu\nu}}{k^2 - m_Z^2} + \frac{ik_\mu k_\nu}{m_Z^2}\left(\frac{1}{k^2 - m_Z^2} - \frac{1}{k^2 - \xi_Z m_Z^2}\right), \tag{D.20}$$

$$W_\mu^\pm : \underset{W^\pm}{\sim\!\sim\!\blacktriangleright\!\sim\!\sim} \quad = \quad \frac{-ig_{\mu\nu}}{k^2 - m_W^2} + \frac{ik_\mu k_\nu}{m_W^2}\left(\frac{1}{k^2 - m_W^2} - \frac{1}{k^2 - \xi_W m_W^2}\right), \tag{D.21}$$

$$S_a^\pm : \underset{S_a^\pm}{- - - \blacktriangleright - - -} \quad = \quad \frac{i}{k^2 - m_a^2}, \tag{D.22}$$

$$G^\pm : \underset{G^\pm}{- - - \blacktriangleright - - -} \quad = \quad \frac{i}{k^2 - \xi_W m_W^2}, \tag{D.23}$$

$$S_b^0 : \underset{S_b^0}{- - - \blacktriangleright - - -} \quad = \quad \frac{i}{k^2 - m_b^2}, \tag{D.24}$$

$$G^0 : \underset{G^0}{- - - \blacktriangleright - - -} \quad = \quad \frac{i}{k^2 - \xi_Z m_Z^2}. \tag{D.25}$$

Selected couplings between bosons:

$S^-S^+A_\mu$:

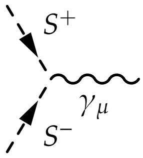

$$= ie(p_- - p_+)_\mu, \tag{D.26}$$

$S^-S^+Z_\mu$:

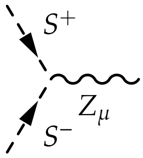

$$= i(p_- - p_+)_\mu \, \frac{g(s_W^2 - c_W^2)}{2c_W}, \tag{D.27}$$

$S^\pm S^0 W_\mu^\mp$:

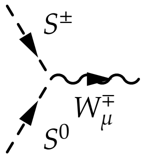

$$= \mp i \, \frac{g}{2} \, (p_\pm - p_0)_\mu, \tag{D.28}$$

$G^\pm W_\mu^\pm A_\nu$:

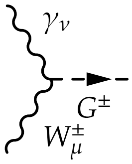

$$= -ie \, m_W \, g_{\mu\nu}. \tag{D.29}$$

Bibliography

[1] M. P. Bento, H. E. Haber, J. C. Romão and J. a. P. Silva, *Multi-Higgs doublet models: physical parametrization, sum rules and unitarity bounds*, *JHEP* **11** (2017) 095 [1708.09408].

[2] L. Susskind, *THE GAUGE HIERARCHY PROBLEM, TECHNICOLOR, SUPERSYMMETRY, AND ALL THAT.*, *Phys. Rept.* **104** (1984) 181.

[3] W. Grimus and L. Lavoura, *Soft lepton flavor violation in a multi Higgs doublet seesaw model*, *Phys. Rev.* **D66** (2002) 014016 [hep-ph/0204070].

[4] S. Davidson and A. Ibarra, *A Lower bound on the right-handed neutrino mass from leptogenesis*, *Phys. Lett.* **B535** (2002) 25 [hep-ph/0202239].

[5] I. Maksymyk, C. P. Burgess and D. London, *Beyond S, T and U*, *Phys. Rev.* **D50** (1994) 529 [hep-ph/9306267].

[6] G. C. Branco, P. M. Ferreira, L. Lavoura, M. N. Rebelo, M. Sher and J. P. Silva, *Theory and phenomenology of two-Higgs-doublet models*, *Phys. Rept.* **516** (2012) 1 [1106.0034].

[7] M. Drewes, *The Phenomenology of Right Handed Neutrinos*, *Int. J. Mod. Phys.* **E22** (2013) 1330019 [1303.6912].

[8] S. Verma, *Theoretical and Phenomenological Status of Neutrino Physics: A Brief Review*, *Adv. High Energy Phys.* **2015** (2015) 385968.

[9] Particle Data Group collaboration, M. T. et al., *Review of Particle Physics (RPP)*, *Phys. Rev.* **D98** (2018) 030001.

[10] E. H. Aeikens, W. Grimus and L. Lavoura, *Charged-lepton decays from soft flavour violation*, *Phys. Lett.* **B768** (2017) 365 [1612.00724].

[11] G. Aldazabal, L. E. Ibanez, F. Quevedo and A. M. Uranga, *D-branes at singularities: A Bottom up approach to the string embedding of the standard model*, *JHEP* **08** (2000) 002 [hep-th/0005067].

[12] J. D. Lykken, *Beyond the Standard Model*, in *CERN Yellow Report CERN-2010-002, 101-109*, 2010, 1005.1676, http://lss.fnal.gov/cgi-bin/find_paper.pl?conf-10-103.

[13] J. Smirnov, *Effects of the Quantum Vacuum in Particle Physics and Cosmology* , dissertation, Universität Heidelberg, 2014. 10.11588/heidok.00017769.

[14] Nobel Media AB, "The 2015 Nobel Prize in Physics - Press release. NobelPrize.org. Nobel Media AB 2018.." https://www.nobelprize.org/prizes/physics/2015/press-release/.

[15] Liverpool Telescope, MAGIC, H.E.S.S., AGILE, Kiso, VLA/17B-403, INTEGRAL, Kapteyn, Subaru, HAWC, Fermi-LAT, ASAS-SN, VERITAS, Kanata, IceCube, Swift NuSTAR collaboration, M. G. Aartsen et al., *Multimessenger observations of a flaring blazar coincident with high-energy neutrino IceCube-170922A*, *Science* **361** (2018) eaat1378 [1807.08816].

[16] C. L. Cowan, F. Reines, F. B. Harrison, H. W. Kruse and A. D. McGuire, *Detection of the free neutrino: A Confirmation*, *Science* **124** (1956) 103.

[17] C. Giunti and C. W. Kim, *Fundamentals of Neutrino Physics and Astrophysics*. 2007.

[18] M. C. Gonzalez-Garcia, M. Maltoni and T. Schwetz, *Global Analyses of Neutrino Oscillation Experiments*, *Nucl. Phys.* **B908** (2016) 199 [1512.06856].

[19] KATRIN collaboration, M. Aker et al., *An improved upper limit on the neutrino mass from a direct kinematic method by KATRIN*, 1909.06048.

[20] K. S. Babu and R. N. Mohapatra, *Quantization of Electric Charge From Anomaly Constraints and a Majorana Neutrino*, *Phys. Rev.* **D41** (1990) 271.

[21] R. Foot, H. Lew and R. R. Volkas, *Electric charge quantization*, *J. Phys.* **G19** (1993) 361 [hep-ph/9209259].

[22] JUNO working group Prof. Dr. Michael Wurm, "mass-hierarchy." http://www.staff.uni-mainz.de/wurmm/juno.html, 2018.

[23] M. D. Schwartz, *Quantum Field Theory and the Standard Model*. Cambridge University Press, 2014.

[24] G. Altarelli, R. Barbieri and S. Jadach, *Toward a model independent analysis of electroweak data*, *Nucl. Phys.* **B369** (1992) 3.

[25] M. Fukugita and T. Yanagida, *Physics of neutrinos and applications to astrophysics*. 2003.

[26] M. E. Peskin and D. V. Schroeder, *An Introduction to quantum field theory*. Addison-Wesley, Reading, USA, 1995.

[27] R. A. Horn and C. R. Johnson, *Matrix Analysis*. Cambridge University Press, 1985.

[28] W. Grimus and L. Lavoura, *The Seesaw mechanism at arbitrary order: Disentangling the small scale from the large scale*, *JHEP* **11** (2000) 042 [hep-ph/0008179].

[29] S. Stone, *New physics from flavour*, *PoS* **ICHEP2012** (2013) 033 [1212.6374].

[30] A. Ibarra, E. Molinaro and S. Petcov, *TeV Scale See-Saw Mechanisms of Neutrino Mass Generation, the Majorana Nature of the Heavy Singlet Neutrinos and $(\beta\beta)_{0\nu}$-Decay*, JHEP **09** (2010) 108 [1007.2378].

[31] E. Akhmedov, A. Kartavtsev, M. Lindner, L. Michaels and J. Smirnov, *Improving Electro-Weak Fits with TeV-scale Sterile Neutrinos*, JHEP **05** (2013) 081 [1302.1872].

[32] W. Grimus, *Lecture notes: Neutrinophysik*, 2016.

[33] W. Grimus, *Neutrino Physics - Models for Neutrino Masses and Lepton Mixing*, PoS **P2GC** (2006) 001 [hep-ph/0612311].

[34] A. Ibarra, *Neutrino Mass Models*, Acta Phys. Polon. Supp. **9** (2016) 741.

[35] S. F. King and C. Luhn, *Neutrino Mass and Mixing with Discrete Symmetry*, Rept. Prog. Phys. **76** (2013) 056201 [1301.1340].

[36] M. Volpp, *Running of radiative neutrino masses - A Study of the Zee-Babu Model*, Master's thesis, Ludwig–Maximilians–Universität München, Germany, 2017.

[37] E. Ma, *Verifiable radiative seesaw mechanism of neutrino mass and dark matter*, Phys. Rev. D **73** (2006) 077301 [hep-ph/0601225].

[38] J. W. F. Valle and J. C. Romao, *Neutrinos in high energy and astroparticle physics*, Physics textbook. Wiley-VCH, Weinheim, 2015.

[39] D. Aristizabal, *Radiative Origin of Majorana Neutrino Masses*, PoS **EPS-HEP2015** (2015) 074.

[40] ATLAS collaboration, G. Aad et al., *Observation of a new particle in the search for the Standard Model Higgs boson with the ATLAS detector at the LHC*, Phys. Lett. **B716** (2012) 1 [1207.7214].

[41] CMS collaboration, S. Chatrchyan et al., *Observation of a new boson at a mass of 125 GeV with the CMS experiment at the LHC*, Phys. Lett. **B716** (2012) 30 [1207.7235].

[42] A. Belyaev, G. Cacciapaglia, I. P. Ivanov, F. Rojas-Abatte and M. Thomas, *Anatomy of the Inert Two Higgs Doublet Model in the light of the LHC and non-LHC Dark Matter Searches*, Phys. Rev. **D97** (2018) 035011 [1612.00511].

[43] G. Branco, L. Lavoura and J. Silva, *CP Violation*, International Series of Monogr. Clarendon Press, 1999.

[44] I. P. Ivanov, *Building and testing models with extended Higgs sectors*, Prog. Part. Nucl. Phys. **95** (2017) 160 [1702.03776].

[45] A. Ibarra and C. Simonetto, *Understanding neutrino properties from decoupling right-handed neutrinos and extra Higgs doublets*, JHEP **11** (2011) 022 [1107.2386].

[46] A. Ibarra and A. Solaguren-Beascoa, *Radiative Generation of Quark Masses and Mixing Angles in the Two Higgs Doublet Model*, Phys. Lett. B **736** (2014) 16 [1403.2382].

[47] A. Ibarra and A. Solaguren-Beascoa, *Standard Model fermion masses and mixing angles generated in 3HDM*, J. Phys. Conf. Ser. **718** (2016) 062055.

[48] L. Lopez Honorez, E. Nezri, J. F. Oliver and M. H. G. Tytgat, *The Inert Doublet Model: An Archetype for Dark Matter*, JCAP **0702** (2007) 028 [hep-ph/0612275].

[49] S. L. Glashow and S. Weinberg, *Natural Conservation Laws for Neutral Currents*, Phys. Rev. **D15** (1977) 1958.

[50] G. Bhattacharyya and D. Das, *Scalar sector of two-Higgs-doublet models: A minireview*, Pramana **87** (2016) 40 [1507.06424].

[51] P. D. M. M. Mühlleitner, *Lecture notes:Beyond the Standard Model Physics*, 2015.

[52] A. Celis, *LHC phenomenology of two-Higgs-doublet models in the LHC era*, Ph.D. thesis, Valencia U., 2014.

[53] W. Grimus, L. Lavoura, O. M. Ogreid and P. Osland, *A Precision constraint on multi-Higgs-doublet models*, J. Phys. **G35** (2008) 075001 [0711.4022].

[54] "higgs-potential-goldstone-mode-higgs-mode." https://francisthemulenews.files.wordpress.com/2013/07/dibujo20130704-higgs-potential-goldstone-mode-higgs-mode.jpg?w=824.

[55] K. Schmidt-Hoberg, *Lecture notes: Phenomenology of Physics beyond the Standard Model*, 2015.

[56] Y. Shapira, "Lecture notes: THE STANDARD MODEL."

[57] D. Aristizabal Sierra and I. de Medeiros Varzielas, *The role of lepton flavor symmetries in leptogenesis*, Fortsch. Phys. **61** (2013) 645 [1205.6134].

[58] W. Grimus and L. Lavoura, *Softly broken lepton numbers and maximal neutrino mixing*, JHEP **07** (2001) 045 [hep-ph/0105212].

[59] L. Megrelidze and Z. Tavartkiladze, *Soft See-Saw: Radiative Origin of Neutrino Masses in SUSY Theories*, Nucl. Phys. B **914** (2017) 553 [1609.07344].

[60] S. Iguro, Y. Muramatsu, Y. Omura and Y. Shigekami, *Flavor physics in the multi-Higgs doublet models induced by the left-right symmetry*, JHEP **11** (2018) 046 [1804.07478].

[61] V. S. Mummidi, V. P. K. and K. M. Patel, *Effects of heavy neutrinos on vacuum stability in two-Higgs-doublet model with GUT scale supersymmetry*, JHEP **08** (2018) 134 [1805.08005].

[62] D. Cogollo, R. D. Matheus, T. B. de Melo and F. S. Queiroz, *Type I + II Seesaw in a Two Higgs Doublet Model*, *Phys. Lett. B* **797** (2019) 134813 [1904.07883].

[63] D. A. Camargo, M. D. Campos, T. B. de Melo and F. S. Queiroz, *A Two Higgs Doublet Model for Dark Matter and Neutrino Masses*, *Phys. Lett. B* **795** (2019) 319 [1901.05476].

[64] A. Ordell, R. Pasechnik and H. Serôdio, *Anomaly-free 2HDMs with a gauged abelian symmetry and two generations of right-handed neutrinos*, 2006.08676.

[65] D. A. Camargo, A. G. Dias, T. B. de Melo and F. S. Queiroz, *Neutrino Masses in a Two Higgs Doublet Model with a U(1) Gauge Symmetry*, *JHEP* **04** (2019) 129 [1811.05488].

[66] K. Cheung, H. Okada and Y. Orikasa, *Neutrinophilic two Higgs doublet model with* $U(1)$ *global symmetry*, 1706.02084.

[67] T. Nomura and H. Okada, *Loop suppressed light fermion masses with* $U(1)_R$ *gauge symmetry*, *Phys. Rev. D* **96** (2017) 015016 [1704.03382].

[68] J. Herrero-Garcia, N. Rius and A. Santamaria, *Higgs lepton flavour violation: UV completions and connection to neutrino masses*, *JHEP* **11** (2016) 084 [1605.06091].

[69] M. Luo and Q. Liu, *Small Neutrino Masses From Structural cancellation In Left-Right Symmetric Model*, *JHEP* **12** (2008) 061 [0812.3453].

[70] D. Borah and A. Dasgupta, *Left–right symmetric models with a mixture of keV–TeV dark matter*, *J. Phys. G* **46** (2019) 105004 [1710.06170].

[71] W. Rodejohann and U. Saldaña-Salazar, *Multi-Higgs-Doublet Models and Singular Alignment*, *JHEP* **07** (2019) 036 [1903.00983].

[72] E. Barradas-Guevara, O. Felix-Beltran, F. Gonzalez-Canales and M. Zeleny-Mora, *Lepton CP violation in a v2HDM with flavor*, *Phys. Rev. D* **97** (2018) 035003 [1704.03474].

[73] E. Barradas-Guevara, O. Félix-Beltrán, F. Gonzalez-Canales, E. Rodríguez-Jáuregui and M. Zeleny-Mora, *Analysis of the Lepton Mixing Matrix in the Two Higgs Doublet Model*, 1606.05388.

[74] M. D. Campos, D. Cogollo, M. Lindner, T. Melo, F. S. Queiroz and W. Rodejohann, *Neutrino Masses and Absence of Flavor Changing Interactions in the 2HDM from Gauge Principles*, *JHEP* **08** (2017) 092 [1705.05388].

[75] D. Atwood, S. Bar-Shalom and A. Soni, *Neutrino masses, mixing and leptogenesis in a two Higgs doublet model 'for the third generation'*, *Phys. Lett. B* **635** (2006) 112 [hep-ph/0502234].

[76] J. D. Clarke, R. Foot and R. R. Volkas, *Natural leptogenesis and neutrino masses with two Higgs doublets*, *Phys. Rev. D* **92** (2015) 033006 [1505.05744].

[77] M. Aoki, S. Kanemura and O. Seto, *Neutrino mass, Dark Matter and Baryon Asymmetry via TeV-Scale Physics without Fine-Tuning*, *Phys. Rev. Lett.* **102** (2009) 051805 [0807.0361].

[78] Z. Liu and P.-H. Gu, *Extending two Higgs doublet models for two-loop neutrino mass generation and one-loop neutrinoless double beta decay*, *Nucl. Phys. B* **915** (2017) 206 [1611.02094].

[79] M. E. Peskin and T. Takeuchi, *Estimation of oblique electroweak corrections*, *Phys. Rev.* **D46** (1992) 381.

[80] J. D. Wells, *TASI lecture notes: Introduction to precision electroweak analysis*, in *Physics in D >= 4. Proceedings, Theoretical Advanced Study Institute in elementary particle physics, TASI 2004, Boulder, USA, June 6-July 2, 2004*, pp. 41–64, 2005, hep-ph/0512342.

[81] J. L. Hewett, *The Standard model and why we believe it*, in *Supersymmetry, supergravity and supercolliders. Proceedings, Theoretical Advanced Study Institute in elementary particle physics, TASI'97, Boulder, USA, June 2-27, 1997*, pp. 3–83, 1997, hep-ph/9810316, http://www-public.slac.stanford.edu/sciDoc/docMeta.aspx?slacPubNumber=SLAC-PUB-7930.

[82] A. S. Kamat, *Phenomenology of the Non-sterile Electroweak-scale Right-handed Neutrino Model*, dissertation, University of Virginia, 2015.

[83] A. Kundu and P. Roy, *A General treatment of oblique parameters*, *Int. J. Mod. Phys.* **A12** (1997) 1511 [hep-ph/9603323].

[84] W. Grimus, L. Lavoura, O. M. Ogreid and P. Osland, *The Oblique parameters in multi-Higgs-doublet models*, *Nucl. Phys.* **B801** (2008) 81 [0802.4353].

[85] A. F. Castillo Ramirez, *Theoretical and phenomenological analyses from vacuum stability, perturbative unitarity, and oblique parameters in the Two Higgs Doublet Model*, Ph.D. thesis, Colombia, U. Natl., 2016.

[86] M. Lucente, *Implication of Sterile Fermions in Particle Physics and Cosmology*, Ph.D. thesis, Orsay, LPT, 2015-09-25. 1609.07081.

[87] M. Drewes, *Theoretical Status of Neutrino Physics*, *PoS* **NUFACT2014** (2015) 001 [1502.06891].

[88] W. Callister and D. Rethwisch, *Materials Science and Engineering: An Introduction, 8th Edition*. Wiley, 2009.

[89] D. J. Griffiths, *Introduction to electrodynamics; 4th ed.* Pearson, Boston, MA, 2013.

[90] M. Pospelov and A. Ritz, *Electric dipole moments as probes of new physics*, *Annals Phys.* **318** (2005) 119 [hep-ph/0504231].

[91] F. Jegerlehner, *The Anomalous Magnetic Moment of the Muon*, *Springer Tracts Mod. Phys.* **274** (2017) pp.1.

[92] P. Frampton, *Gauge Field Theories*, Frontiers in Physics. The Benjamin-Cummings, 1987.

[93] Particle Data Group collaboration, C. Patrignani et al., *Review of Particle Physics*, *Chin. Phys.* **C40** (2016) 100001.

[94] M. Procura, *Lecture notes: Theoretical methods in particle physics*, 2018.

[95] T. Blum, A. Denig, I. Logashenko, E. de Rafael, B. Lee Roberts, T. Teubner et al., *The Muon (g-2) Theory Value: Present and Future*, 1311.2198.

[96] M. Lindner, M. Platscher and F. S. Queiroz, *A Call for New Physics : The Muon Anomalous Magnetic Moment and Lepton Flavor Violation*, *Phys. Rept.* **731** (2018) 1 [1610.06587].

[97] M. Davier, A. Hoecker, B. Malaescu and Z. Zhang, *Reevaluation of the Hadronic Contributions to the Muon g-2 and to alpha(MZ)*, *Eur. Phys. J.* **C71** (2011) 1515 [1010.4180].

[98] K. Hagiwara, R. Liao, A. D. Martin, D. Nomura and T. Teubner, $(g-2)\_muandalpha(M\_Z^2)$ *re-evaluated using new precise data*, *J. Phys.* **G38** (2011) 085003 [1105.3149].

[99] P. J. Mohr, D. B. Newell and B. N. Taylor, *CODATA Recommended Values of the Fundamental Physical Constants: 2014*, *Rev. Mod. Phys.* **88** (2016) 035009 [1507.07956].

[100] D. Hanneke, S. Fogwell and G. Gabrielse, *New Measurement of the Electron Magnetic Moment and the Fine Structure Constant*, *Phys. Rev. Lett.* **100** (2008) 120801 [0801.1134].

[101] Muon g-2 collaboration, G. W. Bennett et al., *Final Report of the Muon E821 Anomalous Magnetic Moment Measurement at BNL*, *Phys. Rev.* **D73** (2006) 072003 [hep-ex/0602035].

[102] Muon g-2 collaboration, J. L. Holzbauer, *The Muon g-2 Experiment Overview and Status*, *PoS* **NuFact2017** (2018) 116 [1712.05980].

[103] R. Kitamura et al., *First Trial of the Muon Acceleration for J-Parc Muon g-2/edm Experiment*, in *Proceedings, 8th International Particle Accelerator Conference (IPAC 2017): Copenhagen, Denmark, May 14-19, 2017*, p. TUPVA097, 2017, DOI.

[104] Webpage of the (g-2) collaboration, "Life of a muon: The (g-2) experiment." https://www.g-2.bnl.gov/physics/g-2.jpg.

[105] D. Aristizabal Sierra and C. E. Yaguna, *On the importance of the 1-loop finite corrections to seesaw neutrino masses*, *JHEP* **08** (2011) 013 [1106.3587].

[106] D. Jurciukonis, T. Gajdosik and A. Juodagalvis, *Seesaw neutrino masses with a second Higgs doublet added*, 1507.03459.

[107] W. Grimus and L. Lavoura, *One-loop corrections to the seesaw mechanism in the multi-Higgs-doublet standard model*, *Phys. Lett.* **B546** (2002) 86 [hep-ph/0207229].

[108] W. Grimus and H. Neufeld, *Radiative Neutrino Masses in an SU(2) X U(1) Model*, *Nucl. Phys.* **B325** (1989) 18.

[109] W. Grimus and H. Neufeld, *Three neutrino mass spectrum from combining seesaw and radiative neutrino mass mechanisms*, *Phys. Lett.* **B486** (2000) 385 [hep-ph/9911465].

[110] W. Grimus and M. Löschner, *Renormalization of the multi-Higgs-doublet Standard Model and one-loop lepton mass corrections*, 1807.00725.

[111] B. Trappl, *One-loop corrections to the seesaw mechanism and models of neutrino masses and lepton mixing*, Master's thesis, Universität Wien, Austria, 2016.

[112] T. Appelquist and J. Carazzone, *Infrared Singularities and Massive Fields*, *Phys. Rev.* **D11** (1975) 2856.

[113] J. C. Collins, *Renormalization*, vol. 26 of *Cambridge Monographs on Mathematical Physics*. Cambridge University Press, Cambridge, 1986, 10.1017/CBO9780511622656.

[114] T. Toma and A. Vicente, *Lepton Flavor Violation in the Scotogenic Model*, *JHEP* **01** (2014) 160 [1312.2840].

[115] MEG collaboration, A. M. Baldini et al., *Search for the lepton flavour violating decay $\mu^+ \to e^+\gamma$ with the full dataset of the MEG experiment*, *Eur. Phys. J.* **C76** (2016) 434 [1605.05081].

[116] K. Hayasaka et al., *Search for Lepton Flavor Violating Tau Decays into Three Leptons with 719 Million Produced Tau+Tau- Pairs*, *Phys. Lett.* **B687** (2010) 139 [1001.3221].

[117] M. De Gerone, F. Gatti, W. Ootani, Y. Uchiyama, M. Nishimura, S. Shirabe et al., *Design and test of an extremely high resolution Timing Counterfor the MEG II experiment: preliminary results*, *JINST* **9** (2014) C02035 [1312.0871].

[118] A. M. Baldini et al., *MEG Upgrade Proposal*, 1301.7225.

[119] A. Blondel et al., *Research Proposal for an Experiment to Search for the Decay $\mu \to eee$*, 1301.6113.

[120] Paul Scherrer Institut (PSI), "Mu3e Experiment - Current news - Second Mu3e DAQ Week in Mainz." https://www.psi.ch/en/mu3e, 2019.

[121] L. Lavoura and W. Grimus, *Seesaw model with softly broken L(e) - L(muon) - L(tau)*, *JHEP* **09** (2000) 007 [hep-ph/0008020].

[122] W. Grimus and L. Lavoura, *Softly broken lepton numbers: An Approach to maximal neutrino mixing*, *Acta Phys. Polon.* **B32** (2001) 3719 [hep-ph/0110041].

[123] Super-Kamiokande collaboration, Y. Fukuda et al., *Evidence for oscillation of atmospheric neutrinos*, *Phys. Rev. Lett.* **81** (1998) 1562 [hep-ex/9807003].

[124] SNO collaboration, Q. R. Ahmad et al., *Measurement of the rate of $\nu_e + d \to p + p + e^-$ interactions produced by ^8B solar neutrinos at the Sudbury Neutrino Observatory*, *Phys. Rev. Lett.* **87** (2001) 071301 [nucl-ex/0106015].

[125] SNO collaboration, B. Aharmim et al., *Combined Analysis of all Three Phases of Solar Neutrino Data from the Sudbury Neutrino Observatory*, *Phys. Rev.* **C88** (2013) 025501 [1109.0763].

[126] S. M. Bilenky and B. Pontecorvo, *Lepton Mixing and Neutrino Oscillations*, *Phys. Rept.* **41** (1978) 225.

[127] S. M. Bilenky and S. T. Petcov, *Massive Neutrinos and Neutrino Oscillations*, *Rev. Mod. Phys.* **59** (1987) 671.

[128] S. M. Bilenky, C. Giunti and W. Grimus, *Phenomenology of neutrino oscillations*, *Prog. Part. Nucl. Phys.* **43** (1999) 1 [hep-ph/9812360].

[129] W. Grimus and L. Lavoura, *Quark mixing from softly broken symmetries*, *JHEP* **05** (2004) 016 [hep-ph/0312330].

[130] G. Senjanovic, *Neutrino mass: From LHC to grand unification*, *Riv. Nuovo Cim.* **34** (2011) 1.

[131] Tobias Koettig, TU Dortmund, "Neutrinoless Double Beta Decay." http://www.cobra-experiment.org/double_beta_decay/.

[132] J. D. Vergados, H. Ejiri and F. Simkovic, *Theory of Neutrinoless Double Beta Decay*, *Rept. Prog. Phys.* **75** (2012) 106301 [1205.0649].

[133] M. Blennow, E. Fernandez-Martinez, J. Lopez-Pavon and J. Menendez, *Neutrinoless double beta decay in seesaw models*, *JHEP* **07** (2010) 096 [1005.3240].

[134] S. Dell'Oro, S. Marcocci, M. Viel and F. Vissani, *Neutrinoless double beta decay: 2015 review*, *Adv. High Energy Phys.* **2016** (2016) 2162659 [1601.07512].

[135] S. Davidson, E. Nardi and Y. Nir, *Leptogenesis*, Phys. Rept. **466** (2008) 105 [0802.2962].

[136] Y. Tang, *Vacuum Stability in the Standard Model*, Mod. Phys. Lett. **A28** (2013) 1330002 [1301.5812].

[137] W. Rodejohann and H. Zhang, *Impact of massive neutrinos on the Higgs self-coupling and electroweak vacuum stability*, JHEP **06** (2012) 022 [1203.3825].

[138] D. Buttazzo, G. Degrassi, P. P. Giardino, G. F. Giudice, F. Sala, A. Salvio et al., *Investigating the near-criticality of the Higgs boson*, JHEP **12** (2013) 089 [1307.3536].

[139] T. Markkanen, A. Rajantie and S. Stopyra, *Cosmological Aspects of Higgs Vacuum Metastability*, 1809.06923.

[140] M. Malinsky, *Fun with the Abelian Higgs Model*, Eur. Phys. J. **C73** (2013) 2415 [1212.4660].

[141] F. Jegerlehner, *The hierarchy problem of the electroweak Standard Model revisited*, 1305.6652.

[142] A. Tomasiello, *Lecture notes: Mathematical Methods for Physics*, 2010.

[143] C. Lüdeling, *Lecture notes: physics751: Group Theory (for Physicists)*, 2010.

[144] M. B. Robinson, K. R. Bland, G. B. Cleaver and J. R. Dittmann, *A Simple Introduction to Particle Physics. Part I - Foundations and the Standard Model*, 0810.3328.

[145] J. Albert, *Lecture notes: Group Theory in Particle Physics*, 2007.

[146] A. Hoang, *Lecture notes: Advanced Topics in Particle Physics*, 2017.

[147] Nobel Media AB, "The 2004 Nobel Prize in Physics - Popular Information."

[148] G. Passarino and M. J. G. Veltman, *One Loop Corrections for e+ e- Annihilation Into mu+ mu- in the Weinberg Model*, Nucl. Phys. **B160** (1979) 151.